Interactions of Cationic Peptides with Anionic Lipid Bilayers and Monolayers

-

Influence of Peptide and Lipid Modifications on Binding

Dissertation

zur Erlangung des Doktorgrades der Naturwissenschaften
(Dr. rer. nat.)

der

Naturwissenschaftlichen Fakultät II
Chemie, Physik und Mathematik

der Martin-Luther-Universität
Halle-Wittenberg

vorgelegt von

Herrn André Hädicke
geboren am 14. Juli 1985 in Köthen

Gutachter:

1. Prof. Dr. Alfred Blume
2. Prof. Dr. Thomas Gutsmann

Tag der Verteidigung: 05.07.2016

to my parents

"An expert is a person who has made all the mistakes that can be made in a very narrow field."

Niels Bohr

Table of Content:

Abbreviations:

Lipids:

PG	phosphatidylglycerol
DMPG	1,2-dimyristoyl-*sn*-glycero-3-phospho-(1'-rac-glycerol) (sodium salt)
DPPG	1,2-dipalmitoyl-*sn*-glycero-3-phospho-(1'-*rac*-glycerol) (sodium salt)
DSPG	1,2-distearoyl-*sn*-glycero-3-phospho-(1'-rac-glycerol) (sodium salt)
POPG	1-palmitoyl-2-oleoyl-*sn*-glycero-3-phospho-(1'-rac-glycerol) (sodium salt)
PC	phosphatidylcholine
DMPC	1,2-dimyristoyl-*sn*-glycero-3-phosphocholine
DPPC	1,2-dipalmitoyl-*sn*-glycero-3-phosphocholine
POPC	1-palmitoyl-2-oleoyl-*sn*-glycero-3-phosphocholine
DOPC	1,2-dioleoyl-*sn*-glycero-3-phosphocholine
PE	phosphatidylethanolamine
DLPE	1,2-dilauroyl-*sn*-glycero-3-phosphoethanolamine
DMPE	1,2-dimyristoyl-*sn*-glycero-3-phosphoethanolamine
N-Me$_2$DPPE	1,2-dipalmitoyl-*sn*-glycero-3-phospho-N-methylethanolamine
N,NMe$_2$DPPE	1,2-dipalmitoyl-*sn*-glycero-3-phospho-N,N-dimethylethanolamine
DPPE	1,2-dipalmitoyl-*sn*-glycero-3-phosphoethanolamine
POPE	1-palmitoyl-2-oleoyl-*sn*-glycero-3-phosphoethanolamine
CL	cardiolipin
TMCL	1,1',2,2'-tetramyristoyl cardiolipin (sodium salt)
PA	phosphatidic acid
DMPA	1,2-dimyristoyl-*sn*-glycero-3-phosphate (sodium salt)
PS	phosphatidylserine
DMPS	1,2-dimyristoyl-*sn*-glycero-3-phospho-L-serine (sodium salt)
POPS	1-palmitoyl-2-oleoyl-*sn*-glycero-3-phospho-L-serine (sodium salt)
Rh-DHPE	1,2-dipalmitoyl-*sn*-glycero-3-phosphoethanolamine-N-(lissamine rhodamine B sulfonyl) (ammonium salt)
lysoPC	1-Oleoyl-2-hydroxy-*sn*-glycero-3-phosphocholine
CTAB	cetyltrimethylammonium bromide
ME	monoelaidin
SA	selachyl alcohol
PHYT	3,7,11,15-tetramethyl-1,2,3-hexadecanetriol
GMO	glycerol monooleate
Dns	Dansyl-

Peptides:

AMP	antimicrobial peptides
MRSA	methicillin-resistant *Staphylococcus aureus*
MDR TB	multidrug resistant *Mycobacterium tuberculosis*
SP-B	lung surfactant protein B
RDS	respiratory distress syndrome

Amino acids:

K	lysine
R	arginine
G	glycine
A	alanine
Abu	α-aminobutyric acid (homoalanine)
V	valine
L	leucine
Orn	ornithine
Dab	α,γ-diaminobutyric acid
Dap	α, β-diaminopropionic acid
TFA	trifluoroacetic acid
PLL	poly(L-lysine)
PLA	poly(L-arginine)

Techniques:

DSC	Differential Scanning Calorimetry
ITC	Isothermal Titration Calorimetry
FT-IR	Fourier Transform Infrared Spectroscopy
IRRAS	Infrared Reflection Absorption Spectroscopy
ATR-IR	Attenuated Total Reflection Infrared Spectroscopy
SFG	Sum Frequency Generation Vibrational Spectroscopy
cryoTEM	cryo Transmission Electron Microscopy
CD	Circular Dichroism
ESR	Electron Spin Resonance
MIC	Minimum Inhibitory Concentration

Variables:

R_c	charge ratio
R	gas constant
R^2	correlation coefficient
CPK model	Corey, Pauling, Koltun model

Phases:

L_α	liquid-crystalline phase
L_β, $L_{\beta'}$	gel, tilted gel phase
L_β^{int}	interdigitated gel phase
L_c	sub-gel phase, crystalline phase
$P_{\beta'}$	rippled gel phase
M_I, M_{II}	micellar, inverted micellar phase
H_I, H_{II}	hexagonal, inverted hexagonal phase
Q_{II}, Q_{II}^{M}	inverted cubic, inverted cubic micellar phase

Calorimetry:

T	temperature / K
T_{pre}	pre-transition temperature / °C
T_m	main transition temperature / °C
T_{mid}	temperature at half integral / °C
ΔT	temperature difference / K
ΔT_{base}	width of the peak at its base / K
I	current / A
β	heating rate / K s^{-1}
Q, G	energy, free energy / J
P	power / W
ΔH	transition enthalpy / kcal mol^{-1}
ΔC_p	differential heat capacity / kcal mol^{-1} K^{-1}

Spectroscopy:

I, I_0	single channel spectra of the sample and the reference
c	concentration / mol l^{-1}
ε	molar extinction coefficient / m^2 mol^{-1}
l, z	length / m
dp	depth of penetration / m
n	refractive index
φ	angle of incidence / °
Γ	polarizer quality
k	absorption coefficient
v_{as}	anti-symmetric stretching vibration / cm^{-1}
v_s	symmetric stretching vibration / cm^{-1}
δ	bending vibration / cm^{-1}
$\Delta\tilde{v}$	wavenumber difference / cm^{-1}

Packing parameter:

V_{hc}, V_{hg}	acyl chain volume, headgroup volume / Å^3
a_0	headgroup cross sectional area / Å^2
l	acyl chain length / nm
cpp	critical packing parameter
d_{hh}	bilayer thickness (head to head distance) / Å
d_{hg}	headgroup thickness / Å
d_{hc}	hydrocarbon thickness / Å
θ	tilt angle / °
ψ	twist angle / °

Monolayer:

G	gas-analogue phase
LE	liquid-expanded phase
LC	liquid-condensed phase
S	solid-condensed phase
A	area / $Å^2$

Tensiometry:

γ	surface tension / mN m^{-1}
F	force / N
ρ	density / g m^{-3}
w, h, t	width, height, thickness / m
q	contact angle / °
Γ	surface excess quantity / mol A^{-1}
π	surface pressure / mN m^{-1}
π_{ini}	initial surface pressure / mN m^{-1}
π_{sp}	superposition surface pressure / mN m^{-1}
$\pi_{LE/LC}$	*LE/LC* phase transition pressure / mN m^{-1}
π_0	equilibrium surface pressure / mN m^{-1}
π_{red}	reduced surface pressure / mN m^{-1}
$\Delta\pi$	difference in surface pressure / mN m^{-1}
n	intercept on y-axis
m	slope
κ	compressibility / m mN^{-1}
$A_{1,2}$	amplitude / mN m^{-1}
t	time / s
$t_{1,2}$	relaxation time / h

1   Introduction

1.1   Biological and Model Membranes

Cells and cell organelles are enclosed of biological membranes. Membranes play a crucial role in almost all cellular phenomena and fulfill several functions. They act as physical barrier to separate the cytosol from the outside, protect the interior from external influences, create a closed reaction volume, and assure a selective transport of material. A gradient of charge and concentration across the membrane drives many biochemical reactions. In biological membranes (see Figure 1.1.1), lipids arrange in a double layer of ca. 5 nm thickness with integral or peripheral proteins. Due to the high mobility of the lipids the bilayer is described as a two-dimensional fluid [1].
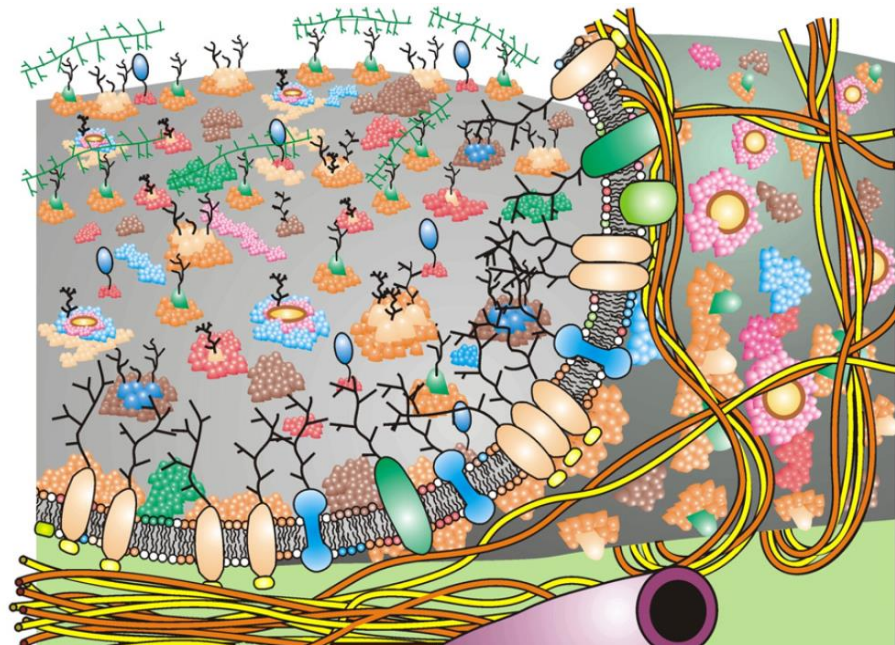
Figure 1.1.1: An updated Fluid-Mosaic Membrane Model that contains information on membrane domain structures and membrane-associated cytoskeletal and extracellular structures. Different integral proteins, glycoproteins, lipids and oligosaccharides are represented by different colors, and where the membrane has been peeled-up to view the inner membrane surface cytoskeletal fencing is apparent that restricts the lateral diffusion of some but not all trans-membrane glycoproteins. Other lateral diffusion restriction mechanisms are also represented, such as lipid domains, integral membrane glycoprotein complex formation (seen in the membrane cut-away), polysaccharide-glycoprotein associations (at the far top left) and direct or indirect attachment of inner surface membrane domains to cytoskeletal elements (at lower left). Although this figure suggests some possible integral membrane protein and lipid mobility restraint mechanisms, it does not accurately present the sizes or structures of integral membrane proteins, cytoskeletal structures, polysaccharides, lipids, submicro- or nano-sized domains or membrane-associated cytoskeletal structures or their crowding in the membrane.

Since the complexity of biological membranes is too high, model membranes composed of one single phospholipid or a defined mixture of some few lipids are often used. They can be easily prepared by dispersing the lipids in aqueous solution. The amphiphilic character forces lipids to form in water various aggregates in a self-assembly process, depending on the lipids and the preparation method. The lipids themselves show a vast variety of self-assembled structures. The most common model system is the vesicle, also named liposome, with different lamellarities. To study specific interactions of lipid membranes with peptides, calorimetric (Differential Scanning Calorimetry (DSC) [2], Isothermal Titration Calorimetry (ITC) [3]) and spectroscopic (Infrared Spectroscopy [4], Fluorescence Spectroscopy, Electron Spin Resonance Spectroscopy [5]) techniques can be applied.

Lipid monolayers, spread at the air-water interface, represent one half of a bilayer [6-8]. During compression, it is possible to investigate the interactions with monolayers in different physical states and packing order of the alkyl chains. Furthermore, monolayers are suitable to study the interaction or binding of molecules, such as peptides [9], polymers [10] or amphiphilic substances [11] to the lipid headgroup region and their possible insertion in between the lipid chains. Monolayer experiments can easily be coupled with fluorescence microscopy [12, 13] or infrared reflection absorption spectroscopy (IRRAS) [14], and other techniques.

1.2 Antimicrobial Peptides

Antibiotics

In 1911, the first report about the "magic bullet" Salvarsan 606, a compound to treat infectious diseases like syphilis was published at Paul Ehrlich´s lab [15]. With this drug the era of "chemotherapy" was started, and led to a tremendous progress in medicine, which finally increased life expectation. The discovery of antibiotics at the beginning and midst of the 20th century seemed to solve all problems concerning bacterial infection, but nowadays these diseases became threatening again due to the resistance of some bacterial strains against these substances.

The drawback of the classical antibiotics is their very specific mode of action, which enables the bacteria to circumvent this mode of action by mutation [16, 17]. Penicillin, a representative of the class of β-lactam antibiotics, for example, inhibits the formation of peptidoglycan cross-links in the cell wall, whereas the class of sulfonamides acts as competitive inhibitors of the enzyme dihydropteroate synthetase, an enzyme involved in folate synthesis [18, 19]. The occurrence of resistant strains like MRSA (methicillin-resistant *Staphylococcus aureus*) and MDR TB (multidrug resistant *Mycobacterium tuberculosis*), is one big problem. This has arisen due to the use antibiotics in animal breeding or overhasty, excessive prescription, and normal adaption of bacteria as reaction to evolutionary pressure. To curtail the development and spread of resistance, the appropriate use of antimicrobials, the development of new antimicrobial classes, and the use of other substances like antimicrobial peptides is required. Since 1968, only two new classes of antimicrobials were developed [20]. The lack of new antimicrobial drugs has several origins, like the high cost for clinical studies, the low profit margin, as a bacterial infection is a short-term medication, the pursuit of companies to earn as much as possible, and the large competition with drugs already on the market.

Antimicrobial peptides

To overcome the drawback of a specific mechanism of action of antibiotics, and to regain a potent drug against bacteria, the use antimicrobial peptides (AMP) might be the method of choice, due to their more general interaction with the bacterial membranes [16, 21]. AMPs or host defense peptides play a key role in the innate immune system and are found in all classes of life. Antimicrobial peptides have been a potent defense for millions of years, without creating any resistance in bacteria. Several reviews are dealing with the interaction of these

peptides with cell lines or lipid membranes [22-25]. Some well-known antimicrobial peptides are indolicidin [26], showing no preferred structure, β-defensin [27] and lactoferricin [28] with mainly β-sheet structures, and the α-helical magainin [29] and LL-37 [30]. The most important feature of these peptides is not their secondary structure, but their cationic and mostly amphipathic character [31, 32]. Antimicrobial peptides show a high abundance (about 10% each) of the amino acids lysine, glycine, alanine and leucine [33]. The positive charge of these peptides promotes the selectivity for bacterial membranes [34], composed of negatively charged lipids, over mammalian cells with mainly zwitterionic lipids. The hydrophobic residues of the peptide enable the interaction with the acyl chain region of the bilayer. The very first interaction of these peptides with the bacterial membrane is driven by electrostatic and hydrophobic interaction. The basics of lipid-peptide interaction are presented in section 2.4.

2 The Model Systems

2.1 Lipids

Lipids are amphiphiles and one of the major components of the cell membrane. Their chemical structures show large differences, but all have in common a hydrophobic and a hydrophilic part. One special class of lipids are phospholipids, composed of a central glycerol, which is esterified at the *sn*-1 and *sn*-2 positions with long fatty acid chains, and at the *sn*-3 position with a phosphoric acid. A general structure of a phospholipid is given in Figure 2.1.1. The hydrophobic acyl chains differ in length between 14 and 24 carbon atoms, and in degree of unsaturation. The hydrophilic headgroup contains the glycerol, the phosphoric acid, and mostly another alcohol, which is esterified at the phosphoric acid. This gives the whole molecule either a neutral or a negative charge. All these variations in the lipid structure open a wide range of properties and enable the opportunity to tune the membrane composition for special needs.

The capability of antimicrobial peptides to distinguish between bacterial cells and mammalian cells has its origin in the different composition, hydrophobicity, and charge of the bilayers. Mammalian cells are composed of mainly zwitterionic lipids like phosphatidylcholine (PC), phosphatidylethanolamine (PE), sphingomyelin, and sterols. Bacterial cells with their high proportion of the negatively charged lipids phosphatidylglycerol (PG) and cardiolipin (CL) beside the zwitterionic PE, sustain a net negative charge [16, 35]. Other negatively charged phospholipids, e.g. phosphatidic acid (PA), phosphatidylserine (PS) and CL can be found as minor components of bacterial membranes, or also in the inner leaflet of mammalian cells or in cancer cells [36]. Since the complexity of bacterial membranes is too high, model membranes containing negatively charged phospholipids are often used to study specific interactions with peptides. As phosphatidylglycerols are the major lipid in bacterial membranes, most of the studies were performed with lipids having PG headgroups.

The properties of the phospholipids used here can be tuned in four major directions to achieve the knowledge about the impact of following parameters (see Figure 2.1.1). The impact of an elongation of the acyl chain length was tested with PG´s having two saturated acyl chains (blue path). With an increased chain length, also the hydrophobic thickness of the membrane is increased from DMPG to DSPG. The effect of a more fluid bilayer compared to saturated lipids was investigated by introducing an unsaturation in the *sn*-2 chain (pink path). Although the oleoyl chain in POPG is two carbon atoms longer, the kink at the double bond in the chain

creates a bilayer thickness, which is comparable to DPPG. The influence of the headgroup charge of the lipid was determined by attaching either a positively charged amino alcohol or a neutral alcohol to the phosphate group. Zwitterionic lipids were formed with ethanolamine (PE) or choline (PC), whereas negatively charged lipids were created by attaching hydrogen (PA), glycerol (PG) or serine (PS) (red path). The attached alcohol also determines the headgroup size (green path) increasing from PA to PS.
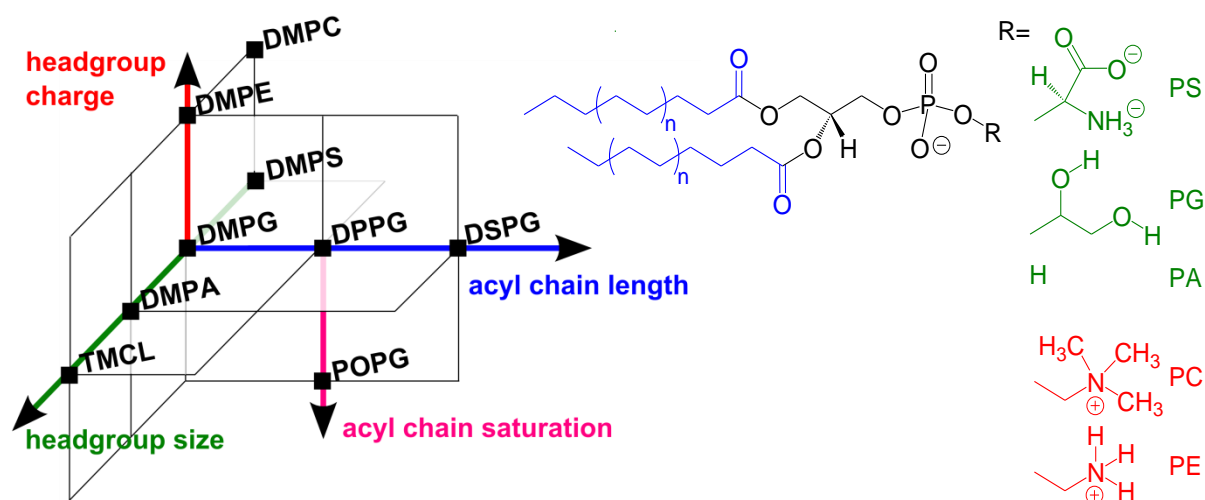
Figure 2.1.1: Left: lipid matrix of the used lipids with the four parameters determining the architecture of the molecule; blue path: acyl chain length variation; pink path: variation of acyl chain saturation; green path: change of headgroup size and structure; red path: different headgroup charges. Right: general chemical structure of the used phospholipids with the different headgroups (same color code as mentioned above).

2.2 Lipid Polymorphism

Lipids dispersed in water spontaneously self-aggregate due to their amphiphilic nature. The driving force of the underlying process, the shielding of the hydrophobic part of the molecule from the surrounding water to minimize unfavored contacts, is known as the hydrophobic effect [37]. Aqueous lipids suspensions show polymorphism (see Figure 2.2.1), depending on the water content (lyotropic mesomorphism), temperature (thermotropic mesomorphism), *pH*, salt concentration and on the lipid architecture itself. Within the structure of phospholipids, the headgroup as well as the acyl chain in its length and saturation has an influence on the phase behavior.
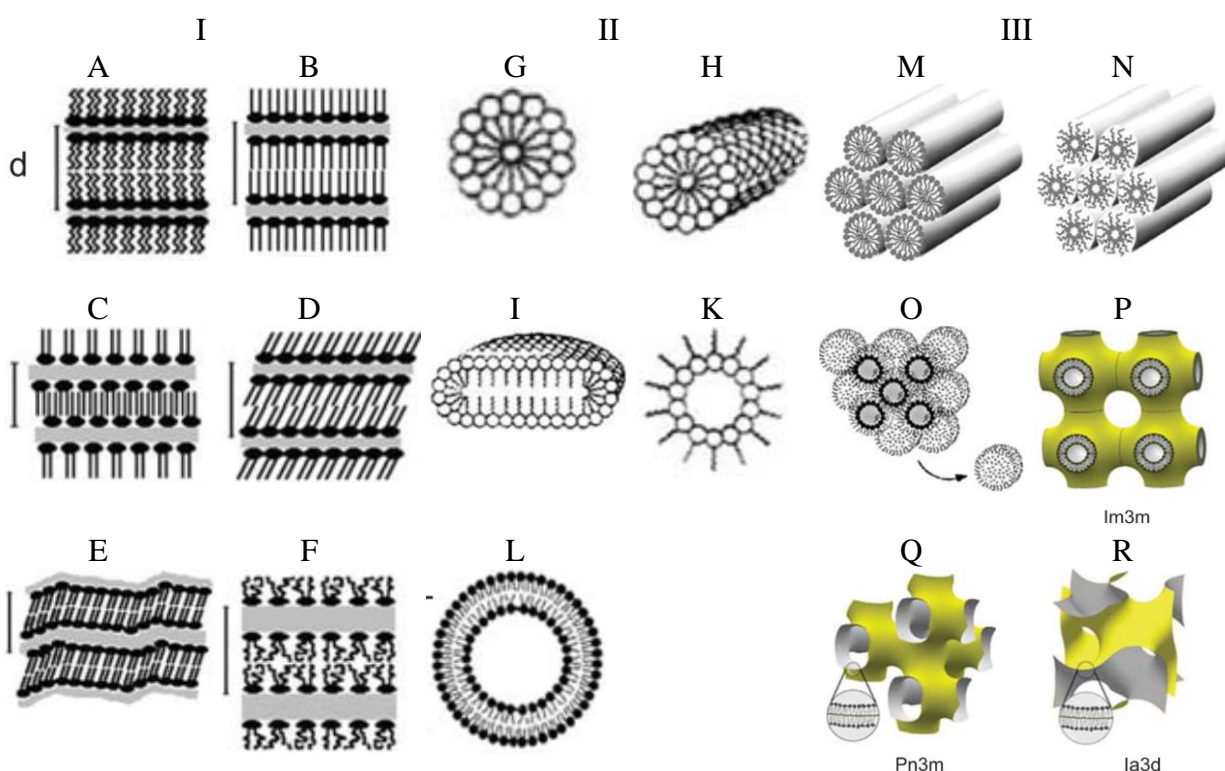
Figure 2.2.1: Structures of lipid phases. I. Lamellar phases: (A) subgel, L_c; (B): gel, L_β; (C) interdigitated gel, L_β^{int}; (D) gel, tilted chains, $L_{\beta'}$; (E) rippled gel, $P_{\beta'}$, (F) liquid crystalline, L_α. II. Micellar aggregates: (G) spherical micelles, M_I; (H) cylindrical micelles (tubules); (J) disks; (K) inverted micelles, M_{II}; (L) liposomes. III. Non-lamellar liquid-crystalline phases of various topology: (M) hexagonal phase H_I; (N) inverted hexagonal phase H_{II}; (O) inverted micellar cubic phase Q_{II}^M; (P) bilayer cubic phase Q_{II} Im3m, primitive; (Q) bilayer cubic phase Q_{II} Pn3m, double diamond; (R) bilayer cubic phase Q_{II} Ia3d, gyroid [38].

Critical packing parameter

The lipid structure with all its parameters shown in Figure 2.1.1 has an influence on the critical packing parameter (*cpp*), introduced by Israelachvili et al. [39]. This parameter derived from geometric considerations predicts the aggregate structures formed by the amphiphiles. The critical packing parameter *cpp* is calculated as follows:

$$cpp = \frac{V_{hc}}{a_0 \cdot l} \tag{2.1}$$

where V_{hc} is the volume of the acyl chain, a_0 the cross sectional area of the headgroup and l the effective length of the acyl chain.

An overview of connection between the *cpp* of a lipid, its shape and the formed aggregates is given in Figure 2.2.2. Thus, lipids with a shape of an ideal cylinder and a *cpp* = 1 form planar lamellar bilayers. Most of the double-chain phospholipids have truncated cone shapes and a *cpp* between 0.5 and 1. They aggregate to vesicles and curved bilayers. Other possible aggregation structures are micelles (*cpp* < 1/3) and hexagonal or cubic phases (*cpp* > 1).

In Table 2.2.1, the structural data to calculate the critical packing parameter of the different lipids used in this study are presented. The calculated critical packing parameters for the used lipids to test their thermotropic behavior in mixtures with peptides are in the range 0.76 up to 1.04 and increase in the order DSPG ≈ DMPS < DMPG ≈ DPPG < DLPE < POPG ≈ DPPC < TMCL ≈ DMPA. All tested lipids are able to build up planar bilayer structures.
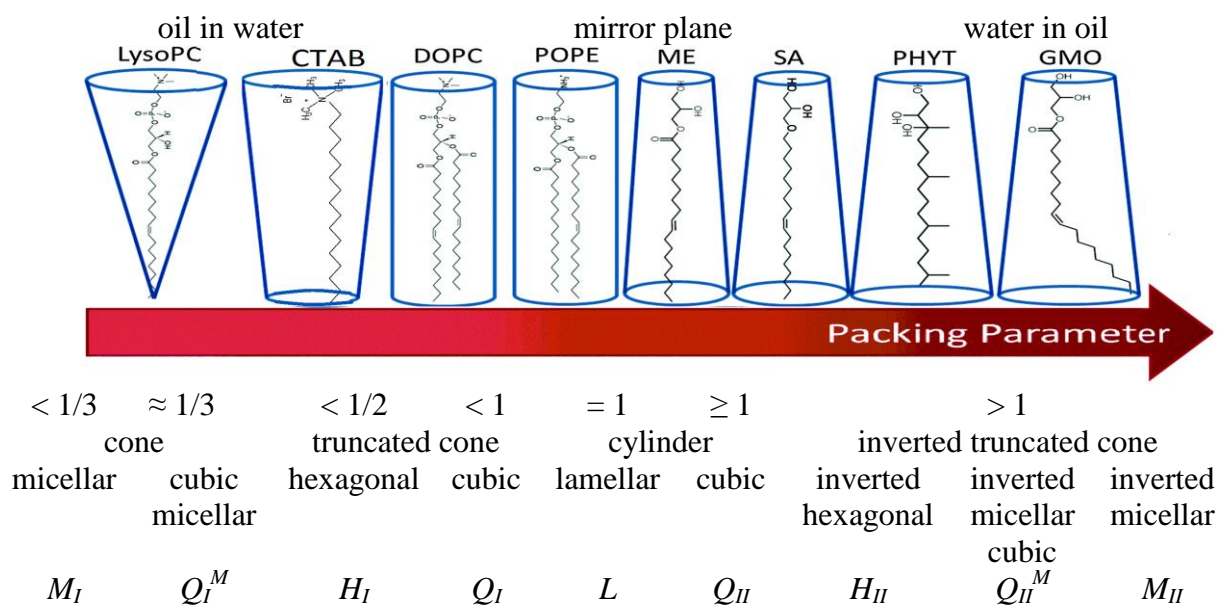
Figure 2.2.2: Critical packing parameter of amphiphiles and their corresponding aggregation structure due to geometrical packing reasons [40-42]. The shape of the lipids can be described by various types of cones. Typical representatives are phosphatidylcholines with one acyl chain (1-Oleoyl-2-hydroxy-*sn*-glycero-3-phosphocholine, lysoPC) for cone shaped lipids; cetyltrimethylammonium bromide (CTAB) for truncated cone shape lipids; 1,2-dioleoyl-*sn*-glycero-3-phosphocholine (DOPC) and 1-palmitoyl-2-oleoyl-*sn*-glycero-3-phosphoethanolamine (POPE) for cylindrical shape lipids; monoelaidin (ME), selachyl alcohol (SA), 3,7,11,15-tetramethyl-1,2,3-hexadecanetriol (PHYT), and glycerol monooleate (GMO) for inverted truncated cone shape lipids.

Comparing lipids with similar headgroups, the critical packing parameter is almost unchanged for homologue phosphatidylglycerols with saturated chains of different length, i.e. DMPG, DPPG, and DSPG, respectively. The higher acyl chain volume is compensated by a larger membrane thickness. This is also shown for PC lipids having chains longer than 12 carbon atoms showing a slight increase of the *cpp* with increasing chain length [43]. Introduction of an unsaturation increases the critical packing parameter, because a reduced order in the chain requires more space. The calculated *cpp* values for DMPA and TMCL are above 1, and the largest, comparing all tested lipids. The shape of these lipids can be illustrated as an inverted cone and an enhanced ability to build up inverted structures is expected. This was found for the influence of the lipids to form inverted hexagonal phases and their effect on the respective phase transition temperature [44, 45].

Table 2.2.1: Comparison of the structural data used to calculate the critical packing parameter for different lipids. Presented data are for the gel and fluid phase, where a_0 is the cross sectional area of the headgroup, d_{hh} the bilayer thickness (head to head distance), V_{hc} the volume of the hydrocarbon chains, V_{hg} the volume of the headgroup, θ the tilt angle in the gel phase bilayer and *cpp* the calculated critical packing parameter. Values without a citation are estimated from other reported values. Uncertainties for the *cpp* are about 0.07.

	a_0 / Å		d_{hh} / Å		V_{hc} / Å^3		V_{hg} / Å^3	θ / °	*cpp*	
lipid	gel	fluid	gel	fluid	gel	fluid			gel	fluid
POPG	48 [46]	64.4 [47]	51	37.3 [47]	930	950 [48]	257 [49]		0.92	1.01
DMPG	48 [46]	65.1 [47]	45.3 [50]	32.5 [47]	730 [48]	780 [48]	257 [49]	29 [51]	0.82	0.98
DPPG	48 [46]	67.0 [47]	51.1 [46]	35.5 [47]	840 [49]	915 [48]	257 [49]	32 [46]	0.81	0.99
DSPG	48 [46]	68.3 [47]	60.0 [49]	38.2 [47]	930 [48]	1030 [48]	257 [49]	27 [49]	0.76	1.00
DMPA	43.2 [50]	55	40.1 [50]	36	730 [48]	780 [48]	220 [52]	31 [50]	1.04	1.00
DMPS	51.3 [53]	64.1 [54]	44.3 [54]	39.0 [54]	735 [54]	780 [48]	244 [54]	0 [54]	0.70	0.76
TMCL	78.9 [55]	~100 [56]	42.8 [56]	37.8 [55]	1460 [48]	1560 [48]	480 [52]	15 [56]	1.03	1.03
DPPC	47.9 [57]	62.7 [57]	47.8 [57]	39.6 [57]	840 [48]	915 [48]	319 [48]	32 [58]	0.94	0.92
DLPE	41 [59]	49 [59]	45 [59]	41 [59]	630 [48]	670 [48]	252 [60]	0 [59]	0.87	0.87

The effective cross-sectional area of a lipid polar headgroup primarily depends on headgroup volume and decreases for lipids with similar acyl chains in the following order PS, PG, PC, CL, PA and PE (taking into account that for CL the volume is halved to be comparable with the other two-chained phospholipids) [45]. Beside the headgroup volume, also shape, charge, orientation, and degree of hydration are important parameters [61-63]. One of these parameters might be the reason for the inverted order of CL and PA in their ability to stabilize the gel phase upon peptide addition. The charge of the phosphatidic headgroup depends on the *pH* of the solution. The single charged phosphate group at neutral *pH* can be deprotonated by decreasing the *pH* below 3.5 (*pK$_1$*) [64]. In vesicles, chain saturated CLs show a second *pK$_2$*

around 7.5 - 9.5 [65, 66]. Thus, in neutral solutions the second proton of the CL headgroup is partly dissociated. To form a stable lipid bilayer, the molecules are forced to tilt the acyl chains, due to the different sterical demands of the headgroup and the attached acyl chains. The mentioned lipids show a tilt angle of the acyl chains between 0° and 30° (see Table 2.2.1).

2.3 Peptides

The used peptides are short linear model compounds to simulate the mode of action of antimicrobial peptides. To study the influence on the amino acid composition of the peptide on the interaction with lipid membranes, a small peptide library was build up. This library was constructed in a way to determine the interplay of electrostatic and hydrophobic contribution on lipid-peptide interactions. All peptides exhibit an alternating sequence of uncharged amino acids of different hydrophobicities inserted between the five positively charged amino acids. The matrix of custom made peptides was used, to address the following questions (see Figure 2.3.1): i) the influence of the increasing hydrophobicity of the uncharged amino acid (blue path), ii) influence of the charge distance and periodicity of the peptide by introducing a second uncharged spacer (red path), iii) influence of arginine instead of lysine (green path).
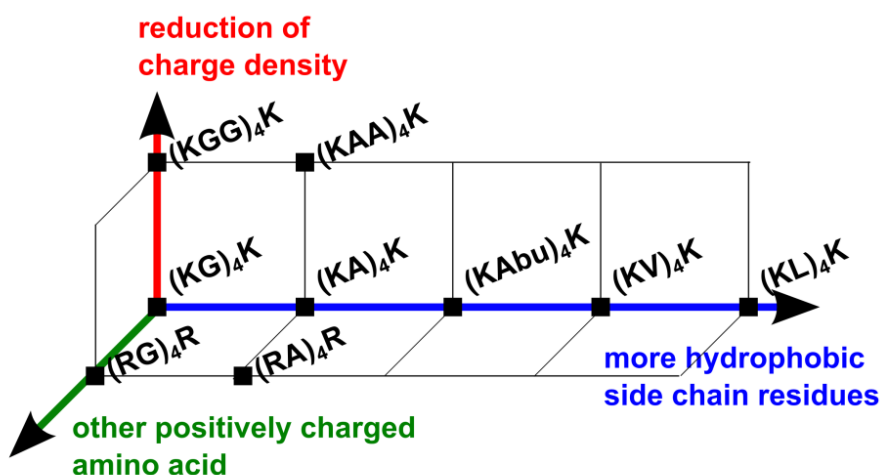
Figure 2.3.1: Peptide library of small linear cationic model peptides used to study their interaction with lipid bilayers and monolayers. All peptides have the same net charge, but the charge distribution, overall hydrophobicity, and the charge localization are tuned by a systematic change of some amino acids.

The exchange of the neutral amino acid X in peptides $(KX)_4K$ of the library from glycine (G) over alanine (A), α-aminobutyric acid (Abu), valine (V), up to leucine (L) enables the possibility to increase and tune the hydrophobicity, the flexibility, and sterical demand of the peptide. A CPK model of all peptides is shown in Figure 2.3.2. The non-natural amino acid (Abu) was used to close the gap between the smaller alanine and larger valine side chain residues. The increments for the side chain residues are -H, $-CH_3$, $-CH_2-CH_3$, $-CH-(CH_3)_2$ and $-CH_2-CH-(CH_3)_2$ for (G), (A), (Abu), (V) and (L), respectively.
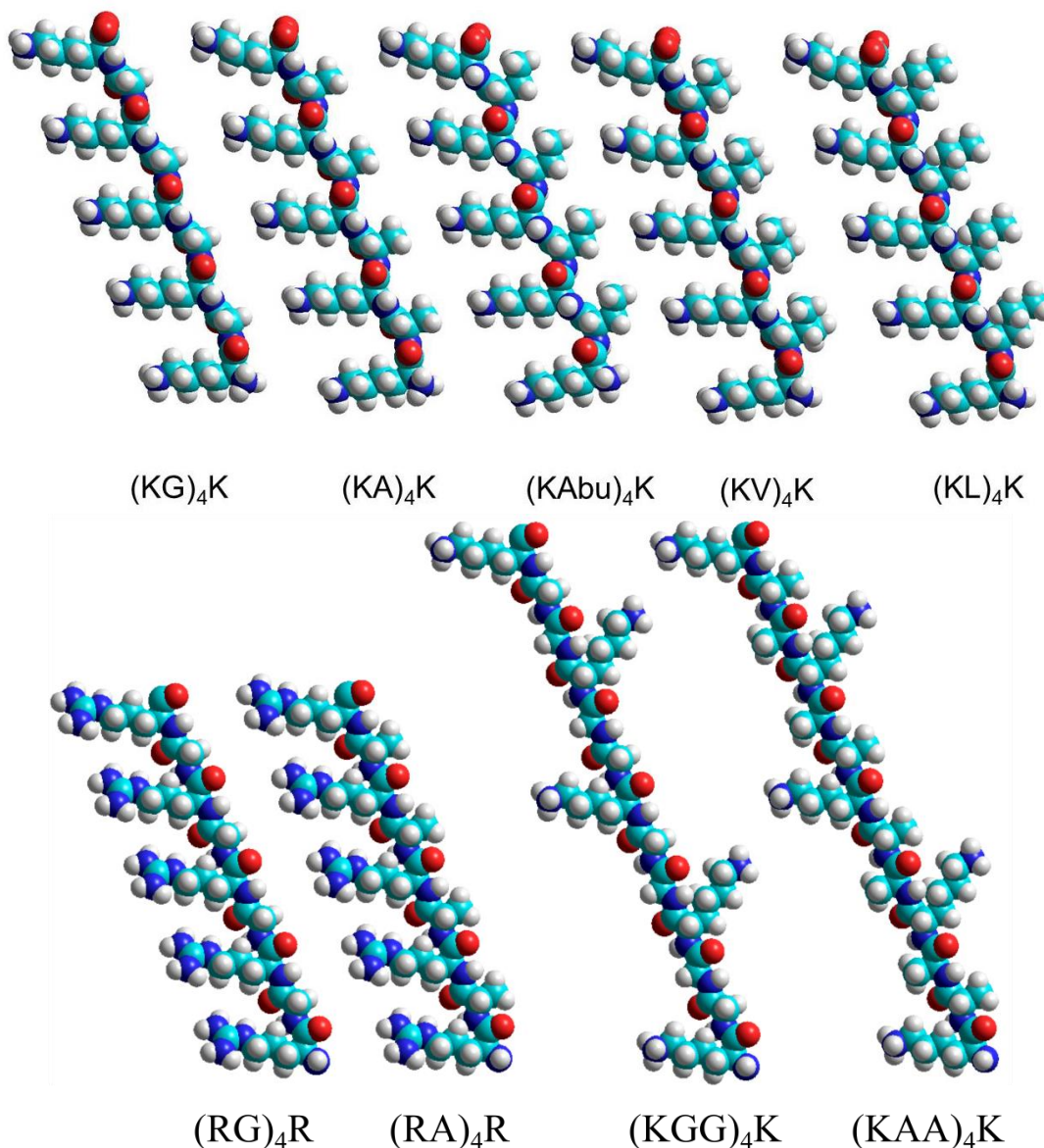
Figure 2.3.2: CPK models of the used linear peptides in an extended conformation. Top: (KX)₄K with X = G, A, Abu, V, and L. Bottom: (RX)₄R and (KXX)₄K with X = G, A.

An introduction of a second uncharged amino acid between two lysines further increases the distance of the charges, and opens the opportunity to build up other secondary structures beside the random conformation and β-sheet structures. The different distribution of hydrophobic amino acids and charged amino acids in a single peptide chain results in different periodicities, which tend to form specific secondary structures, as shown for model peptides containing (L) and (K). An almost unstructured peptide strand in bulk solution [67] is able to build up defined structures upon interaction with interfaces, like the air-water interface [9, 68, 69], lipid-bulk solution interface [70, 71], as well as solid liquid interfaces [72, 73]. For a periodicity of 2 with alternating lysines and leucines, a β-sheet is proposed and experimentally proved by IR [70, 71] and SFG [72] spectroscopic measurements with the

peptide Ac-LKLKLKLKLKLKLKL-NH$_2$, which is a longer analog of the (KL)$_4$K used in this study. An elongation of the periodicity to a value of 3 results in a 3$_{10}$-helix [74, 75], i.e. as observed for Ac-LLKLLKLLKLLKL-NH$_2$. An increased periodicity of 3.5 assumes the formation of α-helixes, as shown for the peptide Ac-LKKLLKLLKKLLKL-NH$_2$ [76]. The minimal length for a stable helix is predicted to be 14 amino acids [77]. All peptides used here are with 13 amino acids and below this value. The very long model peptide (KL$_4$)$_4$K shows a periodicity of 5. In interaction with lipid bilayers, it builds up an α-helix, which inserts parallel to the membrane normal. At the air-water interface the α-helical structure is retained upon interaction with lipid monolayers composed of phosphatidylglycerols [78, 79], but converts to a β-sheet in a phosphatidylcholine monolayer upon film compression [80]. (KL$_4$)$_4$K was used to evaluate the mode of action of lung surfactant protein B (SP-B), and was tested as drug, to treat the respiratory distress syndrome (RDS), a deficiency of surfactants in the alveolar spaces [81-84]. Some of these peptides are acetylated at the beginning and amidated the end, other start with the uncharged leucine in their sequence. This makes it difficult to compare them with (KL)$_4$K, used in this study, but has no influence on the periodicity of the peptide.

The exchange of the charged amino acid from lysine by arginine alters the distance and the distribution of the positive charge in relation to the peptide backbone. Whereas the charge in the lysine side chain is farer apart, but located at the terminal amino group, it is closer, but delocated over the whole guanidinium moiety in the arginine side chain. Thus, the so-called "arginine magic" effect might play a role in peptide-lipid interaction, due to its ability to build up stable hydrogen bonds with lipid phosphate groups [85-87]. Mosior and McLaughlin determined a 2-fold increase of the binding constant, comparing the arginine containing peptides R$_5$, (RA)$_4$R and (RAA)$_4$R with the lysine analogues [88].

2.4 Lipid-Peptide Interactions

The very first step of the peptide-lipid interaction is the approach of the peptide from the bulk medium to the bilayer, which is by itself a complex process. The interaction of both components is driven by electrostatic and hydrophobic contributions. Upon binding of the peptide to the membrane, structural changes of both interaction partners may occur. The variety of the underlying structures of absorbed peptides ranges from unordered conformation, over β-sheets, to α-helices. This makes it difficult to draw a single picture for their mode of action. Some well-known antimicrobial peptides are indolicidin [26], showing no preferred structure, β-defensin [27] and lactoferricin [28] with mainly β-sheet structures and the α-helical magainin [29] and LL-37 [30]. Beside the peptide structure, several other factors like the lipid to peptide ratio, and the lipid composition, are decisive for the mode of action of the cationic antimicrobial peptides [89, 90]. Peptide binding to lipid bilayer can have different effects on the bilayer structure: membrane thinning or thickening, membrane leakage or disruption, lipid sorting, and formation of non-bilayer intermediates [91, 92]. The most common models for peptide induced membrane leakage are the barrel stave, toroidal pore, or the carpet model beside other mechanisms [92-95]. An overview of some possible modes of action is depicted in Figure 2.4.1.

Beside the peptide structure, also the lipid structure also has an influence. Hydrophobic interactions occur with the different acyl chains, whereas the electrostatic contributions of the lipid-peptide interactions are located in the headgroup region. The lipid acyl chain length and saturation changes the fluidity and the thickness hydrophobic region of the membrane, as well as the transition temperature and the area per lipid [96]. An effect of the absolute temperature should be visible with lipids having different chain length, resulting in different trends of the thermotropic behavior. Changing the thickness of the hydrophobic region might stimulate different peptide arrangements, because the ability for membrane thinning or thickening is restricted, and a modified translocation of the peptide through the bilayer is possible [25, 97, 98]. The headgroup charge and the chemical structure of the headgroup play a major role for interaction with charged peptides. For interaction of zwitterionic lipids with peptides, the electrostatic attraction can be neglected.
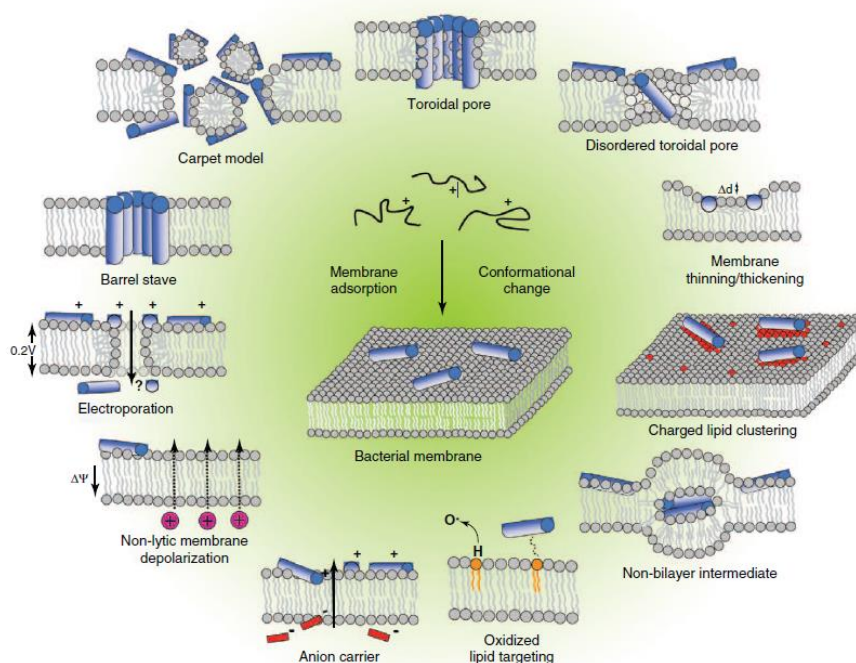
Figure 2.4.1: Events occurring at the bacterial cytoplasmic membrane following initial antimicrobial peptide (AMP) adsorption. These events are not necessarily exclusive of each other. In the classical models of membrane disruption, the peptides lying on the membrane reach a threshold concentration and insert themselves across the membrane to form either peptide-lined pores in the barrel-stave model, solubilize the membrane into micellar structures in the carpet model, or form peptide-and-lipid-lined pores in the toroidal pore model. In the revised disordered toroidal pore model, pore formation is more stochastic and involves fewer peptides. The thickness of the bilayer can be affected by the presence of the peptides, or the membrane itself can be remodeled to form domains rich in anionic lipids surrounding the peptides. In more specific cases, non-bilayer intermediates in the membrane can be induced; peptide adsorption to the membrane can be enhanced by targeting them to oxidized phospholipids; a peptide may couple with small anions across the bilayer, resulting in their efflux; the membrane potential can be dissipated without other noticeable damage; or conversely, in the molecular electroporation model, the accumulation of peptide on the outer leaflet increases the membrane potential above a threshold that renders the membrane transiently permeable to various molecules including the peptides themselves [92].

The arginine with its guanidinium moiety plays an important role for binding to the lipid headgroup as it can build up a stable bidentate hydrogen bond with the phosphate group [85, 86]. The side chain of the arginine with its relative high hydrophobicity shows a 10-fold increase in efficiency for the translocation of the peptide with or without an attached carrier through the lipid bilayer, than lysine analogues [99]. The internalization of the peptide is further enhanced, if the sequence contains 6 or more arginines, and if the alkyl spacer between the guanidinium group and the peptide backbone is elongated [100, 101].

For short homopeptides of lysine (K) or arginine (R) the binding affinity to anionic bilayers composed of PS, PG or CL increases 10-fold with each additional cationic residue [102, 103]. The binding to zwitterionic phosphatidylcholines (PC) is only weak. The longer chain analogues poly(L-lysine) (PLL) and poly(L-arginine) (PLA) with different degrees of

polymerization are frequently used model systems to study the effect of charges with regard to electrostatic binding to negatively charged membranes. [104-111]. Comparing different anionic lipids, the upshift of the main phase transition to higher temperatures is more pronounced for phosphatidic acid (PA) than for PG interacting with PLL. Comparing different peptides, PLL is more potent to stabilize the lipid gel phase than PLA. PLL on its own is able to adopt all three common secondary structures of polypeptides, random coil, β-sheets, or α-helices, depending on the ionic strength, *pH*, and the abundance of lipid membranes [112-114]. Beside the electrostatic interaction, the hydrophobicity, length and sequence of the peptide determines its propensity to build up secondary structures and its ability to be incorporated into membranes. In general, the shorter the chain, the fewer are stable secondary structures, so that a higher probability for random coil structures is present. The interaction of pentalysine and pentaarginine with model membranes was investigated by several other groups, proposing that the binding of oligolysines is of pure electrostatic nature [88, 103, 115-122].

The lysine side chain itself is capable to insert into the headgroup region of the membrane via hydrophobic and electrostatic interaction. Lysine analogs with shorter side chains, namely ornithine (Orn), α,γ-diaminobutyric acid (Dab), and α, β-diaminopropionic acid (Dap), show less hydrophobic contributions and are able to stabilize the gel phase of anionic membranes to a greater extent [123] as charge neutralization is more effective.

2.5 Motivation and Aim of this Work

The interaction of lipid membranes with antimicrobial, cell penetrating, and cationic peptides is an extremely active area of research. The principle findings have been reported in the literature (see chapter 2.4). However, a systematic study on the binding properties, where peptide sequences (see Figure 2.3.1), and lipid structures (see Figure 2.1.1) were altered to determine their influence on the interaction is still missing.

Antimicrobial peptides, originating from biological sources, show a vast variety of different peptide sequences, which lead to different secondary structures. It was found that the exchange of a single amino acid influences the binding properties. The complex behavior of these different cationic peptides with different lipid systems is always a subtle interplay of electrostatics and hydrophobicity.

The main topic of this work is the impact of electrostatic and hydrophobic contributions to the interactions between positively charged peptides and negatively charged lipid membranes.

The question addressed here is, how these interactions are influenced by the peptide sequence, the lipid phase state, and the membrane composition.

Another goal of this work is to study how binding of model peptides influences the membrane properties, i.e. how the thermotropic phase behavior and the structure of the membrane in different phase states are affected. Attention is also directed to the secondary structure of the peptide that possibly forms upon binding to the membrane. Are these secondary structures stable at elevated temperatures and do they influence the binding process?

With regard to the peptide architecture, a small library of tailor-made model peptides was build up, which all contain five positively charged side chains. By introducing several amino acids into the sequence, the parameters depicted in Figure 2.3.1 can be tuned in a systematic manner to investigate their influence. The effect of an increased hydrophobicity of the uncharged amino acid X was tested with the peptides $(KX)_4K$, with X = G, A, Abu, V, and L. The influence of an elongated charge distance was tested with $(KXX)_4K$ peptides, and the exchange of the charged amino acid with $(RX)_4R$ peptides, where X = G or A.

Studies were performed with different model membranes of lipids with varying acyl chain length, acyl chain saturation, headgroup charge, and headgroup structure (see Figure 2.1.1) to evaluate the impact of the lipid component interacting with the peptides. The influence of altered acyl chains was tested with different phosphatidylglycerols: DMPG, DPPG, DSPG, and POPG. The impact of the headgroup structure was revealed by using lipids with negatively charged headgroups, PG, PA, PS, and CL; or zwitterionic headgroups, PC, and PE.

2.6   Methods and Theory

2.6.1   Differential Scanning Calorimetry

Differential Scanning Calorimetry (DSC) is a well-established standard method for the study of thermal induced processes, e.g. chemical reactions or phase transitions. It is used on a large scale in different areas of research to determine thermal effects and the relevant temperature. As physical transitions are connected with the generation or consumption of heat, calorimetry is a universal method for investigating such processes. Caloric values obtained by DSC are heat capacity, heat of transition, kinetic data, and purity. DSC curves serve to identify substances, to set up phase diagrams and to determine degrees of crystallinity [124].

The principles and theory of this method for investigating biological membranes and bilayers of model lipids have been extensively described by Blume [125]. The lipid main phase transition is connected with a transition from an ordered, crystalline-like state at low temperature to a more disordered liquid-crystalline state at higher temperature [126-128]. The high enthalpy of this first order phase transition is associated with the melting of the long acyl chains [129]. Information about the phospholipid conformation, bilayer fluidity, and ligand-vesicle interaction can be derived. DSC has been widely used to measure the phase behavior of phospholipid bilayers in interaction with additives like peptides and proteins [126, 130, 131].

Two types of Differential Scanning Calorimeters must be distinguished: the heat flux DSC and the power compensation DSC. The power compensation DSC in the adiabatic mode of operation measures heat capacities and heat of transitions directly and with a high accuracy. The adiabatic shield guarantees quasi-isothermal conditions, while the heat to be determined is compensated with the aid of electric energy [124]. The sample cell is filled with the sample solution and the reference cell with the pure solvent. The both cells are heated at an equal rate $\beta = dT / dt$ by the same electric current I. The ideally symmetrical arrangement leads to a temperature difference equal to zero.

$$\Delta T = T - T' = 0 \tag{2.1}$$

With an increase of heat capacity C_P in one of the chambers, the computer controlled system adjusts the heating currents so that the occurring temperature difference between the chambers remains zero. An imbalance in one of the chambers increases the heating current by ΔI, while in the second chamber it decreases by ΔI. In this case:

$$\frac{dQ}{dT} = P - P' = R\left\{(I - \Delta I)^2 - (I + \Delta I)^2\right\} = 4RI\Delta I \tag{2.2}$$

The differential heat effect is directly proportional to the compensating current and, consequently, the recording of the heat effect is reduced to the recording of the compensation current [132]. Giving the differential heat capacity of the sample to:

$$\Delta C_p = C_p - C_p' = \frac{4RI\Delta I}{\beta} \qquad (2.3)$$

When in a first order transition the sample temperature remains constant during transition in spite of the fact that heating power is continued to be supplied, the heat of transition is directly determined from the integral of the heating power over the transition time.[124]

$$\Delta H = \int \Delta C_p \, dT = \int 4RI\Delta I dt \qquad (2.4)$$

Thus, the obtained parameters from DSC analysis are the temperature at the peak maximum T_m, half height width of the transition peak $\Delta T_{1/2}$, and the enthalpy of the process ΔH.

2.6.2 Fourier Transform Attenuated Total Reflection Infrared Spectroscopy

FT-IR spectroscopy is a powerful technique to examine the structure and the interaction of molecules on a submolecular level. The infrared light (λ = 0.8 - 1000 µm), as a part of the electromagnetic spectra, is usually divided into three regions: near-infrared, mid-infrared, and far-infrared. Advantages of this technique are there is no need for additional labels and the noninvasive study of samples. The Fourier Transform method enables the measurement of the absorption spectrum for the whole wavelength region at the same time making the single measurements very fast, and increasing the signal to noise ratio.

Irradiation of a sample with mid-infrared light (λ = 2.5 - 25 µm; $\tilde{\nu} = \lambda^{-1}$ = 4000 - 400 cm^{-1}) excites bending and stretching vibrations of different functional groups in the sample molecules [5]. For lipid samples, the wavenumbers of the absorption peaks of the symmetric and asymmetric methylene stretching vibrational bands are of interest. They give information on the *all-trans*/*gauche* ratio of a methylene chain, reflect the order in the chains, and can be used to determine the phase state of the lipid. Beside the methylene vibration in the hydrophobic region, the carbonyl vibration in the polar/apolar region and the phosphate group in the headgroup region can be used for evaluating the mode of action of the lipids with added molecules [4, 133]. The amide-I band gives information about the secondary structure of the added peptide. Variations in the length and direction of the hydrogen bonds influence their strength for different secondary structures resulting in characteristic amide-I frequencies. The stronger the hydrogen bond involving the C=O group the lower the amide-I adsorption appears [134]. β-turns with only one hydrogen bond show a band maximum at 1670 cm^{-1}, the α-helix containing relative long and weak hydrogen bonds exhibits a band maximum at

1648 - 1660 cm^{-1}, unordered structures give a band at 1640 - 1648 cm^{-1}, antiparallel β-sheets with stronger hydrogen bonds showing an intense peak at 1625 - 1640 cm^{-1} and a less intense one at 1680 cm^{-1}, which arises from transition dipole coupling. Band positions may be shifted to lower frequencies for fully H/D exchange, if D_2O is used as solvent [4].

IR radiation is generated by a Globar. The emitted polychromatic infrared light is first guided through a Michelson Interferometer, composed of a beam splitter, a stationary mirror, and a moving mirror. The reflected light from the two mirrors passes into the sample compartment. On leaving the sample compartment, the light is refocused on to the detector. The difference in optical path length between the two arms to the interferometer is known as the retardation. An interferogram is obtained by varying the retardation and recording the signal from the detector for various values of the retardation. A Fourier transformation of the interferogram gives the single channel spectra.

According to Beer-Lambert's law the absorbance of a sample is directly proportional to the concentration c of the absorbing molecules the path length l of the measuring cell and the molar extinction coefficient ε

$$A = \varepsilon \, c \, l \tag{2.5}$$

The different aspects of ATR spectroscopy are discussed in detail in several reviews [4, 135-139]. In ATR spectroscopy and in internal reflection spectroscopy in general, the IR beam is reflected within an IR transparent internal reflection element. Typically, single crystals of germanium, KRS-5, zinc selenide, diamond, or silicon are used as internal reflection elements. An evanescent wave of the same frequency as the incoming IR light is set up in the optically rarer medium, such as an aqueous solution that is adjacent to the interface. The amplitude of the electric field E falls off exponentially with distance z from the interface.

$$E = E_0 \exp(-z/dp) \tag{2.6}$$

with a characteristic decay length (depth of penetration),

$$dp = \frac{\lambda / n_1}{2\pi \sqrt{\left(\sin^2 \gamma - \left[n_3 / n_1 \right]^2 \right)}} \tag{2.7}$$

where λ denotes the wavelength of the IR light, n_3 and n_1 are the refractive indices of the internal reflection element and water, respectively, and γ is the angle of incidence. Because dp is of the order of only a few hundred nm in many typical applications, internal reflection spectroscopy is a surface-sensitive technique.

2.6.3 Monolayer Technique

Amphiphilic molecules spontaneously adsorb to the air-water interface forming a two-dimensional monolayer [140-142]. The free energy of the system is minimized by reducing interactions between nonpolar groups and water molecules. Lipids, as one type of amphiphiles, arrange at an air-water interface in a way that the headgroup points toward the aqueous subphase and the chains toward the air. The lipid monolayer can be used as a model for one leaflet of a cell membrane [143-145]. Although cell membranes are composed of lipid bilayers, the Langmuir lipid monolayers are two-dimensional surface films that have been extensively used to model biological membranes.

Monolayer techniques have been widely employed as potent tools to study interactions of peptides with lipid monolayers at the molecular level [8]. Two types of monolayer experiments have to be distinguished: the time dependent adsorption of the peptide from the subphase to a preformed lipid monolayer at the air-water interface, and the determination of a surface pressure-area isotherm of a co-spread lipid peptide mixture upon compression of the mixed film.

To determine the adsorption process and the phase behavior during compression, the surface pressure is observed in dependence of time or molecular area, respectively. The surface pressure π itself is defined as difference between the surface tension of the modified water surface γ and the surface tension of pure water γ_0.

$$\pi = \gamma - \gamma_0 \qquad\qquad (2.8)$$

The surface pressure can be measured by the Wilhelmy plate-method. The force F on a plate, which is partially immersed into the subphase, is measured. The plate is often very thin and made of platinum, but even plates made of glass, quartz, mica and filter paper can be used. The forces acting on the plate consist of downward forces due to gravity and surface tension, and an upward force due to buoyancy of the displaced water. For a rectangular plate with the length l_p, the width w_p and the thickness t_p, of material density ρ_p, immersed to a depth h_i in a liquid of density ρ_i, the net downward force is given by the following equation:

$$F = \rho_p \cdot g \cdot l_p \cdot w_p \cdot t_p + 2\gamma \cdot (t_p \cdot w_p)\,(\cos q) - \rho_i \cdot g \cdot t_i \cdot w_i \cdot h_i \qquad (2.9)$$

where q is the contact angle of the liquid on the solid plate and g is the gravitational constant. The surface pressure is then determined by measuring the change in F for a stationary plate between a clean surface and the same surface with a monolayer present. If the plate is completely wetted by the liquid (i.e. $q = 0 \Rightarrow \cos q = 1$) the surface pressure is obtained from the following equation

$$\pi = -\Delta\gamma = -\left(\frac{\Delta F}{2(t_p + w_p)}\right) = -\frac{\Delta F}{2w_p} \text{ if } w_p \gg t_p \qquad (2.10)$$

This force is then converted into surface tension (mN m^{-1}) with the help of the dimensions of the plate.

2.6.3.1 Monolayer Adsorption Experiments

The adsorption process of an interaction partner to a phospholipid monolayer is typically measured by the constant area method [10, 146-150] or the constant surface pressure method [9, 151]. In the constant area method used here, the initial surface pressure π_{ini} of the phospholipid monolayer is adjusted by spreading different amounts of lipids (see Figure 2.6.1). Membrane insertion of injected compound is accompanied by a change in the surface pressure, since the area of the trough surface is kept constant. Upon adsorption, the gain of the Gibbs free energy has enthalpic and entropic contributions. Coulomb-, van der Waals forces, and hydrogen bonds have an effect on the enthalpy of the system, whereas the release of water molecules and counter ions and the rearrangement of the molecule, especially of peptides, change the entropy.

The accumulation of the peptide can be expressed with the surface excess quantity Γ according to Gibbs:

$$\Gamma = \frac{n_s - n_b}{A} \qquad (2.11)$$

where n_s are the moles at the surface, n_b are the moles in the bulk phase and A is the interfacial area. For diluted systems, the adsorption process is diffusion controlled. At a higher surface excess, not all molecules reaching the surface are adsorbed caused by a present energy barrier. To ensure that the adsorption maximum is reached, a concentration dependent adsorption isotherm is measured first. There are three main energy barriers, one associated with diffusion from the bulk, another related to the interfacial pressure, and a third to the interfacial electrical potential. It was found that the rate of adsorption depends on the surface pressure of the lipid and the sequence of the peptide. The molecule must do work against the surface pressure in order to create a hole of area A for itself to move into. This amount of work is equal to

$$\Delta G = \int \pi dA \qquad (2.12)$$

The required energy to adsorb to the interface is smaller for small molecules as they tend to adsorb to a greater extent [152].
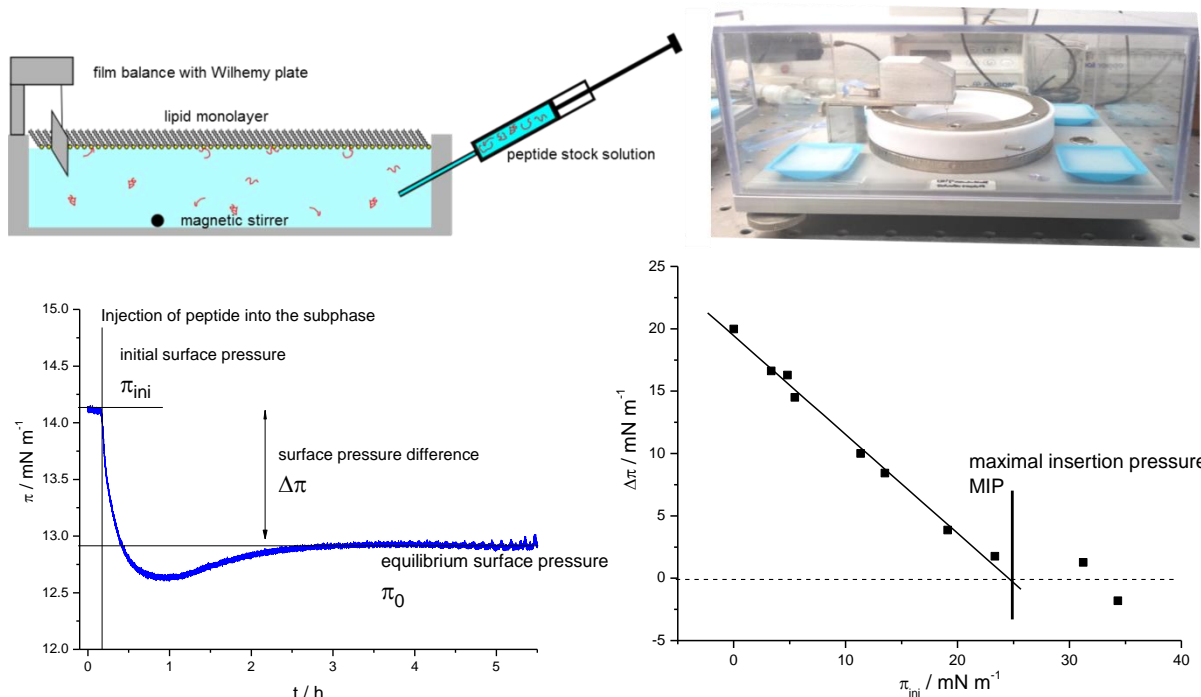
Figure 2.6.1: Top: schematic drawing (left) and picture (right) of the experimental setup to perform adsorption experiments of a peptide solution to a lipid monolayer. The fixed through area is covered with a lipid monolayer, the surface pressure is recorded with a Wilhelmy plate, and the peptide stock solution is injected into the aqueous subphase through a channel in the trough. Bottom left: time dependent development of the surface pressure π of a lipid monolayer after injection of a ligand or peptide solution into the subphase at a starting surface pressure π_{ini}. Bottom right: Difference of surface pressure $\Delta\pi$ after peptide adsorption to a lipid monolayer with different initial surface pressure.

Adsorption experiments of peptides to a lipid monolayer at different initial surface pressures were performed to study the effect of the peptide on physical state of the monolayer and the lipid density at the air-water interface. The kinetics of protein binding onto phospholipid monolayers were monitored until the equilibrium surface pressure π_0 was reached. The kinetic curves show an overlay of two effects, the decrease of π upon lipid condensation and the increase of π upon peptide incorporation into the monolayer. To analyze the kinetics of adsorption quantitatively the experimental adsorption curves were fitted using the following bi-exponential equation:

$$\pi = A_1 e^{-t/t_1} + A_2 e^{-t/t_2} + \pi_0 \tag{2.13}$$

The parameters A_1 and t_1 provide information on the amplitude and rate constant for the peptide incorporation and A_2 and t_2 for the condensation effect, the value π_0 being the final surface pressure at equilibrium after 5 hours. The amplitude of both effects corresponds to the properties of the peptides describing the relative strength of the electrostatic and hydrophobic interaction with the lipid monolayer.

The change in surface pressure $\Delta\pi = \pi_0 - \pi_{ini}$ observed after adsorption of a protein or peptide to a lipid monolayer as a function of the initial surface pressure π_{ini} shows in many cases a linear relationship, from which the maximum insertion pressure MIP is determined, i.e. the value of π_{ini}, where $\Delta\pi = 0$ mN m^{-1}. Per definition MIP is the value above which no incorporation into the lipid bilayer occurs anymore [8, 147-149]. However, for the binding of cationic pentapeptides to DPPG monolayers that this relation was already observed before and the interpretation cannot be used for the electrostatic binding of peptides, as negative surface pressure changes and changes in slope were observed [123].

2.6.3.2 Surface Pressure - Area Isotherms

Monolayer studies with phospholipids and peptides co-spread at an air-water interface can be performed in a well-defined way. The two-dimensional molecular density and composition can be varied, as well as the temperature and the ionic strength conditions of the subphase. Using surface pressure-area (π - A) isotherms [141], one can observe that decreasing the surface area at the interface of the lipid or peptide molecule induces a series of two-dimensional phase transitions due to changes in the molecular packing. The compression rate must be slow enough to ensure that changes occur under thermodynamic equilibrium conditions [8]. Other useful characteristics of monolayers are a planar arrangement over macroscopic dimensions and at least one symmetry axis, the plane normal. This technique is well-known [143] to study the two-dimensional alignment of the molecules with additional techniques, e.g. fluorescence microscopy, infrared reflection absorption spectroscopy (IRRAS), Brewster angle microscopy and X-ray reflectivity and diffraction.

2.6.4 Fluorescence Microscopy of Monolayers

Polychromatic light in the visible range of the electromagnetic spectrum is generated by a mercury-vapor lamp. With the help of an excitation filter, one wavelength is selected, which matches the fluorophore in the sample. The light is then directed onto the sample, where the fluorescence process occurs. Upon radiation, electrons are excited to a higher energy level. When relaxing to a lower level, they emit light of lower energy and longer wavelength. A dichroitic mirror separates the emitted fluorescence light from the reflected light, as it is transparent for the emission wavelength and nontransparent for the excitation wavelength (see Figure 2.6.2). The fluorescing areas appear bright against a dark background with high contrast.
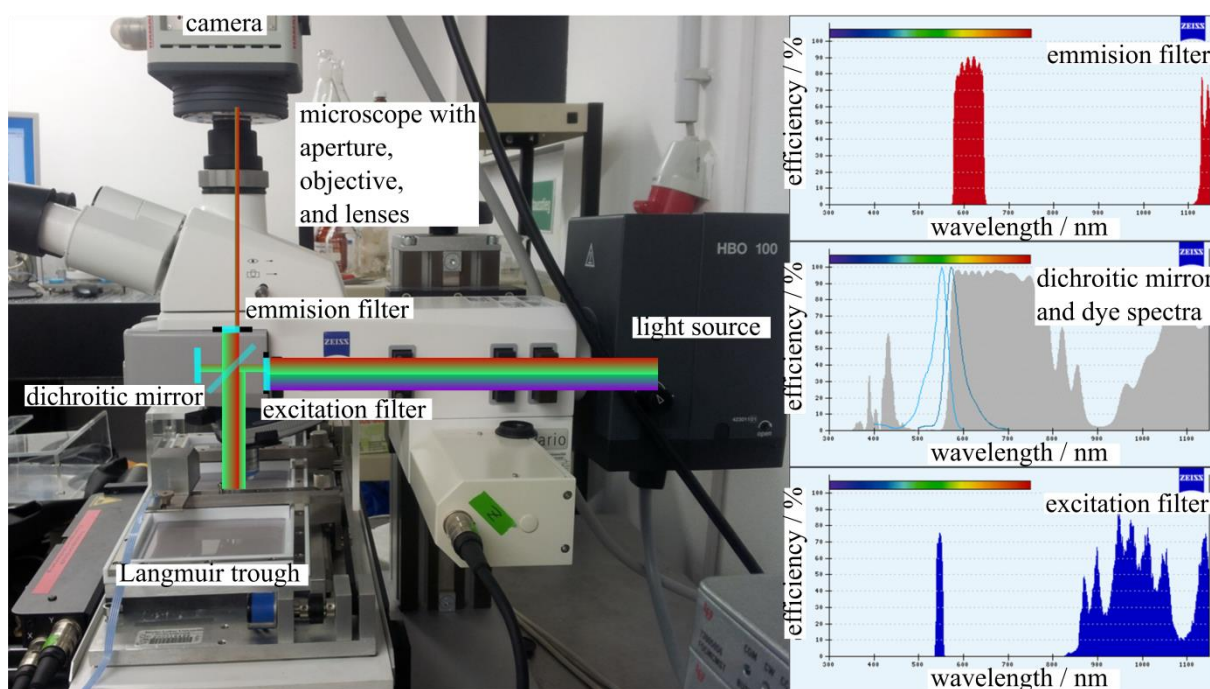
Figure 2.6.2: Left: Fluorescence microscope with a Langmuir film balance underneath. The important parts are labelled and the path of light is inserted. The fluorescence event of the lipid dye takes place at the air-water interface. Right: Transmission efficiencies of light for the excitation filter, dichroic mirror, and emission filter with respect to the wavelength. In the middle panel the excitation and emission spectra of Rh-DHPE is inserted [153].

Fluorescence microscopy of monolayers at the air-water interface as an imaging technique is well suitable to observe directly changes in film morphologies [154-157]. Monolayers were mixed with 0.01 mol% Rh-DHPE to visualize microstructures (domains) during the compression of the film. The added fluorescently labeled lipid has a different solubility in the different phases giving contrast of light and dark in the micrograph. Regions with a high concentration of the dye appear bright and those with no label dark. As experimentally shown and in accordance with literature reports [158], this fluorescence dye used in this work prefers the liquid-expanded (*LE*) phase and is largely excluded from ordered phases (i.e. liquid-condensed phase, *LC*). The added fluorescently labeled lipid acts as an impurity in the observed monolayer, so there might be an additional interaction between the dye and the molecules at the air-water interface, which could alter the shape of the $\pi - A$ isotherm and domains, respectively.

2.6.5 Infrared Reflection Absorption Spectroscopy

The combination of a Langmuir trough with an Infrared Spectrometer opens the possibility to perform Infrared Reflection Absorption Spectroscopy (IRRAS) at the air-water interface. This technique provides detailed information on the molecular conformation, orientation, and thickness of the film at the air-water interface. Although, IRRA spectroscopy has been first

applied to the study of lipid monolayers alone [139, 159, 160], it is well suited to study the interaction of lipid monolayers with other molecules like peptides, proteins or polymers [11, 14, 68, 71, 151, 161-169].

IRRAS experiments can be performed in different ways. Two major techniques have evolved. The one used here is the so-called shuttle technique, where the Langmuir trough has two compartments and is shuttled to two different positions to get single beam reflectivity spectra of the bare water surface and of the water surface covered by a lipid monolayer (see Figure 2.6.3). These two spectra are ratioed to calculate Reflectance Absorbance spectra and to remove water vapor bands [170, 171]. The reflectance absorbance spectra (RA) were calculated from the single-beam reflectance spectra recorded on the reference (I_0) and sample trough (I) according to

$$RA = -\log(I/I_0) \tag{2.14}$$

The second technique widely applied is the polarization-modulation (PM) technique, PM-IRRA spectroscopy. Here, the polarization of the IR-beam is modulated by a photoelastic modulator (PEM) with high frequency [172-174].
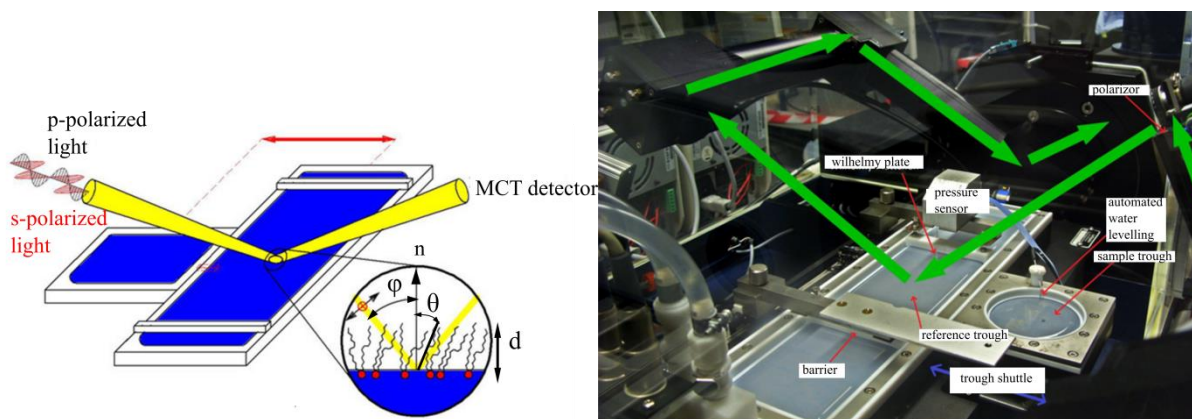
Figure 2.6.3: Schematic drawing (left) and picture (right) of the experimental setup for Infrared Reflection Absorption Spectroscopy of lipid monolayers at the air-water interface [175, 176]. From the angle of incident, φ, dependent measurement with p- and s- polarized IR light the tilt angle of the lipid acyl chains, θ, and the monolayer thickness, d, can be determined. In the right picture, the important parts are labelled and the path of the IR light is inserted.

3   Interaction of Model Peptides with Lipid Bilayers

3.1   Introduction

To understand the complex behaviour of antimicrobial peptides interacting with bacteria, simplified models consisting of short cationic peptides and bilayer membranes with distinct lipid composition are preferentially studied first.

The effect of positively charged amino acids on the electrostatically driven binding of cationic model peptides to lipid bilayers was extensively tested before with homopeptides of lysine or arginine with different degree of polymerisation [97, 104, 105]. The binding affinity of lysine is not only due to the electrostatic attractions [88, 103, 115-120], but has also contributions from the hydrophobic CH_2 groups in the side chain [123].

Introducing other amino acids than lysine and arginine opens the opportunity to tune the charge distance in the peptide and to incorporate hydrophobic residues.

In the following chapter, the thermotropic behavior of lipid-peptide mixtures is presented. The use of the DPPG, which has a transition temperature of 41 °C, in a series of DSC experiments opens the possibility to study the influence of the peptide on the membranes phase behavior with respect to the lipid-to-peptide charge ratio and peptide sequence. On the other hand, the use of the peptides $(KA)_4K$ and $(KAbu)_4K$, which both tend to form β-sheets bound to DPPG, are capable to study the influence of the lipid structure on the membranes phase behavior and secondary structure of the peptide. The combination of DSC studies and temperature dependent ATR-IR measurements show that both components influence each other. The systematic variation of binding parameters yields information about thermodynamics of binding as well as the phase behavior and the structure of the formed complexes. This allows drawing a comprehensive picture of the lipid-peptide interaction. The peptide sequence determines the shift of the main phase transition of the lipid and the lipid headgroup size determines the stability of the formed β-sheet.

3.2   Thermotropic Behavior of Lipid-Peptide Mixtures

3.2.1   Charge Ratio as Unique Parameter

To investigate the impact of increasing peptide content on the thermotropic phase behavior of DPPG mixtures, samples with constant lipid content, but with different peptide concentrations were prepared. To quantify the effect of the added peptide, the charge ratio (R_c) as a unique parameter was used. The charge ratio is the ratio between the concentration of the negatively charged lipid headgroups, i.e. phosphatidylglycerol and the concentration of the positively charged lysine or arginine residues within the used peptides (see equation (3.1)).

$$R_C = \frac{[\text{negatively charged lipid}]}{[\text{positively charged amino acid residue}]}$$

(3.1)

As already stated, all peptides contain five positive charges and thus the concentration of lysines or arginines is five times higher than the peptide concentration. The investigated charge ratios were adjusted to 10:1 over 5:1 and 2:1 up to 1:1 by increasing the amount of added peptide. At a charge ratio DPPG to K of 10:1, a high excess of lipid is present in the mixtures. The negative charge of the phosphatidylglycerol headgroup is completely compensated by the positively charged lysine side chains of the added peptide at a charge ratio of 1:1.

3.2.2   Differential Scanning Calorimetry

Differential Scanning Calorimetry (DSC) is a well-established method for the study of the thermotropic phase behavior of pure phospholipid bilayers and of bilayers in interaction with peptides. A thermal induced phase transition appears as a peak in the recorded thermogram. The enthalpy of the phase transition is associated with the area of this peak and can be obtained from the integral of the curve over the temperature. The observed main phase transition in lipid bilayer systems is connected with the melting of the acyl chains. From DSC experiments and the combination with other temperature dependent techniques, information about the phospholipid conformation, bilayer fluidity and ligand-vesicle interaction can be derived.

3.2.3   Fourier Transform Attenuated Total Reflection Infrared Spectroscopy

IR spectroscopy is a potent method to gain information about the phase state of lipids and induced changes upon peptide addition. Furthermore, the secondary structures of the peptide and possible changes of peptide conformation after binding are detectable.

Important vibrations of lipid molecules are the methylene stretching $v(CH_2)$ and the carbonyl stretching vibrations $v(C=O)$. To determine the acyl chain order in the bilayer and the lipid

phase state, the $v(CH_2)$ is frequently used. Information about the environment of the polar/apolar interfacial region and particularly its hydration can obtained by the band position of $v(C=O)$. The amide-I band of the peptides finally provides information about the secondary structure of the peptide.

3.2.4 Thermotropic Phase Behavior of Pure Lipid Bilayers

The lamellar structures of lipid dispersions exhibit different phase states (see Figure 2.2.1), depending of the temperature (thermotropic mesomorphism). By increasing the temperature first order transitions between these individual phases can be triggered, changing the lateral arrangement of the whole lipid, the order of the hydrocarbon chains, and the hydration of the headgroup. The transition temperatures depend sensitively on the headgroup and the acyl chain length.

As most of the experiments were performed with DPPG as model compound, its thermotropic behavior is presented as an example for all other lipid suspensions. A graphical representation of the different lipid bilayer phases is given in Figure 3.2.1.

At low temperatures shortly after dispersion of DPPG in the aqueous solution, the gel phase is present. Although the dynamics of all motional modes are reduced in the gel phase, the acyl chains show some rotational freedom along their long axis, but they are still organized in a regular hexagonal lattice and the molecule occupies an area of ca. 40 $Å^2$. In the gel phase $L_{\beta'}$ the hydrocarbon chains of DPPG are in an *all-trans* conformation and tilted with respect to the bilayer normal (see Table 2.2.1).

Other lipids form gel phases with different hydrocarbon chain packing and tilt angles or even untilted acyl chains (L_β), depending on the headgroup structure, the length, and degree of unsaturation of the chains, and the mismatch between the two chains in the *sn*-1 and *sn*-2 position.

The fully hydrated bilayers in a pure DPPG suspension in 100 mM NaCl solution show a pre-transition from the lamellar gel phase ($L_{\beta'}$) to the rippled gel phase ($P_{\beta'}$) at $T_{pre} = 33.5$ °C. This phase transition mostly appears just upon heating and is missing during cooling. The flat bilayer system builds up a superlattice of undulated lamellae, but the lipids itself remain in their predominantly *all-trans* conformation. The reproducibility of the pre-transition, especially in unilamellar systems, is low [177, 178], and appears only in pure PG systems.

For lipids where no ripple phase exists, the gel phase is stable until the main phase temperature is T_m is reached [179]. Interaction of lipid bilayer with different components, like antimicrobial peptides [180], surfactants [181, 182], or cholesterol [126], which prevent a

tilting of the lipid acyl chains, abolishes the pre-transition due to a deeper incorporation of these molecules into the lipid bilayer [130].

The DPPG main phase transition from rippled gel phase to liquid-crystalline phase (L_α) occurs at T_m = 40.3 °C with a high cooperativity. A narrow peak width of $T_{1/2}$ = 1.5 °C and an enthalpy of ΔH = 10.4 kcal mol^{-1} is observed [183, 184].
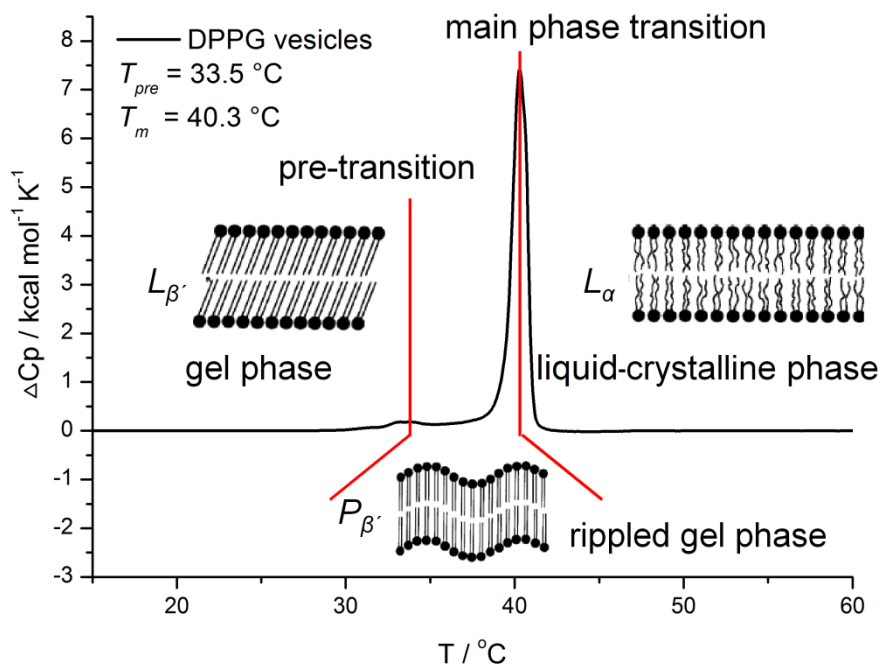
Figure 3.2.1: Schematic representation of the heat capacity profile (ΔC_p) of DPPG bilayers upon heating. The pre-transition at T_{pre} is associated with the transition from the gel phase ($L_{\beta'}$) to ripple phase ($P_{\beta'}$) and the main transition at T_m from the ripple phase ($P_{\beta'}$) to the to the liquid-crystalline phase (L_α). Bilayer phase structure taken from [5].

The asymmetric and the symmetric methylene stretching vibrations ($\nu_{as}(CH_2)$, $\nu_s(CH_2)$) reflect the ordering of the acyl chains in the hydrophobic region of the bilayer. With this first order phase transition the conformation of the acyl chains switch from *all-trans* into a *gauche* conformation [4]. The differences of transition temperature for pure lipid systems and for lipid-peptide mixtures determined by the analysis of the $\nu_{as}(CH_2)$ or $\nu_s(CH_2)$ vibrational band are negligible, and thus only the data from the symmetric vibration are discussed. The symmetric vibration is located at ca. 2850 cm^{-1} and has the advantage of a narrower band width and being undisturbed by the Fermi resonance band of the bending vibration $\delta(CH_2)$ at 2930 cm^{-1} [185].

Upon phase transition every single molecule gains more flexibility, the bilayer becomes more fluid, the van der Waals interactions are reduced, and there are no restrictions for reorientational motions. This high temperature lamellar phase consists of a stack of bilayers separated by aqueous films, where the headgroups are more hydrated than in the gel phase.

Characteristic vibrational bands of the lipid headgroup region are the carbonyl stretching vibration (v(C=O)) and the phosphodiester band. The wavenumbers of these bands are influenced by hydrogen bonding to water or to other hydrogen bond donor groups. For stronger bonds and/or more hydrogen bond donors, the vibrational frequency of the lipid ester C=O group will be shifted to lower wavenumber [186]. Therefore the C=O stretching band is a good indicator for the hydration of a membrane in the headgroup region. Actually, the observed band profile is a superposition of two underlying bands located at 1740 cm^{-1} and 1725 cm^{-1}, originating from non-hydrated and hydrated C=O groups. As the absolute intensity is influenced by sedimentation of lipid-peptide aggregates onto the ATR crystal during the timescale of the experiment, relative band intensities were determined by fitting with two peaks with a Gaussian profile. The band ratio between non-hydrated and hydrated carbonyl groups in the mixture was determined by calculation of the intensity ratio.

$$\frac{A_{1725cm^{-1}}}{A_{1740cm^{-1}} + A_{1725cm^{-1}}} \tag{3.2}$$

The whole lipid occupies an area of 60 - 70 Å^2. Most biomembranes adopt the liquid-crystalline phase, thus its properties are of particular importance for understanding biological membrane functions [187, 188].

PGs, and most of the other negatively charged lipids, show a dependency of their main phase transition on the salt concentration. DPPG suspended in pure water undergoes the main transition at 41.6 °C. Upon addition of low amounts of sodium chloride, the temperature is lowered and reaches a minimum of 39.8 °C at a concentration of 50 mM NaCl. Further increase of the NaCl concentration again increases the phase transition temperature [189].

The acyl chain length and the degree of unsaturation of phospholipids, as well as the headgroup structure, have an influence on the phase behavior. An increase of the acyl chain length also increases the van der Waals forces in the hydrocarbon core of the bilayer and thus the main phase transition is shifted to higher temperatures. A reversed shift of the transition temperature is achieved by introducing an unsaturation in one of the acyl chains. For the tested lipids with a fixed acyl chain length of 14 C-atom, the attached headgroup moiety and their ability to form hydrogen bonds influences the phase transition of the lipid as well. DMPG bilayers show a main phase transition at 23 °C, DMPC at 24 °C, DMPS at 37 °C, TMCL at 40 °C, and DMPA at 50 °C, respectively [2]. The charge repulsion between the negatively charged headgroups in the PG bilayers would lead to a decreased phase transition compared to zwitterionic PC headgroups, but this effect is counterbalanced by the ability of

the glycerol to build up hydrogen bonds to the phosphate group of neighboring lipids. PG and PC bilayers, having the same chain length, show similar phase transition temperatures.

3.2.5 Pure Peptide Solutions

In the thermograms of a pure peptide solution, no peaks are visible. As expected, the highly water-soluble peptides show no secondary structure transitions. In addition, no aggregation due to dehydration at elevated temperature is detectable.

The amide-I band gives information about the secondary structure of the added peptide. The most likely structure for these short peptides is unordered structure with possible additional β-turns. The short peptide sequence hinders any effective stabilization originating from larger secondary structure elements like α-helices or β-sheets. The pure peptide solutions show spectral features of unordered structures and β-turns. A typical spectrum of the amide region is given in Figure 3.2.2. Former studies of oligomers and polymers of $(KL)_nK$ prove the existence of random coil structures at low peptide concentration. However, increasing the peptide concentration or adding salts triggers the formation of antiparallel β-sheets [190]. A concentration, time and solvent dependent CD and Raman spectroscopy study also showed that the β-sheet is the most stable conformation for $(KL)_nK$ peptides [191, 192].
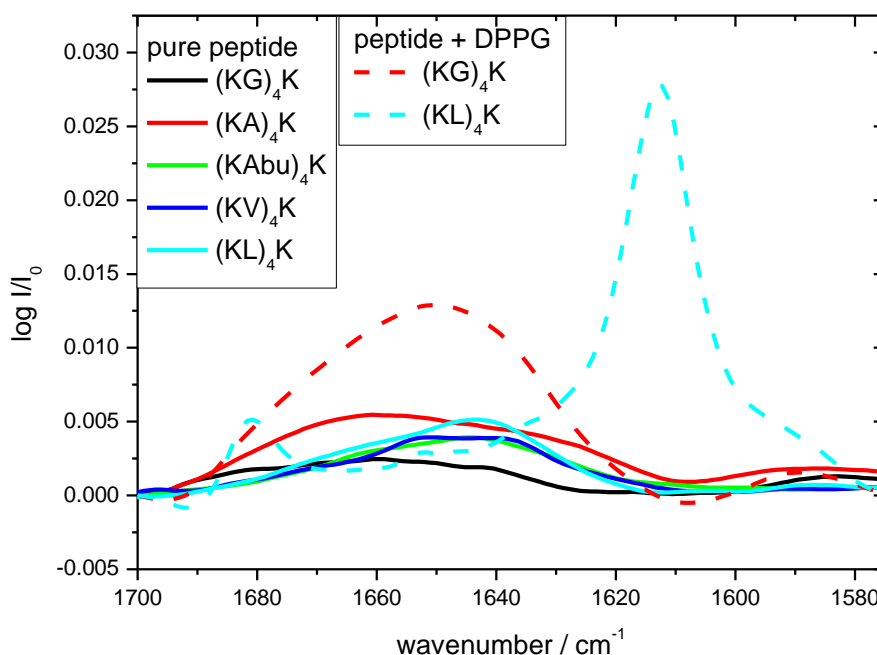

Figure 3.2.2: Amide-I region of pure peptides $(KX)_4K$ in solutions (5 mM peptide solved in D_2O containing 100 mM NaCl at $pD = 7.2$ and $T = 10\ °C$) and lipid-$(KX)_4K$ mixtures of a charge ratio of 1:1 (1 mM peptide mixed with 5 mM lipid in D_2O containing 100 mM NaCl at $pD = 7.2$ and $T = 10\ °C$).

3.2.6 General Behavior of Vesicle Samples after Peptide Binding

The first heating scan after mixing the lipid suspension with the peptide solution at room temperature was always slightly different compared to the following ones. Therefore, the presented curves for lipid-peptide mixtures, investigated by DSC and temperature dependent ATR-IR, are from the second heating scan. The reason for the difference between the first and the following other scans is due to incomplete equilibration after mixing at room temperature. Reasons might be that the added peptide first binds preferentially on the outside of the vesicle. Upon passing the phase transition after heating, the peptides are able to cross the membrane and reach the inside of the vesicles. For samples with a low charge ratio, it also remains unclear whether the vesicles are still intact after peptide addition.
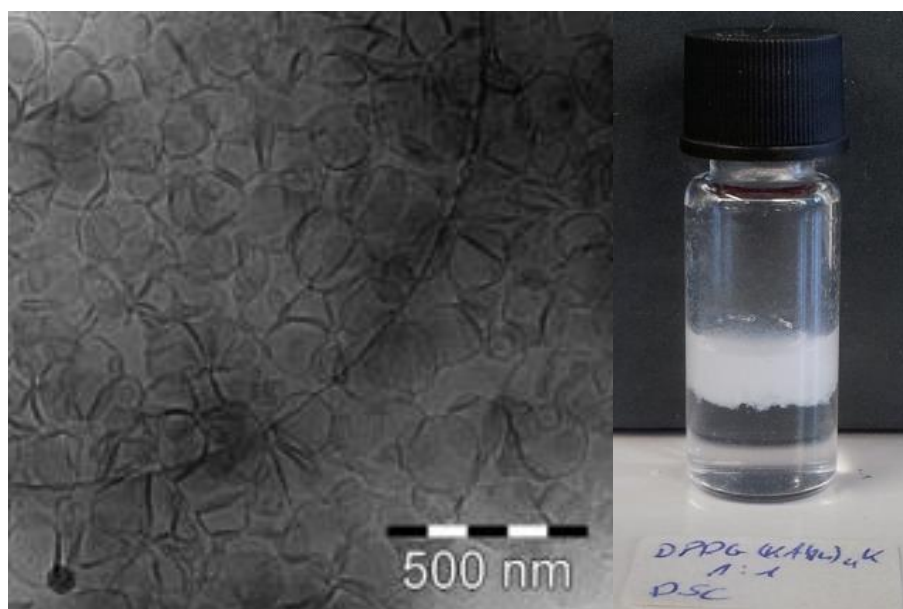
Figure 3.2.3: Mixtures of DPPG vesicles with (KAbu)$_4$K showing aggregation. Left: cryoTEM micrograph of a charge ratio of 10:1. Right: photo with a higher charge ratio of 1:1. For both samples, lipid vesicle suspensions were prepared by extrusion through a 100 nm polycarbonate membrane. The mixture was fresh prepared from pure lipid and peptide solution and allowed to mix for 30 s prior plunging into liquid ethane for the cryoTEM sample or vortexed after mixing for the DSC sample, respectively. The final lipid concentration in both samples was adjusted to 2 mM in 100 mM NaCl.

With decreasing charge ratio, i.e. higher peptide content, the samples became increasingly turbid and the lipid suspension immediately aggregated upon mixing. For a charge ratio of 1:1 the sample separated into a clear bulk solution and flaky white lipid-peptide aggregates. Although the aggregates are on top of the bulk solution in the picture, they settle down with time or upon centrifugation. The inclusion of small air bubbles during the vortexing process might be a reason for the floating of the aggregates. This aggregation was independent of the peptide sequence, thus it must be driven by charge compensation. A sample image obtained by cryoTEM and an optical image of a sample vial are shown in Figure 3.2.3. It remains

unclear to which structure the lipids are assembled, because the aggregates are too bulky to be investigated by cryoTEM.

Similar effects have been observed before after binding of poly(L-lysines), polyamines, or cyclic antimicrobial peptides to negatively charged PG vesicles [104, 193, 194]. In these cases charge compensation is the leading cause.

To compare the results of the ATR-FT IR experiments with the previous DSC measurements, a similar sample preparation method was used. The lipid suspension and the peptide solution were directly mixed on the crystal of the BioATR II cell, followed by a heating cycle to 70°C with subsequent cooling to ensure equilibration of the sample. Data of the temperature dependent ATR-FT IR spectra of a charge ratio of 1:1 originate from the second upscan.

The transition temperature determined for pure DPPG is observed at slightly higher temperature, namely 42 °C in the ATR-FT IR experiment. This upshift may be due to experimental reasons as spectra were taken in an interval of 2 degree centigrade and an equilibrium time of at least 10 min. In contrast, a DSC curve is recorded with a heating rate of 1 K min^{-1} and a higher temperature resolution. In addition, the temperature is not measured directly in the sample solution, but outside in a drill hole on top of the sample chamber.

Although, the concentration of the pure peptides is higher than in the lipid-peptide mixtures, the obtained signals are very broad and of low intensity. A clear assignment of the peptide structure in solution is hardly possible, because the signal ranging over the whole amide-I region showing only hints for unordered structures. For lipid-peptide mixtures, the advantage of the precipitation of the aggregates is visible, leading to a higher signal.

3.3   Interaction of DPPG with Cationic Model Peptides - Influence of Peptide Sequence

To study the influence of the peptide sequence on the thermotropic behavior of DPPG vesicles after binding, the lipid was mixed with different peptide solutions. The peptide sequence was altered to reveal the following effects: i) increase in hydrophobicity of the uncharged spacer amino acid X in the sequence (KX)$_4$K, ii) reduction of the charge density in the peptide by introducing a second uncharged amino acid in the sequence (KXX)$_4$K, iii) exchange of the charged amino acid from lysine by arginine with a concomitant delocalization of the charge in the sequence (RX)$_4$R.

3.3.1   Influence of Increased Hydrophobicity of the Uncharged Spacer Amino Acid X in the Peptides (KX)$_4$K

DPPG-(KG)$_4$K mixtures with low peptide content

The effect of (KG)$_4$K addition on the phase transition of DPPG vesicles is presented in Figure 3.3. At high charge ratios of 10:1 or 5:1 the pre-transition has disappeared and the main phase transition temperature of DPPG is slightly increased. The transition enthalpy in the mixtures is lowered upon peptide addition. All obtained parameter from DPPG-(KG)$_4$K samples with different charge ratios are summarized in Table 3.3.1.

The occurrence of the pre-transition is very sensible to interactions of the added peptide with the headgroup region. (KG)$_4$K disturbs the regular arrangement of the headgroups or even penetrates into the headgroup region preventing the formation of the rippled gel phase. An incorporation of the peptide into the acyl chain region is possible, but unlikely, as it would destabilize the ordered arrangement in the gel phase leading to a reduced phase transition temperature [180, 195]. It is reported that the pre-transition is coupled with a partial melting of the acyl chains [177] increasing the molecular flexibility and the demanded space in the hydrophobic region. The peptide with its five positively charged side chains is capable to bridge several lipid molecules. Thus, the diffusion in the plane of the bilayer is hindered. The defined arrangement of the lipid-peptide aggregates leads to a prevention of this partial chain melting due to sterical constraints.

An increase in T_m implies that the peptide interacts more favorably with the ordered gel phase of the lipid than with the fluid phase. The origin of this stabilizing effect could be the release of counter ions upon peptide binding and the reduction of lipid headgroup hydration. The explicit arrangement of the peptide bound to the bilayer remains unclear from DSC measurements.
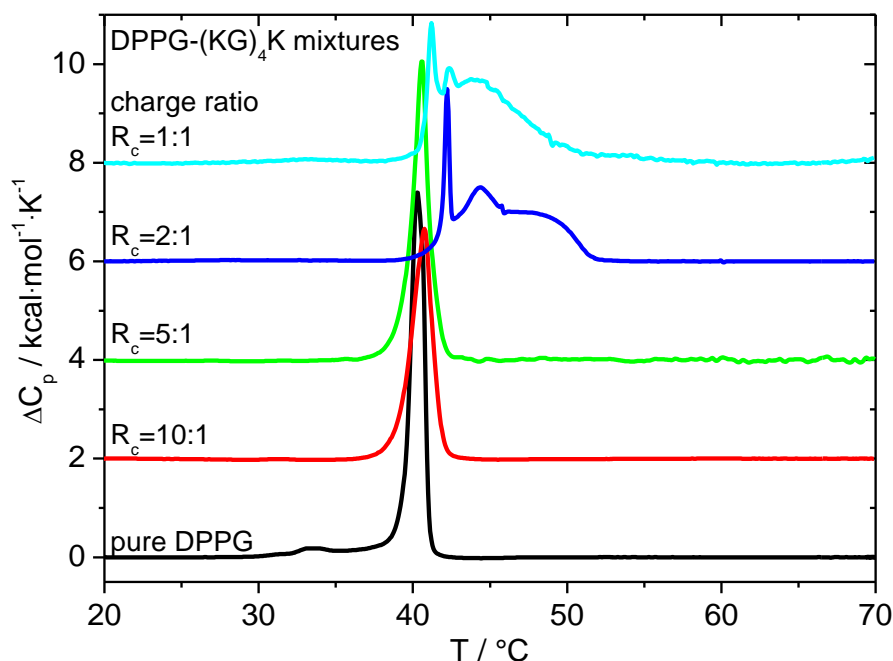
Figure 3.3.1: Thermogram of pure DPPG vesicles and different DPPG-(KG)$_4$K mixtures with increasing charge ratio. The 2nd heating scan is shown, because equilibrium was only reached after passing the phase transition. Samples were prepared in aqueous 100 mM NaCl with a fixed lipid concentration of 2 mM.

The transition enthalpy of charged lipids has contribution from van der Waals interactions of the hydrocarbon chain, possible hydrogen bonds at the headgroup and the electrostatic contributions. The observed reduction of the transition enthalpy is an effect of the electrostatic binding of the peptide to the lipid bilayer. Addition of peptide may hinder the formation of intermolecular hydrogen bonds between lipids in the headgroup region, and instead electrostatic attractions between the lipid headgroup and the lysine side chain are built up.

DPPG-(KG)$_4$K mixtures with high peptide content

With higher peptide content, i.e. a charge ratio of 2:1 the transition peak becomes much broader, although a sharp peak at 42.2 °C is still visible. The overall enthalpy of the whole process is similar to pure lipid systems. A charge ratio of 2:1 hypothetically may create intact vesicles with a complete peptide layer on the outside of the vesicle shortly after mixing and binding. Such an arrangement is energetically and entropically unfavorable, as there are two completely different layers connected with each other, a negatively charged inner layer, and a nearly neutral outer layer with bound peptide.

It was shown that large lysine containing peptides can cross the lipid bilayer [196]. With time or by heating over the phase transition, the vesicles become leaky and a uniform distribution of the peptide is reached. Also peptide binding by itself can induce vesicle leakage as

proposed in several reviews [92, 93] with different modes of action depending on the peptide. It is suggested that at high charge ratios, a planar bilayer structure is favored and the vesicles are disrupted upon peptide binding. Otherwise, the strong aggregation of the system is not explainable.

Mixtures of negatively charged DPPG and positively charged lysine residues with a charge ratio of 1:1 also show a broad phase transition region with several peaks, possibly due to domain formation. The transition enthalpy is 2.8 kcal mol^{-1} higher than the one of pure DPPG and exceeds the observed enthalpy of all other mixtures discussed before. The enthalpy is drastically reduced upon addition of low amounts of peptide, but increases again by adding more peptide. The chain melting and the headgroup dehydration are main contributions to the transition enthalpy beside other possible processes.

Table 3.3.1: Overview of the thermodynamic data obtained from DPPG-(KG)$_4$K mixtures with different charge ratios. T_m is the main phase transition and marked by the peak with the highest heat capacity and $T_{1/2}$ the full width of this peak at half maximum. Especially for the asymmetric peaks with several shoulders T_{mid} obtained from the midpoint of the integral of the curves, is more suitable for a comparison. ΔT_{base} is the width of the peak at its base and ΔH is the transition enthalpy.

charge ratio	T_m / °C	T_{mid} / °C	$T_{1/2}$ / °C	ΔT_{base} / K	ΔH / kcal mol^{-1}
pure DPPG	40.3	40.2	1.5	3.5	10.4
10:1	40.8	40.7	1.5	3.9	7.7
5:1	40.6	40.5	1.1	3.8	8.7
2:1	42.2	45.1	0.4	10.4	10.6
1:1	41.3	44.2	5.6	10.7	13.2

As reported by Zhang et al. [184], the building of quasi-crystalline layer with less hydrated lipids, which are restricted in rotation, leads to a higher transition temperature as well as a higher transition enthalpy compared to the well-known main phase transition of DPPG. A hint for the occurrence of uncharged and dehydrated bilayer is the highly turbid or even segregated lipid suspension. To prove this notion spectroscopic experiments were performed.

The electrostatic binding of the peptide to the lipid coupled with the stabilization due to hydrogen bonding between the lipid phosphate group and the amine group of the lysine side chain is suggested to be the reason for thermal stabilization of the lipid-peptide aggregate. As shown for pure lipid systems, additional hydrogen bonds in the headgroup region shift the transition temperature e.g. from 42 °C of DPPC, 48 °C of N-MeDPPE, 58 °C of N,NMe$_2$DPPE to 64 °C of DPPE [197].

The appearance of several peaks in thermograms of mixtures DPPG with polylysine of different chain length (5 up to ~1000) was also observed in previous studies and explained as domain formation within the bilayer upon peptide binding [107, 108, 198, 199]. Lipid-rich bilayer patches show a phase transition in close proximity to pure DPPG, whereas domains with higher peptide content show a transition at higher temperature with a lowered cooperativity.

Molecular crowding at the surface of the vesicle occurs during the binding of peptides with several charges. This leads to a partial or complete exclusion of molecules, if the available free space is not sufficient anymore. This occurs particularly at high charge ratios. The occurrence of a mixture of partially bound peptides, and a concomitant possible separation into different domains explains DSC curves with several peaks at different transition temperatures. This problem has been known for a long time, and has been addressed in several articles by Stankowski for different shapes of bound molecules, including also cooperative binding [200-202]. Unfortunately, the electrostatic binding observed here with the peptides cannot be described, using the models by Stankowski due to a superposition of electrostatic effects and possible contributions from hydrophobic effects to the binding. Furthermore, the explanation with molecular crowding may hold for mixtures with low peptide content, where vesicles remain intact, but does not explain the resharpening of the transition peaks for mixtures with a charge ratio of 1:1 of more hydrophobic peptides and lipid discussed in the next sections.

It is difficult to compare these results with findings from previous studies as the peptide sequence, as well as the structure of the used peptide, plays an important role for the interaction with membranes. The simplest peptide sequence, which is related to $(KG)_4K$, is pentalysine and the longer chain homologues, polylysine. Pentalysine and its interaction with PG membranes was studied very intensely in the past [88, 103, 115, 120, 122, 203], but the peptide lacks the ability to build up any stable secondary structures due to its short chain length. Longer polylysine chains might be able to form stable structures, e.g. α-helixes or β-sheets. Polylysines cannot be compared with $(KG)_4K$ due to an increase in charge and smaller charge distance.

The results obtained from the mixtures of DPPG and $(KG)_4K$ are consistent with previous results of a mixture of DPPG with lys_5 and other pentapeptides containing shorter α,ω-diaminoacids as building blocks. For these peptides an upshift of the phase transition as well as the increase of transition enthalpy [123, 204] at a charge ratio of 1:1 was seen. The charge

ratio itself affects the thermotropic behavior of these mixtures as discussed above. In the study of Papahadjopoulos et al. [198], peptides like polylysine were thought to bind mainly electrostatically and form a surface layer on top of the lipid bilayer, but without any penetration or interaction with the hydrocarbon region. Based on the results it is suggested that the interaction of DPPG and (KG)$_4$K is also mainly driven by electrostatics.

The repulsive coulomb interaction between the former negatively charged lipids is reduced upon peptide binding and charge screening. Simultaneously, the effective area of the headgroup is decreased and thus the packing of the lipids is increased.

DPPG-(KA)$_4$K mixtures

The thermotropic behavior of DPPG mixed with (KA)$_4$K is depicted Figure 3.3.2, left panel. In the peptide (KA)$_4$K, glycine was exchanged by the bulkier and more hydrophobic amino acid alanine to test the influence of the uncharged spacer X. The thermograms of DPPG with (KA)$_4$K and (KG)$_4$K and a charge ratio of 10:1 are similar. A transition peak at slightly elevated temperature is visible. The results obtained with higher peptide content are different compared to mixtures with (KG)$_4$K. At a charge ratio of 5:1, a second peak at 44.3 °C with a low transition enthalpy appears, and the main transition peak is slightly downshifted compared to pure DPPG. The appearance of two separated peaks indicates possibly the formation of domains enriched with bound peptide or different adsorption stoichiometries.

With decreasing charge ratio (R_c = 2:1) a very broad peak with several maxima appears, perhaps as a result of molecular crowding of the peptide at the lipid bilayer surface. The mixture DPPG-(KA)$_4$K with a charge ratio of 1:1 shows a completely different behavior, compared to all mixtures discussed before. The stability of the gel phase of the DPPG bilayer is drastically increased and the transition temperature is shifted to 60.2 °C. Only one transition peak is seen. Complete charge compensation seems to induce the formation of uniform and stable lipid-peptide aggregates without any domain formation. The transition enthalpy is drastically reduced. Data from IR measurements confirm that during the phase transition also a structural transition of the peptide occurs (see below). The bound peptide covers the gel phase bilayer in an antiparallel β-sheet arrangement and converts into an unordered or even unbound state after the lipid phase transition.

ITC measurements with lipid vesicles reveal that the phase state of the lipid plays an important role for the binding (data not shown). The strong exothermic binding of the peptide to gel phase liposomes is in contrast to the low binding enthalpy observed for fluid phase liposomes.
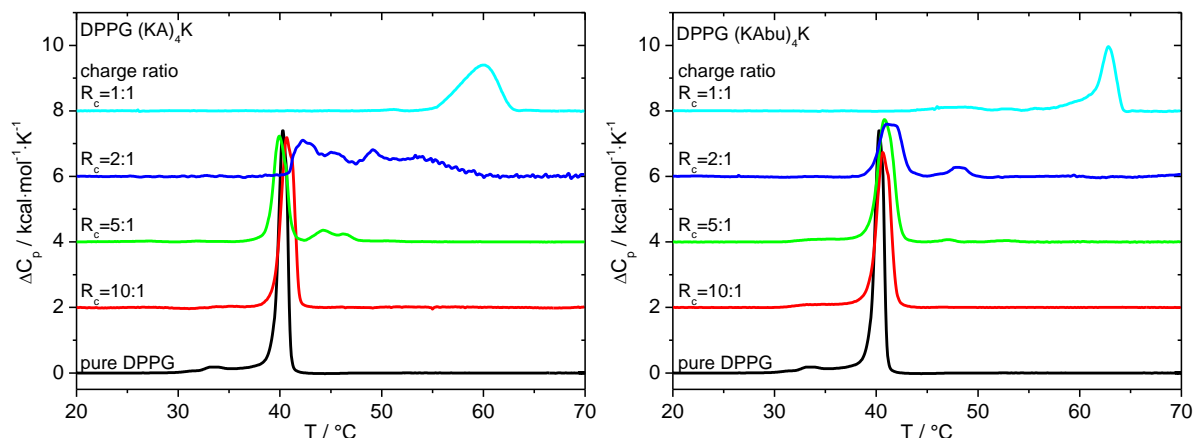
Figure 3.3.2: Thermogram of pure DPPG vesicle and different DPPG-(KA)4K mixtures (left panel) and different DPPG-(KAbu)4K mixtures (right panel) with increasing charge ratio. The 2nd heating scan is shown, because equilibrium was only reached after passing the phase transition. Samples were prepared in aqueous 100 mM NaCl with a fixed lipid concentration of 2 mM.

DPPG-(KAbu)$_4$K mixtures

The hydrophobicity of the peptide is further increased, when the non-natural amino acid aminobutyric acid is inserted into the sequence. Mixtures of DPPG with the peptide (KAbu)$_4$K and different charge ratios show peaks at 3 distinct temperatures as depicted in Figure 3.3.2, right panel. The tendency to form distinct lipid-peptide aggregates, which have a defined transition temperature, is enhanced compared to (KA)$_4$K. As already suggested, aggregates with higher peptide content show an elevated transition temperature. A peak located at 40 °C, which corresponds mainly to pure DPPG, is only visible up to a charge ratio of 2:1. A second peak at about 47 °C appears at charge ratios 5:1 and lower, increasing its enthalpy with higher peptide content. The third peak at 64 °C is only visible at a charge ratio of 1:1. With more hydrophobic amino acid spacers, an additional ordering effect seems to counteract the effect above and a sharper transition occurs upon heating.

The concentration dependent DSC measurements of DPPG mixtures with the more hydrophobic peptides (KV)$_4$K and (KL)$_4$K are comparable with those of (KAbu)$_4$K and show no new features (see Figure 8.3.1).

Overview DPPG-(KX)$_4$K mixtures of a charge ratio $R_c = 1:1$

DSC curves of DPPG-(KX)$_4$K with a charge ratio of 1:1 are depicted in Figure 3.3.3. A clear upshift of the transition temperature of the lipid-peptide complexes compared to pure DPPG is visible. The stabilization of the gel phase upon peptide binding becomes more prominent, if the side chain of the uncharged amino acid X in the added peptide becomes larger and more hydrophobic. The upshift of the transition temperature increases from G over A and reaches

its maximum for Abu and V, which show similar behavior. In contrast to the general trend, T_m for complexes with (KL)$_4$K is at slightly lower temperatures than for the complexes with (KV)$_4$K. The interaction of positively charged peptides with negatively charged DPPG membranes affects the phase transition temperature as well as the transition enthalpy. All determined data of the thermotropic behavior of DPPG-peptide mixtures are summarized in Table 3.3.2.

Upon peptide binding, the negative charges of the membrane are screened by positively charged lysine residues of the peptide. Thus, the electrostatic repulsion between neighboring headgroups is reduced and a better chain packing as well as higher van der Waals interaction leads to a higher main phase transition temperature. In addition, a dehydration of the headgroup region might occur, shifting the phase transition to higher temperatures. Increasing van der Waals forces can be also obtained by elongation of the acyl chains.
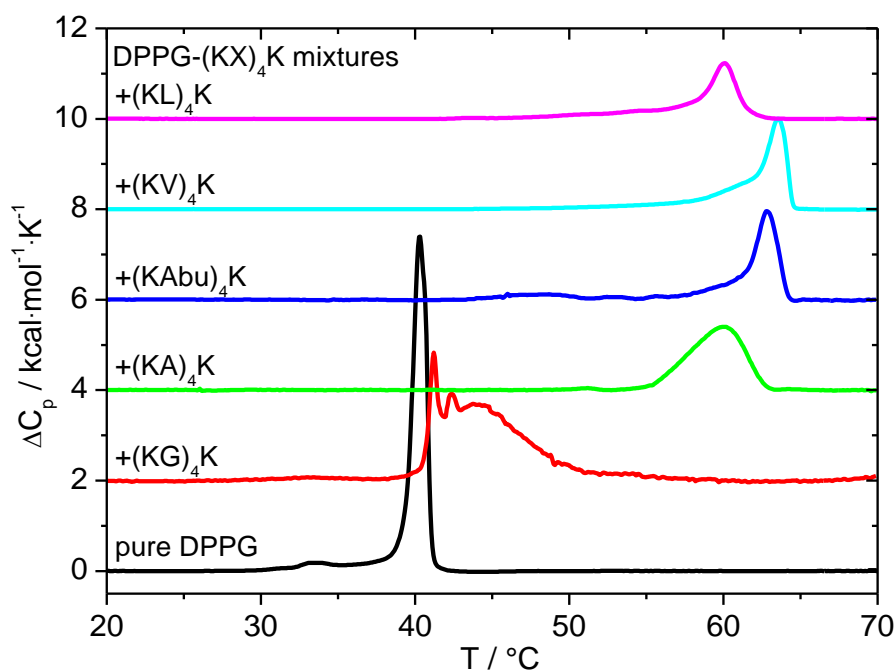
Figure 3.3.3: Thermogram of pure DPPG vesicle (black) and different DPPG-(KX)$_4$K mixtures with a charge ratio R_c = 1:1. The 2nd heating scan is shown, because equilibrium was only reached after passing the phase transition. Samples were prepared in aqueous 100 mM NaCl with a fixed lipid concentration of 2 mM.

Similar results of a reduced transition enthalpy were obtained with DPPG and polylysines of different lengths [205]. This is somehow contradictory as lipid-peptide interactions enable a better acyl chain packing leading to increased van der Waals interaction in the hydrophobic region. Furthermore, an intermolecular hydrogen bonding network between the glycerol and phosphate groups is formed during long time incubation at low temperature results in an upshift of T_m and transition enthalpy as seen for DMPG. This proves that hydrogen bonds

between lipids brake up at elevated temperatures and contribute to the transition enthalpy [206]. The influence of increased van der Waals contacts and lower charge repulsion in the headgroup region is overcompensated by altered hydrogen bond network and electrostatic lipid-peptide attraction. In contrast to the intermolecular hydrogen bonds between lipids the electrostatic lipid-peptide binding remains stable also in the liquid-crystalline phase and does no contribute to the transition enthalpy resulting in an overall reduced transition enthalpy. A change of the lipid arrangement especially the tilt angle of the hydrocarbon chain might be also the reason for a reduced transition enthalpy [207].

Table 3.3.2: Overview of the thermodynamic data obtained from DPPG-(KX)$_4$K mixtures with a charge ratio of 1:1. T_m is the main phase transition and marked by the peak with the highest heat capacity and $T_{1/2}$ the full width of this peak at half maximum. Especially for the asymmetric peaks with several shoulders T_{mid} obtained from the midpoint of the integral of the curves, is more suitable for a comparison. ΔT_{base} is the width of the peak at its base and ΔH is the transition enthalpy.

	T_m / °C	T_{mid} / °C	$T_{1/2}$ / °C	ΔT_{base} / K	ΔH / kcal mol^{-1}
pure DPPG	40.3	40.2	1.5	3.5	10.4
+ (KG)$_4$K	41.3	44.2	5.6	10.7	13.2
+ (KA)$_4$K	60.0	59.4	4.3	7.7	6.3
+ (KAbu)$_4$K	62.9	62.2	1.7	8.1	5.3
+ (KV)$_4$K	63.6	62.4	1.6	7.4	5.7
+ (KL)$_4$K	60.1	59.2	2.0	4.1	4.4

Beside the theoretical explanation, there might be some uncertainties in the calculation of the transition enthalpy, because during sample preparation the system starts to aggregate and some lipid content remains in the vial. To minimize this error the volume of the prepared samples was reduced, so that almost the complete sample in the vial was transferred into the calorimetric cell. This experimental drawback should be more problematic for mixtures with high peptide content. The reduced transition enthalpy must have other origins.

Lipid CH$_2$ stretching bands of DPPG-(KX)$_4$K mixtures

As observed before by DSC (Figure 3.3.3), an increase of the transition temperature after peptide addition is visible as depicted in Figure 3.3.4, left panel, where v_s(CH$_2$) as a function of temperature is shown. ΔT_m increases as follows: (KG)$_4$K < (KA)$_4$K ≈ (KAbu)$_4$K < (KV)$_4$K ≈ (KL)$_4$K. The midpoint of the lipid transition in the mixture of (KG)$_4$K is upshifted to 47 °C and agrees with DSC results. The phase transition temperatures of DPPG mixtures with (KA)$_4$K and (KAbu)$_4$K appear at 54 °C and 57 °C, respectively, and are slightly lower compared to the DSC (60 and 64 °C, respectively). The largest ΔT_m with a transition

temperature around 62 °C is observed for the two peptides (KV)$_4$K and (KL)$_4$K bound to DPPG. For these two mixtures, T_m-values determined by IR and DSC results agree very well. The CH$_2$ stretching vibrations in DPPG-(KX)$_4$K mixtures are shifted to lower wavenumber in the fluid phase with $\Delta\tilde{v}$ = -0.3 up to -0.6 cm^{-1} for all tested peptides. The trend shows a larger decrease the more hydrophobic the added peptide is. For peptides bound to gel phase DPPG vesicles, only (KG)$_4$K and (KA)$_4$K lead to a lower wavenumber, i.e. $\Delta\tilde{v}$ = -0.4 cm^{-1}, whereas the binding of the more hydrophobic peptides induces no shift. The extent of the wavenumber shift seems to be the same for (KG)$_4$K and (KA)$_4$K, suggesting similar effects of the bound peptide. Such downshift indicates that the binding of the peptide induces a higher order in the hydrophobic part of the membrane. The charge screening and the coupled reduction of the effective headgroup area due to bound peptide allows a better packing of the molecule and increases the van der Waals interaction. A possible decrease of the tilt angle of the acyl chains in the membrane can occur.

This was also suggested as an effect of the binding of polylysine to DPPG bilayer by Takahashi et al. [111]. This would be observable in IR experiments with linear polarized light or in X-ray studies using stacked bilayers. The observed downshift of the wavenumber in the gel phase is absent for the two more hydrophobic peptides (KV)$_4$K and (KL)$_4$K. Here the wavenumbers are similar to unperturbed lipid. (KAbu)$_4$K shows an intermediate behavior with features of both groups discussed before. There are two explanations for this behavior. First, there is an additional effect of an incorporation of the hydrophobic side chains into the acyl chain region, counteracting the charge screening effect mentioned above, or second, the lipid bilayer is more or less undisturbed and the shift in the phase transition is a result of local dehydration upon peptide binding. The second explanation is favored, as results from the carbonyl vibration show dehydration in the interfacial region of the bilayer (see below).

A further influence of the stretching vibrational frequencies is observed for an increased vibrational coupling of neighboring acyl chains, either intramolecularly [176] or intermolecularly [208]. This could be accomplished by a restriction of the rotational motion of the acyl chains, induced by peptide headgroup interaction. Comparing the reduction of the vibration frequencies induced by peptide binding with effects induced by polylysines [205] or their short chain analogues [204], the shift observed here is less pronounced. This suggests that the rotational motion of the acyl chains is unperturbed, as the bandwidths show no significant changes.
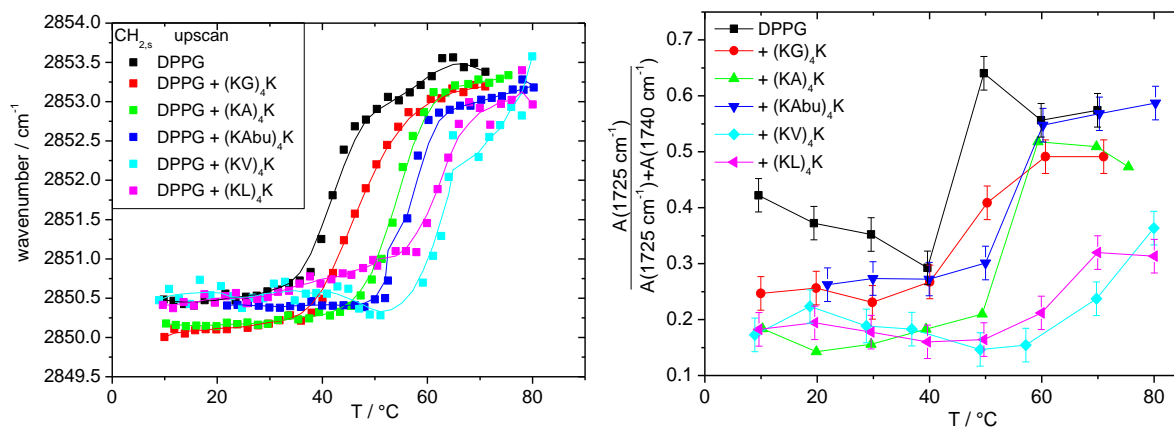
Figure 3.3.4: Left: wavenumber of the maximum of the symmetric CH$_2$ stretching band of pure DPPG and DPPG mixtures with peptides of increasing hydrophobicity: (KG)$_4$K, (KA)$_4$K, (KAbu)$_4$K, (KV)$_4$K, (KL)$_4$K, respectively. Lines to guide the eye were constructed by an adjacent averaging of 5 points. Right: ratio of the area of hydrogen bonded ν(CO) vibrational band compared to the whole area of the carbonyl vibrational peak of pure DPPG and DPPG mixtures with peptides. All samples had a charge ratio $R_c = 1:1$ and were prepared in D$_2$O containing 100 mM NaCl at $pD = 7.2$.

Lipid C=O bands of DPPG-(KX)$_4$K mixtures

In Figure 3.3.4, right panel, the band ratio of the intensity of the hydrated carbonyl group to the total carbonyl band intensity is plotted against the temperature for all tested DPPG-peptide mixtures. For pure DPPG in the gel state, approximately 30 to 40 % of the C=O bands correspond to the hydrogen bonded state. Above the phase transition the bilayer becomes more hydrated with the result that water molecules penetrate more deeply into the interfacial region as reported before [186].

The binding of the peptide influences the hydration level of the lipid bilayer in both phases. For bilayers in the gel phase, a general decrease of hydration is observed after peptide binding. Upon (KG)$_4$K addition, the hydrogen-bonded carbonyl fraction is reduced to 25 %, for the binding of the other peptides even lower values of 20 - 15 % are observed. Pure DPPG vesicles show an increase in the hydrogen-bonded fraction to ~ 60% above T_m. When the peptides are bound, this effect occurs to a lesser extent, particularly when (KV)$_4$K and (KL)$_4$K are bound. These more hydrophobic peptides are able to prevent hydration also at 80 °C. Peptide binding reduces the available space for hydration water, as it is assumed that complexes of stacked lipid bilayers are formed, which are bridged by the peptide. The remaining water of hydration will be shared by bound peptide and the lipid headgroups. This dehydration of the bilayer after charge compensation is the main reason for the upshift of the transition temperature. It is known from binary lipid water systems with a low water content that the phase transition temperature is increased [209]. In contrast, a direct hydrogen bond between the carbonyl groups of the lipid and the lysine -NH$_3^+$ moiety of the added peptide is

unlikely, because it would act as hydrogen bond donor and increase the band at 1725 cm^{-1}. It might be possible that the phosphate group is also influenced by the peptide. Upon charge attraction and binding of the lysine side chain to the phosphate group a stronger hydrogen bonding might be possible as both moieties carrying the highest charge density. However, the phosphodiester vibrational band ($v_{as}(\text{PO}_2^-)$ = 1228 cm^{-1}) could not be analyzed, due to an overlay with the D$_2$O bending vibration ($\delta(\text{D}_2\text{O})$ = 1210 cm^{-1}).

Peptide amide-I bands of DPPG-(KX)$_4$K mixtures

The spectral region of the amide-I bands for the mixtures of DPPG with (KG)$_4$K, (KA)$_4$K and (KL)$_4$K are shown in Figure 3.3.5 (see Figure 8.3.3 for data of DPPG-(KAbu)$_4$K and DPPG-(KV)$_4$K mixtures). The observed amide-I bands show distinctly different contours depending on the structure of the peptide. (KG)$_4$K as flexible and least hydrophobic peptide shows a broad band, indicating the presence of mostly unordered structures (1646 cm^{-1}) with some β-turns (1670 cm^{-1}). This conformation is observed for the complete temperature range. The peptides (KA)$_4$K and (KAbu)$_4$K show a different conformation at low temperatures compared to (KG)$_4$K. They form predominantly antiparallel β-sheets (1615 cm^{-1} and 1680 cm^{-1}) when bound to lipid bilayer in the gel phase. However, upon heating, the peptide reorganizes to an unordered conformation at high temperature above the phase transition (see Figure 3.3.5, bottom right panel). The transition from the β-sheet to unordered structure occurs for (KA)$_4$K in a temperature range between 50 and 60 °C with a midpoint at 56 °C. The peptide (KAbu)$_4$K is less temperature stable (T_m = 53 °C) and the transition occurs in a narrower temperature range (49 - 56 °C) compared to (KA)$_4$K. These three peptides are thus bound to the DPPG bilayers in an unordered structure at high temperature. A complete dissociation at higher temperature is unlikely, as there are still differences compared to the behavior of pure lipid. The β-sheet arrangement of the peptide creates a highly amphipathic molecule structure. The charged side containing the lysine side chains, faces the lipid headgroups, and the uncharged and hydrophobic part is composed of the side chains of the uncharged spacer. Upon heating, a solvation of the uncharged part is possible and increased water content can lead to swelling of the membrane stacks.

In contrast, the more hydrophobic peptides (KV)$_4$K and (KL)$_4$K show no temperature dependent reorganization and build up stable β-sheets bound to the lipid bilayer surface independent of the lipid phase state. Thus, an extensive incorporation of water is hindered.

The hydrophobicity of the peptide is the decisive property, determining which secondary structure is build up upon binding to the vesicles. The FT-IR measurements clearly show that

lipids, as well as peptides are influenced after binding. The lipid becomes less hydrated and the phase transition is shifted to a higher temperature. The peptide can build up β-sheet structures with a tight hydrogen bond network. The wavenumber of the β-sheet component at 1615 cm^{-1} is also sensitive for the strength of the hydrogen bond in the structure. The wavenumber observed at 10 °C decreases from (KA)$_4$K to (KL)$_4$K from 1614 to 1612.5 cm^{-1}, indicating stronger hydrogen bonds within the β-sheet layer for the more hydrophobic peptides. Increasing the temperature weakens the hydrogen bonds resulting either a breakup of this structure, as seen for (KA)$_4$K and (KAbu)$_4$K, or leading to a value of 1616 cm^{-1} for temperature stable β-sheets.
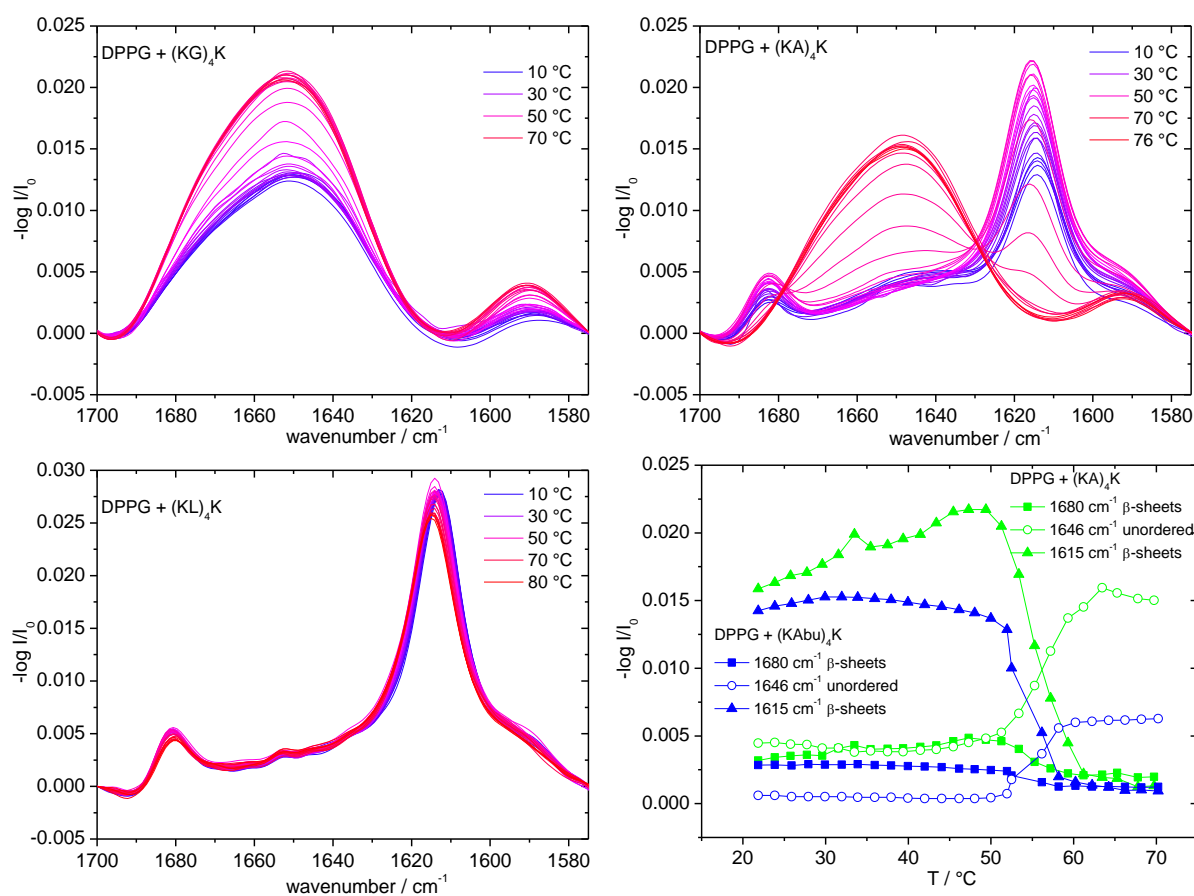
Figure 3.3.5: Temperature dependent behavior of the amide-I band for DPPG mixtures with different peptides during the heating. Top left: (KG)$_4$K-DPPG mixtures. Top right: (KA)$_4$K-DPPG mixtures. Bottom left: (KL)$_4$K-DPPG mixtures. Bottom right: peak intensity of amide-I band components as a function of temperature clearly showing changes in secondary structures upon heating. DPPG-(KA)$_4$K mixtures (green symbols) and DPPG-(KAbu)$_4$K mixtures (blue symbols) show a β-sheet secondary structure at low temperatures with amide peaks at 1680 cm^{-1} (■) and 1615 cm^{-1} (▲), which converts into an unordered structure at higher temperature (amide-I peak at 1646 cm^{-1} (O)). All samples had a charge ratio R_c = 1:1 and were prepared in D$_2$O containing 100 mM NaCl at pD = 7.2.

Comparison with published results shows that the hydration of the peptide backbone is crucial for the formation of secondary structures of the peptide, especially for polylysine. An increased hydration induces the change from β-sheets over α-helices to random coil structure [210, 211]. The low hydration of the carbonyl group of the lipid and the appearance of the β-sheet structure found here fits together well and suggests that most of the water is expelled from the mixed lipid-peptide bilayer stacks.

3.3.2 Influence of a Reduced Charge Density - Introduction of a Second Uncharged Amino Acid Spacer

To test the influence of an increased distance between the charged lysine side chains on the thermotropic phase behavior of DPPG, different numbers of spacers between the charged residues were introduced and thus the periodicity of the peptide is changed. The peptides with alternating sequences $(KX)_4K$ and a periodicity of 2 are predestinated to form β-sheets, because an uncharged and/or hydrophobic side opposes a highly positively charged side. However, data from ATR-IR show that the stability of the proposed β-sheets is determined by the hydrophobicity of the spacer X (see above). The peptides with a sequence of $(KXX)_4K$ exhibit a periodicity of 3 and therefore favor a 3_{10}-helix [67, 72]. Whether these structures are built up depends on the one hand on the interaction partner, and on the other hand on the peptide length [69]. With a further increased periodicity, the probability to form helices is enhanced, a periodicity of 3.6 would lead to α-helices, but glycine as the smallest amino acid is known as helix breaker due to its flexibility and the missing side chain [212]. The minimal length for a stable helix is predicted to be 14 amino acids [77]. The peptides used here are with maximal 13 amino acids are below this value. Therefore, it is expected that these peptides do not form stable secondary structures in solution.

In the DSC studies, both peptides $(KGG)_4K$ and $(KAA)_4K$ are also able to stabilize the DPPG bilayer in its gel phase and shift the phase transition temperature to higher values. The extent of stabilization is larger for $(KAA)_4K$ than for $(KGG)_4K$. The whole transition spans the temperature range from 40 °C up to 50 °C for both peptides $(KXX)_4K$ and for all other peptides mentioned in Table 3.3.3.

The appearance of different pronounced peaks for all DPPG-peptide mixtures indicates possible domain formation (see Figure 3.3.6). The separation into immiscible lipid-rich and peptide-rich aggregates is suggested. The transition enthalpies for 1:1 mixtures of DPPG-

(KXX)$_4$K are increased compared to pure DPPG vesicles. For detailed comparison of the obtained parameters, see Table 3.3.3.

The transition temperature and enthalpy increases in the order pure DPPG, mixtures with (K)$_5$ [123] and mixtures with (KG)$_4$K and decreases again for (KGG)$_4$K. Thus, (KG)$_4$K stabilizes the gel phase of the DPPG most effectively, but has the broadest transition range. To exclude an effect of the peptide chain length on the thermotropic behavior, data of DPPG-(K)$_{14}$ mixtures were added to the Table 3.3.3. (K)$_{14}$ is one amino acid longer than the peptides (KXX)$_4$K with 13 amino acids. The chain length of the added peptide seems to be less important as results from (K)$_5$ and (K)$_{14}$ are similar concerning the phase transition temperature [104]. Based on these results, one can conclude that the different phase transition temperatures for DPPG mixtures with (K)$_5$, (KG)$_4$K and (KGG)$_4$K are related to the different charge separation, and are independent of the peptide chain length.
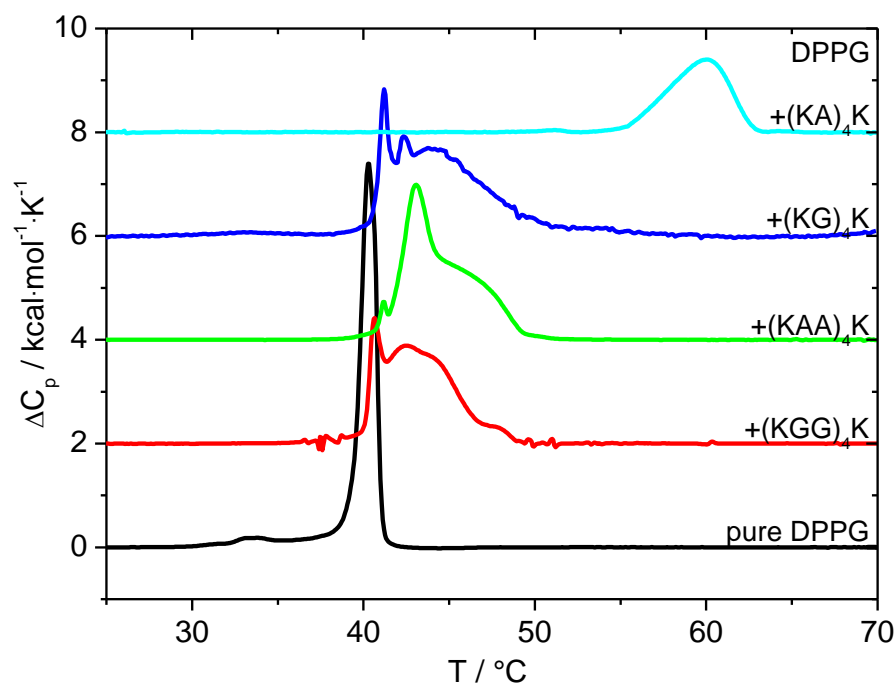
Figure 3.3.6: Thermogram of pure DPPG vesicles and different DPPG-peptide mixtures with a charge ratio R_c =1:1. The 2nd heating scan is shown, because equilibrium was only reached after passing the phase transition. Samples were prepared in aqueous 100 mM NaCl with a fixed lipid concentration of 2 mM.

Similar trends concerning the transition temperature are obtained within the series (K)$_5$, (KA)$_4$K and (KAA)$_4$K. However, here the thermotropic behavior of DPPG-(KA)$_4$K mixtures is an exception showing a much higher T_m with a reduced transition enthalpy. Data obtained from FT-IR measurements show a completely different arrangement for (KA)$_4$K, building β-sheets upon binding to DPPG vesicles, whereas all other peptides having mostly unordered structures.

An important role for the interaction with DPPG bilayer systems is the charge separation, which is directly coupled to the periodicity of the peptide. Beside the general distance of the charge in the peptide, the flexibility, bulkiness and hydrophobicity of the introduced uncharged spacer amino acid is also decisive. The general stabilization effect of the gel phase is visible for all added peptides and may be attributed to the charge neutralization upon peptide binding, because all peptides exhibit the same charge. Peptides with one uncharged spacer show a greater upshift than pentalysine and peptides with two uncharged spacers.

Table 3.3.3: Overview of the thermodynamic data obtained for DPPG-peptide mixtures with a charge ratio of 1:1. The peptides had different sequences and thus different distances between the charged lysines. T_m is the main phase transition and marked by the peak with the highest heat capacity and $T_{1/2}$ the full width of this peak at half maximum. Especially for the asymmetric peaks with several shoulders T_{mid} obtained from the midpoint of the integral of the curves, is more suitable for a comparison. ΔT_{base} is the width of the peak at its base and ΔH is the transition enthalpy.

	T_m / °C	T_{mid} / °C	$T_{1/2}$ / °C	ΔT_{base} / K	ΔH / kcal mol^{-1}
pure DPPG	40.3	40.2	1.5	3.5	10.4
+ (K)$_5$ [123]	42.2	42.2			10.7
+ (KG)$_4$K	41.3	44.2	5.6	10.7	13.2
+ (KGG)$_4$K	40.7	42.9	4.8	9.0	10.8
+ (KA)$_4$K	60.0	59.4	4.3	7.7	6.3
+ (KAA)$_4$K	42.1	44.0	2.7	8.7	11.4
+ (K)$_{14}$ [104]	42	42			10.9

Lipid CH$_2$ stretching bands of DPPG-(KXX)$_4$K mixtures

Mixtures of DPPG with (KGG)$_4$K show a lower v_s(CH$_2$) in the gel phase and fluid phase compared to pure DPPG (see Figure 3.3.7, left panel). Such a decrease in the vibration wavenumber is interpreted with a better ordering of the acyl chains [4]. The phase transition of the DPPG-(KGG)$_4$K mixture occurs at 43 °C and is in good agreement with the results from the DSC experiments. In the IR data, a hint of a second step is visible at 59 °C. Such two-step behavior was also observed by Schwieger [104] for DPPG-polylysine complexes and was discussed as a proof for domain formation.

In mixtures of the lipid with (KAA)$_4$K, an increase in chain order in the gel phase is not seen, but significant in the fluid phase. The increase of the wavenumber at the phase transition is less pronounced.

Comparing thermotropic behavior of DPPG-(KXX)$_4$K mixtures with DPPG-(KX)$_4$K shows that the midpoint of the lipid transitions is upshifted in mixtures containing peptides with only one spacer.

Introducing a spacer amino acid between the lysine changes the ability of the peptide to increase the chain order of the lipid upon binding. Comparing the peptides (K)$_5$, (KG)$_4$K and (KGG)$_4$K as well as (K)$_5$, (KA)$_4$K and (KAA)$_4$K for their influence on the wavenumber of the v_s(CH$_2$), the effect of the better acyl chain ordering is most pronounced for (K)$_5$ ($\Delta\tilde{v}$ = - 1.08 cm^{-1}) [123], lower for the peptides with glycine spacers (KG)$_4$K and (KGG)$_4$K and (KA)$_4$K ($\Delta\tilde{v}$ = -0.5 cm^{-1}), and absent for (KAA)$_4$K. Reasons might be the increased binding constants for peptides with no or only one spacer to negatively charged lipids [88] or a better charge compensation due to geometrical reasons.
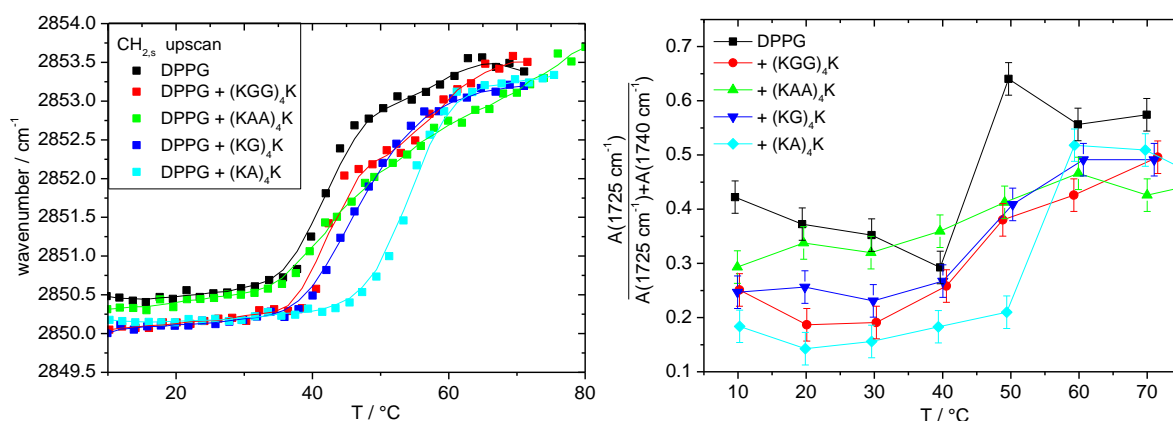
Figure 3.3.7: Left: wavenumber of the maximum of the symmetric CH$_2$ stretching band of pure DPPG and DPPG mixtures with peptides of increasing charge distance and hydrophobicity: (KG)$_4$K, (KA)$_4$K, (KGG)$_4$K, (KAA)$_4$K, respectively. Lines to guide the eye were constructed by an adjacent averaging of 5 points. Right: ratio of the area of hydrogen bonded v(CO) vibrational band compared to the whole area of the carbonyl vibrational peak of pure DPPG and DPPG mixtures with peptides. All samples had a charge ratio R_c = 1:1 and were prepared in D$_2$O containing 100 mM NaCl at pD = 7.2.

Lipid C=O bands of DPPG-(KXX)$_4$K mixtures

Peptide addition influences the hydration level of the lipid bilayer in both phases and an upshift of the transition temperature is visible (see Figure 3.3.7, right panel). It is shown that the bound lysine containing peptides reduce the hydration of the lipid headgroup. The hydrogen bonded carbonyl fraction in gel phase at 20 °C is reduced after peptide binding in the order (K)$_5$ (66 %) [123], (KG)$_4$K (25%), (KGG)$_4$K (20%). For the gel phase, the hydration level is constant below T_m, but at the phase transition of the system an increase of the

hydrogen bonded fraction is visible. The headgroup hydration of DPPG mixed with $(KAA)_4K$ is slightly below those of pure lipid in the gel phase. Phase transition temperatures determined for DPPG mixtures with $(KGG)_4K$ and $(KAA)_4K$ from the carbonyl vibrations the are in good agreement with the results from the CH_2 stretching vibrations.

The increased hydration of DPPG mixed with $(K)_5$ was explained by the hydration water molecules, shared by lipids and the bound peptides, become better orientated and the peptide side chains are inserted into the lipid headgroup region [123].

Peptide amide-I bands of DPPG-(KXX)₄K mixtures

Spectra of the peptides $(KGG)_4K$ and $(KAA)_4K$ bound to DPPG bilayers are shown in Figure 3.3.8. The secondary structure of the tested peptides $(KXX)_4K$ is a mixture of β-turns and unordered conformations. The structure remains upon binding of the peptide to the lipid bilayer and upon heating over the phase transition of the lipid.
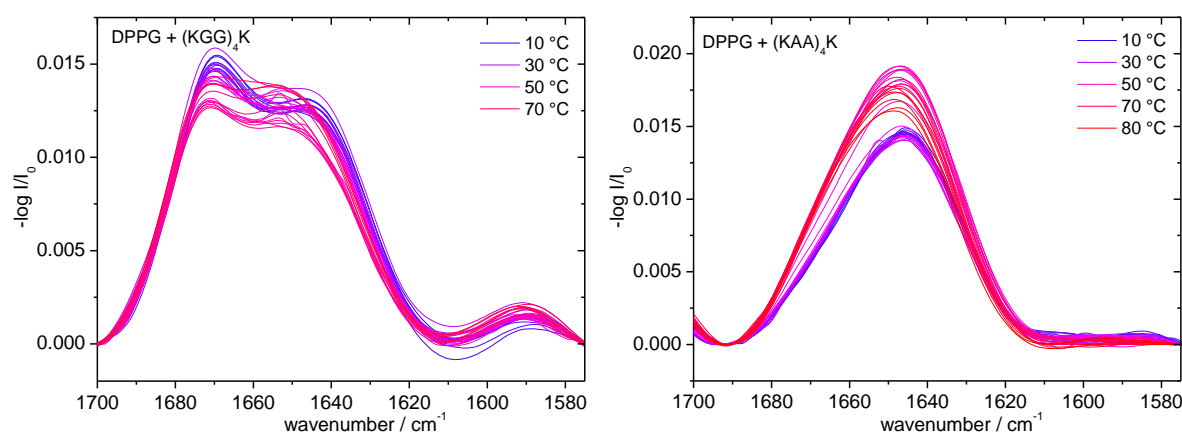
Figure 3.3.8: Temperature dependent behavior of the amide-I band for DPPG mixtures with different peptides $(KXX)_4K$ during the heating. Left: $(KGG)_4K$-DPPG mixtures. Right: $(KAA)_4K$-DPPG mixtures. All samples had a charge ratio R_c = 1:1 and were prepared in D_2O containing 100 mM NaCl at pD = 7.2.

A fitting of the obtained spectra in the amide-I region with two peaks, centered at 1670 cm^{-1} for β-turns and 1646 cm^{-1} for unordered conformations, with a Gaussian profile were used to determine the relative areas of the peaks. The higher content of β-turns in the spectra of $(KGG)_4K$ (ca. 45%) compared to $(KG)_4K$ with 25 % turn content and nearly exclusively unordered structures for $(K)_5$ [123] could be explained with the higher flexibility of the peptide backbone. In general, the probability for β-turns [213] is enhanced in glycine containing peptides and increases further, if 3 out of 4 residues are glycines. The most likely turn arrangement is the one with the charged amino acid lysine in position 2 and the hydrogen bond between position 1 and 4 (see Table 3.3.4).

Table 3.3.4: Turn potentials of single amino acids for different positions in the β-turn structures [213]. The overall turn potential for a β-turn composed of different peptide sequences, consisting of K, G, and A.

amino acid \ position	i	i+1	i+2	i+3
K	0.80	1.22	0.94	1.10
G	1.09	1.04	2.14	1.64
A	0.81	0.96	0.66	0.89
sequence	KKKK	KAAK	AAKA	AKAA
turn potential	1.01	0.56	0.65	0.58
sequence	KGKG	GKGK	KAKA	AKAK
turn potential	1.28	3.13	0.64	0.72
sequence	KGGK	GGKG	GKGG	
turn potential	1.96	1.75	4.67	

An exception to all these lipid-peptide mixtures with unordered peptide structures is the mixture of DPPG with (KA)₄K. In the gel phase, an antiparallel β-sheet layer is build up on top of the bilayer. This stabilization due to an additional level of self-organization shifts the phase transition of DPPG up to 60 °C, as discussed above for the other peptides of the series (KX)₄K. The peptide rearranges into an unordered structure in the fluid phase. For the peptides (KXX)₄K a 3_{10}-helix is predicted, which would be visible by a band at 1660 cm^{-1} [72]. As no contribution to the amide-I band in this spectral region occurs the existence of a 3_{10}-helix is excluded for both tested peptides.

For all 1:1 complexes, one negative headgroup charge should be compensated by the positive charge of the lysine side chain. In the gel phase, the area of a PG headgroup is estimated to be 48 Å^2. Thus, a distance between two neighboring headgroups of 6.9 Å must be bridged by the peptide [46, 214]. For geometrical reasons, the different lysine chains at different positions in the peptides with different sequences have to adapt to this distance. The distance of two neighboring positively charged nitrogens in a lysine side chain is about 13.0 Å. The charge distance of the residues i and i+2 is only 7.3 Å for a β-sheet structure. This motif is also found in peptides (KX)₄K. The largest distance of 16.6 Å of the residues i and i+3 can be reduced to 7 Å in a β-turn, but requires a glycine in position i+2, and a lipid layer to screen the charges and the repulsion of equal charges. Such sequence can be found in the peptides (KXX)₄K.

A schematic representation of the calculated distances of a polylysine chain in its extended conformation is given in Figure 3.3.9. These maximal charge distances are not found for

lysine containing peptides in 100 mM NaCl, because the repulsion of the charges is screened by the added ions.

For oligolysines, i.e. (K)$_5$ only a small stabilization at the gel phase is found, due to the close proximity of neighboring lysine chains. Heptalysine in its extended conformation, lying flat on top of the lipid bilayer covers an area of ~ 530 Å^2 (17 x 31 Å). This conformation would cause a charge density of 1 positive charge per 75 Å^2, compared to a charge density of 1 negative charge per 70 Å^2 for lipids in the fluid phase and 48 Å^2 for gel phase lipids. Assuming a binding of all lysine residues no complete charge compensation can achieved, because more than seven lipids are covered [119]. The increased distance of lysines in the peptide backbone in (KX)$_4$K enables a regular peptide arrangement on top of the lipid bilayer without any constraints, resulting in a further increased stabilization of the gel phase. A distance of 7.3 Å between the positively charged nitrogens in the side chains fits nicely to the distance of the lipid headgroups in the gel phase and enables the formation of β-sheets for further stabilization. Peptides with two spacers are thought to arrange in other conformations than β-sheet to maximize the charge compensation with the lipid bilayer.
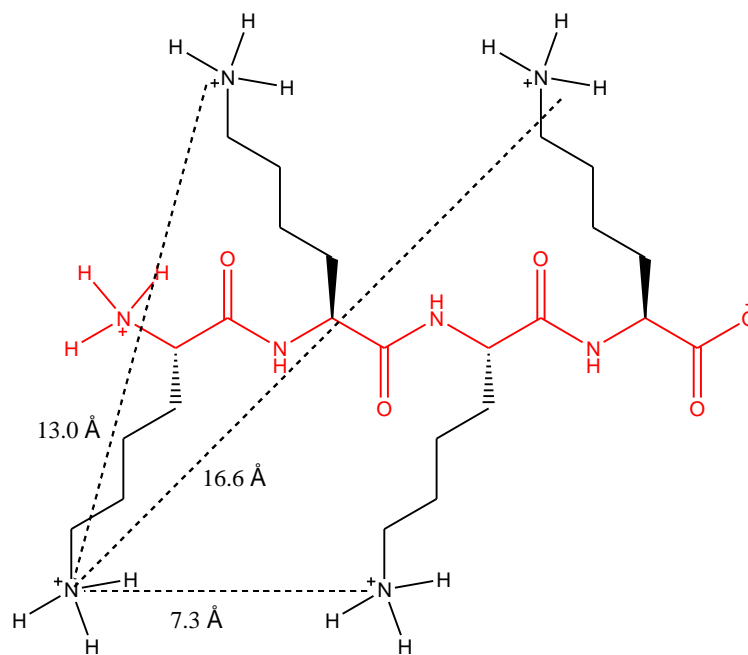
Figure 3.3.9: Schematic representation of the charge distances in a polylysine chain in its extended conformation.

Beside the distance between the charges, the relative orientation of the peptide backbone with its amide groups to the lipid bilayer may also play a role. For pentalysine, the amide groups are mostly aligned parallel to the membrane normal, resulting in a flat arrangement on top of the bilayer without the possibility to build up intermolecular hydrogen bonds for stabilization between adjacent peptide strands [119, 215].
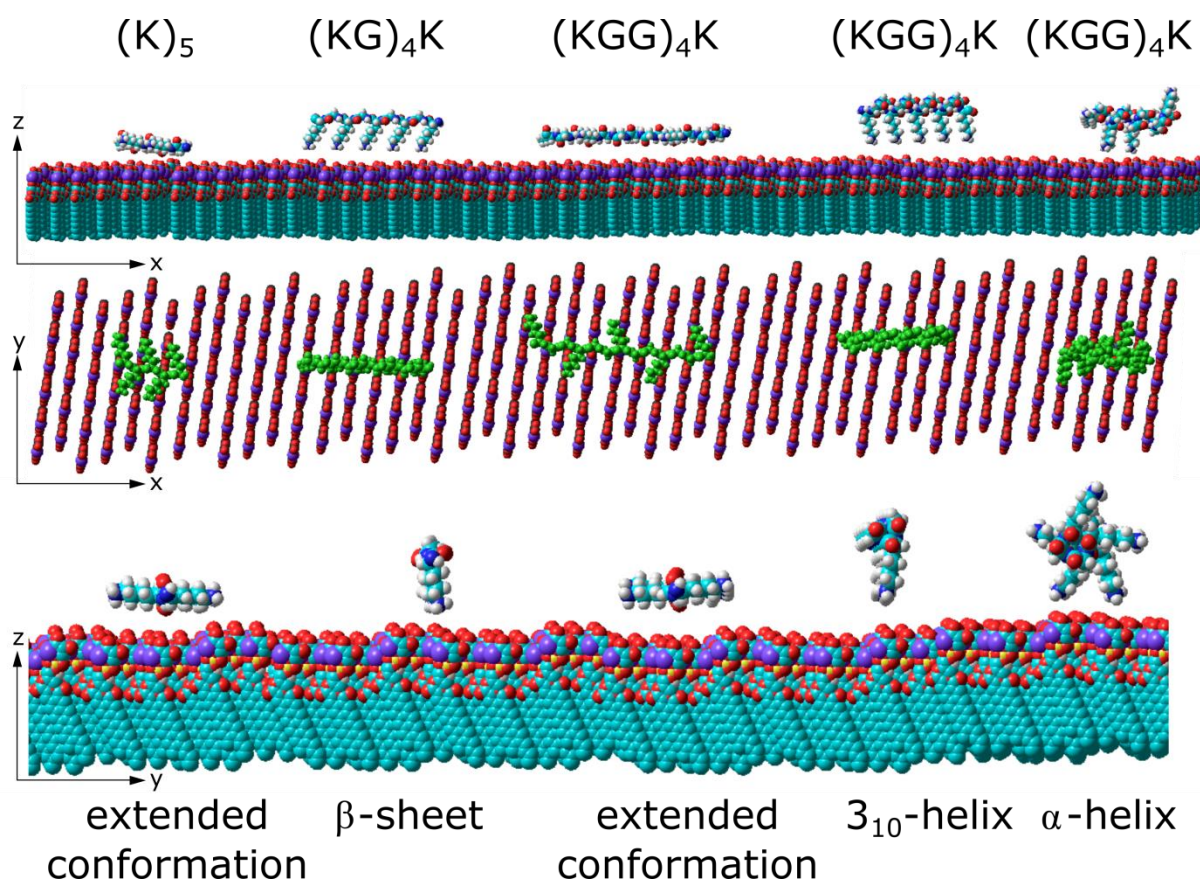
Figure 3.3.10: Possible arrangements of the peptides on top of the lipid layer: $(K)_5$ in extended conformation, $(KG)_4K$ in β-sheet conformation, and $(KGG)_4K$ in extended, 3_{10}-helical, and α-helical conformation. Structures are presented along the three dimensions of space (top: side view along y-axis, middle: top view along z-axis, bottom: side view along molecule longitudinal axis along x-axis). The secondary structures presented here are a selection of the possible conformations determined by the peptide sequence. Peptide molecules are turned in such direction that the maximal numbers of positive charged lysine side chains are directed to the negatively charged lipid headgroups.

With one uncharged spacer, the peptide has the ability to be orientated perpendicular to the bilayer so that most of the amide groups are now parallel to bilayer surface. This leads to an effective stabilization for a β-sheet arrangement via intermolecular hydrogen bonds in y-direction. For peptides with the sequence $(KXX)_4K$, an extended conformation lying flat on the bilayer, as discussed for pentalysine, a turn structure (not shown), 3_{10}- or α-helical structures are possible and depicted in Figure 3.3.10. The turn and α-helical structure induce no preferred direction of the amide bonds, but stabilization through intramolecular hydrogen bonds within the structure is possible. A with an additional hydrogen bond in the peptide strand also fits to the lipid headgroup distance of 6.9 Å in the gel phase. A drawback for a β-turn is that only a part of the peptide is stabilized, and the rest of the molecule is thought to exhibit a random conformation. Comparing the β-sheet arrangement of $(KG)_4K$ and the 3_{10}-helix of $(KGG)_4K$, both structures have in common that all lysine side chains point towards

the negatively charged lipid headgroups, but the lateral distance of two neighboring lysines is different. A further stabilization of several peptide strands is possible by hydrophobic interactions between the uncharged spacer. This is possible for both structures and is supplemented by hydrogen bonds in the β-sheet arrangement of (KX)$_4$K.

The importance or the effect of the peptide backbone can be evaluated by comparing the results obtained here for peptides with increasing charge distances the study by Ye et al. [216]. The charge distance can be altered by insertion of additional uncharged amino acids or by ω-amino acids of different chain length. The phase transition is upshifted because of electrostatic interaction, whereas influence on the phase transition upon binding of peptide analogues depends on the spacer length and its hydrophobicity. For peptides with the short spacer 5-amino pentanoic acid a slight upshift is observed. Here the distance of two charged residues is comparable with those in (KXX)$_4$K. For the medium spacer 8-amino octanoic acid, both effects compensate each other, and for the longest spacer 12-amino dodecanoic acid, the phase transition decreases the due to incorporation of the uncharged spacer into the acyl chain region.

Model peptides composed of the two amino acids lysine and leucine with other periodicities were used to determine the interplay of hydrophobic and charge interaction for the peptide structure itself, as well as for the interaction with other components. Beside the periodicity, also the length of the peptide plays a role for the formed structure at the air-water interface and in interaction with lipid monolayer. Peptides composed of lysine and leucine with a ratio K$_i$L$_{2i}$ show for 9 residues a β-sheet structure. For the 15 residue analogue, an α-helical arrangement is detected although a 3$_{10}$-helix is predicted for this peptide sequence [69, 162]. (LLK)$_n$L with $n = 2$ or 4 show a helical structure and bind tightly to hydrophobic surface of polystyrene resin [74]. CD and IR spectroscopy measurements show that the longer peptide (KL$_4$)$_4$K has an α-helical structure and orients its helical axis parallel to the acyl chains in a mixed DPPC/DPPG bilayer [78]. In contrast, it shows a β-sheet structure in the denser DPPC bilayer [79].

3.3.3 Influence of Delocalization of the Side Chain Charge - Exchange of Lysine by Arginine

The DSC curves of DPPG mixtures with the arginine containing peptides (RG)$_4$R and (RA)$_4$R of a charge ratio of 1:1 are shown in Figure 3.3.11. As known from previous studies, arginine homopolymers are capable to cross the bilayer even at low temperatures [101, 217]. Introducing a spacer into the sequence of polyarginine, forming alternating peptide sequences (RX)$_n$R, influences the efficiancy to pass bilayer membranes. The length of the spacer between two neighboring arginines plays an inportant role in their ability to penetrate the bilayer. An echange of the natural occuring glycine spacer by the much longer artificial amino acid 6-amino-caproic acid shows an 2.5 fold increases of the cellular uptake measured by fluorescence spectroscopy [218]. With the ability of the peptide to cross the bilayer the question arises, if the enhanced permeability of the lipid bilayer also affects their thermotropic behavior.
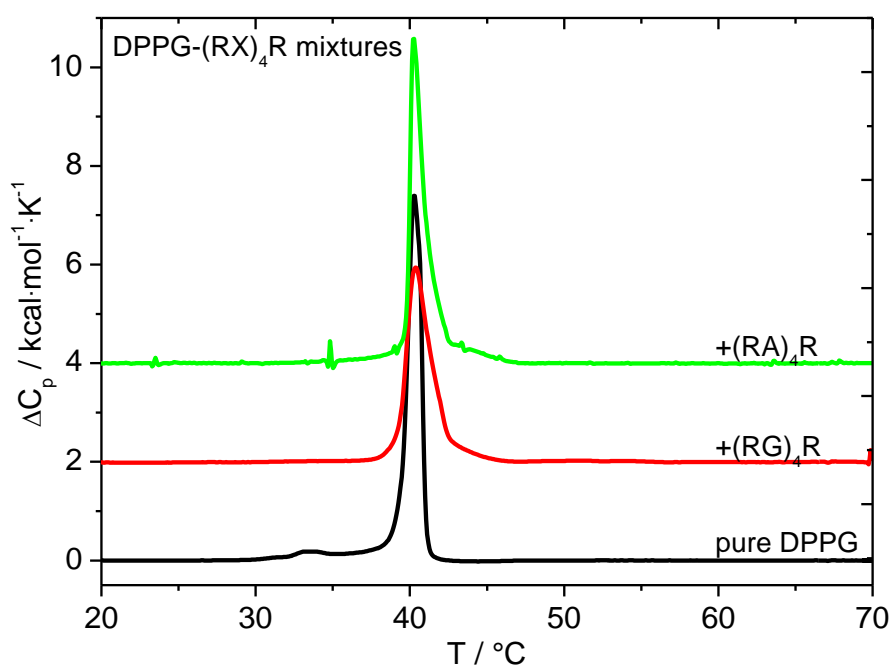
Figure 3.3.11: Thermogram of pure DPPG vesicles and different DPPG-(RX)$_4$R mixtures with a charge ratio R_c=1:1. The 2nd heating scan is shown, because equilibrium was only reached after passing the phase transition. Samples were prepared in aqueous 100 mM NaCl with a fixed lipid concentration of 2 mM.

The effect of added peptide on the phase transition temperature is marginable. Even at charge ratios of 1:1 no stabilization or destabilization of the gel phase is detectable, and a peak at 40.3 °C, the same temperature as for pure DPPG, is visible. The transition is boader and exhibits a small shoulder at the high temperature regime shifting the T_{mid} 0.5 °C upwards. For detailed comparison of the obtained parameters, Table 3.3.5.

Table 3.3.5: Overview of the thermodynamic data obtained from DPPG-(RX)$_4$R mixtures with a charge ratio of 1:1. T_m is the main phase transition and marked by the peak with the highest heat capacity and $T_{1/2}$ the full width of this peak at half maximum. ΔT_{base} is the width of the peak at its base and ΔH is the transition enthalpy.

	T_m / °C	T_{mid} / °C	$T_{1/2}$ / °C	ΔT_{base} / K	ΔH / kcal mol^{-1}
pure DPPG	40.3	40.2	1.5	3.5	10.4
+ (RG)$_4$R	40.4	40.7	1.8	3.7	8.4
+ (RA)$_4$R	40.3	40.6	1.0	2.9	9.6

Comparing the arginine containing with lysine containing peptides, an extensive domain formation is absent. Mosior and McLaughlin observed a ten-fold higher binding constant for arginine containing peptides [88]. An unaltered phase transition temperature can be a result of two competing processes which overlay each other, or a hint that there is no peptide binding to the bilayer. The latter explanation is unlikely as the sample shows also peptide induced aggregation.

Lipid CH$_2$ stretching bands of DPPG-(RX)$_4$R mixtures

For mixtures of DPPG with arginine containing peptides (RG)$_4$R and (RA)$_4$R the clear upshift of the phase transition to 48 °C is visible (see Figure 3.3.12, left panel). The transition ranges from 40 - 54 °C. The differences between both peptides are marginable. The ordering effect in the gel phase is visible, but levels off at the end of the transition at 54 °C. Based on the IR experiments there are no significant differences between (RG)$_4$R and (KG)$_4$K with respect to their influence on the acyl chain ordering in the DPPG bilayer.
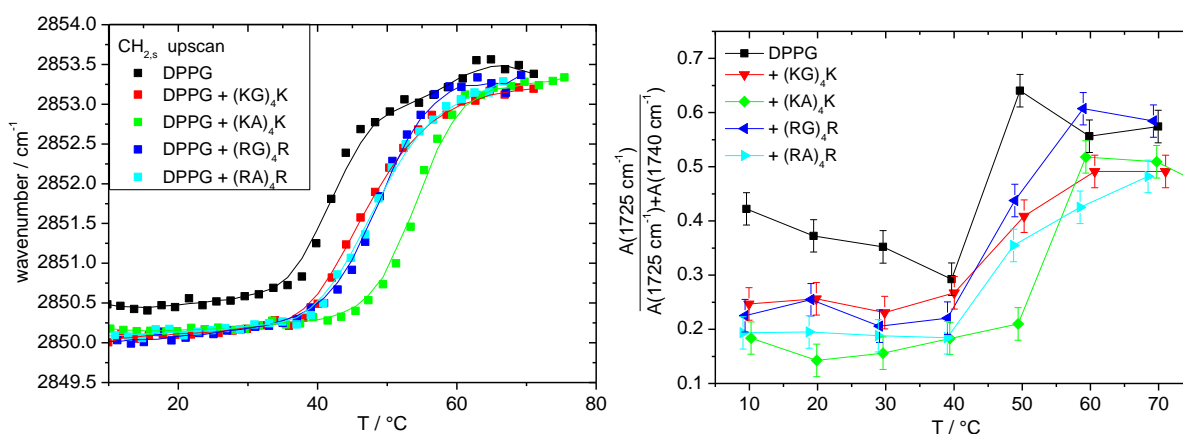
Figure 3.3.12: Left: wavenumber of the maximum of the symmetric CH$_2$ stretching band of pure DPPG and DPPG mixtures with peptides. The charged amino acid lysine was exchanged by arginine: (KG)$_4$K, (KA)$_4$K, (RG)$_4$R, (RA)$_4$R, respectively. Lines to guide the eye were constructed by an adjacent averaging of 5 points. Right: ratio of the area of hydrogen bonded ν(CO) vibrational band compared to the whole area of the carbonyl vibrational peak of pure DPPG and DPPG mixtures with peptides. All samples had a charge ratio R_c = 1:1 and were prepared in D$_2$O containing 100 mM NaCl at pD = 7.2.

Lipid C=O bands of DPPG-(RX)$_4$R mixtures

The added arginine peptides (RG)$_4$R and (RA)$_4$R behave similar to the corresponding lysine peptides and cause a reduction of the lipid hydration to the same extent in the gel phase (see Figure 3.3.12, right panel). At higher temperature the effect of (RG)$_4$R is imperceptible and the system shows similar behavior as pure lipid vesicles. The peptide (RA)$_4$R also reduces the hydrogen bonded fraction in the fluid state.

Peptide amide-I bands of DPPG-(RX)$_4$R mixtures

Spectra of the peptides (RG)$_4$R and (RA)$_4$R bound to DPPG bilayer are shown in Figure 3.3.13. The secondary structure of the tested peptides (RX)$_4$R is a mixture of turns and unordered arrangements.

Peptides with arginine show an additional band in their spectra due to the contributions of the antisymmetric and symmetric guanidyl stretching vibrations located at 1608 cm^{-1} and 1582 cm^{-1}, respectively [219]. A downshift of the absolute number of the guanidyl stretching vibrations from free peptide in aqueous solution compared to the bilayer bound arrangement is likely due to the hydrogen bonding with the phosphate group of the lipid. The slight linear reduction of these vibrations with temperature is thought to be an effect of decreased hydration at elevated temperatures.
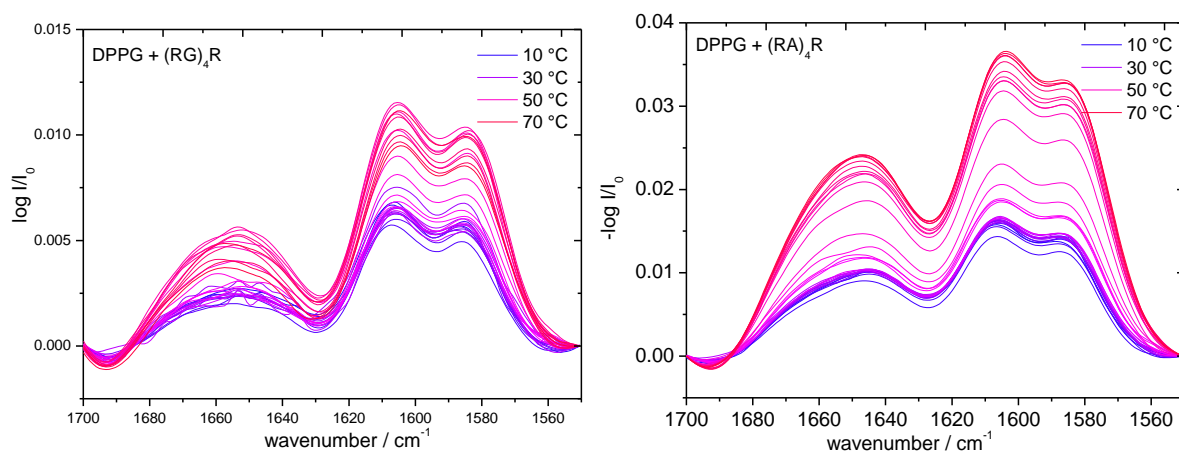
Figure 3.3.13: Temperature dependent behavior of the amide-I band for DPPG mixtures with different peptides (RX)$_4$R during the heating. Left: (RG)$_4$R-DPPG mixtures. Right: (RA)$_4$R-DPPG mixtures. The sample had a charge ratio R_c = 1:1 and was prepared in D$_2$O containing 100 mM NaCl at *pD* = 7.2.

Comparing the three tested peptides (RA)$_4$R, (RG)$_4$R and (KA)$_4$K reveals follows: the exchange of the charged amino acid of arginine by lysine shifts the phase trasition of DPPG mixed with (RA)$_4$R or (KA)$_4$K from 40 °C to 60 °C, whereas the exchange of the uncharged spacer amino acids in mixtures of DPPG with (RA)$_4$R or (RG)$_4$R causes no shift of the

transition temperature. Thus, the charged amino acid has a greater influence on the thermotropic behavior than the uncharged one. The electrostatic shielding is opposed by nonelectrostatic contribitions leading to a zero net effect on the DPPG phase transition.

Similar effects were also reported for homopeptides of argenine and lysine [104, 105]. An overlay of hydrophobic and electrostatic contributions was also discussed in DSC studies of DMPG or DPPG vesicles interacting with polyarginines of different chain length. Adittion of shorter polypeptides (R)$_9$ up to (R)$_{184}$ show a slight downshift of the lipid main transition, whereas the longer peptides increase T_m [105, 220]. The arginine side chain is more hydrophobic compared to lysine side chain [105, 221]. Additionally, the positive charge of arginine is delocalized in the guanidyl residue over at least four atoms in a π-system. It is known that the guanidinium moity is capable to build up a bidentate hydrogen bond with the lipid phosphate group [85, 86].

Furthermore, a different interaction between two charged residues was found in studies of separated ions, as well as small tri-peptides. The terminal ammonium moiety in the lysine side chain is completely surrounded by a layer of water and a repulsion of the two equal charges is present. The delocalization and the increased hydrophobicity of the guanidinium moiety enables a stacked conformation, stabilized by π-π interaction with the result of a less hydrated face above and below the molecular plane [222]. Guanidinium pairing, a structural motif for stabilization in several proteins, was also present in a theoretical calculation of the more biological tri-peptide RAR showing a distance of about 4 Å of both planes [223].

3.4   Interaction of (KA)₄K and (KAbu)₄K with Lipid Vesicles - Influence of the Lipid Structure

To study the influence of the lipid structure on binding, the peptides (KA)₄K and (KAbu)₄K were mixed with vesicles composed of different lipids. These peptides were chosen, because they already showed the large upshift of the main transition temperature upon interacting with DPPG vesicles, as discussed above. The lipid were altered in different ways to reveal the following effects a) increase the acyl chain lengths in PGs, b) introduction of one unsaturated chain into PG, c) change in size of the negatively charged headgroups, d) attachment of a zwitterionic headgroup.

3.4.1 Influence of Different Acyl Chains Attached to a Phosphatidylglycerol Headgroup

To test the influence of the acyl chain length and acyl chain saturation on the behavior of the lipid-peptide aggregates, measurements with DMPG, DPPG, DSPG, and POPG were performed.

3.4.1.1 Influence of Lipid Acyl Chain Lengths

The length of the acyl chain increases in the order DMPG, DPPG and DSPG concomitantly the main phase transition temperature increases from 23.2 °C, 40.3 °C to 53.3°C, and the transition enthalpy from 5.6 kcal mol⁻¹, 10.4 kcal mol⁻¹ to 12.3 kcal mol⁻¹ for DMPG, DPPG and DSPG, respectively. The results obtained here are in agreement with reported data [184]. The packing parameter for all three lipids is similar, as the headgroup is the same and differences in the length of the acyl chain compensate the effect of different chain volumes (see Table 2.2.1). For a better comparison of the DSC thermograms, a reduced temperature $T_{red} = T - T_m$, scaled to the main phase transition temperature of the pure lipid suspension was applied. Thus, the gel phase exists at negative values and the liquid-crystalline phase at positive ones.

Figure 3.4.1 shows thermograms of the pure PGs and their mixtures with (KA)₄K of a charge ratio PG:K of 1:1. For PGs with saturated acyl chains, two peaks are visible, one with a small transition enthalpy close to the transition temperature of the pure lipid, and the other main peak at elevated temperature. These both peaks are well separated for DMPG and DPPG, whereas the transition in mixtures with DSPG is very broad, unseparated and ranges over 20 K. The upshift of the transition scales with the length of the acyl chain, the shorter the chain, the larger the upshift. DMPG shows a $\Delta T = 22.3$ K, DPPG a $\Delta T = 19.7$ K and DSPG a $\Delta T = 15.8$ K. A reduced transition enthalpy for all three tested PG-peptide mixtures reveals a

similar effect of (KA)$_4$K, independent of the acyl chain length of the lipid. The increased transition enthalpy for DSPG-(KAbu)$_4$K mixtures is an exception and might be due to the very broad transition and the coupled uncertainties in ΔH determination.

All other parameters determined from mixtures of PGs with (KA)$_4$K and (KAbu)$_4$K are presented in Table 3.4.1. The stabilization of the gel phase is slightly enhanced in mixtures with the more hydrophobic peptide (KAbu)$_4$K.
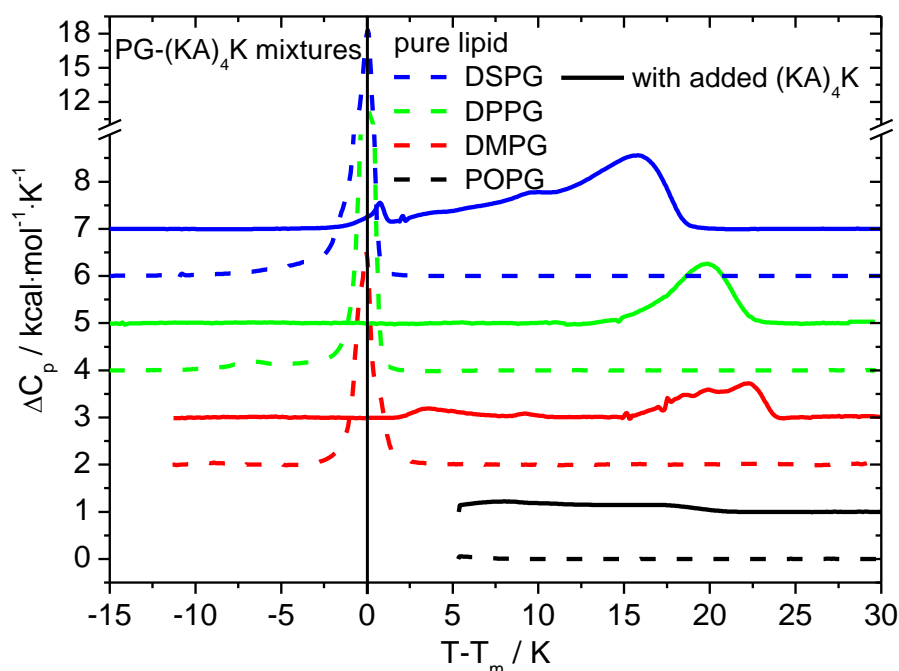
Figure 3.4.1: Thermogram of pure PG vesicles and different PG-(KA)$_4$K mixtures with a charge ratio R_c= 1:1. To compare all data a reduced temperature scale T - T_m, referring to the main transition temperature of the pure lipid is applied. The used PGs differ in acyl chain length or saturation. The 2nd heating scan is shown, because equilibrium was only reached after passing the phase transition. Samples were prepared in aqueous100 mM NaCl with a fixed lipid concentration of 2 mM.

3.4.1.2 Influence of Lipid Acyl Chain Unsaturation

DPPG with its two saturated palmitoyl chains is capable to arrange them in an *all-trans* conformation in the gel phase. This enables a relative dense packing of the molecules within the bilayer. In contrast, in the POPG molecule only the *sn*-1 chain can arrange in an *all-trans* conformation, whereas the unsaturation in the *sn*-2 chain inhibits such conformation. With the increased volume of the chain, the packing in the bilayer is less dense and a shorter effective length of the hydrophobic region increases the packing parameter.

Thermograms of pure POPG show only a baseline, as the instrument is not capable to measure below 0 °C. The phase transition of POPG was reported to be -2 °C [224]. In the mixture POPG with (KA)$_4$K, a transition starting below 2 °C up to 19 °C having its maximum at 6 °C is visible (see Figure 3.4.1). Thus, a similar stabilizing effect of the gel phase as

reported above is also possible for unsaturated lipids. The effect of the increased van der Waals interaction is less pronounced due to unsaturation and the coupled inherent looser packing. Compared with saturated PGs, the upshift with 8 K is much lower. The effect of peptide binding to bilayers composed of lipids with either multiple unsaturation in one chain or lipids with two unsaturated chains remains unclear, but it can be speculated that the phase transition temperature is upshifted by ca. 5 K as predicted for a complete charge neutralization [225].

Table 3.4.1: Overview of the thermodynamic data obtained from different PGs and their mixtures with (KA)$_4$K and (KAbu)$_4$K of a charge ratio of 1:1. The used PGs differ in acyl chain length or saturation. T_m is the main phase transition and marked by the peak with the highest heat capacity and $T_{1/2}$ the full width of this peak at half maximum. Especially for the asymmetric peaks with several shoulders T_{mid} obtained from the midpoint of the integral of the curves, is more suitable for a comparison. ΔT and ΔT_{mid} are the differences between the phase transition temperatures of the lipid in the mixture compare with them of pure lipid suspension. ΔT_{base} is the width of the peak at its base and ΔH is the transition enthalpy. n.d. not determined

	T_m / °C	T_{mid} / °C	ΔT / K	ΔT_{mid} / K	$T_{1/2}$ / °C	ΔT_{base} / K	ΔH / kcal mol^{-1}
pure POPG [224]	-2.0						6.2
+ (KA)$_4$K	6.2	9.5	8.2	11.5	n.d.	>20	>2.3
+ (KAbu)$_4$K	18.5	14.3	20.5	16.3	n.d.	>28	>4.8
pure DMPG	23.2	23.2			1.0	2.6	5.6
+ (KA)$_4$K	45.5	43.1	22.3	19.9	5.7	8.7	4.4
+ (KAbu)$_4$K	46.3	44.8	23.1	21.6	5.0	12.1	6.3
pure DPPG	40.3	40.2			1.5	3.5	10.4
+ (KA)$_4$K	60.0	59.4	19.7	19.2	4.3	7.7	6.3
+ (KAbu)$_4$K	62.9	62.2	22.6	22.0	1.7	8.1	5.3
pure DSPG	53.3	53.1			0.7	4.4	12.8
+ (KA)$_4$K	69.1	66.0	15.8	12.9	6.6	17.2	13.8
+ (KAbu)$_4$K	71.6	67.5	18.3	14.4	12.6	17.6	13.6

Lipid CH$_2$ stretching bands of PG mixed with (KAbu)$_4$K or (KL)$_4$K

The wavenumber of the symmetric methylene stretching vibration of pure PG vesicles and their mixtures with (KAbu)$_4$K are depicted in Figure 3.4.2, left panel. The curves obtained for the pure lipids are superimposed using the reduced temperature scale. Thus, a similar ordering of the acyl chains of the different lipids is evident independent of the acyl chain length and number of unsaturation.

For mixtures of DMPG and POPG with (KAbu)$_4$K of a charge ratio of 1:1, the phase transitions are shifted to higher temperatures similar to the discussed behavior in systems with DPPG. For pure POPG with a transition temperature of -2 °C the gel phase is experimentally unreachable. In mixture of POPG with (KAbu)$_4$K lower wavenumbers of ν_s(CH$_2$) are visible up to $\Delta T = 12$ K. The stabilization of the gel phase up to $\Delta T = 15$ K is seen for DMPG and DPPG. The ordering effect of the added peptide for fluid phase POPG vesicles is smaller as the wavenumber of the stretching vibration is comparable with that obtained for pure POPG vesicles.
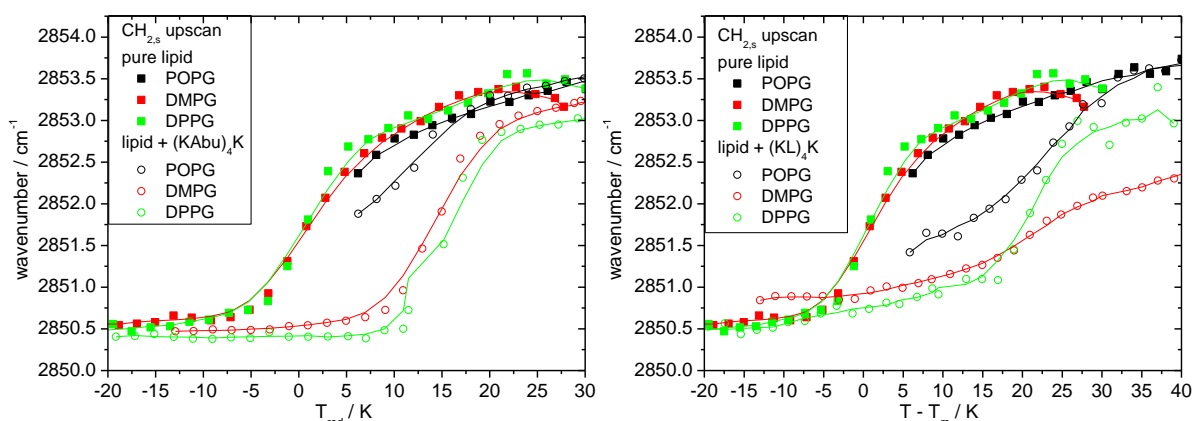

Figure 3.4.2: Wavenumber of the maximum of the symmetric CH$_2$ stretching band of pure PG and PG mixtures with (KAbu)$_4$K (left panel), or with the more hydrophobic peptide (KL)$_4$K (right panel). To compare all data a reduced temperature scale $T - T_m$, referring to the main transition temperature of the pure lipid is applied. The used PGs differ in acyl chain length or saturation. All samples had a charge ratio $R_c = 1$:1 and were prepared in D$_2$O containing 100 mM NaCl at $pD = 7.2$. Lines to guide the eye were constructed by an adjacent averaging of 5 points.

After binding of (KL)$_4$K, ΔT is higher for all three lipids compared to PG-(KAbu)$_4$K mixtures. The lipid phase transition appears to be broader or no clear transition is visible for DMPG-(KL)$_4$K mixtures. This more continuous increase might be a result of the tightly bound peptide layer on top of the bilayer, which hinders lipid rotation.

Lipid C=O bands of PG mixed with (KAbu)$_4$K or (KL)$_4$K

With the addition of the peptide, the interfacial region of the lipid bilayer becomes less hydrated, independent of the lipid, its phase state, or the added peptide. Lipid mixtures with (KAbu)$_4$K show an increase of hydration in the same temperature range, where the acyl chain melting occurs. Interestingly, there are no differences between the three PGs, underlining the finding that the main interaction takes place in the headgroup region. The acyl chain region plays only a minor role. The lowest ratio of hydrogen bonded carbonyl groups are found in mixtures with (KL)$_4$K (see Figure 3.4.2, right panel). The very effective shielding of the lipid

bilayer against water penetration by $(KL)_4K$ is very likely a result of the stable β-sheet layer on top of the lipid membrane (see below).
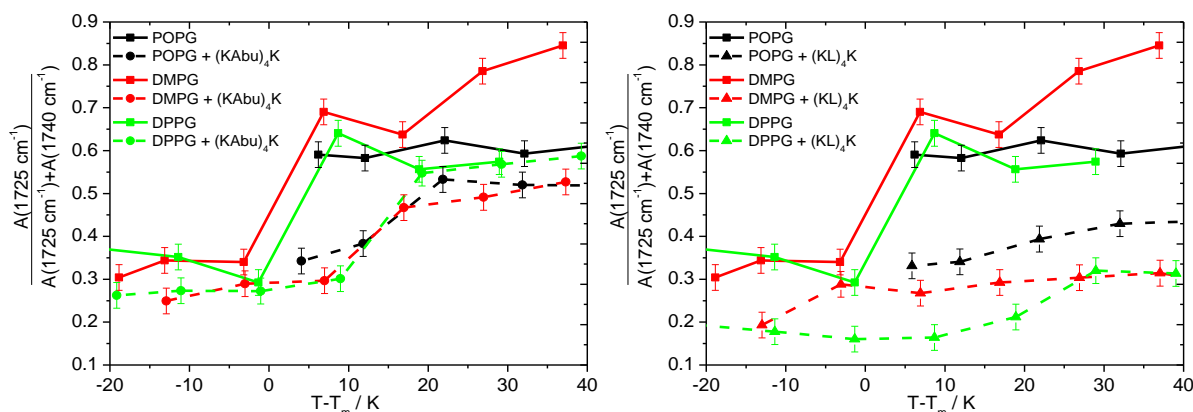

Figure 3.4.3: Ratio of the area of hydrogen bonded ν(CO) vibrational band compared to the whole area of the carbonyl vibrational peak of pure PG and PG mixtures with $(KAbu)_4K$ (left panel), or with the more hydrophobic peptide $(KL)_4K$ (right panel). To compare all data a reduced temperature scale $T - T_m$, referring to the main transition temperature of the pure lipid is applied. The used PGs differ in acyl chain length or saturation. All samples had a charge ratio $R_c = 1:1$ and were prepared in D_2O containing 100 mM NaCl at $pD = 7.2$.

Peptide amide-I bands of PG mixed with $(KAbu)_4K$ or $(KL)_4K$

The mixtures with $(KAbu)_4K$ show a rearrangement of the secondary structure from a β-sheet to unordered structure, which is connected with the phase transition of the lipid (see Figure 3.4.4, left panel). The rearrangement appears at 12 °C, 38 °C, and 57 °C for mixtures with POPG, DMPG, and DPPG, respectively. The adsorbed β-sheet structure remains stable up to 14 or 16 K above the phase transition temperature of the pure lipid. The analysis of the amide-I bands reveals some structural differences of the peptide, when bound to PGs with saturated acyl chains compared to POPG with one unsaturated chain. In mixtures of $(KAbu)_4K$ with DMPG (see Figure 8.3.3) and DPPG, nearly no contribution from unordered structures is visible. The fraction of bound peptide in a β-sheet conformation to gel phase lipids is higher, compared to mixtures with POPG. In these mixtures more than 25 % unordered structures are found (see Figure 3.4.5). The explanation for this behavior might be that the chain order at low temperature is much higher for saturated lipids. Thus, the headgroup distances match better for a β-sheet adsorption.

After addition of $(KL)_4K$ to different PGs, no β-sheet rearrangement is observed upon heating. The bound antiparallel β-sheet structure remains stable above the acyl chain melting temperature of the lipid.

To further analyze the peptide conformation, a fitting of the obtained spectra in the amide-I region with three peaks, centered at 1670 cm^{-1} for β-turns and 1646 cm^{-1} for unordered

conformations and 1616 cm^{-1} for β-sheets, with a Gaussian profile were used to determine the relative areas of the peaks. The mixture POPG-(KL)$_4$K shows 24% unordered conformation, 66% β-sheet, and 10% β-turns. This fits quite well with the structural data found for (KL)$_{10}$, a longer chain homologue, bound to POPG vesicles (30% unordered conformation, 52% β-sheet, and 18 % β-turns) [226].
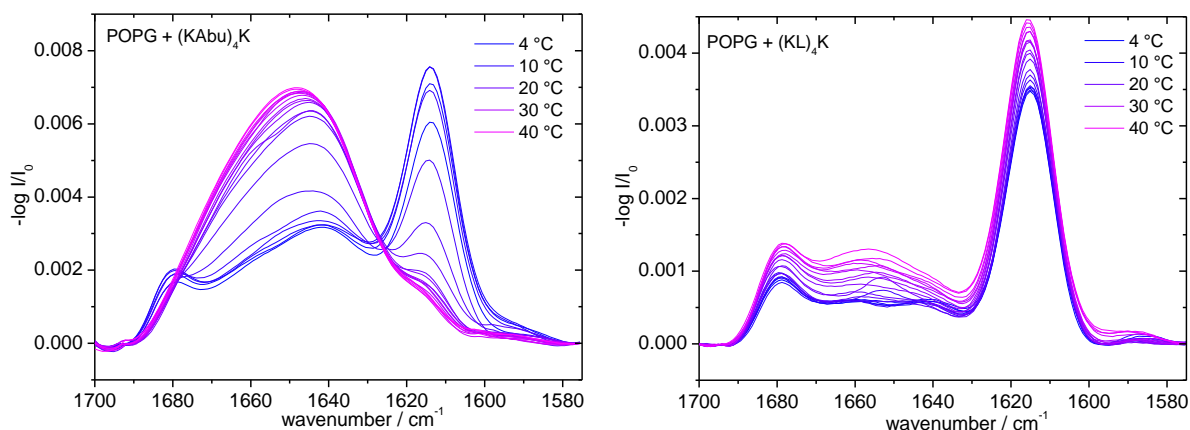

Figure 3.4.4: Temperature dependent behavior of the amide-I band for POPG mixtures with (KAbu)$_4$K (left panel), or with the more hydrophobic peptide (KL)$_4$K (right panel). POPG-(KAbu)$_4$K mixtures show a β-sheet secondary structure at low temperatures with amide peaks at 1680 cm^{-1} and 1615 cm^{-1}, which converts into an unordered structure at higher temperature (amide-I peak at 1646 cm^{-1}). POPG-(KL)$_4$K mixtures show a β-sheet secondary structure for the whole tested temperature range. All samples had a charge ratio R_c = 1:1 and were prepared in D$_2$O containing 100 mM NaCl at pD = 7.2.

The bound peptide with its positively charged lysine residues screens the negative charges of the PG headgroups. Thus, the electrostatic repulsion between neighboring headgroups is reduced, the headgroup demands less space, and a better chain packing leads to a higher T_m. A dehydration of the headgroup region contributes to the upshift. PGs of different chain length have similar headgroup areas and tilt angle of the acyl chains in the gel phase, only the bilayer thickness is altered (see Table 2.2.1). Upon peptide addition, the change in interfacial headgroup area is thought to be similar, but the relative increase of the van der Waals attraction is different for the different acyl chains. The short myristoyl chains have fewer contacts compared to the longer stearoyl chains.

Studies of DMPG and DPPG bilayer systems with pentalysine and peptides with shorter side chains reveal some contribution of hydrophobic interaction between the peptide side chains and the lipid acyl chain region [123]. However, the chain length dependence of the T_m shift found here, clearly shows that electrostatic effects mainly drive the interaction between peptides and PG. With increasing the chain length of the PGs, the effect of additional stabilization of the gel phase by peptide binding is reduced.
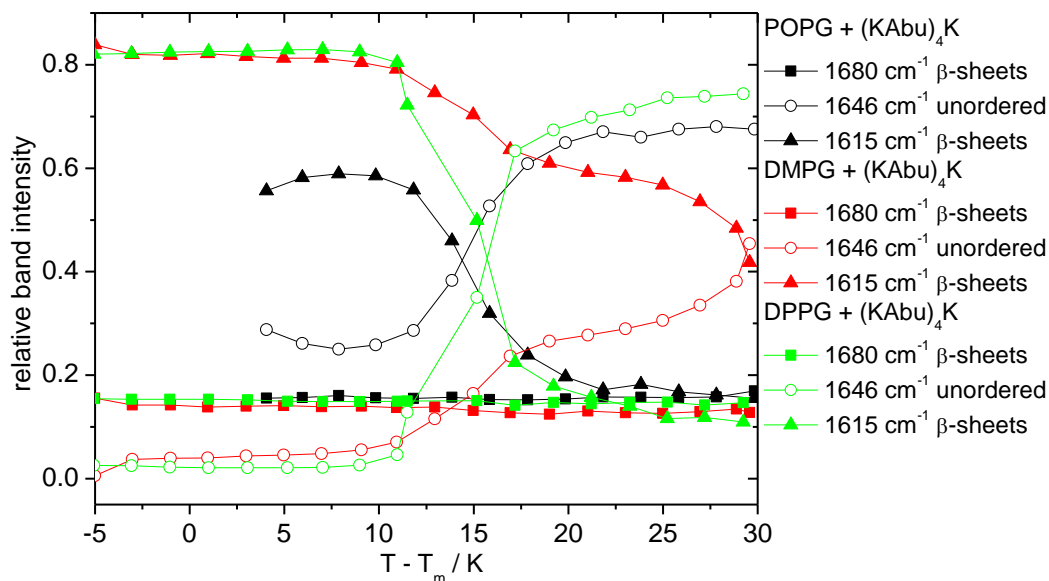
Figure 3.4.5: Peak intensity of amide-I band components as a function of temperature clearly showing changes in secondary structures upon heating. To compare all data a reduced temperature scale $T - T_m$, referring to the main transition temperature of the pure lipid is applied. The used PGs differ in acyl chain length or saturation. Mixtures of (KAbu)$_4$K with POPG (black symbols), DMPG (red symbols), and DPPG (green symbols) and show a β-sheet secondary structure at low temperatures with amide peaks at 1680 cm^{-1} (■) and 1615 cm^{-1} (▲), which converts into an unordered structure at higher temperature (amide-I peak at 1646 cm^{-1} (O)). All samples had a charge ratio R_c = 1:1 and were prepared in D$_2$O containing 100 mM NaCl at pD = 7.2.

3.4.2 Influence of the Lipid Headgroup Structure on Peptide Binding

The dependence on the lipid-peptide interaction on the anionic headgroup structure was tested by using lipid systems with myristoyl chains of phosphatidic acid (PA), phosphatidylserine (PS), cardiolipin (CL), and PG: DMPA, DMPS, TMCL, and DMPG, respectively.

All tested lipids adopt lamellar phases at neutral pH and a NaCl concentration of 100 mM. Common for all lipids is their ability to build up hydrogen bonds between neighboring lipids in the headgroup region. DMPA has the smallest headgroup among the lipids mentioned above. Direct hydrogen bonds between the lysine or arginine side chain and the lipid headgroup may build up after binding. DMPS has a special headgroup structure as the attached amino acid serine is itself zwitterionic, but the headgroup charged due to the negative charge at the phosphate group. The positive charge (-NH$_3^+$) might cause some local repulsion and decrease the stabilizing effect of the bound peptide. TMCL is a lipid with formally two negative charges. Due to its four acyl chains the packing parameter is slightly larger than 1. Several studies have shown that the charge of a TMCL molecule is between -1 and -2 at neutral pH [65, 66, 227].

Although all tested lipids have myristoyl chains, their transition temperature is quite different. DMPG shows a phase transition at 23 °C, DMPS at 37 °C, TMCL at 40 °C, and DMPA at 50 °C, respectively [2]. To compare all tested lipid systems and their mixtures with (KA)$_4$K a reduced temperature scale (scaled to pure lipid phase transition temperature) is applied. The obtained results are presented in Figure 3.4.6 and Table 3.4.2.

All lipid-peptide mixtures show an upshift of the phase transition to higher temperature after peptide binding. The shape of the transition peak is different for all lipid-peptide mixtures. The occurrence of several peaks is a hint for domain formation in the sample, as seen before for DPPG mixture with different peptides (KX)$_4$K (section 3.3.1) or polylysines [104]. A separation in lipid-rich and peptide-rich domains occurs, because of local differences upon incomplete mixing or sterical crowding. The extent of the upshift of T_m increases for lipids with myristoyl chains as follows: PS < PG < PA < CL and ranges from 14 up to 29 K (see Table 3.4.2).
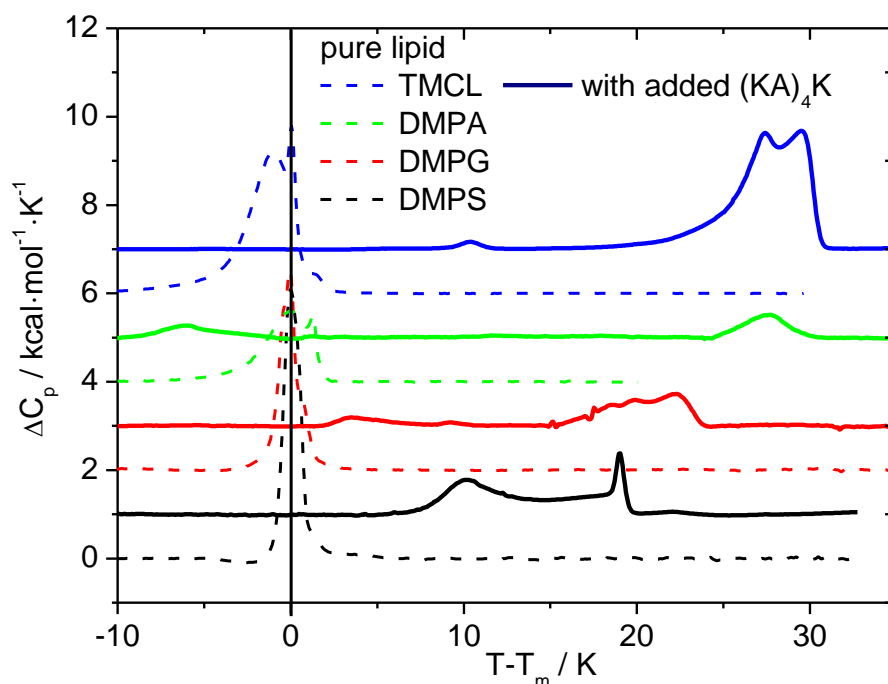
Figure 3.4.6: Thermogram of pure lipid vesicles and different lipid-(KA)$_4$K mixtures with a charge ratio R_c = 1:1. To compare all data a reduced temperature scale $T - T_m$, referring to the main transition temperature of the pure lipid is applied. The used anionic lipids had different headgroup structures. The 2nd heating scan is shown, because equilibrium was only reached after passing the phase transition. Samples were prepared in aqueous 100 mM NaCl with a fixed lipid concentration of 2 mM.

The observed upshift of the transition temperature in the lipid mixtures with peptides has several origins. Probably the packing parameter plays a role for the extent of the stabilization of the lipid gel phase with the overall trend, the smaller the headgroup, the larger the upshift.

Sterical constraints, which allow a better packing of the peptide on bilayers with smaller headgroups could be also present.

The binding constant of the peptide to the corresponding lipid headgroup might also be different. A stronger interaction of the peptide with the headgroups of DMPA or TMCL over DMPG and DMPS is possible. Experimental evidence was found for the association of polylysine to vesicles of PG, PS, or CL, revealing a relative association constant of 1.0, 1.1, and 1.7, respectively [228]. A comparison of the binding constants of Ac-(KA)$_4$K-NH$_2$ to POPG and POPS vesicle reveal similar binding stoichiometries for charge neutralization, but a 20 % steeper slope for PS vesicles indicating slightly stronger binding [88].

Table 3.4.2: Overview of the thermodynamic data obtained from different anionic lipids and their mixtures with (KA)$_4$K and (KAbu)$_4$K of a charge ratio of 1:1. The used anionic lipids had different headgroup structures. T_m is the main phase transition and marked by the peak with the highest heat capacity and $T_{1/2}$ the full width of this peak at half maximum. Especially for the asymmetric peaks with several shoulders T_{mid} obtained from the midpoint of the integral of the curves, is more suitable for a comparison. ΔT and ΔT_{mid} are the differences between the phase transition temperatures of the lipid in the mixture compare with them of pure lipid suspension. ΔT_{base} is the width of the peak at its base and ΔH is the transition enthalpy. n.d. not determined

	T_m / °C	T_{mid} / °C	ΔT / K	ΔT_{mid} / K	$T_{1/2}$ / °C	ΔT_{base} / K	ΔH / kcal mol^{-1}
pure DMPS	37.3	37.2			1.1	4.0	7.6
+ (KA)$_4$K	56.2	51.3	18.9	14.1	9.7	12.3	5.8
+ (KAbu)$_4$K	55.7	51.7	18.4	14.5	0.7	10.0	5.7
pure DMPG	23.2	23.2			1.0	2.6	5.6
+ (KA)$_4$K	45.5	43.1	22.3	19.9	5.7	8.7	4.4
+ (KAbu)$_4$K	46.3	44.8	23.1	21.6	5.0	12.1	6.3
pure DMPA	51.3	50.1			0.8	5.9	5.8
+ (KA)$_4$K	77.6 (43.7)	77.6 (44.1)	26.3	27.5	5.3 (3.0)	8.7 (5.8)	1.8 (1.0)
+ (KAbu)$_4$K	78.0	77.9	26.7	27.8	4.0	7.5	4.0
pure TMCL	40.3	38.9			2.6	5.0	12.7
+ (KA)$_4$K	69.8	67.9	29.5	29.0	4.3	7.3	13.5
+ (KAbu)$_4$K	70.5	69.0	30.2	31.1	4.6	7.4	4.9

The exception of this general behavior is DMPA. It is the only sample in this study, where a transition peak below the phase transition of the pure lipid is visible. This destabilization of the gel phase might be explained with another lipid-peptide arrangement, where the

hydrophobic parts of the peptide insert into the acyl chain region and perturb the van der Waals interaction. This is more probable for DMPA because sterical shielding is absent, and a closer contact between lipid acyl chain and peptide is possible. Another explanation of the peak might be the formation of domains composed of fully protonated DMPA in the sample. The phase transition observed at 44 °C coincides with those observed for fully protonated DMPA [64].

The hydrogen bonds in the headgroup region also influence the main phase transition temperature. DSC and ESR measurements show an upshift of the transition temperature up to 19 K for DMPG, DPPG and DMPS vesicles upon protonating the headgroup, whereas the transition temperature of DMPA is only 3 K upshifted [229, 230].

Lipid CH$_2$ stretching bands of anionic lipids mixed with (KAbu)$_4$K or (KL)$_4$K

To monitor the phase state and the acyl chain order of the lipid the symmetric stretching vibration of the methylene group in the acyl chains of the lipids was chosen. To compare all tested lipids with their different transition temperatures, again a reduced temperature scale is used. The obtained wavenumbers in both phases are similar for all tested lipids showing a comparable acyl chain order in the hydrophobic region independent of the attached lipid headgroup. The phase transition temperatures of the pure lipids determined by ATR-IR are 24 °C, 39 °C, 42 °C, and 52 °C and thus slightly higher compared to the DSC results showing a T_m of 23.2 °C, 37.3 °C, 40.3 °C, and 51.3 °C for DMPG, DMPS, TMCL, and DMPA, respectively.

Binding of (KAbu)$_4$K

Addition of (KAbu)$_4$K to the lipids has no significant influence on the v(CH$_2$) wavenumbers in the gel phase The peptide side chains apparently do not penetrate the acyl chain region and do not disturb their order. The lipid-peptide interaction is restricted to the headgroup region. As seen before in DSC experiments, the phase transition of the lipid occurs at higher temperatures compared to pure lipid systems (see Figure 3.4.7 left panel). The upshift of phase transition ranges from $\Delta T = 11$ K for DMPS, 12 K for DMPA over 15 K for DMPG up to 19 K for TMCL.

Comparing the results from DSC and ATR-IR experiments, all T_m-values determined by IR are 6 °C up to 14 °C below those obtained from DSC experiments. The different temperatures of the transition in both experiments might have an origin in the different heating rates used in both experiments. In ATR-IR experiments, a slower heating rate (roughly 6 K h^{-1} compared to

60 K h^{-1} in DSC) is employed. The obtained midpoints of the transition are in good agreement with the onset temperatures of the peaks in the DSC experiments. In the DSC thermograms, the peak is smeared out over a temperature range of 10 K and the temperatures T_{mid} and T_m differ up to 5 K.

For all the mixtures, the stretching vibrations in the fluid phases of are located at similar or slightly lower wavenumbers compared to pure lipid systems suggesting an unperturbed hydrophobic acyl chain region of the lipid bilayer.
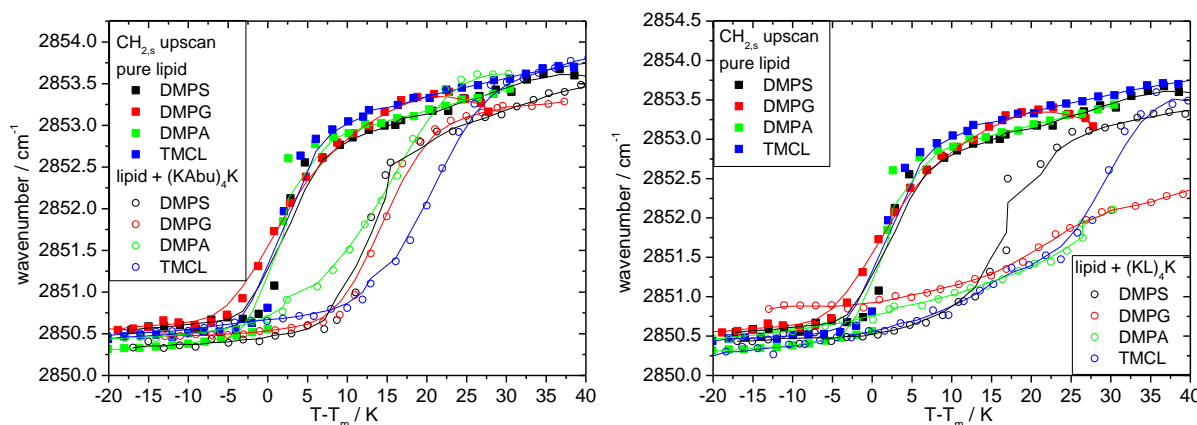

Figure 3.4.7: Wavenumber of the maximum of the symmetric CH₂ stretching band of pure anionic lipid and lipid mixtures with (KAbu)₄K (left panel), or with the more hydrophobic peptide (KL)₄K (right panel). To compare all data a reduced temperature scale $T - T_m$, referring to the main transition temperature of the pure lipid is applied. The used anionic lipids had different headgroup structures. All samples had a charge ratio R_c = 1:1 and were prepared in D₂O containing 100 mM NaCl at pD = 7.2. Lines to guide the eye were constructed by an adjacent averaging of 5 points.

Binding of (KL)₄K

The analysis of $\tilde{v}$ vs. T_{red} for mixtures of negatively charged lipids with (KL)₄K are more complicated compared to mixtures with (KAbu)₄K (see Figure 3.4.7, right panel). Addition of (KL)₄K to DMPS stabilizes the gel phase of DMPS and increases the phase transition to 54 °C. This shift is larger than the one observed after binding of (KAbu)₄K.

From the $\tilde{v}$ vs. T_{red} plots of DMPG, DMPA, and TMCL it is difficult to decide, if a phase transition occurs or only a continuous process takes place. DMPG was discussed above comparing PGs with different acyl chains. Briefly, the wavenumber of the vibration is increased in the gel phase and decreased in the fluid phase, thus the difference in $\Delta\tilde{v}$ between gel and fluid phase is halved.

In DMPA-(KL)₄K mixtures in the gel phase, the peak maxima are similar to pure DMPA. In the observed temperature range only a slight increase of $\tilde{v}$ (CH₂) is visible and the wavenumbers are 2 cm^{-1} below the ones for pure DMPA at the same temperature. In the DSC curves of DMPA-(KAbu)₄K, the transition takes place at 78 °C and it is probable that the

transition of DMPA mixtures with (KL)$_4$K takes place at even higher temperature and thus above the tested experimental range.

The acyl chain vibrations of TMCL in the mixtures with (KL)$_4$K are comparable to those obtained for pure lipid. Upon heating the wavenumbers only slightly increase up to 25 K above the phase transition of pure TMCL. A phase transition at 30 K is detected due to a sharp increase of the wavenumber. The observed transition temperature is in good agreement with the peak obtained in the thermogram.

Lipid C=O bands of anionic lipids mixed with (KAbu)$_4$K or (KL)$_4$K

For the mixtures of DMPG, DMPA, DMPS, and TMCL with the peptides the following general trends are observed. Peptide binding to anionic lipid bilayer lowers the ratio of hydration in the gel phase due to coverage of the interfacial region with a peptide layer built up of antiparallel β-sheets. As known from DSC experiments and the results from the acyl chain vibration, the lipid phase transition is upshifted to higher temperature. For mixtures of DMPS and DMPG with (KAbu)$_4$K, the increase of hydrogen bonded carbonyl groups occurs 10 K above the transition of pure lipids (see Figure 3.4.8, left panel), corresponding with the acyl chain melting.
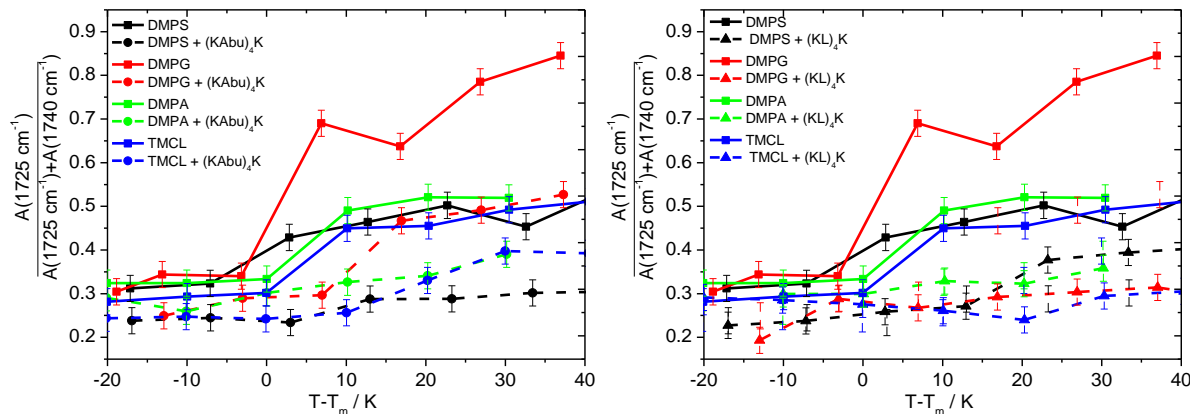
Figure 3.4.8: Ratio of the area of hydrogen bonded v(CO) vibrational band compared to the whole area of the carbonyl vibrational peak of pure anionic lipid and lipid mixtures with (KAbu)$_4$K (left panel), or with the more hydrophobic peptide (KL)$_4$K (right panel). To compare all data a reduced temperature scale $T - T_m$, referring to the main transition temperature of the pure lipid is applied. The used anionic lipids had different headgroup structures. All samples had a charge ratio R_c = 1:1 and were prepared in D$_2$O containing 100 mM NaCl at pD = 7.2.

The other two lipids DMPA and TMCL mixed with (KAbu)$_4$K show no strong increase of the ratio. Thus, it is suggested that there is no transition, which leads to increased hydration. In the mixtures with (KL)$_4$K, little changes in hydration occur over the whole temperature range for DMPG, DMPA, and TMCL, and just DMPS shows a slight increase (see Figure 3.4.8, right panel).

Similar effects of a lower hydration of the bilayer were also reported for vesicles composed of POPC/POPS with bound (K)$_{10}$ or (R)$_{10}$ [231].

Peptide amide-I bands of anionic lipids mixed with (KAbu)$_4$K or (KL)$_4$K

For all different anionic lipids, the added peptide forms defined secondary structures, when bound to the bilayers. The peptides (KAbu)$_4$K and (KL)$_4$K are hydrophobic enough to self-assemble into a β-sheet at lower temperature bound to gel phase lipids (see Figure 3.4.9 and Figure 8.3.3). The headgroup structure of the used lipid is irrelevant as long as a negative charge is present. The stability of the β-sheet upon heating is determined by the critical packing parameter, i.e. the size of the headgroup and to some extent on the hydrophobicity of the uncharged spacer.
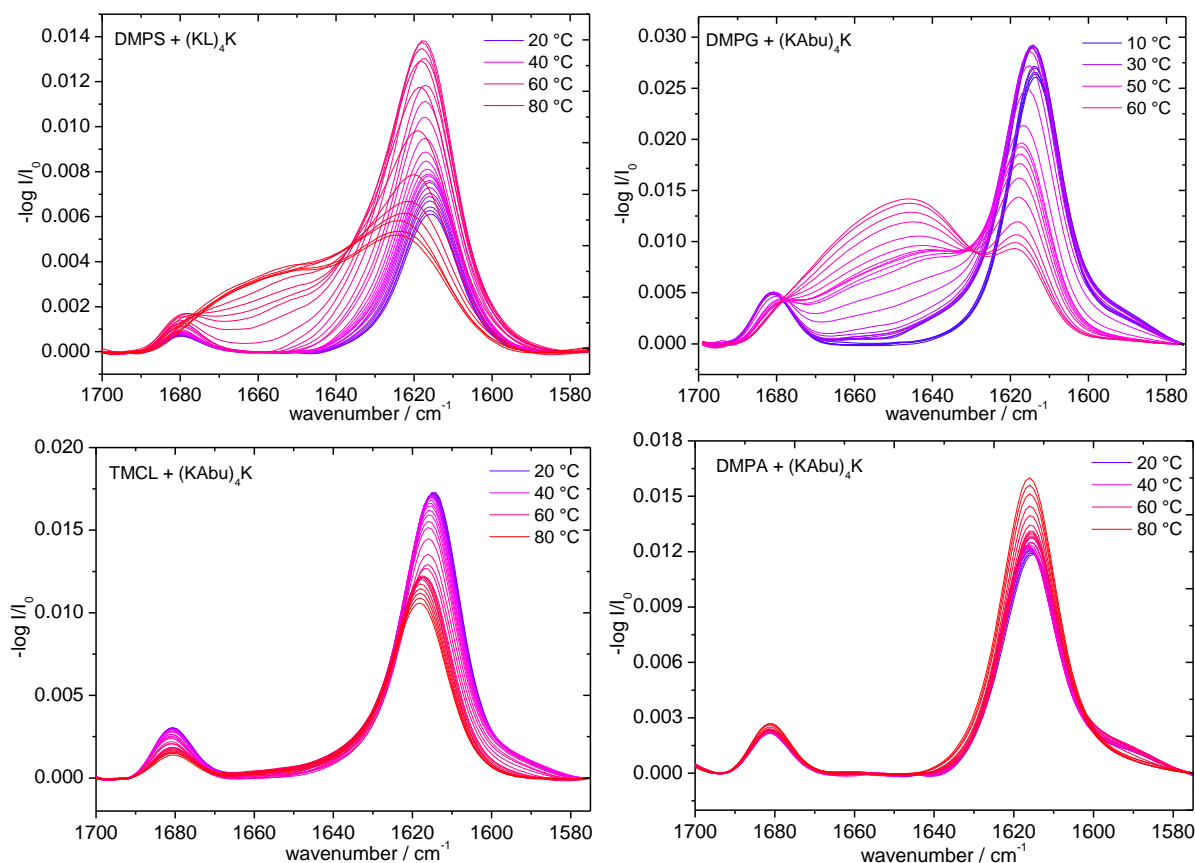
Figure 3.4.9: Temperature dependent behavior of the amide-I band for anionic lipids mixed with (KAbu)$_4$K or with the more hydrophobic peptide (KL)$_4$K. DMPS-(KL)$_4$K mixtures (top left) and DMPG-(KAbu)$_4$K mixtures (top right) show a β-sheet secondary structure at low temperatures with amide peaks at 1680 cm^{-1} and 1615 cm^{-1}, which converts into an unordered structure at higher temperature (amide-I peak at 1646 cm^{-1}). TMCL-(KAbu)$_4$K mixtures (bottom left) and DMPA-(KAbu)$_4$K mixtures (bottom right) show a β-sheet secondary structure for the whole tested temperature range. All samples had a charge ratio R_c = 1:1 and were prepared in D$_2$O containing 100 mM NaCl at pD = 7.2.

For mixtures with DMPS, having the largest headgroup, a rearrangement from β-sheets to random coil structures occurs for (KAbu)$_4$K and for (KL)$_4$K. The conformational transition of (KAbu)$_4$K bound to DMPS bilayers occurs at 52 °C. A decrease of the bands originating from the β-sheet at 1680 and 1615 cm^{-1} and an increase of the band located at 1646 cm^{-1}, representing unordered structures, is observed. In (KL)$_4$K-DMPS mixtures, the β-sheet is more stable due to a higher hydrophobicity of the uncharged spacer leucine. The conformational change of the peptide occurs at 61 °C.

A similar rearrangement was observed for (KAbu)$_4$K bound to DMPG, where the peptide undergoes a reordering, which is coupled with the lipid chain melting. In DMPG-(KL)$_4$K mixtures, the β-sheet structure remains stable in the fluid phase of the lipid bilayer at elevated temperatures (see section 3.3.1).

The lipids DMPA and TMCL with smaller headgroups compared to DMPG and DMPS are able to stabilize (KAbu)$_4$K as well as (KL)$_4$K in its antiparallel β-sheet arrangement over the whole temperature range without any rearrangement.

Beside the changes of the thermotropic behavior of the mixtures induced upon lipid-peptide interaction, other features like the peptide arrangement, or the tilt angle of the lipid acyl chains are also affected and contribute to the stabilization of the gel phase.

A selectivity of antimicrobial peptides towards different kinds of anionic lipid headgroups was presented before, revealing some specific modes of interaction beside the effect of charge compensation and hydrophobic contributions. The α-helical magainin effectively forms pores in vesicles containing PG at a low peptide to lipid ratio. For the other tested lipids PS, PA and CL much higher peptide ratios are necessary to induce leakage [232]. Protegrin-1, a small β-sheet forming peptide, distinguishes between different negatively charged headgroups. The bound peptide shows minor effects on the main phase transition of PA membranes, whereas a preferential interaction with fluid phase PS reduces the phase transition temperature. An induced phase separation into lipid-rich and peptide-rich domains creates an additional peak in the thermograms of PG membranes [233]. All those results show that in addition to the overall negative charge, the structural features of the phospholipid headgroups and the lipid packing are important for the interaction with the peptide. A coupling of the thermotropic phase behavior of the lipid-peptide mixtures with the critical packing parameter is discussed in the next section.

Connection of cpp with ΔT after peptide binding

A direct connection of the critical packing parameter *cpp* with the extent of the upshift of the main phase transition *ΔT* is found for all negatively charged lipids and their interaction with the cationic model peptide (KAbu)$_4$K (see Figure 3.4.10). The larger the headgroup of the lipid, and the smaller the cpp, the lower the upshift of the main phase transition of the lipid-peptide mixture.

This effect seems to have geometrical reasons, as a better lipid-peptide binding is achieved for lipids with smaller headgroups. The stabilization of the gel phase of PGs is similar for lipids with saturated acyl chains. Comparing anionic lipids with myristoyl chains, the upshift of the phase transition increases in the same order as the calculated critical packing parameter.

Comparing the published results, the secondary structure of peptides bound to anionic lipid bilayers is determined on the one hand by the peptide sequence and length, and on the other hand on the lipid headgroup. The stability of the peptide structure is determined by its length, short PLL chains rearrange to unordered structures at the lipid phase transition and long PLL retain their structure also in the fluid phase [234]. Binding of these peptides lead to effective different cross sectional areas of the lipid headgroups, because the charge repulsion is reduced upon binding of positively charged molecules. In the gel phase the tilt angle for the acyl chains of PA is reduced from 27° obtained for pure lipid system [235] to nearly 0° when PLL is bound as β-sheet [236]. Furthermore, the small headgroup of PA and the direct ability to build up hydrogen bonds between the lysine side chains and the easy accessible lipid phosphate group may be contribute to the interaction.
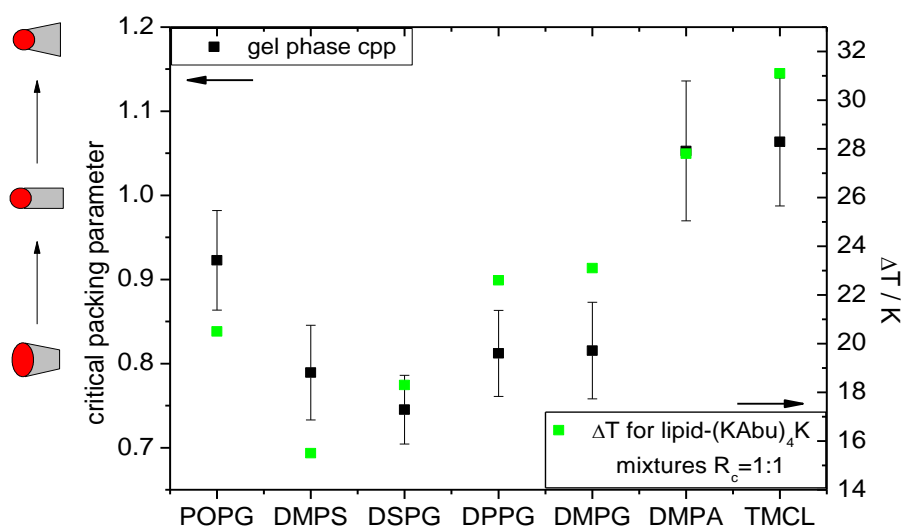

Figure 3.4.10: Comparison of thermotropic behavior and the critical packing parameter for negatively charged lipids

In contrast, PLL adsorption to PG and PS membranes induces the formation of α-helices [108, 109, 237]. This is true for long PLL chains. Shorter chains retain their unordered structures. The larger headgroups of PG and PS prevent a β-sheet arrangement as the cross sectional area of one lysine residue is calculated to 31-33 Å^2 [236]. The differences between the sterical demand of the acyl chain and cross sectional area of the lipid headgroup forces some lipids to tilt the acyl chains with respect to the bilayer normal. The acyl chain tilt angle of DPPG without and with bound α-helical PLL remains unaltered at a value of 30° [109]. The situation with the alternating peptides $(KX)_4K$ used in this study is more complicated. A detailed discussion how a stable peptide-bilayer stack can be formed, is given below.

3.4.3 Influence of the Headgroup Charge - Peptide Interaction with Zwitterionic Lipids

The experiments discussed above were performed with PG, a negatively charged lipid, which can bind the added peptides through electrostatic interaction. By changing the headgroup from the glycerol to an ethanolamine or choline residue the headgroup becomes zwitterionic and the whole lipid formally uncharged. In the absence of a net negative charge, the peptide should bind only due to hydrophobic interaction or some specific headgroup peptide interaction.
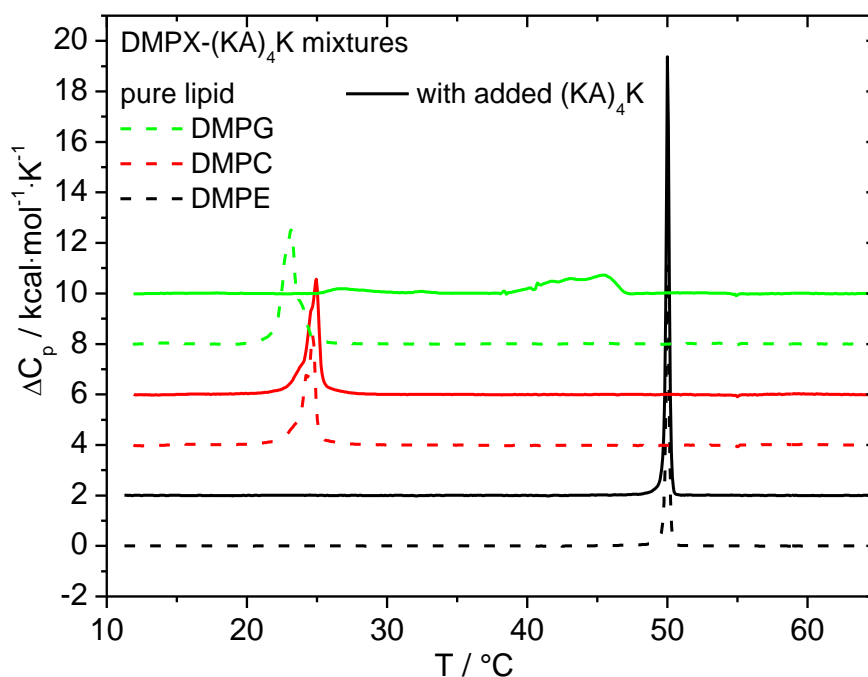

Figure 3.4.11: Thermogram of pure lipid vesicles and different lipid-$(KA)_4K$ mixtures with a charge ratio R_c = 1:1. DMPC and DMPE are zwitterionic, whereas DMPG is negatively charged. The 2nd heating scan is shown, because equilibrium was only reached after passing the phase transition. Samples were prepared in aqueous 100 mM NaCl with a fixed lipid concentration of 2 mM.

In Figure 3.4.11 it is clear visible that the thermotropic behavior of the mixtures is not changed after peptide addition. For PE and PC, no shift of the phase transition occurs and the transition enthalpy remains unaltered. Without negatively charge headgroups, the binding of the peptide is weak and nearly all peptide remains in the bulk solution. (KA)$_4$K is relative hydrophilic, but adding the more hydrophobic (KV)$_4$K to PE and PC shows also no changes of the phase transition temperatures. Although, both tested headgroup contain a negatively charged phosphate group, which is capable to build up electrostatic interaction with the lysine side chains, the close proximity of the positively charged nitrogen in the headgroup hinders an approach of the peptide due to its positive charge. Thus, the repulsion of both positive charges is larger than the possible hydrophobic interaction.

The effect of the lipid headgroup on the interaction with cationic peptides, e.g. polylysines of different chain length, was tested is several studies before, mixing zwitterionic and anionic lipids. The negative charge of acidic lipids, independent of its chemical structure was found to be crucial for an effective binding of the peptide to the membrane, although the strength of the binding is different [228], whereas zwitterionic lipids show no binding [103, 116]. The underlying process of lipid sorting upon peptide binding results in a domain formation of a local enrichment of acidic lipids [120], which leads to broader phase transition or even peak separation in the DSC plots. The percentage of the acidic lipids in mixed PC/PG vesicles determines the amount of the bound cationic peptide [88] and thus the stabilizing of the gel phase, which finally increases the phase transition temperature of the lipids [104].

The peptide Gramicidin S, a cyclic peptide isolated from *Bacillus brevis* with antimicrobial activity, inhibits some structural identities with the model peptides of this study. On one side of the antiparallel β-sheet the four hydrophobic residues are located, whereas on the other side the charged side chains are clustered, forming two distinct regions in the peptide structure [238, 239]. Gramicidin S also shows a preferred interaction with negatively charged bilayer system and induces only a modest decrease of the phase transition temperature and enthalpy of zwitterionic vesicles composed of DMPC, DPPC or DMPE, implying the importance of the charge and structure of the lipid headgroup in interactions with cationic peptides [240]. Although Gramicidin S contains two ornithine residues, its lacks the ability to effectively stabilize the gel phase of DMPG as predicted for positively charged peptides. Large amounts of added peptide induce domain formation, a reduction of the transition enthalpy and a downshift of the transition temperature.

3.5 Summary of Bilayer Experiments

3.5.1 Influence of Peptide Sequence

The results obtained from DSC and FT-IR experiments for DPPG-peptide mixtures are compared to each other with respect to the different peptide sequences. Based on the shift of the transition enthalpy ΔH, the transition temperature T_m and the peptide secondary structure, the peptides are grouped into three main categories (see Table 3.5.1).

Table 3.5.1: Comparison of the effects observed after binding of different proteins[198] or our model peptides to DPPG bilayers. Their effect on the transition enthalpy ΔH and the transition temperature T_m of the lipid component is denoted with arrows, where ↑ means an increase, ↓ a decrease and → no differences compared to pure lipid.

		protein [198]	mode of action	ΔH	T_m	peptide structure
literature		ribonuclease	electrostatic binding	↑	→	
		polylysine	electrostatic binding	↑	↑	
		cytochrome c	fluidization of bilayer + hydrophobic interaction	↓	↓	
		gramicidin A	non-polar interactions	↓	→	
own results	1a	$(K)_5$, $(KAA)_4K$	electrostatic binding	↑	↑	random
	1b	$(KG)_4K$, $(KGG)_4K$	electrostatic binding	↑	↑	random and turn
	2a	$(KA)_4K$, $(KAbu)_4K$	electrostatic binding + β-sheet formation	↓↓	↑↑	antiparallel β-sheet to random transition
	2b	$(KV)_4K$, $(KL)_4K$	electrostatic binding + β-sheet formation	↓↓	↑↑	stable antiparallel β-sheet
	3	$(RG)_4R$, $(RA)_4R$	electrostatic binding + hydrophobic interaction no/weak binding?	↓	→	random

DPPG mixtures with the peptides $(K)_5$, $(KG)_4K$, $(KGG)_4K$ and $(KAA)_4K$ belong to the first category, 1a or 1b, where at a charge ratio of 1:1 the enthalpy and temperature of the lipid phase transition are increased after peptide binding. This is the case when electrostatic effects are dominating, i.e. the screening of charges of the lipid headgroup is the main effect of binding, resulting in a stabilization of the gel phase. For a complete shielding of all headgroup charges an increase in T_m of 5.5 K would be expected [225]. This was found for binding of oligolysines or polylysines to negatively charged membranes [104, 198]. Shortening of the lysine side chain leads to a larger increase in T_m as theoretically predicted [123]. The upshift of T_m of up to 4 K for the peptides in category 1 is slightly below the theoretically predicted increase because of additional hydrophobic interactions of the lysine side chain.

The two subgroups 1a and 1b are due to the different structures of the bound peptide strands. In both categories, the added peptide adopts an unordered structure when bound to DPPG bilayers. Additionally, in the subcategory 1b the peptide backbone of $(KG)_4K$ and $(KGG)_4K$ seems to be flexible enough due to insertion of glycine spacers to adopt an unordered structure with a high content of β-turns. It could be concluded that these peptides bind mainly due to the electrostatic interaction to the lipid bilayer surface without any incorporation into the hydrocarbon region.

The second class of peptides are the more hydrophobic ones with the general structure $(KX)_4K$ with X = A, Abu, V, and L. After binding they lead to a much larger increase of the transition temperature combined with a decrease of the transition enthalpy. An increase of the phase transition temperature by 19 up to 23 K is far above the value predicted for purely electrostatic binding, thus an additional stabilizing effect must be present. For binding of the peptides $(KX)_4K$, the formation of β-sheet structures is an additional driving force. The possible arrangements of the peptides and a graphical representation are given in section 3.5.3. Results from FT-IR measurements show that this class can also be subdivided into two subclasses determined by the stability of the secondary structure of bound peptide.

In subclass 2a the peptides $(KA)_4K$ and $(KAbu)_4K$ with intermediate hydrophobicity form intermolecular β-sheets upon binding to gel phase bilayers, which convert to an unordered structure at the temperature of the lipid chain melting. Thus, the lipid chain melting is coupled to the structural transition of the peptide. This additional level of self-organization of peptides bound to the lipid bilayer stabilizes the gel phase of the lipids, whereas the unstructured peptides of category 1 only show minimal stabilization. The defined structure of the adsorbed peptide leads to a distinct separation of the lipid bilayer from the peptide layer without any incorporation into the acyl chain region. Vesicle aggregation, as observed by visual inspection and by cryo-TEM, is caused by a cross-linking of the bilayers via the peptide and a dehydration of the bilayer surface after peptide binding. This is clearly evident from the change in the C=O vibrational band of the lipids. When the peptide undergoes the transition into an unordered structure, this dehydration is reduced and the C=O groups become more hydrated again to an extent very similar to the hydration level of pure DPPG in the fluid phase.

The class 2b is composed of the more hydrophobic peptides: $(KV)_4K$ and $(KL)_4K$. Their influence on the thermotropic behavior of the DPPG system is similar to the group 2a, as they also form intermolecular β-sheets after binding to gel phase DPPG and increase the transition

temperature much more than expected from simple charge screening effects. The important difference is the stability of the bound intermolecular β-sheet due to the increased hydrophobicity (see section 3.5.3). The antiparallel β-sheet on top of the lipid bilayer remains also stable when the lipid performes the phase transition from gel into the liquid-crystalline phase. A penetration of bulk water into the lipid headgroup region is hindered, so that the headgroup region stays less hydrated even in the liquid-crystalline phase. For $(KL)_4K$, the transition temperature decreases to some extent compared to $(KV)_4K$. This indicates that the most hydrophobic amino acid used in this study seems to slightly perturb the lipid bilayer, meaning that the hydrophobic side chain might be in contact with the lipid headgroup region.

The third group of peptides are the arginine containing peptides $(RG)_4R$ and $(RA)_4R$ which behave differently than those mentioned before. The transition enthalpy is slightly lowered at a constant transition temperature. Similar effects for binding to DPPG vesicles were observed for peptides with non-polar interactions without any electrostatic contributions, e.g. gramicidin A [198]. However, the arginine plays an important role in these interactions, showing a more complex behavior. The superposition of the counteracting effects, namely the binding to the bilayer upon electrostatic interaction, the formation of bidentate hydrogen bonding, and the hydrophobic interaction of the guanidinium moiety with the lipid headgroup, causes a zero net effect on the phase transition.
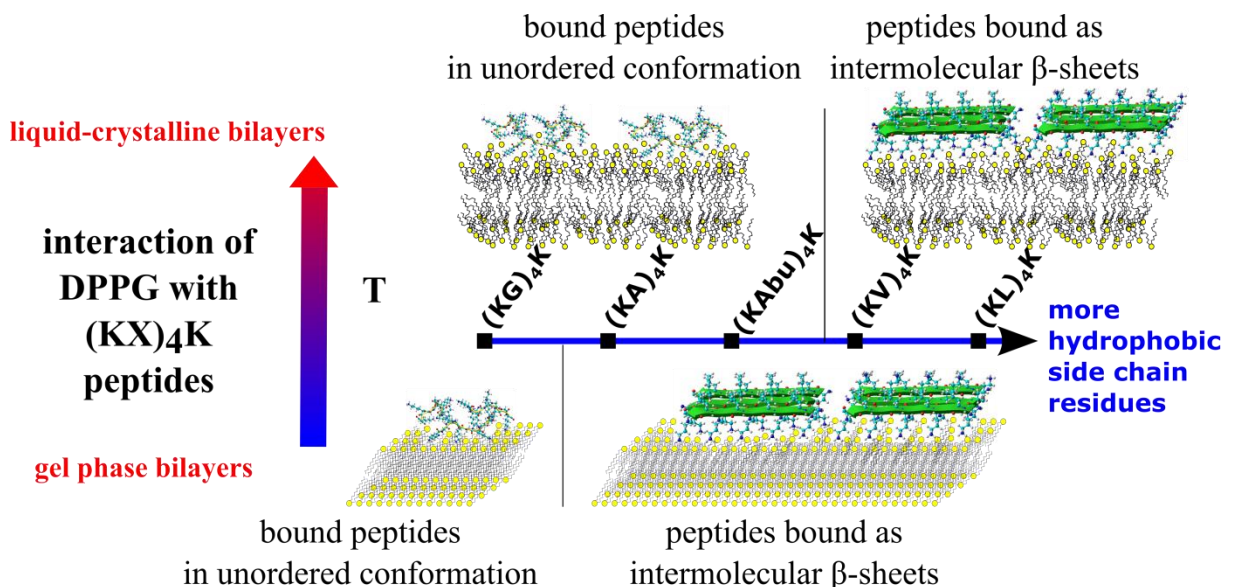
Figure 3.5.1: Binding of the peptides $(KX)_4K$ to DPPG membranes studied by DSC and FT-IR: The hydrophobicity of the uncharged amino acid X determines the secondary structure of the bound peptide. For hydrophilic G unordered conformations are detected. For X = A or Abu, the secondary structure changes with temperature, whereas for X = L or V, stable β-sheets are formed at all temperatures. The bound β-sheets strongly increase the phase transition temperature of DPPG.

Comparing the results shown in Table 3.5.1 with the matrix of the peptides in Figure 2.3.1 reveals a distinct influence of the peptide sequence on the termotropic behavior of DPPG bilayers after peptide binding. The effects upon peptide binding on the phase behavior of DPPG are larger comparing peptides of two different groups as the difference within the groups themselves. The introduction of an uncharged amino acid reduces the hydrophobic contribution of the lysine side chain and increases the electrostatic effect of charge screening. Tuning the hydrophobicity of the side chain of the uncharged amino acid enables the formation of an additional level of self-organization resulting in an extensive stabilization of the lipid gel phase. Exchanging lysine by arginine further enhances the hydrophobic contributions of the side chain counteracting the electrostatic effect.

3.5.2 Influence of Lipid Structure

Influence of the headgroup charge - peptide interaction with zwitterionic lipids

The direct comparison of experiments using negatively charged lipids and zwitterionic ones reveals that the interaction of the cationic peptide with the lipid bilayer is mainly driven by electrostatic attractions. The lack of a net negative charge in the headgroup region disables a binding of the lysine residues to the headgroup region, leading to an undisturbed phase behavior without any changes compared to pure lipid systems.

Influence of different acyl chains attached to a phosphatidylglycerol headgroup

The effect of different acyl chain lengths on the thermotropic phase behavior of PG-(KA)$_4$K mixtures is marginal, when analyzed on a reduced temperature scale. The main phase transition was upshifted by 16 to 22 K for DSPG < DPPG < DMPG due to a reduced headgroup area and a higher van der Waals interaction as a result of the decreased repulsion of the negatively charged headgroup upon binding of the cationic peptide. The influence of the acyl chain length seems to be less important than the saturation of the lipid. For lipids with an unsaturated acyl chain, the upshift of T_m was reduced by 50 %.

It can be concluded that the main part of the lipid-peptide interactions take place in the headgroup region via electrostatic attractions. The acyl chain region of the lipid bilayer remains undisturbed having a comparable acyl chain order as pure lipids. The headgroup region becomes less hydrated after peptide binding. The observed peptide transition from antiparallel intermolecular β-sheets to unordered structures occurred at similar temperatures

on a reduced scale, underlining similar interactions of the peptide with the headgroup region of the lipids.

Influence of the lipid headgroup structure

The observed upshift of the main phase transition temperature in DMPG-peptide mixtures was confirmed for other negatively charged lipids (DMPS, DMPA, and TMCL), underlining the suggested, charge driven interaction. For other negatively charged lipid headgroups, the stability of the β-sheets depends on the size of the lipid headgroup. The gel phase was more stabilized for lipids with smaller headgroups, resulting in an order for T_m: DMPS < DMPG < DMPA < TMCL. A direct correlation between the critical packing parameter and the extent of the upshift of the lipid main phase transition temperature in mixtures with the cationic peptides was found for all studied negatively charged lipids.

Table 3.5.2: Lipid headgroup dependence of the stability of the formed β-sheet layer of $(KAbu)_4K$ and $(KL)_4K$, having different hydrophobic side chains, bound to gel phase lipid systems and the response of the system upon heating above the phase transition.

	packing parameter	+ $(KAbu)_4K$	+ $(KL)_4K$
DMPS	0.70	β-sheet to unordered	β-sheet to unordered
DMPG	0.82	β-sheet to unordered	stable β-sheet
DMPA	1.04	stable β-sheet	stable β-sheet
TMCL	1.03	stable β-sheet	stable β-sheet

The FT-IR results show that the negatively charged headgroups act as a template for the peptide self-assembly. The unordered structure in the bulk solution is converted to a intermolecular β-sheet structure bound to the lipid headgroups in the gel phase (see section 3.5.3). The stability of the β-sheet is determined by the hydrophobicity of the peptide and the effective headgroup size (see Table 3.5.2). The smaller the headgroup, the more stable are the β-sheets. The intercalated water between the bilayer stacks of pure lipids is replaced by the bound peptide, resulting in less hydrated carbonyl groups in the headgroup region of the lipids. For lipid-peptide mixtures with a stable peptide structure the changes of the acyl chain vibration are smeared out upon heating, whereas the interfacial region retains its initial state with a low fraction of hydrogen bonded carbonyl groups. For bilayers, composed of lipids with large headgroups, all the observed changes of the FT-IR bands after peptide binding seem to be correlated. At temperatures, where the wavenumber of the acyl chain vibration increases, the lipid headgroup becomes more hydrated and the peptide converts from a β-sheet to an unordered conformation.

3.5.3 Peptide Structure

Inspection of the amide-I band of FT-IR measurements shows that the peptides $(KX)_4K$ bound to an anionic bilayer form antiparallel intermolecular β-sheets covering the bilayer surface. The question now arises whether specific interactions "gluing" the vesicles together also occur or solely charge interactions take place. In principle, two different β-sheet structures can be formed. One, where all charged lysine side chains are pointing to one side of the β-sheet and the hydrophobic residues to the other side (syn-orientation). The other possible structure contains an alternating orientation of the single strands (anti-orientation). These two different structures are shown in Figure 3.5.12 from the side and end-on.
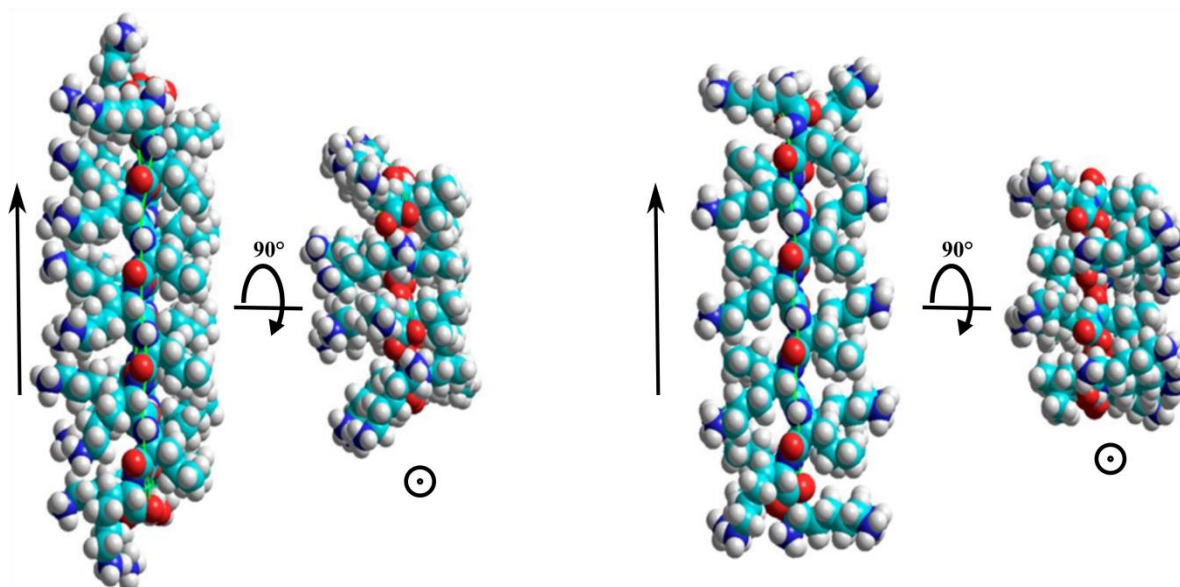
Figure 3.5.12: Possible structures of small patches of aggregated β-sheets composed of $(KL)_4K$. viewed side-on and end-on. Left: syn-orientation. Right: anti-orientation.

The syn-orientation leads to an asymmetric β-sheet with a high charge density on one face and a completely hydrophobic and uncharged opposing face. If the β-sheets would be bound in the syn-orientation a completely hydrophobic surface would be created. To shield this from bulk water it can be expected that a second layer of peptide is attached driving the aggregation of the vesicles and the formation of two β-sheets sandwiched between bilayers. The hydrogen bonds within the peptide layers and the hydrophobic interaction between the uncharged spacer connecting the two peptide layers would stabilize the whole peptide bilayer in its β-sheet conformation. The final stability of the formed β-sheet is determined by the size of the uncharged amino acid side chain, where leucine shows the highest stability, because of the largest hydrophobic residue.

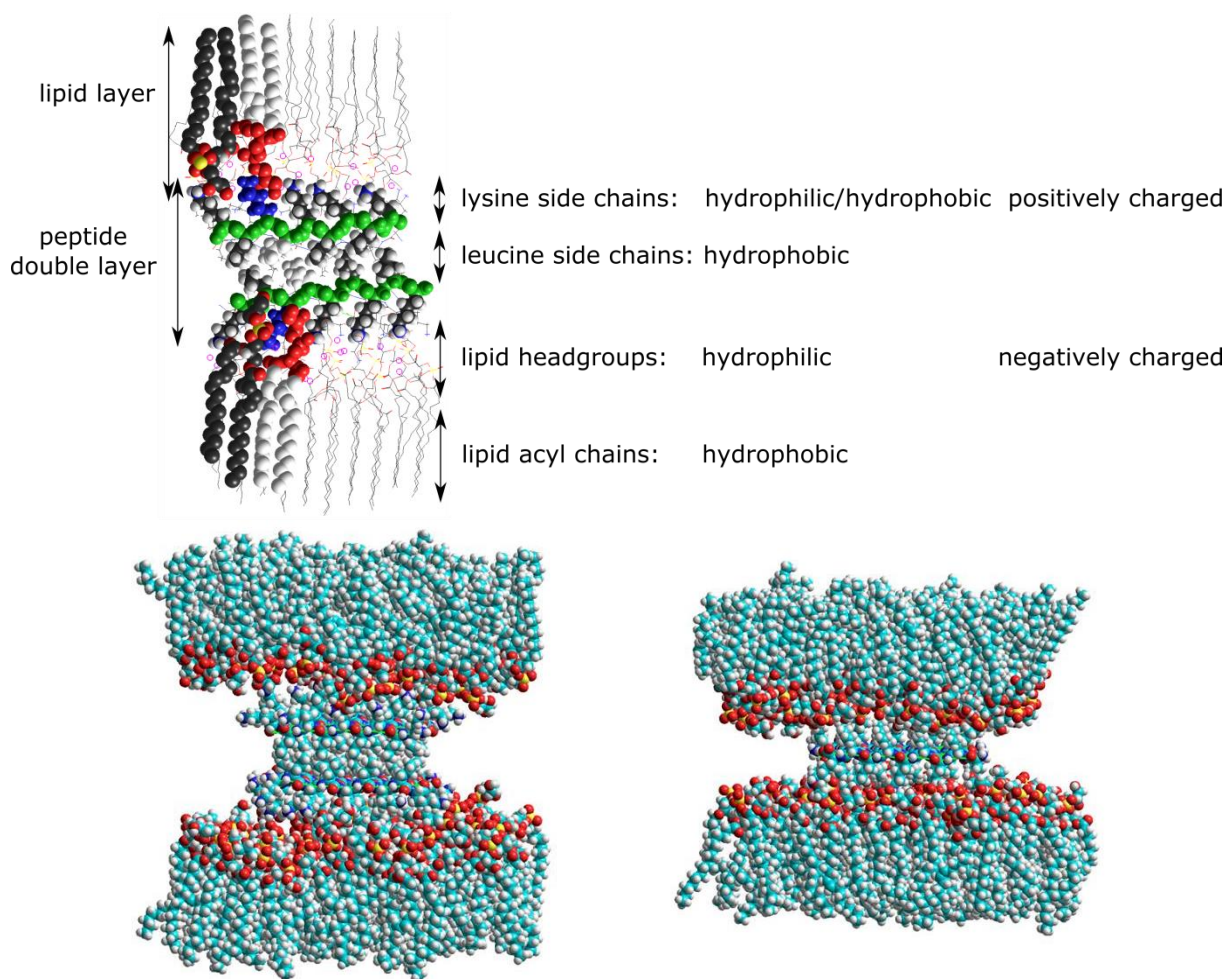Figure 3.5.13: Proposed models of aggregated lipid bilayers. Top: peptide layer, composed of two β-sheets, sandwiched by two individual lipid layers forming aggregated bilayer stacks. The different regions of the stack are colored individually: acyl groups in gray, lipid headgroups in red, peptide backbones in green, lysine side chains in blue. Bottom: Two opposing monolayers of PG "glued" together by two short pieces of β-sheets in the syn-orientation (left) or by a single β-sheet in the anti-orientation (right).

In the anti-orientation the overall charge density on both sides of the β-sheets is the same, but with a reduced number of lysine side chains. Thus, a symmetric β-sheet is formed with intermediate charge densities on both sides. In this case the aggregation would be driven by charge interactions by the lysine side chains with the negatively charged PG vesicle surface and the vesicles would be "glued" together by single layer β-sheets. These two different possibilities are shown in Figure 3.5.13.

From the experiments it is not possible to distinguish between these two possibile models. Based on the finding of an increase of dehydration of the lipid headgroup regions with increasing hydrophobicity of the amino acid X, the second possibility is favored, namely that the vesicles are "glued" together by a single β-sheet peptide layer, where the charged and hydrophobic amino acids are oriented in the anti-orientation. As can be seen from the

structure in Figure 3.5.12, the voids between the charged lysine side chains are filled with the hydrophobic side chains of leucine. When bound to the vesicle surface this anti-orientation therefore leads to a higher stability of the β-sheets and to an expulsion of water from the lipid headgroup region, as the available space for hydration water will be reduced. The slight reduction of the phase transition temperature of the DPPG mixtures with the most hydrophobic peptide (KL)$_4$K compared to the DPPG mixtures with (KV)$_4$K supports the anti-orientation. The interaction of the leucine side chains with the lipid headgroup causing a perturbation of the lipids is only possible in this orientation.

By shortening the side chain length of the hydrophobic amino acid, i.e. (KA)$_4$K and (KAbu)$_4$K to DPPG, the voids between the charged lysine side chains now have to be filled with water. When bound to gel phase DPPG, the β-sheet structure is still stable, but upon heating it converts to an unordered structure and the hydration level of the lipid headgroups increases again. The residual water of hydration will be shared by bound peptide and the lipid headgroups. This shielding of the bilayer is probably the main reason for the upshift of the transition temperature, as it is already known from binary lipid water systems with a low water content that the phase transition temperature is increased with decreasing hydration of the bilayers [60].

For a dense peptide packing in the syn-conformation, a charge density of 1 positive charge per 34 Å^2 within the peptide layer is created, which is higher than the charge density of the DPPG bilayer in the gel (1 negative charge per 50 Å^2) and the liquid-crystalline phase (1 negative charge per 65 Å^2). For the anti-conformation, the charge density on one side would be 1 positive charge per 68 Å^2. Thus, from purely geometrical arguments the anti-conformation fits better to the charge density of the DPPG surface in the liquid-crystalline state. However, as there is some flexibility in the lysine side chains, they might adapt to yield optimal electrostatic interactions. As the aggregation is dependent on the charge ratio, the formation of the β-sheets may also depend on it. A possible change or mixture of syn- and anti-orientation for different peptides and charge ratios cannot be excluded.

4 Interaction of Model Peptides with Lipids at the Air-Water Interface

4.1 Introduction

In addition to bilayer experiment presented in section 3.3, the interactions of the peptides with lipid monolayers at the air-water interface were investigated. A lipid monolayer represents half of a bilayer [6-8] and is particularly suitable to study the interaction or binding of molecules, such as peptides and proteins [9, 241], polymers [10] or amphiphilic substances [11] to the lipid headgroup region and their penetration into the lipid acyl chain region. The monolayer is very well defined, as the number of accessible lipids is precisely known, and the phase state can be controlled by the number of spread lipids, and by the available surface area. Furthermore, the changes in area or surface pressure can easily be measured and controlled.

The combination of the monolayer technique with fluorescence microscopy enables the visualization of the formation of liquid-condensed domains upon peptide interaction and allows monitoring morphological changes of the domains during film compression.

IRRA spectroscopy of monolayer films provides additional information on the phase state of the lipid as well as about the secondary structure and orientation of the peptide.

4.1.1 Phase Behavior of Lipid Monolayers at the Air-Water Interface

The phase state of a lipid monolayer spread on an aqueous subphase is also dependent the parameters discussed for the bilayer systems. The temperature T, the concentration of added salt and the pH of the subphase determine the surface pressure-area (π - A) isotherm of a monolayer [8].

As a representative saturated lipid 1,2-dipalmitoyl-sn-glycero-3-phosphoglycerol (DPPG) was used in this work beside other lipids mentioned above. The π - A isotherm of DPPG shows a typical phase behavior (see Figure 4.1.1). The different phases are named according to Adamson [140]. At large areas per molecule and very low surface pressure, no interactions between the molecules occur, and the DPPG molecules at the air-water interface behave like a two-dimensional gas. In this so-called gas-analogue region (G) of the isotherm, the hydrocarbon chains lie flat on the surface. Lateral compression condenses the lipid monolayer and a transition from the gas-analogue state to the liquid-expanded state (LE) is triggered at a certain transition pressure. The coexistence region of the gas and the LE phase occurs at a very low surface pressure, usually not resolvable by the used method. In the liquid-expanded

state, described as an isotropic two-dimensional fluid, the molecules diffuse rapidly on the surface having a substantial conformational disorder in the alkyl chains. In the isotherm, the surface pressure shows a liftoff from almost zero surface pressure. Further compression increases the surface pressure up to the next phase transition region. The phase transition of the liquid-expanded to liquid-condensed state (*LC*) creates an almost horizontal plateau in the π - *A* isotherm [242]. In the liquid-condensed state, the hydrocarbon chains are tilted towards the surface arranged in *all-trans* conformation. The compressibility of the film is much lower due to a denser packing. A perpendicular alignment and a tight packing of the molecules in the solid-condensed phase (*S*) is achieved upon further compression. The film is relatively incompressible and finally collapses [129].
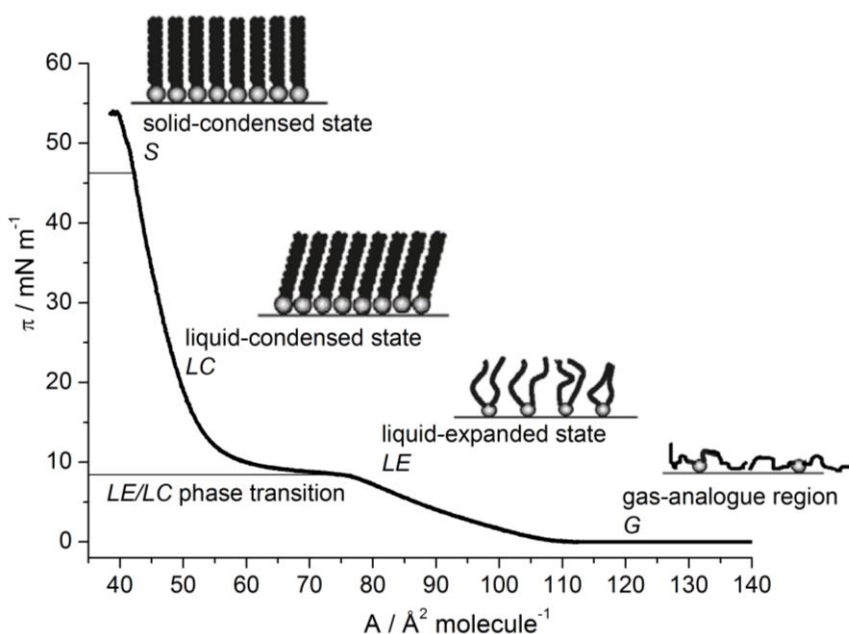
Figure 4.1.1: π - *A* isotherm obtained by compressing an DPPG lipid monolayer formed at an air-water interface [243].

The π - *A* isotherms of phosphatidylglycerols with other acyl chains than two palmitoyl chains are less complex. The film of 1-palmitoyl-2-oleoyl-*sn*-glycero-3-phosphoglycerol (POPG) at the air-water interface is more expanded due to unsaturation. Only the gas-analogue and the liquid-expanded phases occur [244]. For DSPG, increased lipid-lipid interaction due to the longer acyl chains prevent the occurrence of an *LE* phase and the monolayer shows a direct transition from the gas-analog phase to the *LC* phase [245].

4.2   Adsorption to Lipid Monolayers

The interaction of antimicrobial peptides with bacterial membranes is a complex interplay of charge and hydrophobicity. Due to their positive charge, they show preferred interactions with negatively charged lipid headgroups, but at the same time, the hydrophobic residues interact with the lipid acyl chain region. To get further insights into the mode of interaction of antimicrobial peptides with membranes, it is necessary to understand the very first binding step of these peptides and the resulting effects on lipid membrane properties.

In contrast to bilayer experiment, where premixed samples were investigated, adsorption experiments open the opportunity to study the binding process of the peptide in direct way. The adsorption of the peptide from the subphase to a preformed lipid monolayer can be followed as a function of time to extract the binding kinetics and to monitor the effect of peptide binding on the lipids.

4.3 Interaction of DPPG with Cationic Model Peptides - Influence of Peptide Sequence

To study the influence of the peptide sequence, different peptide solutions were injected into the subphase of a DPPG monolayer at the air-water interface. DPPG was chosen, because the monolayer exhibits an *LE* and *LC* phase transition upon compression at the given experimental conditions. The peptide sequence was altered, to reveal the following effects: i) increase in hydrophobicity of the uncharged spacer amino acid X in the sequence (KX)$_4$K, ii) reduction of the charge density in the peptide by introducing a second uncharged amino acid in the sequence (KXX)$_4$K, iii) exchange of the charged amino acid (lysine by arginine) with a concomitant delocalization of the charge in the sequence (RX)$_4$R.

4.3.1 Influence of an Increased Hydrophobicity of the Uncharged Spacer Amino Acid X in the Peptides (KX)$_4$K

All peptides depicted in Figure 2.3.1 are soluble in water and are not surface active, i.e. they show no adsorption to the air-water interface, if no lipid is present. Thus, in experiments performed without a lipid monolayer the surface pressure remains constant at 0 mN m^{-1} as depicted in Figure 4.3.2 in panels a-e (black curves). Although hydrophobic amino acids like valine and leucine are incorporated into peptides, their presence does not lead to enhanced surface activity as the charged residues (lysine and arginine) ensure good water solubility.

4.3.1.1 Adsorption Isotherm for Binding of (KG)$_4$K and (KL)$_4$K to a DPPG Monolayer

The adsorption isotherm of (KG)$_4$K and of (KL)$_4$K to a DPPG monolayer was studied by injecting different amounts of a peptide solution into the subphase underneath the DPPG monolayer with an initial surface pressure of 25 mN m^{-1} for (KG)$_4$K and 5 mN m^{-1} for (KL)$_4$K (see Figure 4.3.1). These values were chosen to obtain significant changes in π (see Figure 4.3.2).

Depending on the initial surface pressure, the total amount of spread lipids differ and the theoretical lipid concentration at the air-water surface of the trough ranges from 0.6 up to 1.1 µM. Binding of (KG)$_4$K to the DPPG monolayer of 25 mN m^{-1} in the *LC* phase decreases the surface pressure. For higher peptide concentrations, a stronger decrease of π is observed. Above a peptide concentration of 3 µM a constant decrease in surface pressure of about - 9 mN m^{-1} was obtained. Upon additional hydrophobic interaction, the binding of (KL)$_4$K to the DPPG monolayer of 5 mN m^{-1} increases the surface pressure. An increase in surface pressure of about 9 mN m^{-1} was seen. Saturation for binding of (KG)$_4$K and (KL)$_4$K, the most

hydrophilic and most hydrophobic one of the peptides (KX)$_4$K, to a DPPG monolayer was reached above a peptide concentration of 3 μM and 0.6 μM, respectively (see Figure 4.3.1). Assuming that a DPPG molecule at 5 mN m^{-1} covers an area of 90 Å^2 at the monolayer the beginning plateau value of $\Delta\pi$ for (KL)$_4$K coincides with a lipid to peptide ratio of 1 at the given trough dimensions. Charge compensation is reached at even lower concentrations, because one peptide carries five positive charges. The used peptide concentration of 3.0 μM provides an excess of peptide for all initial surface pressure and ensures that saturation is reached. However, most of the peptides stay in the subphase.
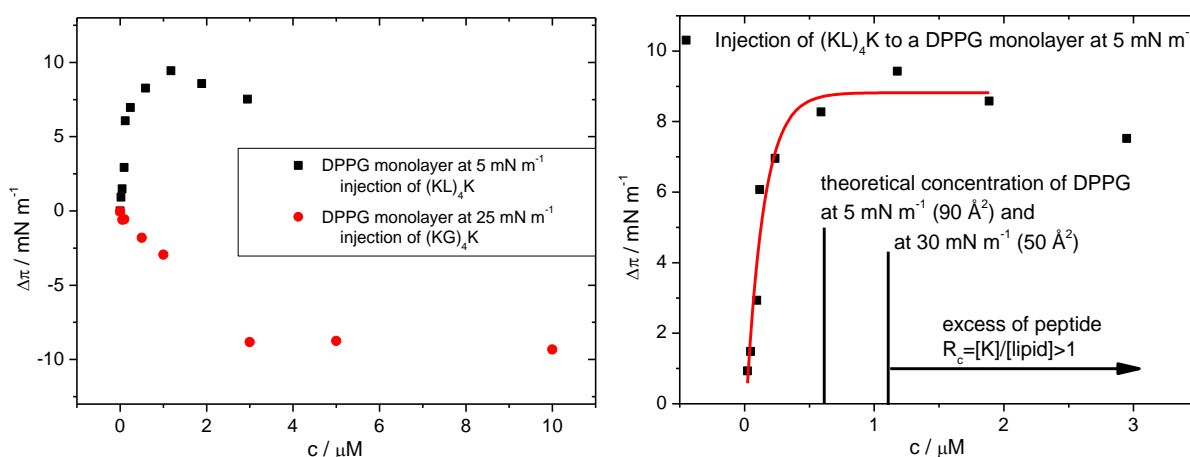

Figure 4.3.1: Left: Adsorption isotherms of (KG)$_4$K and (KL)$_4$K determined by difference in surface pressure obtained after 5 h of adsorption to a DPPG monolayer of π_{ini} = 25 mN m^{-1} ((KG)$_4$K) or π_{ini} = 5 mN m^{-1} ((KL)$_4$K) as a function of their subphase concentration. Right: Adsorption isotherm of (KL)$_4$K. Red curve is drawn to guide the eye. Depending on the initial surface pressure the total amount of spread lipids differ, the theoretical lipid concentration at the air-water interface of the trough thus ranges from 0.6 up to 1.1 μM. For the peptide concentration of 3 μM, which has been used in all experiments the amount of peptide is in excess compared to that of the lipid.

For pure electrostatic binding of a peptide with five cationic charges, e.g. (K)$_5$, one would estimate an apparent binding constant to purely negatively charged lipid bilayers of 1-2 10^5 M^{-1}, a value supported by experimental results obtained by isothermal titration calorimetry using different pentapeptides [103, 117, 123]. Separating the charged lysine residues by introducing alanine into the peptides sequence reduces the binding constant 3-fold [88]. Except for (KG)$_4$K, all other peptides have amino acids more hydrophobic than alanine in their sequence. Therefore, higher binding constants can be assumed due to the additional hydrophobic interaction.

For a binding constant of 10^6 M^{-1} it can be calculated that under the experimental conditions 75 % of all lipids have bound peptides assuming a stoichiometry of binding of 5 lipids per peptide. The adsorption curves presented in Figure 4.3.1 show that saturation is reached at a

concentration of 3 µM peptide, thus the binding constant must be higher than estimated above and must have a value of ca. 10^7 M^{-1} for (KG)$_4$K and even higher for (KL)$_4$K.

4.3.1.2 Adsorption of Peptides (KX)$_4$K to DPPG Monolayers at Different Initial Surface Pressure

Adsorption experiments of peptides (KX)$_4$K to DPPG monolayers at different initial surface pressures were performed to study the effect of the peptide on physical state of the monolayer, to monitor the kinetics of binding, and a possible incorporation of the peptide into the DPPG monolayer. After injection of a peptide solution into the subphase underneath the DPPG monolayer, the surface pressure changed due to interaction of the peptides with the lipid molecules. This change of surface pressure depends on the initial surface pressure π_{ini} of the lipid monolayer, and on the sequence of the peptide. Adsorption of basic peptides to negatively charged lipids is mainly driven by electrostatic interactions, zwitterionic lipids showing no significant binding [119, 246, 247]. A decrease in surface pressure is observed as a result of condensation of the monolayer due to electrostatic interactions leading to a shielding of the repulsive head group charges when the total area of the monolayer is constant [123]. Lipid condensation is also seen for electrostatic binding of divalent cations to PG monolayers [248].

The net charge of all tested peptides is +5 at neutral *pH*, and due to length and flexibility of lysine side chains, it might be possible to bridge more than one lipid molecule upon binding, the oligopeptide thus functioning as a pentadentate ligand. That an oligopeptide with several basic residues can act as a bridging agent and binds to more than one lipid, was shown theoretically and proven experimentally. It was found that the apparent free energy of binding becomes more negative by ca. 1 kcal mol^{-1} with every additional basic residue [103, 117]. The efficacy of bridging depends also on the charge distance between the cationic charges in the side chain of the peptide compared to the average distance of the lipid molecules.

A mean distance of 7.2 Å between two α-carbon atoms in the peptide backbone of neighbouring lysine residues was calculated for the sequence (KX)$_4$K. As DPPG molecules carry their negative charge at the phosphate group in close proximity to the air-water interface it is possible to access, the charged phosphate group and build up hydrogen bonds with the ammonium group of the lysine residues. In a DPPG monolayer in the liquid-expanded phase at a surface pressure of 5 mN m^{-1}, one lipid occupies roughly 90 Å^2 and thus two headgroups are 9.5 Å apart. Based on this simple calculation, lipid condensation in the liquid-expanded

phase is likely to occur to reach optimal lipid-peptide contacts. Compression of the monolayer to 30 mN m^{-1} reduces the area per lipid, and in the *LC* phase, the molecules now are closer together having a distance of 7.1 Å. However, a condensation effect caused by electrostatic shielding of negative lipid headgroup charges is still possible as the side chains of the peptide can adapt to smaller distances. As the DPPG isotherm has a very steep slope at this surface pressure in the *LC* phase, the resulting surface pressure decrease can be very significant, even if the area change is small.

To study the effect of additional hydrophobic interactions, peptides with amino acids of increased hydrophobicity were used. Peptides interacting with the acyl chain region are located between the lipid molecules occupying space at the air-water interface, thus the surface pressure will increase at constant total area [198].

Membrane anchors of proteins or peptides often contain either a prenyl or a farnesyl moiety [249, 250], which inserts into the lipid monolayer. Upon insertion of the membrane anchor into the lipid monolayer a strong increase of surface pressure is observed also for zwitterionic lipids [167]. Although lysine as charged amino acid preferentially acts via electrostatics the lysine side chain contributes to hydrophobic interactions [105, 123].

A superposition of electrostatic and hydrophobic interaction is observed, when peptides are charged on the one hand, and have hydrophobic side chains on the other hand, i.e. α-helical antimicrobial peptides KLAL and (LKKL)$_4$ [105, 251, 252]. First, the injected positively charged peptide is attracted to the lipid monolayer driven by electrostatic interactions between phosphate moieties and lysine residues. Second, the bound peptide inserts deeper into the headgroup region due to hydrophobic interactions. A following clustering of the leucine residues enables a maximal interaction with the hydrophobic region of the bilayer. To tune the contributions of additional hydrophobic interactions, the amino acid X was changed systematically from G to A, Abu, V, and L.

Adsorption kinetics of (KG)$_4$K to a DPPG monolayer

(KG)$_4$K has the least hydrophobic amino acid glycine G. The adsorption kinetics of (KG)$_4$K to a DPPG monolayer differ below and above *LE*/*LC* phase transition region at 8 - 10 mN m^{-1} (see Figure 4.3.2a). After the injection of (KG)$_4$K under a DPPG monolayer in the *LE* phase with a surface pressure lower than 10 mN m^{-1}, first a decrease of the surface pressure over a period of half an hour is detected, followed by a much slower increase in surface pressure. This indicates that at least two consecutive processes take place, the initial fast one reducing the surface pressure, followed by a slower process leading to an increase in π.

The explanation for the observed two processes is the following: the electrostatic adsorption of the highly charged peptide to the lipid headgroup region first causes a shielding of the headgroup charges and a concomitant reduction in repulsive forces. The resulting increase in chain order and the reduction of the area per lipid molecule with possible bridging of more than one lipid due to binding of a peptide molecule decreases the surface pressure. The following slower increase in surface pressure is then probably caused by a rearrangement of the orientation of the peptides, so that partial insertion of the side chains in between the lipid headgroups can occur. A two-step model during binding of cationic peptide to a lipid layer composed of negatively charged molecules has been suggested before and observed experimentally for monolayers [123] as well as for bilayer systems [253].

Injections of (KG)$_4$K into the subphase of a DPPG monolayer with an initial surface pressure above 10 mN m^{-1}, i.e. in the *LC* phase, lead only to a decrease of the surface pressure without any second process. The decrease in surface pressure becomes higher with increasing surface pressure of the film. This can be explained by the form of the monolayer surface pressure-area isotherm of DPPG (see Figure 4.3.2f), which becomes steeper with increasing compression of the film. A change of the area per lipid of 0.5 Å^2, for instance, has a larger effect on the surface pressure in the *LC* phase (25.0 mN m^{-1} - 23.5 mN m^{-1}) than in the *LE* phase (5.0 mN m^{-1} - 4.8 mN m^{-1}).

The shielding of the repulsion between the headgroups by electrostatic adsorption of the peptides induces a chain ordering and condensation of the film, although the lipid order in the *LC* phase is higher compared to the *LE* phase. Incorporation of the peptide into the densely packed lipid monolayers is less likely so that the condensation effect dominates. The condensing effect of the adsorbed peptides was also seen in fluorescence microscopy and IRRAS experiments and will be discussed later. From these findings it can be concluded that the peptide (KG)$_4$K is not hydrophobic enough to penetrate tightly packed DPPG monolayers in the *LC* phase and is only electrostatically adsorbed to the lipid headgroup region, whereas it can partially penetrate a less dense monolayer in the *LE* phase.
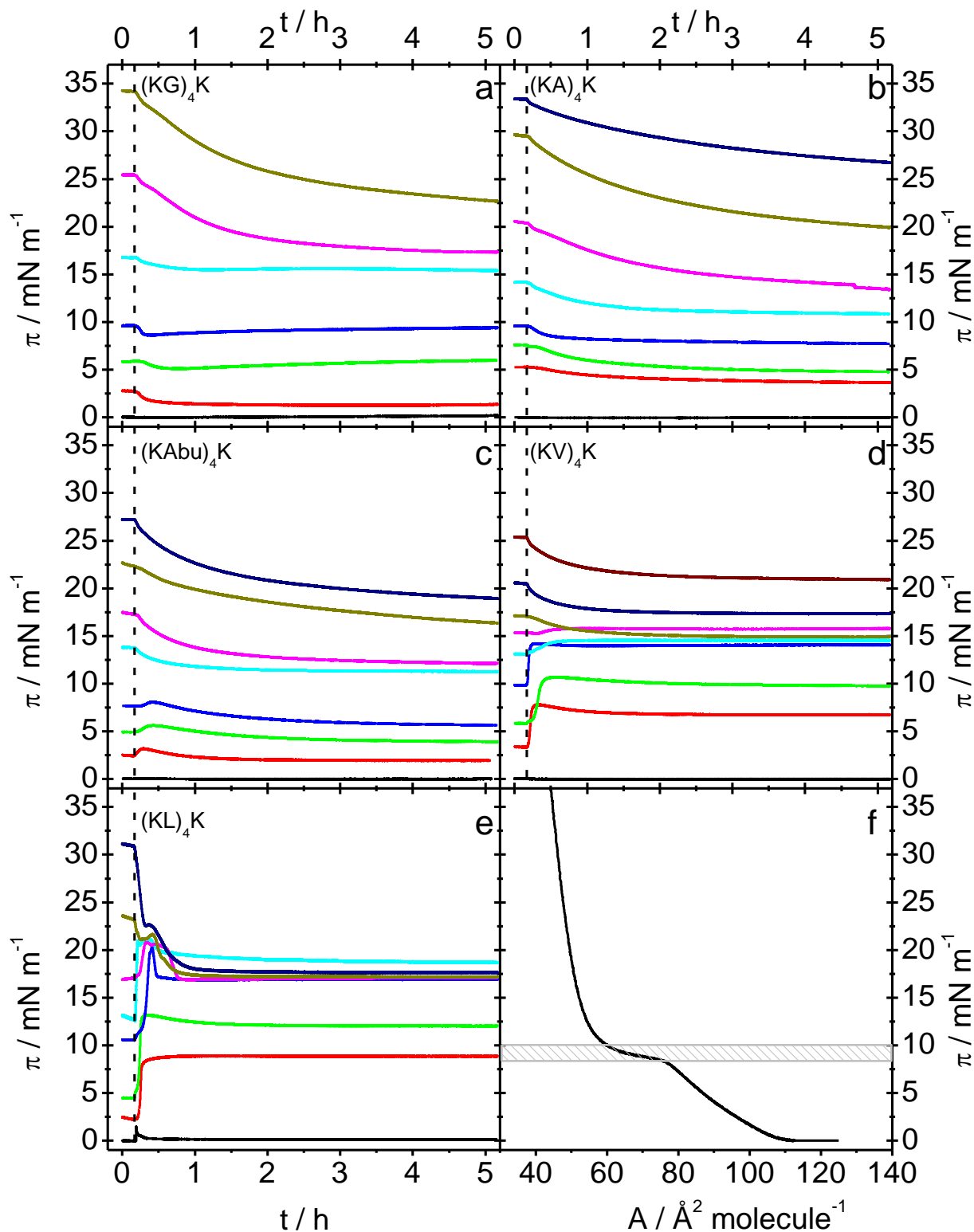
Figure 4.3.2: Change in surface pressure of a DPPG monolayer as a funktion of time after injection of different peptides $(KX)_4K$ into the subphase ($T = 20$ °C, 100 mM NaCl) at various initial surface pressure. The lipid monolayer remains at a constant surface pressure prior to peptide injection at $t = 600$ s (marked with the dashed line). The final concentration of the peptides (panel a-e) in the subphase was 3.0 μM. Adsorption equlibrium was reached within 5 h. Surface pressure - area isotherm of pure DPPG monolayer (panel f), the *LE/LC* phase transition region between 8 mN m^{-1} and 10 mN m^{-1}is highlighted by shading.

Adsorption kinetics of $(KA)_4K$ to a DPPG monolayer

The peptide $(KA)_4K$ contains the more bulky and more hydrophobic amino acid alanine instead of glycine in the peptide $(KG)_4K$. The adsorption kinetics of the peptide $(KA)_4K$ are independent of the initial surface pressure π_{ini} and no influence of the phase state of the lipid monolayer was detected (see Figure 4.3.2b). All kinetic curves show a decrease of the surface pressure over time, the decrease becoming more prominent at higher π_{ini}. At the highest value of π_{ini} the slow kinetics prevents the determination of the equilibrium value.

Adsorption kinetics of $(KAbu)_4K$ to a DPPG monolayer

For a systematic increase of the hydrophobicity and bulkiness of the side chain of the uncharged amino acid in the peptide, the unnatural amino acid α-amino butyric acid, having an intermediate hydrophobicity, was also used to bridge the gap between the natural amino acids alanine and valine. The attached residues are a methyl group, an ethyl group and an isopropyl group for alanine, amino butyric acid and valine, respectively. For $(KAbu)_4K$, a distinct dependence of the adsorption kinetics on the phase state of the lipid was observed (see Figure 4.3.2c). For DPPG in the *LE* phase, first an increase in surface pressure is visible followed by a slower decrease of π. Compared to the adsorption kinetics of $(KG)_4K$, a reversed sequence of surface pressure increase and decrease is thus observed.

The initial electrostatic adsorption leads immediately to hydrophobic interactions with concomitant insertion of $(KAbu)_4K$ into the lipid monolayer and thus to an increase in π. After 30 min, the following slower decrease in π is due to a reorientation of $(KAbu)_4K$ with concomitant better electrostatic interaction. This then overcompensates the hydrophobic interactions. The final equilibrium surface pressure is then below π_{ini}, resulting in an overall negative $\Delta\pi$. For binding to the *LC* phase, only the decrease of the surface pressure is visible due to lipid condensation.

Adsorption kinetics of $(KV)_4K$ to a DPPG monolayer

The amino acid valine in $(KV)_4K$ has an even larger hydrophobic side chain. Therefore, immediately an incorporation of the peptide into the lipid monolayer with an increase in surface pressure can be detected when $(KV)_4K$ is adsorbed to a DPPG monolayer up to an initial surface pressure of 16 mN m^{-1}. The condensation effect is present, but masked by the surface pressure increase due to insertion. Only at low surface pressure, an overshoot of the surface pressure above the final equilibrium surface pressure is visible with a consecutive

slight decrease of π (see Figure 4.3.2d). The comparison with the kinetics of the (KAbu)$_4$K incorporation reveals that the adsorption becomes faster with increasing hydrophobicity of the peptide. At the beginning of the *LC* phase, in the range from 10 mN m^{-1} up to 17 mN m^{-1}, all adsorption experiments end up at a surface pressure of about 16 mN m^{-1}. Above an initial surface pressure of 16 mN m^{-1}, a similar behaviour was detected as observed before for (KAbu)$_4$K, namely only a decrease of the surface pressure after adsorption.

Adsorption kinetics of (KL)$_4$K to a DPPG monolayer

Leucine is the amino acids with the highest hydrophobicity used here. The kinetics of the adsorption of (KL)$_4$K to a DPPG monolayer are clearly dominated by the insertion of the hydrophobic peptide into the monolayer. Immediately after injection into the subphase, π increases and at intermediate values of π_{ini} an overshoot is visible followed by the slower condensation of the monolayer coupled with the decrease of π. Independent of the initial surface pressure in the *LC* phase a final surface pressure of ca. 17 mN m^{-1} is reached (see Figure 4.3.2e).

4.3.1.3 Kinetic Analysis of (KX)$_4$K Adsorption to a DPPG Monolayer

The kinetics of the two observed effects, the decrease of the surface pressure upon lipid condensation, and the increase of the surface pressure upon incorporation into the monolayer, change their relative order by increasing the hydrophobicity of the added peptide. Lipid condensation shows faster kinetics during adsorption of (KG)$_4$K followed by a slower process of peptide incorporation.

A quantitative analysis of the kinetics of adsorption was tried by fitting the experimental adsorption curves obtained for the five different peptides at a specific initial surface pressure using the following bi-exponential equation:

$$\pi = A_1 e^{-t/t_1} + A_2 e^{-t/t_2} + \pi_0 \tag{4.1}$$

The parameters A_1 and t_1 provide information on the amplitude and rate constant for the peptide incorporation and A_2 and t_2 for the condensation effect, the value π_0 being the final surface pressure at equilibrium after 5 hours. The amplitudes of both effects correspond to the properties of the peptides describing the relative strength of the electrostatic and hydrophobic interaction with the DPPG monolayer.

Figure 4.3.3 shows the experimental and fitted curves for the adsorption of the different peptides to a DPPG monolayer starting from a surface pressure ca. 5 - 7 mN m^{-1}, where the pure DPPG monolayer is in the *LE* phase. Fitting the adsorption kinetics to the *LC* phase was

omitted, because only a decrease of surface pressure is observed with the exception of the most hydrophobic peptide (KL)$_4$K. A separation in two processes is therefore not possible. An overview of the obtained parameters is given in Table 4.3.1.
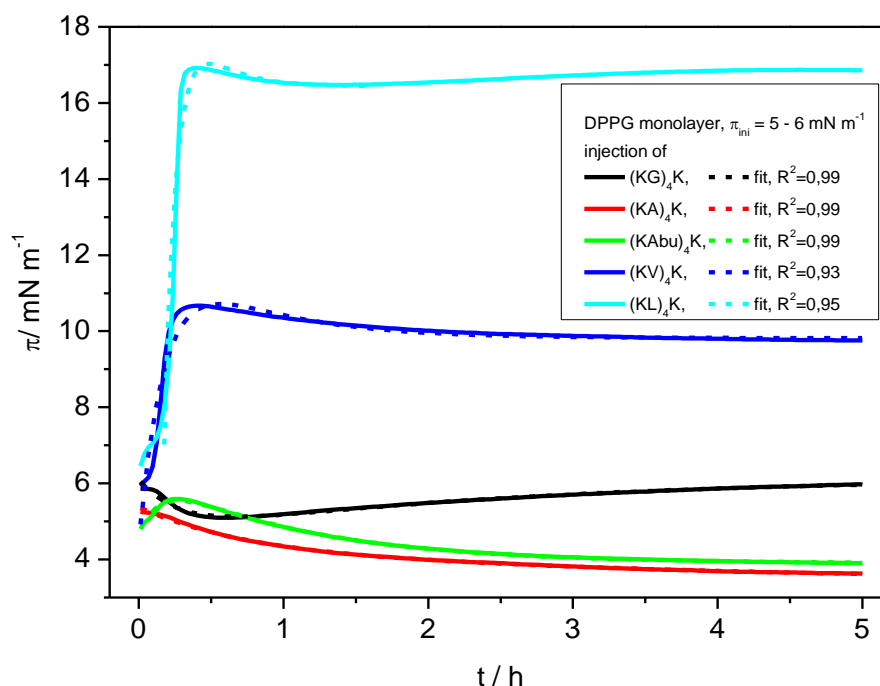

Figure 4.3.3: Time dependent development of the surface pressure of a DPPG monolayer after injection of different solutions of the peptides (KX)$_4$K into the subphase at a starting surface pressure of 5 - 7 mN m^{-1} in the *LE* phase ($T = 20$ °C, 100 mM NaCl). The final concentration of the peptide in the subphase was 3.0 µM. Adsorption equlibrium was reached within 5 h.

These data reveal certain trends. The amplitude A_2 for the lipid condensation effect should be similar for all peptides, because all peptides have the same overall charge. Indeed, the value for A_2 increases only slightly with the hydrophobicity of the peptide, as stronger hydrophobic interactions lead to a closer location of the charged lysine side chains at the surface and lead to more effective lipid condensation. The relaxation time t_2 shows first an increase starting from (KG)$_4$K and then a significant decrease going from (KA)$_4$K to (KL)$_4$K. In the case of (KA)$_4$K binding only the slow condensation effect was visible. It could be that both processes have similar relaxation times so that they cannot be separated.

The relaxation time t_1 describing the effect of peptide incorporation becomes shorter, the more hydrophobic the peptide is, the relaxation times for (KAbu)$_4$K and (KV)$_4$K being very similar. In this case, it could be excluded that the diffusion of the peptide to the air-water interface is the rate-limiting step, because for the most hydrophobic peptide an even shorter relaxation time is observed. The amplitude A_1 of this effect correlates with the hydrophobicity and increases from (KG)$_4$K to (KL)$_4$K due to a deeper incorporation of the peptides into the lipid headgroup region. Assuming that the adsorption of the peptide to the air-water interface

requires the opposite charge of the lipid headgroup it is surprising that the rate constant for lipid incorporation seems to be faster than the rate constant of the lipid condensation due to the charge compensation.

Table 4.3.1: Fit values for the adsorption kinetics of an injected peptide (KX)$_4$K into the subphase of a DPPG monolayer at 5 - 7 mN m^{-1}. Values for (KA)$_4$K in parenthesis are for a mono-exponential fit, as a bi-exponential fit could not reliably be performed. A_1, A_2: amplitudes of the two processes, t_1, t_2: relaxation rates, π_0: final surface pressure after 5 h. Data obtained by least square fit with the given bi-exponential equation. Errors are from numerical fitting routine of Origin 8.0.

	peptide incorporation		lipid condensation		
peptide	A_1 / mN m^{-1}	t_1 / h	A_2 / mN m^{-1}	t_2 / h	π_0 / mN m^{-1}
(KG)$_4$K	-1.55 ± 0.02	2.48 ± 0.14	1.49 ± 0.03	0.28 ± 0.01	6.17 ± 0.03
(KA)$_4$K			(1.66 ± 0.01)	(1.25 ± 0.02)	3.64 ± 0.01
(KAbu)$_4$K	-1.66 ± 0.03	0.15 ± 0.01	2.45 ± 0.02	1.08 ± 0.01	3.90 ± 0.01
(KV)$_4$K	-8.41 ± 0.61	0.18 ± 0.01	2.94 ± 0.64	0.65 ± 0.09	9.82 ± 0.02
(KL)$_4$K	-15.00 ± 0.49	0.08 ± 0.01	3.53 ± 0.50	0.23 ± 0.04	16.44 ± 0.08

Comparison with literature data shows that similar adsorption kinetics were observed for the binding of poly(L-lysine) or poly(L-arginine) to a DPPG monolayer [105] with no additional intervening hydrophobic amino acids. For poly(L-arginine), however, the arginine side chain is more hydrophobic so that even for DPPG in the *LC* phase a surface pressure increase is observed due to an insertion of the side chain into the headgroup region. For the pentapeptide lys$_5$, which is less hydrophobic, this surface pressure increase is reduced. Further reduction of spacer length enhances the effect of condensation [123].

4.3.1.4 Changes of Surface Pressure as a Function of π_{ini}

The change in surface pressure $\Delta\pi = \pi_0 - \pi_{ini}$, observed after adsorption of a protein or peptide to a lipid monolayer shows in many cases a linear relationship as a function of the initial surface pressure π_{ini}, from which the maximum insertion pressure (MIP) is determined. MIP is the value of π_{ini}, where $\Delta\pi = 0$ mN m^{-1}. Per definition MIP is a value above which no incorporation into the lipid bilayer occurs anymore [8, 148, 149]. However, as observed before for the binding of cationic pentapeptides to DPPG monolayers, this relation and the interpretation cannot be used for the electrostatic binding of peptides, as negative surface pressure changes and changes in slope were observed [123].

This is again found for the peptides used in this study (see Figure 4.3.4). All peptides show a biphasic adsorption mainly dependent on the phase state of the DPPG monolayer. For (KG)$_4$K, $\Delta\pi$ values are very small and only a tendency for becoming more negative with

increasing π_{ini} is visible. For (KA)$_4$K and (KAbu)$_4$K with low hydrophobicity, all values for $\Delta\pi$ are negative and a linear behaviour is seen, although the slopes in both phase are slightly different. For the more hydrophobic peptides (KV)$_4$K and (KL)$_4$K a different behaviour is observed. At low initial surface pressure π_{ini} an increase of $\Delta\pi$ up to a certain maximum value of π_{ini} is seen, followed by a decrease in $\Delta\pi$, which becomes then negative at higher values of π_{ini}. Thus, the adsorption of the peptides studied here leads to a completely different behaviour of $\Delta\pi$ *vs.* π_{ini} as observed before for proteins, where a linear behaviour and only positive $\Delta\pi$ values and not negative ones were observed [147, 149, 150, 244]. The reason for these differences is the condensation of the lipid monolayer due to electrostatic shielding of charges.

As shown in Figure 4.3.4, $\Delta\pi$ decreases linearly with increasing π_{ini} only at initial surface pressure $\pi_{ini} > 10$ mN m^{-1}, where a DPPG monolayer is in the *LC* state, i.e.

$$\Delta\pi = m\pi_{ini} + n \tag{4.2}$$

The values for m, n, and π_{sp}, as shown in Table 4.3.2, were all obtained at a given subphase concentration and for the binding to a DPPG monolayer in the *LC* phase. As the peptides themselves are not surface active, the parameter n obtained from the fits have no physical meaning. The observed value of $\Delta\pi$ is determined by a superposition of condensing and insertion effects. When $\Delta\pi = 0$ mN m^{-1} both effects exactly compensate, which occurs at the value $\pi_{ini} = \pi_{sp}$ and called here superposition surface pressure π_{sp}. By rearranging equation (4.2), the superposition surface pressure is calculated as follows:

$$\pi_{sp} = -\frac{n}{m} \tag{4.3}$$

For adsorption of (KG)$_4$K at initial surface pressures below 10 mN m^{-1} (DPPG in *LE* phase), no notable changes are visible. As the kinetics show two distinct processes of peptide insertion and lipid condensation, they compensate each other so that finally $\Delta\pi = 0$ mN m^{-1}. For the *LC* phase, the surface pressure decreases linearly with increasing π_{ini} and thus the lipid condensation becomes more prominent. The break in the plot corresponds with the transition region of the lipid monolayer and the calculated value for π_{sp}.

The slope m in the plot $\Delta\pi$ vs. π_{ini} is connected with the strength of the interaction between peptide and lipid. Similar explanations about the strength of lipid-peptide interactions are given by Calves et al. [149]. Regression lines with a slope $m = -1$ would represent an ideal situation, where the binding of the peptide is not favoured or no interaction exists at all. A steeper slope with absolute values larger than 1 ($m < -1$) indicates repulsive interactions and a

slope with absolute values lower than 1 attractive interactions ($0 > m > -1$). A comparison of the slopes determined for lipid-peptide interactions [147, 149, 150, 244] with those obtained here is difficult due to the following reasons. First, the peptide itself is not surface active. Second, only an apparent slope is detectable, because two competing processes overlay with each other. However, the determined m value of -0.44 suggests attractive interaction between the bound (KG)$_4$K and DPPG.
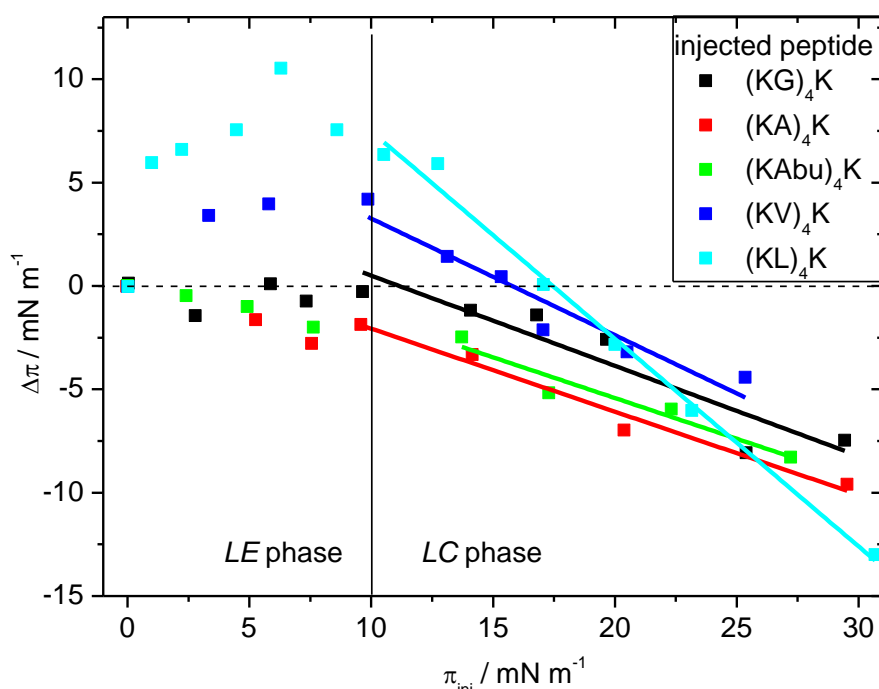

Figure 4.3.4: Difference of surface pressure $\Delta\pi$ after 5 h of adsorption of the peptides (KX)$_4$K to a DPPG monolayer with different initial surface pressure π_{ini}, the lines at $\Delta\pi = 0$ and $\pi_{ini} = 10$ mN m^{-1} are drawn to guide the eye and to distinguish between the different phases of the DPPG monolayer. The final concentration of the peptide in the subphase was 3.0 μM.

Although, there are differences in the adsorption kinetics between (KA)$_4$K and (KAbu)$_4$K, the dependence of $\Delta\pi$ on π_{ini} is similar. Adsorption of these peptides causes a decrease in surface pressure at all initial surface pressure values. There are only slight differences for the behaviour in the LE and LC phase. The calculated compensation of incorporation and condensation by extrapolation of data from the LC phase is reached at $\pi_{sp} = \sim 5 - 6$ mN m^{-1}. The m value of -0.40 implies comparable attractive forces as determined for (KG)$_4$K.

For the binding of (KV)$_4$K to the DPPG monolayer a different behaviour is seen. Up to $\pi_{ini} = 16$ mN m^{-1} incorporation of the peptide into the lipid monolayer dominates and a positive $\Delta\pi$ is observed which reaches a maximum at 10 mN m^{-1}. The dependence of $\Delta\pi$ from π_{ini} in the LC phase shows a linear relationship with a slope of $m = -0.56$. The superposition surface pressure π_{sp} of the peptide (KV)$_4$K is much higher with ~ 16 mN m^{-1}, indicating the

increasing dominance of the insertion effect. The obtained value for π_{sp} corresponds with the observed equilibrium surface pressure after peptide adsorption of medium initial surface pressure ($\pi_{ini} = 10 - 17$ mN m^{-1})

Table 4.3.2 Values of n, m, π_{sp} and R^2 obtained from the fitting of data for binding of the peptides $(KX)_4K$ to a DPPG monolayer in the *LC* phase presented in Figure 4.3.4. Errors of the parameters m, n, and π_{sp} from least square fit of the regression lines calculated with Origin 8.0.

peptide	intercept n / mN m^{-1}	slope m	superposition surface pressure, π_{sp} / mN m^{-1}	R^2
$(KG)_4K$	4.9 ± 1.6	-0.44 ± 0.08	11.0 ± 4.2	0.849
$(KA)_4K$	2.0 ± 0.9	-0.40 ± 0.04	4.9 ± 2.2	0.967
$(KAbu)_4K$	2.5 ± 1.5	-0.39 ± 0.07	6.3 ± 3.9	0.910
$(KV)_4K$	8.9 ± 1.4	-0.56 ± 0.08	15.9 ± 3.4	0.904
$(KL)_4K$	17.5 ± 0.9	-1.00 ± 0.04	17.5 ± 1.1	0.990

Adsorption of $(KL)_4K$ to a DPPG monolayer in the surface pressure range up to 10 mN m^{-1} first leads to an increase in surface pressure. In the range of π_{ini} from 10 mN m^{-1} up to 30 mN m^{-1} a linear decrease in $\Delta\pi$ is seen. The superposition surface pressure π_{sp} of 17.5 ± 1.1 mN m^{-1} is the highest observed for all peptides and fits with the equilibrium surface pressure of the adsorption studies. The slope $m = -1.00$ of the linear fit is much steeper compared to all other peptides. According to the theory of Calves [148] no attractive interactions between the peptide $(KL)_4K$ and DPPG monolayer should be present. After peptide adsorption, an equilibrium surface pressure of about 17 mN m^{-1} is observed, independent of the initial surface pressure.

Comparing all peptides (see Figure 4.3.4), the decrease of the surface pressure is similar in the range $\pi_{ini} = 25 - 30$ mN m^{-1} for all peptides. For this dense DPPG monolayer in the *LC* phase lipid condensation is dominating and results a decrease in surface pressure of about 6 mN m^{-1}, highlighting the importance of the electrostatic attraction. The differences in the peptide hydrophobicity are unimportant. The hydrophobic interaction between the lipids and the peptide play a role for the less dense lipid monolayer in the *LE/LC* phase transition region and close above. The more hydrophobic the peptide, the higher is the increase of the surface pressure. Lipid condensation and peptide insertion overlay each other and have opposite effects on the change in surface pressure. The overall strength of interaction between the lipids and peptides should be the sum of the hydrophobic and electrostatic contributions.

Assuming the two counteracting effects having similar strength a slope $m = -1$ is detected, as seen for (KL)$_4$K and DPPG. For the peptides (KX)$_4$K, the slope m is related to the extent of the hydrophobic contribution. A steeper slope for peptides with more hydrophobic amino acids, such as (KV)$_4$K, and (KL)$_4$K compared to (KG)$_4$K is determined. Thus, it is concluded that the strongest attractions exists between (KL)$_4$K and DPPG.

When the values m, n, and π_{sp} were analyzed, a coupling of these three parameters was observed as shown in Figure 4.3.5. All three parameters have minimal values for peptides with intermediate hydrophobicity, i.e. (KA)$_4$K or (KAbu)$_4$K.
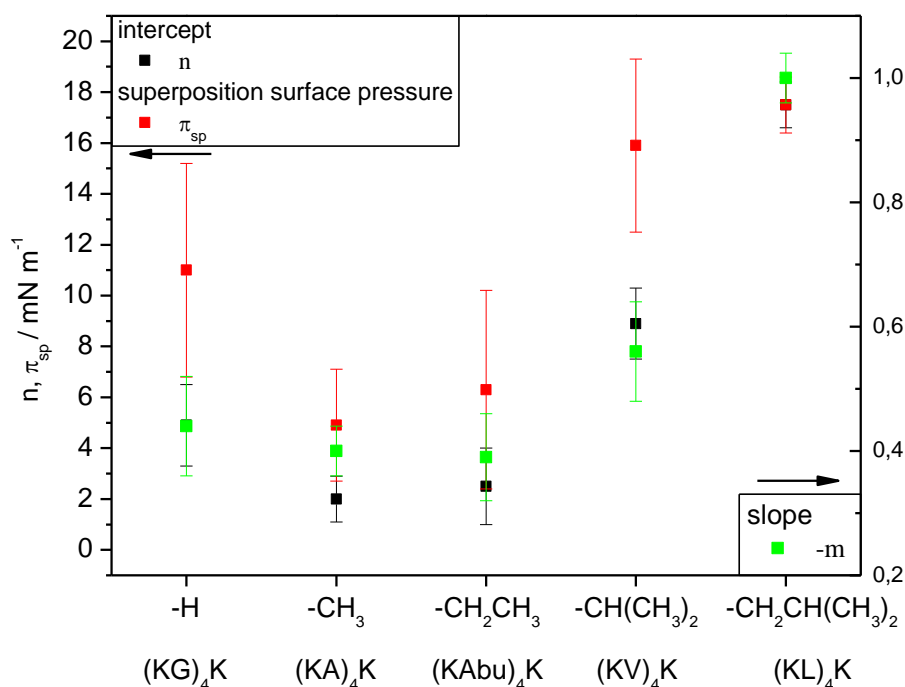

Figure 4.3.5: Graphical representation of the values n, m, and π_{sp} for peptides (KX)$_4$K with different side chain residues of the uncharged amino acid X.

4.3.1.5 Adsorption of Peptides (KX)$_4$K to DPPG Monolayers Studied with Fluorescence Microscopy

To investigate whether the adsorption of the peptide to the lipids and the possible incorporation has an effect on the domain formation and the shape of the lipid *LC*-domains, fluorescence microscopy experiments were performed.

In the *LE* phase of a pure DPPG monolayer at 3.4 mN m^{-1} the fluorescence marker Rh-DHPE is homogeneously distributed and the fluorescence micrograph shows a uniform bright monolayer (see Figure 4.3.6), as the onset of the *LE/LC* phase transition occurs at a surface pressure of about 8 - 10 mN m^{-1}. Upon peptide addition, the formation of *LC*-domains is

triggered in all cases, despite the fact that π can increase or decrease, depending on the added peptide. The *LC*-domains appear dark as the fluorescence marker molecule is excluded from them [158]. Within each image, all domains have similar sizes. After 4h of adsorption of (KG)$_4$K, (KA)$_4$K and (KAbu)$_4$K, ca. 17 % of the total monolayer area is covered with circular *LC*-domains, although the surface pressure is lower compared to the pure DPPG monolayer before peptide injection. It is also still way below the phase transition pressure of pure DPPG (see Figure 4.3.6). This confirms the assumption stated above that upon electrostatic binding of the peptides to the DPPG monolayer the lipid condensation occurs and the acyl chains become more ordered with the result of the formation of *LC*-domains [254].
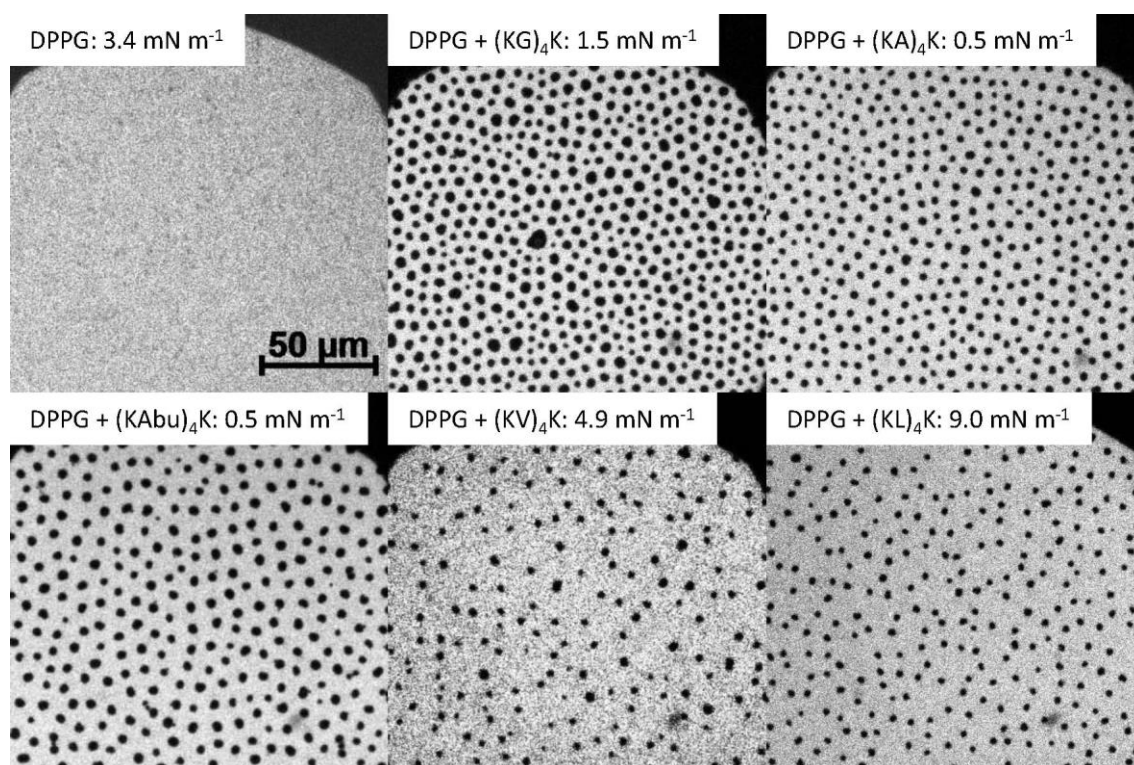

Figure 4.3.6: Fluorescence microscopy images of a DPPG monolayer at the air-water interface before peptide adsorption and after 4 - 5 h of adsorption of the linear peptides reaching final surface pressures as indicated. The final concentration of the peptide in the subphase was 3.0 μM. Lipid dye: 0.01 mol% Rh-DHPE. The scale bar given in the image for a pure DPPG is the same for all other images.

After adsorption of (KV)$_4$K and (KL)$_4$K, only 6 % and 11 %, respectively, of the monolayer show condensed domains (for comparison see Figure 8.3.4, right panel). After binding of these two peptides, the surface pressure increases, indicating that hydrophobic parts of the peptide are incorporated into the acyl chain region of the lipid monolayer overcompensating the effect of electrostatic condensation and thus leading to a smaller number of *LC*-domains.

After 5 h of adsorption of the peptides to the lipid monolayer, a slow compression of the monolayer was started, the surface pressure was monitored and fluorescence microscopy

images were acquired during the compression process. The compression isotherms and the calculated compressibility data for pure DPPG and for DPPG with adsorbed peptide from the subphase are shown in Figure 4.3.7. The fluorescence microscopy images recorded during the compression of the monolayer are depicted in Figure 4.3.8.
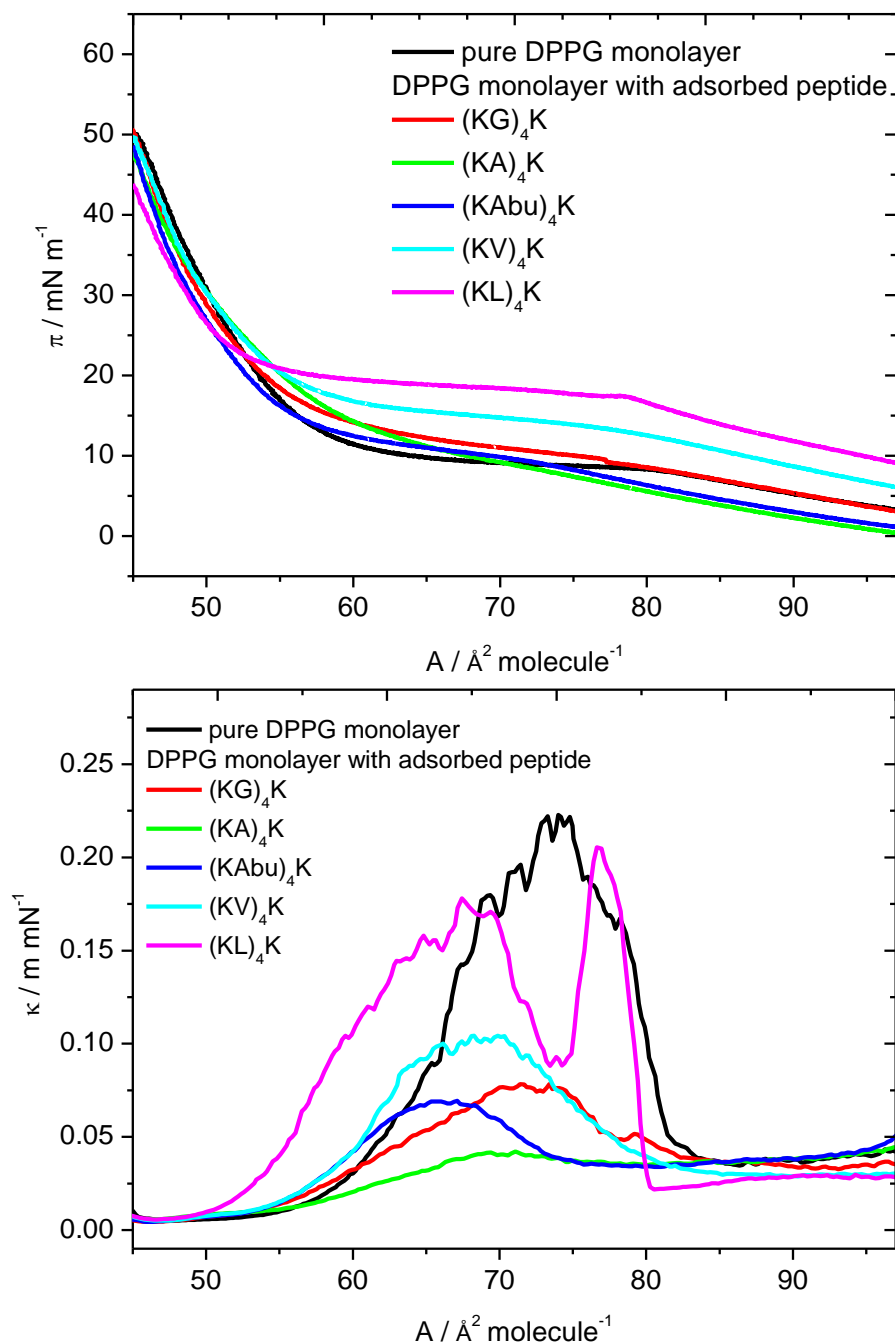

Figure 4.3.7: Top: Surface pressure - area isotherm of a pure DPPG monolayer and DPPG monolayer with adsorbed peptide from the subphase. Bottom: Compressibility of a pure DPPG monolayer and DPPG monolayers with adsorbed peptide.

The observed compression isotherm of pure DPPG with its characteristic plateau starting at about 8 mN m^{-1} for the phase transition from the *LE* to the ordered *LC* phase is in good agreement with literature data [229, 255, 256]. Micrographs of pure DPPG monolayers (Figure 4.3.8, upper row) show a homogeneous bright monolayer in the *LE* phase. The appearance of the first irregular dark domains of condensed lipids fits with the *LE/LC* phase transition with its high compressibility between 80 and 65 Å^2 molecule^{-1} (see Figure 4.3.7 bottom). Further compression increases the area covered with condensed lipids. The dye is excluded from the ordered domains and is forced to accumulate at the domain boundaries, giving the image a higher contrast.

The compression isotherm obtained after binding of (KG)$_4$K is similar compared to the pure DPPG isotherm, only the phase transition region seems to be smeared out after (KG)$_4$K adsorption leading to a reduced compressibility. At high surface pressure, the isotherms overlap indicating that the peptide is apparently only bound to the lipid headgroup region.

Adsorption of (KA)$_4$K and (KAbu)$_4$K first lowers the surface pressure of the DPPG monolayer and the compression isotherm therefore starts below the one of pure DPPG at high molecular areas. During compression of the mixed films, only a smeared-out plateau is visible as seen before for (KG)$_4$K, which is slightly more prominent for binding of (KAbu)$_4$K. Comparing all results the condensing effect of the bound peptide can be seen as a decrease of surface pressure in adsorption measurements coupled with the occurrence of *LC*-domains and a lowered compressibility of the mixed monolayer.

The adsorption of the more hydrophobic peptides (KV)$_4$K and (KL)$_4$K increase the surface pressure due to insertion into the monolayer in the *LE* phase at high molecular areas. The largest effect is seen for (KL)$_4$K. Compression of the DPPG/(KV)$_4$K film shows a broad phase transition starting at 15 mN m^{-1}. For DPPG/(KL)$_4$K, the phase transition pressure is even higher with 19 mN m^{-1}. These two peptides with their larger hydrophobic side chains insert in between the lipid chains in the *LE* phase and apparently reach the air-water surface thus increasing the phase transition pressure. An upshift of the *LE/LC* phase transition is interpreted as effect of a disturbed acyl chain ordering upon incorporation of the adsorbed molecule into the acyl chain region. Both values of the phase transition are comparable with the calculated superposition surface pressure from the adsorption experiments. The compressibility in the transition region is reduced for mixed monolayers compared to pure DPPG, although compressibility increases again with the hydrophobicity of the added peptide from (KA)$_4$K to (KL)$_4$K.
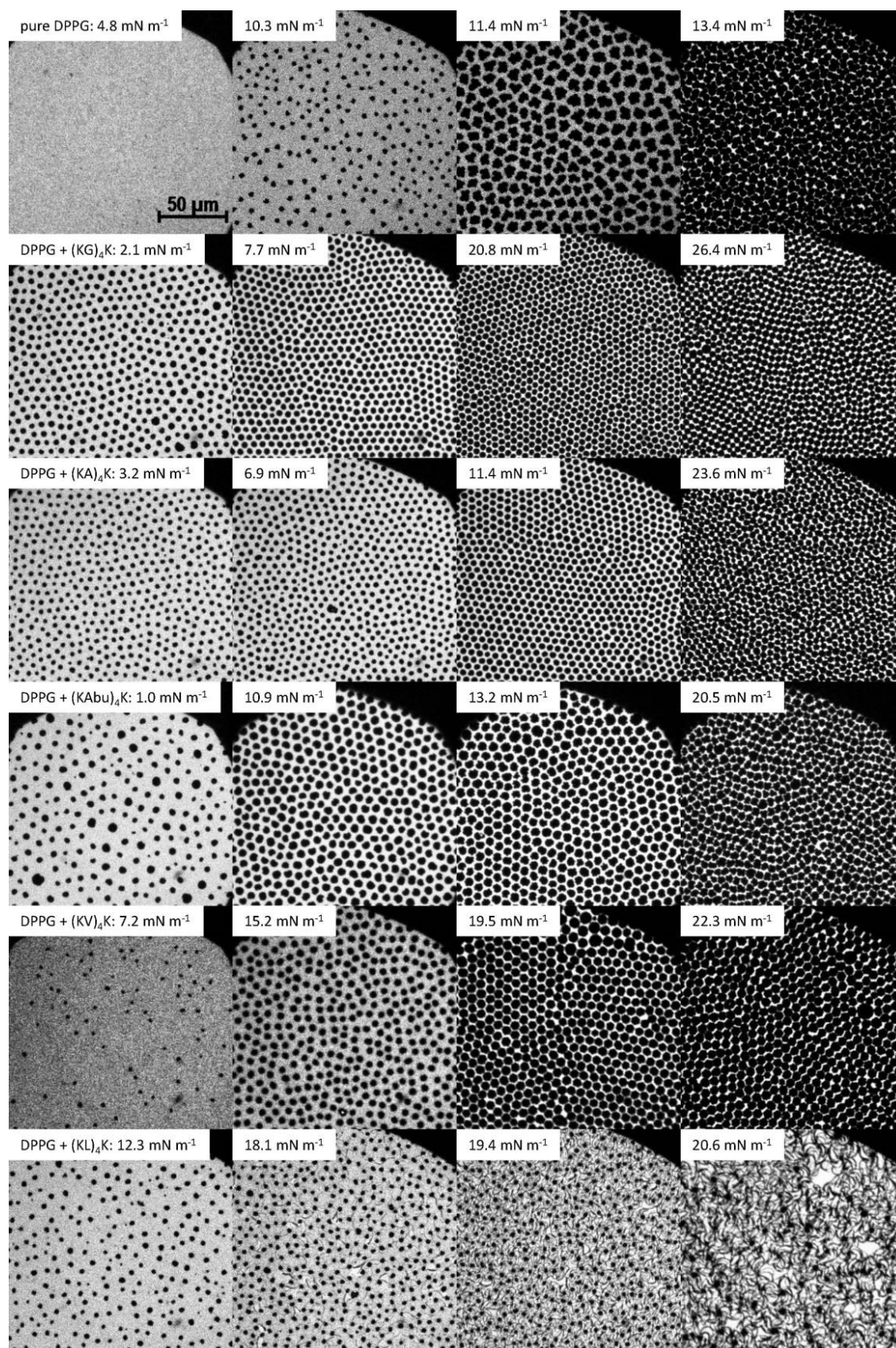
Figure 4.3.8: Fluorescence microscopy images of pure DPPG monolayer (upper row) and DPPG monolayer with adsorbed peptide (row 2 - 6) at the air-water interface ($T = 20$ °C, 100 mM NaCl subphase) recorded at different surface pressure. Lipid dye: 0.01 mol% Rh-DHPE. The scale bar given in the image for a pure DPPG is the same for all other images.

The fluorescence micrographs taken during the compression of the DPPG monolayer after peptide binding are quite similar for the adsorbed peptides (KG)$_4$K, (KA)$_4$K, (KAbu)$_4$K and (KV)$_4$K. Dark condensed domains are visible, even at a surface pressure below the *LE/LC* phase transition region of pure DPPG and the plateau surface pressures of the film with bound peptides (see Figure 4.3.8). The fluorescence images therefore prove that lipid condensation occurs after adsorption of the peptide to the monolayer in the *LE* phase. Compression of these mixed monolayers from 90 Å^2 molecule^{-1} to 55 Å^2 molecule^{-1} also increases the area covered by the condensed domains as expected. However, compared to the domains seen for pure DPPG films, the arrangement of the *LC*-domains is not random, but becomes highly ordered.
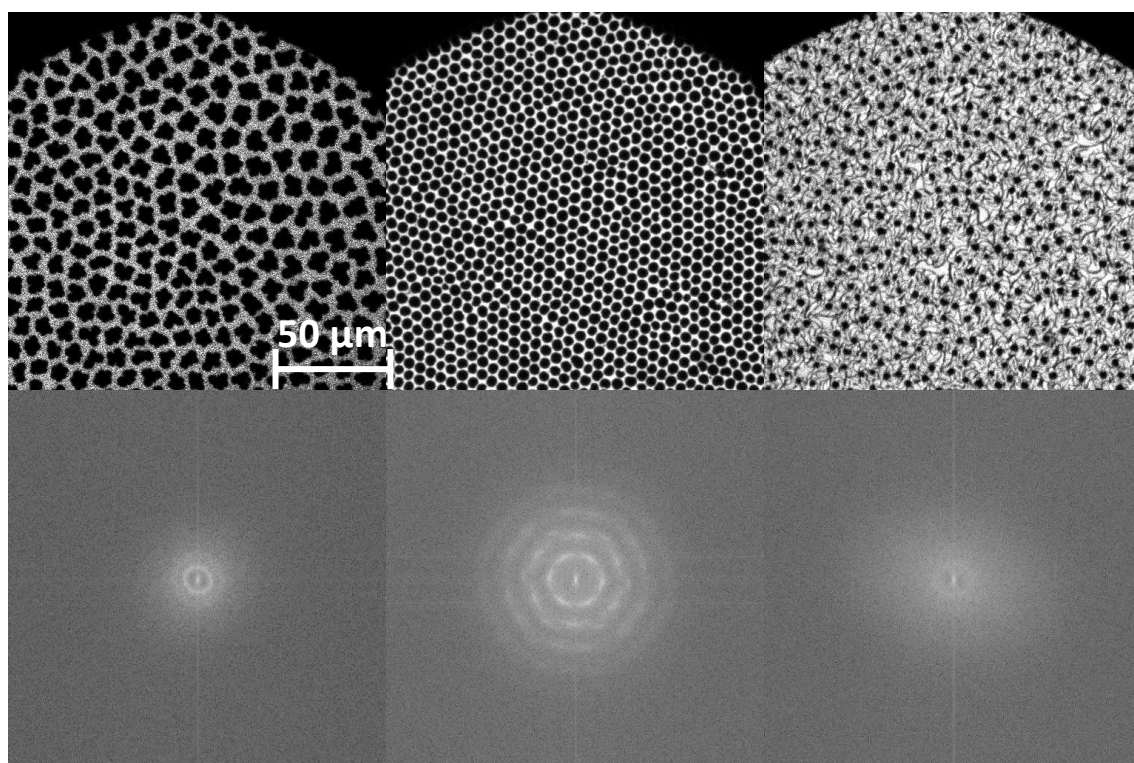

Figure 4.3.9: Upper row: pure DPPG (11.4 mN m^{-1}, left): *LC*-domains have irregular size and random orientation during compression; DPPG + adsorbed (KG)$_4$K (20.8 mN m^{-1}, middle): *LC*-domains have similar size and regular sixfold symmetry during compression, ordered pattern of domains with a sixfold local arrangement; DPPG + adsorbed (KL)$_4$K (19.4 mN m^{-1}, right): *LC*-domains have a nucleation core in the middle of the domain with long filaments. Lower row Fourier transformed pictures showing a random orientation of neighboring domains for pure DPPG and DPPG with adsorbed (KL)$_4$K, a sixfold symmetry of domain orientation for DPPG with (KG)$_4$K. The scale bar given in the image for a pure DPPG is the same for all other images.

In addition, all domains have similar sizes, are almost round at low surface pressure, and form hexagonal shapes at higher surface pressure and lower surface area. The domains are stable and seem not to fuse upon compression. Thus, it can be concluded that binding of peptides lowers the line tension between *LE* phase and *LC*-domains. An additional effect, preventing

growth of *LC*-domains might be the different dipole densities between *LE* phase and *LC*-domains after peptide binding.

A closer look at the organization of the domains reveals a six-fold symmetry. This becomes much clearer after a Fourier-transformation of the image (see Figure 4.3.9). The peptides seem to have a higher concentration at the edges of the condensed domains (data from double label experiments, not shown). Electrostatic repulsion between the single domains then leads to a quasi-hexagonal arrangement of domains. The occurrence of these hexagonal patterns results thus from an equilibrium between electrostatic repulsion and line tension as shown before [257, 258].

A significantly different behaviour is observed for mixed monolayers of DPPG after adsorption of the peptide with the highest hydrophobicity, (KL)$_4$K (see Figure 4.3.8, bottom row). At the beginning of the compression isotherm, at high areas per molecule, also condensed domains are visible due to the adsorbed peptide. The plateau in the compression isotherm region appears at 19 mN m^{-1} and corresponds to the onset of changes in the domain shape seen in the fluorescence micrographs. At the beginning of this plateau at 17 mN m^{-1}, very thin filaments of condensed lipid grow from the existing domains, which act like nucleation sites. Further compression increases the number and the length of these filaments. Over the whole compression range, the initially formed round domains are still present. Adsorption of (KL)$_4$K lowers the line tension between *LC*-domains and the surrounding *LE* phase much more compared to the other tested peptides in this study, due to the bulkier side chain of leucine.

A reduced line tension between the *LE* phase and *LC*-domains is observed for DPPC mixtures with cholesterol [259], perfluoroalcohols [260], 5-cyanobiphenyl [261] or semitelechelic polymers [262]. This is always combined with an elongation of the observed domains due to the accumulation of the additional agent at the edge of the condensed domain and a creation of a new phase boundary.

4.3.1.6 Time Dependent Adsorption of Peptides (KX)$_4$K to DPPG Monolayers Studied with Infrared Reflection Absorption Spectroscopy

The combination of the monolayer technique with infrared spectroscopy provides additional information on the phase state of the lipids as well as the orientation and secondary structure of the peptide. The changes in surface pressure upon peptide binding were discussed separately in the previous section (see section 4.3.). Conformational changes of the lipid at the air-water interface due to adsorption of the injected peptide to the monolayer can be resolved by time dependent recording of IRRA spectra. The following vibrational bands are of interest for mixed lipid-peptide films: the OH stretching vibration of the aqueous subphase, the CH$_2$ and C=O stretching vibration of the lipid and the amide vibrations of the adsorbed peptide (see Figure 4.3.10).

The OH stretching bands [4] and the integral absorption between 3800 cm^{-1} - 3000 cm^{-1} provide information on the thickness of the monolayer at the air-water interface [164] and possible changes upon interaction with the injected peptide.
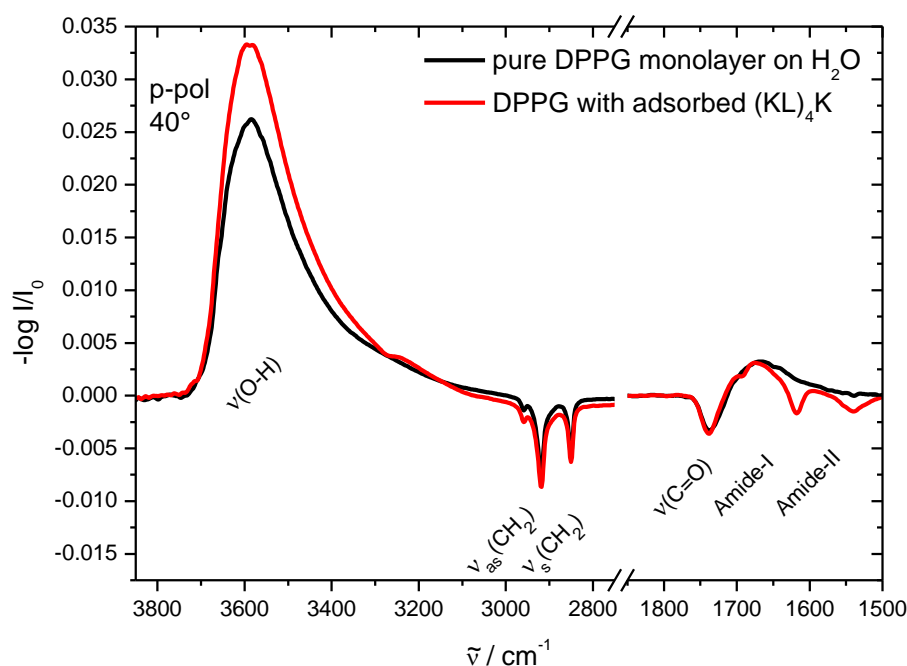
Figure 4.3.10: FT-IRRA spectra with all characteristic vibrational bands discussed in the text.

Peptide binding to the lipid monolayer can be directly proved by the appearance of the amide bands and indirectly by OH-absorption increase indicating an increase of the layer thickness of the mixed film. Different arrangements of the bound peptide can be distinguished. An incorporation of single peptide strands into the lipid monolayer would lead appearance of amide vibrational bands combined with minor changes in the OH stretching mode region, as

seen for the binding of KLAL to POPG [251]. Observed changes in layer thickness of lipid monolayer in the *LC* phase can be a result of the adsorption of peptide as well as a change in tilt angle of the lipid acyl chains. An increase in the intensity of the OH stretching band with a concomitant occurrence of amide bands indicates a peripheral adsorption of the peptide to the headgroup region of the monolayer, increasing the film thickness [263, 264].

In the experiments, pure DPPG monolayers in the *LC* phase had similar surface pressure of ca. 19 mN m^{-1} - 23 mN m^{-1}, prior to injection. The water bands had integrals values of 6.2 - 7.2 absorb. cm^{-1}. The integrals of the OH stretching bands increased short after peptide binding. It can be deduced that the layer thickness is increased upon binding of the peptide. Due to slightly different starting values of the integral of the OH band, the increase of the integral was evaluated.

The increase of the water band integral upon peptide binding is similar for all peptides, except for (KL)$_4$K. After 8 h the adsorption equilibrium was reached. Binding of the hydrophilic peptides creates an increase of 8 - 13 %, whereas the binding of the more hydrophobic peptide (KL)$_4$K increases the water band integral up to 30 % (see Figure 4.3.11, left panel). These findings correlate with the differences in peptide structure, where also (KL)$_4$K behaves different from the other peptides (KX)$_4$K (see discussion below). The similar changes in ΔH$_2$O of the other peptides suggest a similar interaction of these peptides with the lipid monolayer and a similar effect on the layer thickness. For the peptides (KG)$_4$K up to (KV)$_4$K, the interaction with the DPPG monolayer is driven by electrostatics, without any incorporation of the peptides into the lipid acyl chains. It seems that these peptides are not hydrophobic enough to penetrate the lipid monolayer in the *LC* phase and are only weakly adsorbed via charge interaction. The ordered lipid arrangement in the *LC* phase prevents the peptide incorporation into the hydrophobic region of the monolayer. For the peptide (KL)$_4$K, the hydrophobicity of the leucine side chain is higher so that incorporation into the monolayer seems to occur.

The band position of the CH$_2$ vibration (2970 cm^{-1} - 2840 cm^{-1}) depends on the phase state of the monolayer and the conformational order of the acyl chains of the lipids [170, 185]. In the *LE* phase, a position of ca. 2925 cm^{-1} and 2855 cm^{-1} is observed and in the *LC* phase, the bands are located at lower wavenumber (2920 cm^{-1} and 2850 cm^{-1}), indicating that the acyl chains are in *all-trans* conformation.
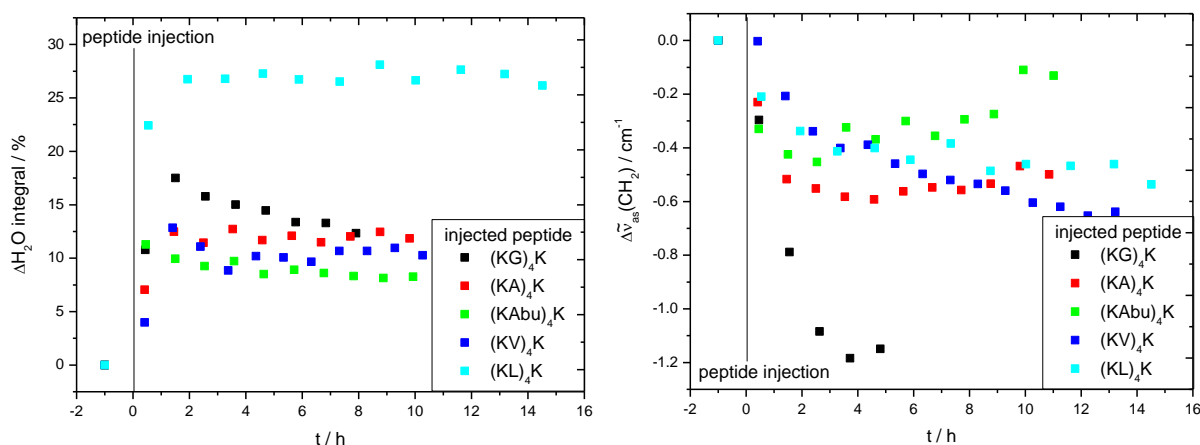
Figure 4.3.11: Time dependent differences of the integral of the water band (3000 cm^{-1} to 3800 cm^{-1}, left panel) and of the asymetric CH$_2$ vibrational band of the lipid acyl chain (right panel) upon peptide adsorption (averaged values of 5 individual spectra). For all graphs the data point (-1;0) refers to the initial state of a pure DPPG monolayer prior to peptide injection.

The asymmetric CH$_2$ vibrational band is located at about 2919.1 ± 0.1 cm^{-1} for a pure DPPG monolayer in the *LC* phase at a surface pressure of about 20 mN m^{-1}. This indicates a relative high acyl chain order and a high proportion of *all-trans* conformers. Upon peptide adsorption, the wavenumber of the asymmetric CH$_2$ vibration decreases by 0.2 - 1.2 cm^{-1} (see Figure 4.3.11, right panel). The observed decrease of the CH$_2$ vibrational band positions, indicating a condensation effect, is similar for all tested peptides. Only the adsorption of (KG)$_4$K shows a stronger decrease of the wavenumber, which might be a result of the flexible peptide chain enabling a better electrostatic interaction. The order of the acyl chains increases further due to a shielding of the repulsive interactions in the headgroup region after peptide binding. The condensation effect of the bound peptide on the lipid was shown before using fluorescence microscopy, as dark condensed domains appear after peptide binding.

Peptide, adsorbed to a bare air-water interface or to a lipid monolayer, can be detected by the occurrence of bands in the amide-I (1700 cm^{-1} to 1610 cm^{-1}) and amide-II region (1575 cm^{-1} to 1500 cm^{-1}). The characteristic bands in the amide-I region allow the determination of the secondary structure of the peptide. For the experiments shown here, it is difficult to draw a conclusion on the secondary structure of the adsorbed peptides, as the observed intensities are very low (see Figure 8.3.7, left panel). For all tested peptides (KX)$_4$K the occurrence of weak and broad amide-II bands around 1545 cm^{-1} indicate the presence of peptide, but no significant intensity is seen in the region of the amide-I band. For the peptides (KG)$_4$K, (KA)$_4$K, (KAbu)$_4$K, and (KV)$_4$K, thus no statement about the secondary structure can be made, but an unordered conformation is assumed from bulk measurements (broad band at

1648 cm^{-1}). The most hydrophobic peptide (KL)$_4$K shows a different behavior compared to the other peptides. The stronger accumulation of the peptide at the air-water interface enhances the band intensities in the spectra. The intense peaks at 1689 cm^{-1} and 1617 cm^{-1} show that (KL)$_4$K forms a β-sheet structure upon interaction with the DPPG monolayer in the *LC* phase.

(KL)$_4$K Adsorption to DPPG Monolayers in Different Phases

Injection experiments to investigate the adsorption behavior of (KL)$_4$K to an *LE* monolayer were performed to compare them with the fluorescence microscopy experiments on the one hand, and to determine the effect of the different phase states of the DPPG monolayer on the other hand. In the *LE* phase, the lipid molecules occupy a larger area at the air-water interface and the acyl chains are in an unordered conformation with a high fraction of *gauche* conformers, thus peptide incorporation between the lipid molecules should be easier.

The effect of the bound peptide on the lipid monolayer is similar for both tested surface pressures and phases. The OH vibration increases 30 % upon peptide injection for both phases of the DPPG monolayer (see Figure 8.3.7, right panel).
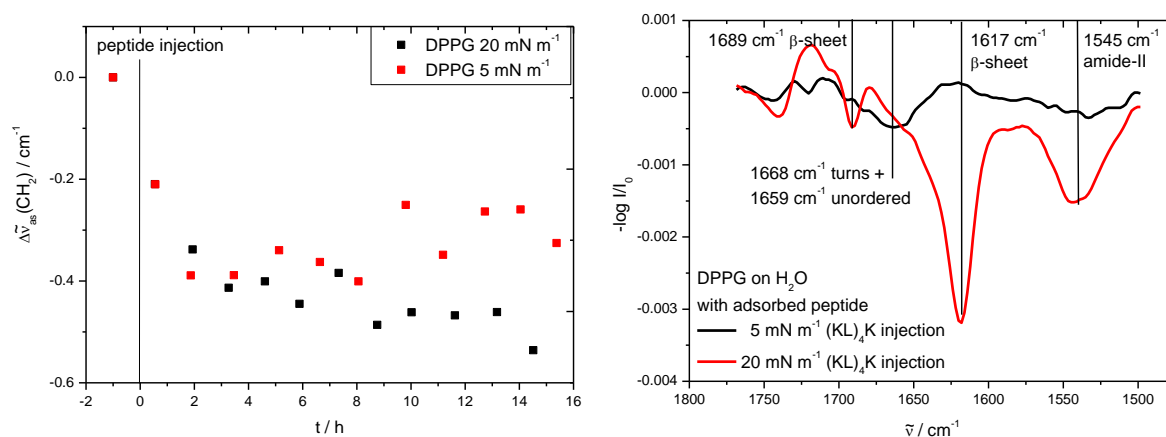

Figure 4.3.12: Left: time dependent differences in the wavenumber of the asymetric CH$_2$ vibration of the lipid acyl chain upon (KL)$_4$K adsorption to a DPPG monolayer in the *LE* or *LC* phase (avered values of 5 individual spectra). The data point (-1;0) refers to the initial state of a pure DPPG monolayer prior to peptide injection. Right: Difference spectra (calculated from the spectra obtained from the lipid monolayer with the adsorbed peptide minus the spectra of pure DPPG prior to peptide adsorption) of the amide region of (KL)$_4$K, adsorbed to a DPPG monolayer of different phase states.

Binding of (KL)$_4$K reduces the wavenumber of asymmetric CH$_2$ vibration for both phases (see Figure 4.3.12 left panel). Although the relative changes are similar ($\varDelta \tilde{\nu}$ = -0.3 cm^{-1}), the order of the lipid in the *LE* phase is lower than in the *LC* phase. Fluorescence microscopy measurements showed already the formation of *LC*-domains upon peptide binding at very low surface pressures, below the *LE/LC* phase transition pressure of pure DPPG.

The formation of *LC* domains with a more ordered and upright acyl chain region and adsorbed peptide to the lipid headgroup fits to the observation of a reduced wavenumber of the CH$_2$ vibration, an increased thickness of the mixed layer and the occurrence of dark domains in the fluorescence microscopy.

The amide-I band reveals differences of the secondary structure of the adsorbed peptide. After binding of (KL)$_4$K to an *LC* monolayer, a β-sheet was formed. Binding of (KL)$_4$K to an *LE* monolayer induces another secondary structure (see Figure 4.3.12, right panel). The weaker binding can be confirmed by the peptide amide-II vibration and the broad band in the amide-I region suggesting a mix of unordered (1659 cm^{-1}) and turn (1668 cm^{-1}) structures.

4.3.2   Influence of a Reduced Charge Density - Introduction of a Second Uncharged Amino Acid Spacer

4.3.2.1 Adsorption of Peptides (KXX)$_4$K to DPPG Monolayers at Different Initial Surface Pressure

Adsorption kinetics of (KGG)$_4$K to a DPPG monolayer

For (KGG)$_4$K the distances between the charged side chains is increased due to the insertion of a second glycine. In addition, all lysine side chains are pointing now towards opposite sides in the extended conformation of the peptide (see Figure 2.3.2). Adsorption of (KGG)$_4$K to the DPPG monolayer in the *LE* phase as well as the *LC* phase triggers a decrease of the surface pressure until the equilibrium surface pressure is reached after ca. 4 h (see Figure 4.3.13, left panel). The higher molar mass of (KGG)$_4$K slows down the binding kinetics compared to (KG)$_4$K.

Adsorption kinetics of (KAA)$_4$K to a DPPG monolayer

The peptide (KAA)$_4$K has an increased hydrophobicity compared to (KGG)$_4$K. For (KAA)$_4$K, a distinct dependence of the adsorption kinetics on the phase state of the lipid was observed (see Figure 4.3.13, right panel) comparable to the behaviour of (KAbu)$_4$K, although the peptide is larger. It seems that two alanines between the lysines have a similar effect on the adsorption kinetics as one amino butyric acid. For DPPG in the *LE* phase, first an increase in surface pressure is visible followed by a slower decrease of π. Thus, a reorientation of the peptide after binding to the lipid monolayer takes place to achieve a better electrostatic interaction. Compared to (KGG)$_4$K, the adsorption kinetics are different in the *LE* phase

For binding to the *LC* phase, only a decrease of the surface pressure is visible due to lipid condensation. Compared to (KGG)₄K, the adsorption kinetics of peptide insertion into the *LC* phase monolayer become faster and insertion is enhanced in its strength, with the result of a lower decrease of the surface pressure in the adsorption equilibrium.
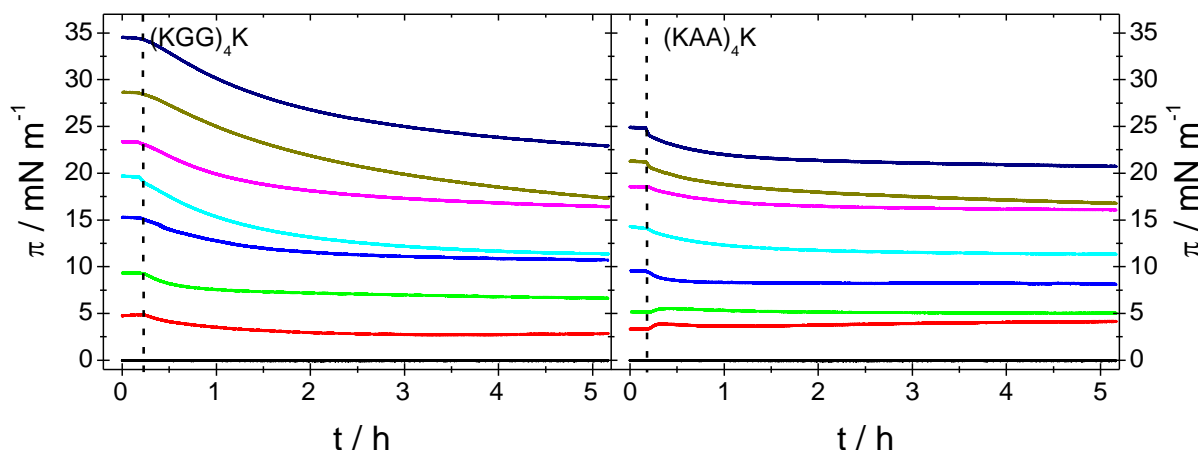

Figure 4.3.13: Change in surface pressure of a DPPG monolayer as a funktion of time after injection of different peptides (KXX)₄K into the subphase ($T = 20$ °C, 100 mM NaCl) at various initial surface pressure. The lipid monolayer remains at a constant surface pressure prior to peptide injection at $t = 600$ s (marked with the dashed line). The final concentration of the peptides in the subphase was 3.0 µM. Adsorption equlibrium was reached within 5 h.

4.3.2.2 Kinetic Analysis of (KXX)₄K Adsorption to a DPPG Monolayer

Similar to the kinetic analysis of the adsorption process of peptides (KX)₄K to a DPPG monolayer it was also attempted to entangle the two observed effects, the decrease of π upon lipid condensation and the increase of π upon incorporation into the monolayer, by fitting the experimental curves with the bi-exponential equation (4.1). In the case of (KGG)₄K binding only the slow condensation effect was visible. Therefore, the curve was fitted with a mono-exponential equation. It could be that both processes have similar relaxation times so that they cannot be separated.

Figure 4.3.14, left panel, shows the experimental and fitted curves for the adsorption of the different peptides to a DPPG monolayer starting from a surface pressure of ca. 5 - 6 mN m⁻¹, where the monolayer is in the *LE* phase. An overview of the obtained parameters is given in Table 4.3.3.

Comparing the peptides with two uncharged spacer completely reversed trends for all determined parameters were observed. As stated above, the amplitude A_2 describing the lipid condensation effect should be similar for all peptides, because all peptides have the same overall charge. For (KGG)₄K the amplitude A_2 is increased compared to (KG)₄K. Apparently, a more flexible peptide chain enables a better orientation of the charged lysine side chains,

fitting better to the distances between lipid phosphate groups, and thus leading to more effective lipid condensation. In contrast, the amplitude A_2 of (KAA)$_4$K is the smallest of all studied peptides. The relaxation times t_2 are similar for (KXX)$_4$K, underlining the reduced adsorption kinetics due to a higher molecular mass. The observed relaxation time t_2 of (KAA)$_4$K and (KAbu)$_4$K are also similar.
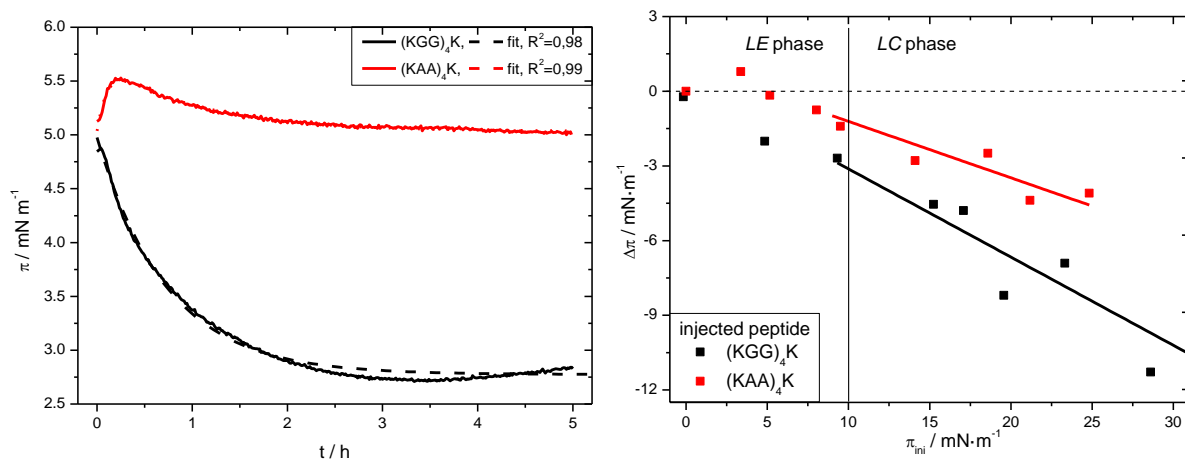

Figure 4.3.14: Left: Time dependent development of the surface pressure of a DPPG monolayer after injection of different solutions of the peptides (KXX)$_4$K into the subphase at a starting surface pressure of 5 mN m^{-1} in the *LE* phase (T = 20 °C, 100 mM NaCl). The final concentration of the peptide in the subphase was 3.0 µM. Adsorption equilibrium was reached within 5 h. Right: Difference of surface pressure $\Delta\pi$ after 5 h of adsorption of the peptides (KXX)$_4$K to a DPPG monolayer with different initial surface pressure π_{ini}, the lines at $\Delta\pi$ = 0 and π_{ini} = 10 mN m^{-1} are drawn to guide the eye and to distinguish between the different phases of the DPPG monolayer. The final concentration of the peptide in the subphase was 3.0 µM.

For (KGG)$_4$K no bi-exponential behaviour is seen, thus a comparison with the peptides (KX)$_4$K is not possible. Reasons might be a low amplitude A_1, a very long relaxation time t_1, or the overlay with the relaxation time for lipid condensation. For (KAA)$_4$K, the observed amplitude A_1 has the lowest values found for all peptides, whereas the relaxation time t_1 is comparable with the most hydrophobic peptide (KL)$_4$K. Thus, it can be concluded that already alanines contribute to the hydrophobicity of the peptide.

Table 4.3.3: Fit values for the adsorption kinetics of the injected peptides (KXX)$_4$K into the subphase of a DPPG monolayer at 5 - 6 mN m^{-1}. Values for (KGG)$_4$K in parenthesis are for a mono-exponential fit, as a bi-exponential fit could not reliably be performed. A_1, A_2: amplitudes of the two processes, t_1, t_2: relaxation rates, π_0: final surface pressure after 5 h. Data obtained by least square fit with the given bi-exponential equation. Errors are from numerical fitting routine of Origin 8.0.

peptide	peptide incorporation		lipid condensation		
	A_1 / mN m^{-1}	t_1 / h	A_2 / mN m^{-1}	t_2 / h	π_0 / mN m^{-1}
(KGG)$_4$K			(2.20 ± 0.01)	(0.74 ± 0.01)	(2.77 ± 0.10)
(KAA)$_4$K	-0.74 ± 0.01	0.11 ± 0.01	0.69 ± 0.01	0.98 ± 0.03	5.03 ± 0.01

4.3.2.3 Changes of Surface Pressure as a Function of π_{ini}

To gain comparable values of (KXX)$_4$K for m, n, and π_{sp}, only data of $\Delta\pi$ vs. π_{ini} of the *LC* phase were fitted as depicted in Figure 4.3.14, right panel.

Adsorption of (KGG)$_4$K causes a decrease in surface pressure for all initial surface pressure. The superposition of incorporation and condensation is extrapolated to $\pi_{sp} \approx 1$ mN m^{-1}. Thus, it can hardly proved experimentally. The shift of π_{sp} towards lower values compared to the value obtained for (KG)$_4$K is in accordance with the lower hydrophobicity of the peptide. The m value of -0.35 highlights the importance of the electrostatic attraction between the cationic peptide and negatively charged lipid.

For the binding of (KAA)$_4$K to the DPPG monolayer, a different behaviour for both phase states is seen. Up to $\pi_{ini} = 5$ mN m^{-1} incorporation of the peptide into the lipid monolayer slightly dominates and a slightly positive or zero $\Delta\pi$ is observed. The superposition surface pressure $\pi_{sp} = 4.8 \pm 1.8$ mN m^{-1} found for (KAA)$_4$K is comparable with that found for (KA)$_4$K, but higher than the value found for (KGG)$_4$K, indicating the increasing dominance of the insertion effect. The dependence of $\Delta\pi$ from π_{ini} in the *LC* phase shows a linear relationship with a slope of $m = -0.23$. This value is less negative than all determined values before, indicating weak interaction. Due to an increased charge distance, the impact of lipid condensation is lowered compared to (KX)$_4$K. In addition, the two glycines show the least contributions to the hydrophobic interaction. ATR-IR data from bulk samples indicate a different arrangement of the (KAA)$_4$K compared to alternating peptides(KX)$_4$K.

Table 4.3.4: Values of n, m, π_{sp} and R^2 obtained from the fitting of data for binding of the peptides (KXX)$_4$K to a DPPG monolayer in the *LC* phase presented in Figure 4.3.14. Errors of the parameters m, n, and π_{sp} from least square fit of the regression lines calculated with Origin 8.0.

peptide	intercept n / mN m^{-1}	slope m	superposition surface pressure, π_{sp} / mN m^{-1}	R^2
(KGG)$_4$K	0.4 ± 1.0	-0.35 ± 0.04	1.1 ± 2.9	0.913
(KAA)$_4$K	1.1 ± 0.4	-0.23 ± 0.03	4.8 ± 1.8	0.910

4.3.3 Influence of Delocalization of the Side Chain Charge - Exchange of Lysine by Arginine

4.3.3.1 Adsorption of Peptides (RX)₄R to DPPG Monolayers at Different Initial Surface Pressure

Adsorption kinetics of (RG)₄R to a DPPG monolayer

$(RG)_4R$ is the arginine analogue of $(KG)_4K$, also having an alternating sequence, but the positive charge of the peptide is delocated over the guanidinium moiety and the whole arginine side chain is more hydrophobic compared to the lysine side chain. The time dependent development of the surface pressure of a DPPG monolayer after injection of an aqueous $(RG)_4R$ solution into the subphase is depicted in Figure 4.3.15, left panel. The phase dependence of the adsorption kinetics on the phase state of the lipid is comparable to the behaviour for $(KG)_4K$. Peptide binding to DPPG monolayers in the *LE* phase shows first a decrease in surface pressure followed by a slower increase of π. Lipid condensation overcompensates the effect of peptide incorporation, if the DPPG monolayer is in the *LC* phase with the result that only a decrease of the surface pressure is visible.
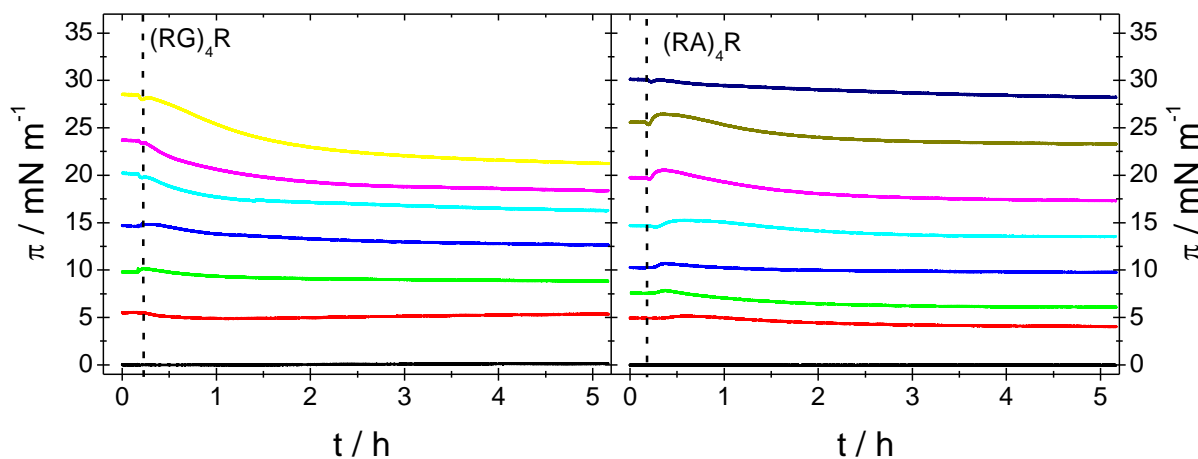

Figure 4.3.15: Change in surface pressure of a DPPG monolayer as a funktion of time after injection of different peptides $(RX)_4R$ into the subphase (T = 20 °C, 100 mM NaCl) at various initial surface pressure. The lipid monolayer remains at a constant surface pressure prior to peptide injection at t = 600 s (marked with the dashed line). The final concentration of the peptides in the subphase was 3.0 µM. Adsorption equlibrium was reached within 5 h.

Adsorption kinetics of (RA)₄R to a DPPG monolayer

$(RA)_4R$ is the arginine analogue to $(KA)_4K$. The time dependent development of the surface pressure of DPPG monolayers after injection of an aqueous $(RA)_4R$ solution into the subphase is depicted in Figure 4.3.15, right panel. Independent of the phase states of the lipid monolayer, the adsorption kinetics show first an increase of the surface pressure, followed by

a slower decrease of the surface pressure also in the *LC* phase. Due to the increased incorporation into the monolayer, the effect of lipid condensation is less pronounced leading to smaller values of $\Delta\pi$.

4.3.3.2 Kinetic Analysis of (RX)$_4$R Adsorption to DPPG Monolayer

Similar to the kinetic analysis of the adsorption process of peptides (KX)$_4$K to a DPPG monolayer the experimental curves were fitted with the bi-exponential equation (4.1).

Figure 4.3.16, left panel, shows the experimental and fitted curves for the adsorption of the different peptides to a DPPG monolayer starting from a surface pressure of ca. 5 - 6 mN m^{-1}, where the monolayer is in the *LE* phase. An overview of the obtained parameters is given in Table 4.3.6.
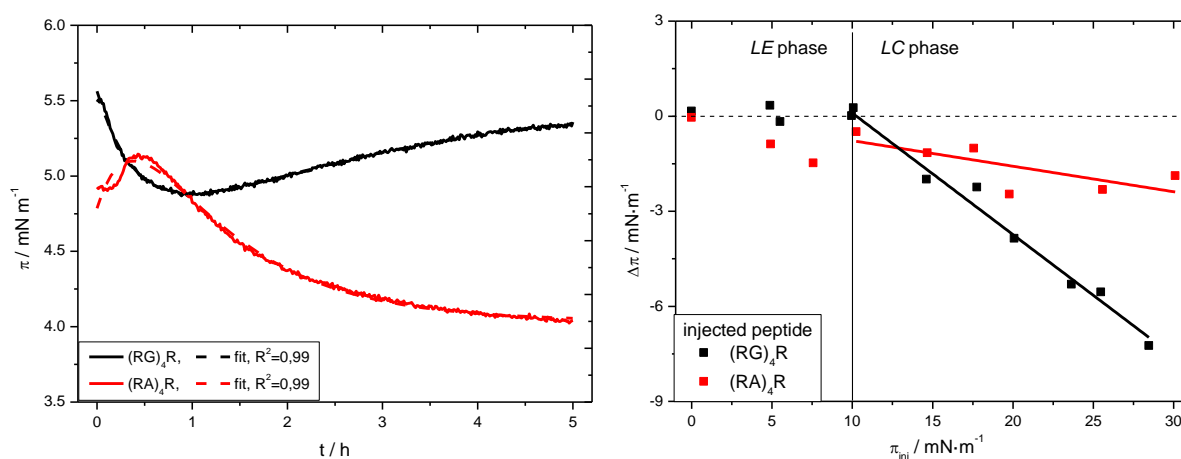

Figure 4.3.16: Left: Time dependent development of the surface pressure of a DPPG monolayer after injection of different solutions of the peptides (RX)$_4$R into the subphase at a starting surface pressure of
4 - 6 mN m^{-1} in the *LE* phase (T = 20 °C, 100 mM NaCl). The final concentration of the peptide in the subphase was 3.0 µM. Adsorption equilibrium was reached within 5 h. Right: Difference of surface pressure $\Delta\pi$ after 5 h of adsorption of the peptides (RX)$_4$R to a DPPG monolayer with different initial surface pressure π_{ini}, the lines at $\Delta\pi = 0$ and $\pi_{ini} = 10$ mN m^{-1} are drawn to guide the eye and to distinguish between the different phases of the DPPG monolayer. The final concentration of the peptide in the subphase was 3.0 µM.

Comparing the parameters for (RG)$_4$R and (KG)$_4$K, both relaxation times for lipid condensation and peptide incorporation are similar. Although the arginine side chain should be more hydrophobic, the amplitude A_2 of lipid condensation is slightly enhanced, whereas the amplitude of peptide incorporation A_1 is slightly decreased. An explanation might be the ability of the guanidinium moiety to bridge two lipids [85, 86], which is impossible for lysine residues.

(RA)$_4$R shows a similar behaviour as found for all peptides (KX)$_4$K tested before. The incorporation of a more hydrophobic amino acid than glycine slows down the relaxation time

t_2 of the lipid condensation and concomitant increases the amplitude A_2. On the other hand, t_1 becomes faster and the amplitude of A_1 of peptide incorporation is increased in its strength. Although these universal statements are all true for (RA)$_4$R, the amplitude for lipid condensation is larger than the one for peptide incorporation leading to the observed small decrease of the surface pressure. The obtained parameters for (RA)$_4$R are to those obtained for (KAbu)$_4$K, confirming the proposed increased hydrophobicity of the arginine side chain, as well as the increased condensation ability due to the bidentate guanidinium moiety.

Table 4.3.5: Fit values for the adsorption kinetics of the injected peptides (RX)$_4$R into the subphase of a DPPG monolayer at 4 - 6 mN m^{-1}. A_1, A_2: amplitudes of the two processes, t_1, t_2: relaxation rates, π_0: final surface pressure after 5 h. Data obtained by least square fit with the given bi-exponential equation. Errors are from numerical fitting routine of Origin 8.0.

	peptide incorporation		lipid condensation		
peptide	A_1 / mN m^{-1}	t_1 / h	A_2 / mN m^{-1}	t_2 / h	π_0 / mN m^{-1}
(RG)$_4$R	-1.11 ± 0.01	2.83 ± 0.02	1.14 ± 0.03	0.45 ± 0.01	5.54 ± 0.01
(RA)$_4$R	-1.68 ± 0.02	0.38 ± 0.02	2.41 ± 0.02	1.05 ± 0.04	4.04 ± 0.01

4.3.3.3 Changes of Surface Pressure as a Function of π_{ini}

The plot $\Delta\pi$ vs. π_{ini} for (RG)$_4$R is comparable with the one for (KG)$_4$K. For adsorption of (RG)$_4$R at low initial surface pressure to DPPG monolayer in the *LE* phase below 10 mN m^{-1}, no notable changes are visible. As the kinetics show two distinct processes of peptide insertion and lipid condensation they compensate each other so that finally $\Delta\pi = 0$ mN m^{-1}. For the *LC* phase, the surface pressure decreases linearly with increasing π_{ini} and thus the lipid condensation becomes more prominent (see Figure 4.3.16, right panel). The break in the plot corresponds with the *LE/LC* transition region of the DPPG monolayer at 10 mN m^{-1} and the fitted value for π_{sp}. The determined *m* value of -0.38 suggests strong attractive interaction between the peptide comparable to (KG)$_4$K.

Table 4.3.6: Values of *n*, *m*, π_{sp} and R^2 obtained from the fitting of data for binding of the peptides (RX)$_4$R to a DPPG monolayer in the *LC* phase presented in Figure 4.3.16. Errors of the parameters *m*, *n*, and π_{sp} from least square fit of the regression lines calculated with Origin 8.0.

peptide	intercept n / mN m^{-1}	slope m	superposition surface pressure, π_{sp} / mN m^{-1}	R^2
(RG)$_4$R	3.9 ± 0.5	-0.38 ± 0.02	10.3 ± 1.4	0.978
(RA)$_4$R	0.0 ± 0.8	-0.08 ± 0.04	0.0 ± 10.0	0.440

Adsorption of (RA)$_4$R causes only a small decrease in surface pressure at all initial surface pressure values. There is no difference in behaviour in the *LE* and *LC* phase. As explained above, both processes nearly compensate each other with the result that the extrapolated superposition of incorporation and condensation is extrapolated $\pi_{sp} \approx 0$ mN m^{-1}. The low value of π_{sp} coupled with the large error, allows no conclusion.

The adsorption of short arginine containing peptides to a POPG monolayer was also studied by Alhakamy et al. [12]. As POPG exhibits only an *LE* phase, the presented results are only partly comparable. Compared to (R)$_9$, incorporation of alanines into the peptide sequence increases the ability of the peptide to penetrate into the lipid monolayer with a concomitant increase of the surface pressure. Incorporation of the more hydrophobic amino acid leucine results in a stronger increase of the surface pressure and accelerates the peptide binding. Similar results were obtained for the tested peptides above.

4.3.4 DPPG Monolayers with Adsorbed Peptides Studied with Infrared Reflection Absorption Spectroscopy

To determine values for the thickness of the monolayer and to calculate the tilt angle of the lipid acyl chains, angle and polarization dependent IRRA spectroscopy was performed. Spectra were collected at angles of incidence (φ) from 26° to 70° and in p- and in s-polarization. From the angle of incidence and polarization dependence of the v(OH) or v(CH$_2$) band shape and intensity, the layer thickness and the acyl chain tilt angle can be determined by fitting simulated spectra to the experimental ones. The pure DPPG monolayer in the liquid condensed phase at a surface pressure of 20 mN m^{-1} is the reference for the comparison of the DPPG monolayer with adsorbed peptides. The maximal intensities of simulated and experimental spectra of the pure DPPG monolayer at different surface pressure, and with bound (KL)$_4$K as a function of φ and polarization are shown in Figure 4.3.17.

4.3.4.1 Monolayer Thickness *d*

By fitting the experimental data obtained for a pure DPPG monolayer in the *LC* phase (20 mN m^{-1}) at the air-water interface a thickness of 2.5 nm and a tilt angle of 33° was determined. These values agree with literature data for DPPG monolayer, measured by PM-IRRAS or GIXD [265-267].

Upon binding of the peptide to an *LC* monolayer, both parameters were altered. The results of the fits for the DPPG monolayer with the different adsorbed peptides are presented in Table 4.3.7.

Binding of the peptides $(KX)_4K$ to the DPPG monolayer can be divided into two groups. The DPPG monolayer becomes slightly thicker when the peptides $(KG)_4K$, $(KA)_4K$, $(KAbu)_4K$, and $(KV)_4K$ were adsorbed. The thickness of the monolayer increases from 2.5 nm to 2.6 or 2.7 nm, but there is no correlation with the side chain volume of the uncharged amino acid. For the most hydrophobic peptide $(KL)_4K$, a thickness of 3.1 nm was calculated. This much larger increase cannot simply be explained by the longer side chain of the peptide. $(KL)_4K$ bound to the DPPG monolayer forms of an ordered β-sheet structure. The orientation of the peptide is discussed below.

Adsorption of $(RG)_4R$ and $(RA)_4R$ also increases the thickness of the mixed monolayer. The differences in film thickness between the both peptides are marginal.
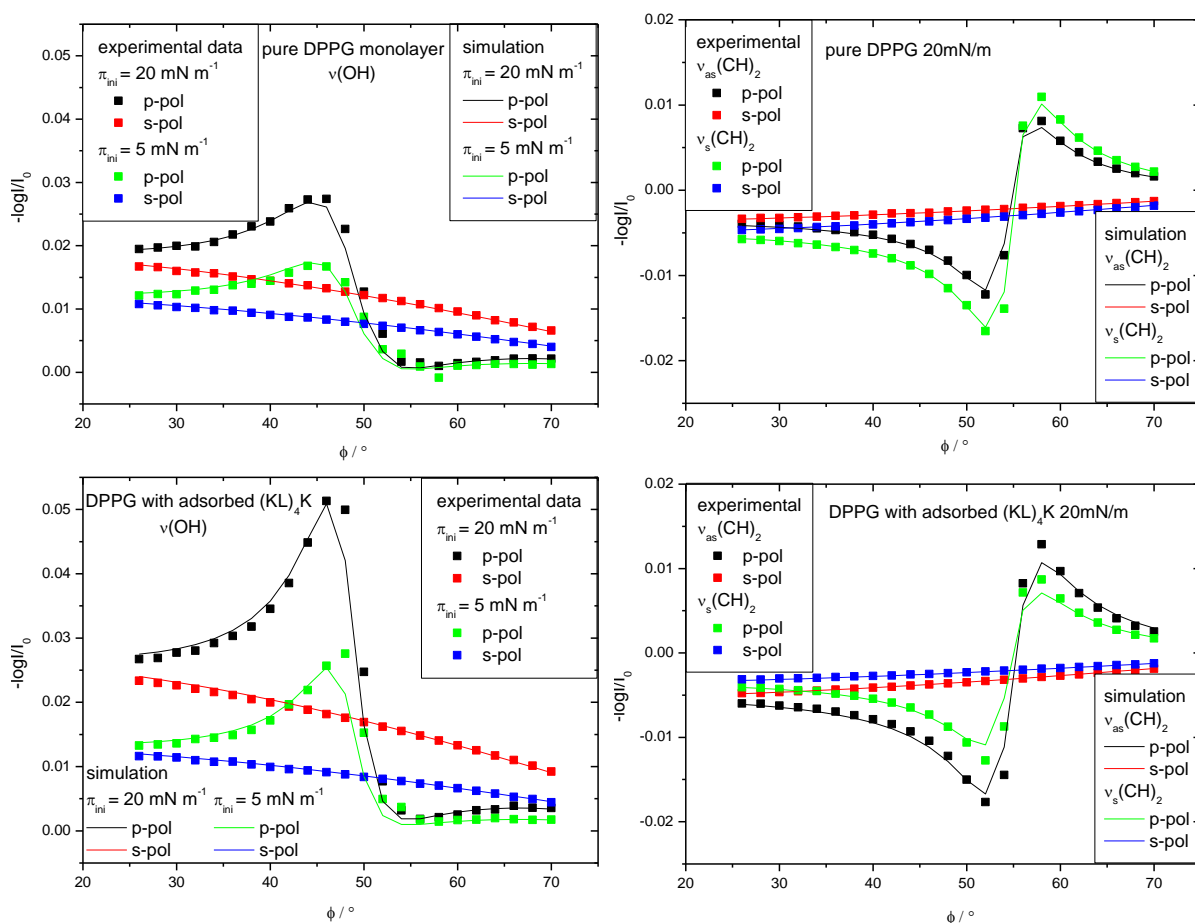

Figure 4.3.17: Left: Intensities of $v(OH)$ bands as a function of the angle of incidence φ measured for pure DPPG monolayer (top) and with adsorbed $(KL)_4K$ (bottom) at $\pi_{ini} = 20$ mN m^{-1} and 5 mN m^{-1} in p- and s-polarization, and intensities of best fitting simulated spectra for films of a thickness of 3.1 nm (20 mN m^{-1}), 1.6 nm (5 mN m^{-1}). Right: Intensities of symmetric and antisymmetric $v(CH_2)$ bands as a function of the angle of incidence measured for pure DPPG monolayer (top) and with adsorbed $(KL)_4K$ (bottom) at $\pi_{ini} = 20$ mN m^{-1}.

Peptides with two uncharged spacers seem to behave differently. For $(KGG)_4K$, nearly no change in monolayer thickness was calculated due to its weak binding, whereas $(KAA)_4K$ causes a slight increase comparable with $(KA)_4K$.

As already discussed in the time dependent adsorption process, the peptide amide bands are hardly detectable in the IRRA spectra. This might be a result of the low binding of the peptides to the dense *LC* monolayer and the suggested inability of the peptides to incorporate into a dense *LC* phase due to their low hydrophobicity. A general slight increase of the monolayer thickness can be explained by a binding of the peptides in an unordered conformation by electrostatic interaction. An exception to this general increase of the thickness is observed for the interaction of DPPG with $(KGG)_4K$.

Table 4.3.7: Comparison of a pure DPPG monolayer in the *LC* phase at 20 mN m^{-1} and the DPPG monolayer with adsorbed peptide. The thickness of the monolayer d and the tilt angle θ of the hydrocarbon chains were obtained by fitting the experimental data of the v(OH) and v(CH$_2$), respectively. With these parameters, the monolayer can be divided into the hydrocarbon region and the headgroup region. The thickness of the hydrocarbon region was calculated $d_{hc} = \cos(\theta) \cdot l_{hc}$. The length of a palmitoyl hydrocarbon chain in an *all-trans* conformation is $l_{hc} = 1.905$ nm. The thickness of the headgroup region was calculated $d_{hg} = d - d_{hc}$.

	d / nm	θ / °	d_{hc} / nm	d_{hg} / nm
DPPG	2.48	33.0	1.60	0.88
+ $(KG)_4K$	2.56	17.9	1.81	0.74
+ $(KA)_4K$	2.68	26.5	1.70	0.97
+ $(KAbu)_4K$	2.60	30.2	1.65	0.95
+ $(KV)_4K$	2.73	18.6	1.81	0.92
+ $(KL)_4K$	3.10	20.3	1.79	1.31
+ $(KGG)_4K$	2.44	29.4	1.66	0.78
+ $(KAA)_4K$	2.64	17.8	1.81	0.80
+ $(RG)_4R$	2.67	25.9	1.71	0.96
+ $(RA)_4R$	2.64	28.4	1.68	0.96

Although, the integral of the OH band shows an increase upon binding of $(KGG)_4K$ in the time dependent experiments, a slightly lower, nearly unchanged layer thickness compared to pure DPPG, is calculated for the mixed film. This might be contradictory on the first sight. The angle dependent measurements were performed with the same monolayer subsequent to the time dependent adsorption. Within the angle dependent measurement the OH band integrals, show a decrease over time. A possible explanation for a decrease of the monolayer thickness might be the reduction of the order in the acyl chain region. This can be excluded, because the wavenumber for the CH$_2$ vibrations are also lowered, indicating a higher acyl

chain order after peptide binding. Furthermore, the refractive index of the mixed film can be altered due to peptide binding.

4.3.4.2 Acyl Chain Tilt Angle θ

Besides the thickness of the films, also the tilt angle of the acyl chain can be determined. In general, the binding of the peptide reduces the tilt of the lipid acyl chains (see Table 4.3.7) independent of the peptide sequence and underlines the condensing effect discussed above. Because of the lower tilt angle and a more upright position of the acyl chains, the monolayer becomes thicker. The electrostatic interaction of the positively charged peptide side chain with the negatively charged lipid headgroup results in charge screening. The repulsion becomes less prominent and the effective headgroup area becomes smaller, leading to a decrease of chain tilt, which enables a better van der Waals interaction in the acyl chain region.
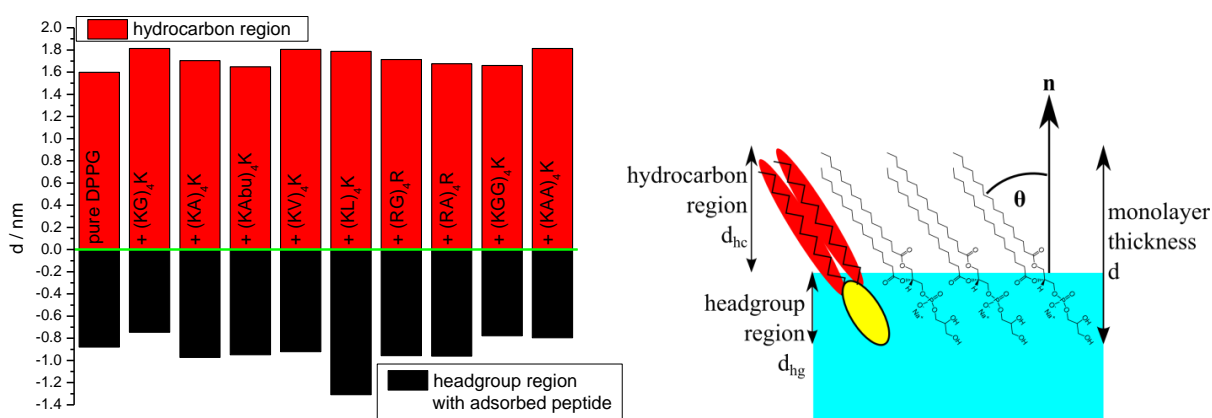

Figure 4.3.18: Left: calculated monolayer thicknesses of pure DPPG monolayer at a surface pressure of 20 mN m^{-1} and DPPG monolayer with adsorbed peptide. The monolayer can be separated into a hydrophobic region of the acyl chains, which are in an *all-trans* conformation, and a hydrophilic region. The hydrophilic region is composed of the lipid headgroup with adsorbed or inserted peptide. Right: schematic representation of the lipid arrangement at the air-water interface determining the monolayer thickness *d* and the acyl chain tilt angle θ. The lipid monolayer is composed of a hydrophobic acyl chain region and a hydrophilic headgroup region.

θ is lowered to 18° upon binding of $(KG)_4K$ and then increases for the more hydrophobic peptides $(KA)_4K$ and $(KAbu)_4K$. For the even more hydrophobic peptides, a smaller tilt angle is again observed. Binding of $(KV)_4K$ reduces the tilt of the acyl chains to 19° and $(KL)_4K$ to 20°. By separating the mixed monolayer into the hydrocarbon region and into the headgroup region (see Figure 4.3.18, left panel), the combination of tilt angle and bilayer thickness reveals the following results: For $(KG)_4K$, the reduction in thickness of the headgroup region of the monolayer is compensated by the more upright position of the hydrocarbon region. For

$(KA)_4K$, $(KAbu)_4K$, and $(KV)_4K$, the headgroup regions have a similar thickness, slightly thicker than for pure DPPG (+0.1 nm). DPPG films with $(KL)_4K$ are 0.6 nm thicker than without any adsorbed peptide additionally to an increased hydrocarbon region. For all systems, the sum of both effects yields an overall increase of the monolayer thickness.

Experiments with adsorbed $(KGG)_4K$ and $(KAA)_4K$ as well as $(RG)_4R$ and $(RA)_4R$ show individual results. The tilt angle is reduced to 18° for $(KAA)_4K$ and 26° - 29° for the other peptides. The hydrocarbon chains occupy a more upright conformation, increasing the thickness of the hydrophobic region. The headgroup layer thickness is increased for arginine containing peptides and decreased for peptides with two uncharged amino acid spacer.

A different mode of action for arginine than for lysine at the air-water interface is assumed as already observed for the bilayer systems. These results confirm that both components of the adsorbed peptide the charged as well as the uncharged amino acids play a role for the interaction with the DPPG monolayer in the *LC* phase. Taking the results of the determination of the monolayer thickness and the tilt angle of the hydrocarbon chains together three different modes of lipid-peptide interaction are observed. In the first place, the adsorption of $(KGG)_4K$ to the monolayer, a reduced thickness of the hydrophilic region and a reduced tilt angle is seen. The second group contains peptides with uncharged amino acids of intermediate hydrophobicity and the arginine containing peptides. They show a slightly increased thickness of the monolayer as well as of the headgroup region combined with a reduced tilt angle of the acyl chain region. Finally, for DPPG with adsorbed $(KL)_4K$ a strong increase of the monolayer thickness is observed upon binding of the peptide in a β-sheet conformation.

4.3.4.3 Peptide Orientation

Adsorption of $(KL)_4K$ to a DPPG monolayer in the *LC* phase at 20 mN m^{-1} results in a strong contribution of the amide region. Bands from the amide-I vibration at 1617 cm^{-1} and 1680 cm^{-1} as well as from the amide-II vibrations around 1535 cm^{-1} are visible in the spectra. From these band positions, it is concluded that an antiparallel β-sheet is formed during the adsorption process. By fitting the experimental data with two bands (1617 cm^{-1} and 1535 cm^{-1}) it is possible to evaluate the orientation of the adsorbed peptide at the air water interface.

From sterical reasons and due to the peptide sequence, it was supposed that the formed β-sheet is adsorbed in a flat conformation underneath the lipid monolayer. The directions of the transition dipoles of the amide vibrations [268] are depicted in Figure 4.3.20, left panel. From IRRAS experiments, twist angle $\psi = 29°$ and a tilt angle $\theta = 90°$ was obtained. The experimental and simulated spectra for this conformation are depicted in Figure 4.2.19.

Although there are some derivations in intensities, this fit matches the experimental data best. For other twist and/or tilt angle the bands have different intensities or directions in the spectra. Some simulations for mismatched ψ and θ are given in Figure 8.3.8.

This orientation of the β-sheet underneath a lipid monolayer is depicted in Figure 4.3.20, right panel. A flat orientation of the β-sheet comparable to the situation at the lipid monolayer was also found for the deposited peptide $(KL)_7K$ on CaF_2 with an twist angle $\psi = 13°$ [268].

The hydrophilic region of the monolayer is calculated to 0.9 nm for DPPG, and 1.3 nm for DPPG with bound $(KL)_4K$. The distance of the methyl group of the leucine side chain and the terminal amine group of the lysine side chain in its extended conformation about 1 nm. Thus, the peptide in its β-sheet conformation fits into the hydrophilic region of the lipid monolayer. The increase of the thickness assumes that only a part of the peptide is inserted into the hydrophilic region.
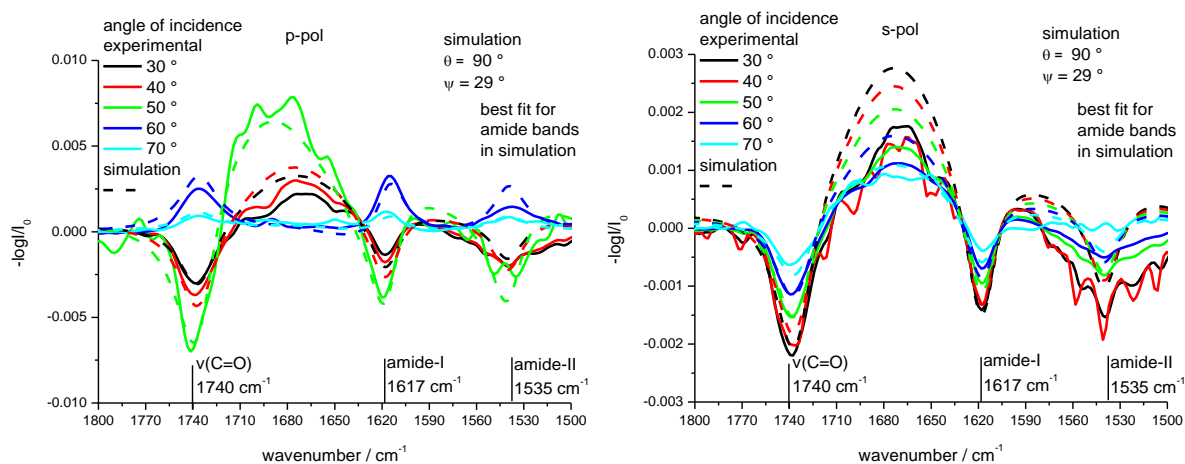

Figure 4.2.19: Left: experimental and simulated spectra (p-polarization) of the mixed DPPG/$(KL)_4K$ monolayer in the amid region, Right: experimental and simulated spectra (s-polarization) of the mixed DPPG/$(KL)_4K$ monolayer in the amid region.

Although, the conformation of the whole β-sheet is determined, it remains an open question, in which direction a single peptide strand is oriented. Are the hydrophobic leucine side chains or the charged lysine residues pointing towards the lipid headgroups in the monolayer?

A first possible orientation is that the charged lysine side chains pointing towards the lipids, as discussed before for the syn-orientation in lipid bilayer systems. On the one hand, direct charge compensation is achieved upon strong electrostatic interactions. On the other hand, a hydrophobic surface by leucine side chains is created, which is in contact with the aqueous subphase. To shield the hydrophobic surface, addition of a second peptide layer underneath from bulk water might be possible, creating a peptide bilayer. In contrast to the bilayer system, a second lipid layer is missing, reducing the stability of the formed β-sheet.

The second orientation is a β-sheet structure, where the hydrophobic leucine side chains facing towards the lipid headgroups. Here, no hydrophobic surface is formed. In addition, the leucine side chains can interact with the hydrophobic acyl chain region, but charge compensation is only partly possible, due to their long range.

The third peptide conformation might be an overlay of the two extrema describe before. Similar to the discussion in the bilayer systems also a mixed arrangement in an anti-conformation might be possible, mixing hydrophobic and charged residues. Thus, the formation of a hydrophobic surface is inhibited, and electrostatic interactions between the lysine side chains and the lipid headgroups are possible.

Based on the experimental data, an exclusion of one or two possibilities is not possible. Nevertheless, the third possible orientation is favored, because for monolayer systems the electrostatic interactions are dominating, due to their long range. The short ranged hydrophobic interactions alone are not sufficient. The addition of a second peptide layer is unlikely, due to the remaining charge repulsion of the lysine side chains and the missing second lipid layer for stabilization.
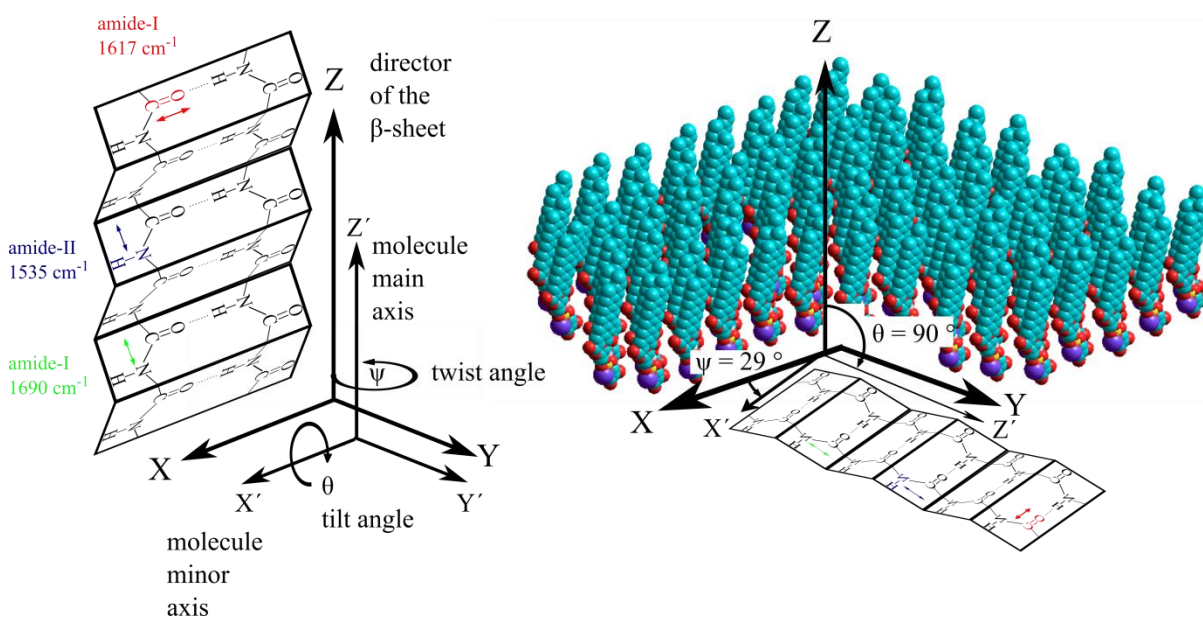

Figure 4.3.20: Left: vibrations of the amide-I and amide-II bands of a β-sheet with their direction and the definition of the twist angle ψ and the tilt angle θ. Right: visualization of the adsorbed β-sheet of $(KL)_4K$ underneath the lipid monolayer.

4.4 Interaction of (KL)$_4$K with Lipid Monolayers - Dependence on Lipid Structure

To study the influence of the lipid structure on binding properties, a (KL)$_4$K solution was injected into the subphase of different lipid monolayers at the air-water interface. The peptide (KL)$_4$K was chosen, because it showed the largest changes in surface pressure upon interacting with the DPPG monolayer discussed above. The lipids were altered in different ways, to reveal the following effects a) increase the acyl chain lengths in PGs, b) introduction of one unsaturated chain into PG, c) change in size of the negatively charged headgroups, d) attachment of a zwitterionic headgroup.

4.4.1 Influence of Different Acyl Chains Attached to a Phosphatidylglycerol Headgroup

4.4.1.1 Influence of Acyl Chain Lengths

With an elongation of the acyl chains in the lipids DMPG, DPPG, and DSPG, the hydrophobic compartment of the monolayer becomes thicker [47] and the increased strength of the van der Waals forces leads to a shift in the phase behavior. For a subphase temperature of 20 °C DMPG and DPPG show an *LE/LC* phase transition of the monolayer at 40 mN m^{-1} and 9 mN m^{-1} [229, 255, 256], respectively. For DSPC monolayers, a direct transition from the gas-analog phase to the *LC* phase is observed [245]. Thus, for monolayers at varying fixed surface pressures different phase states of the monolayers are present.

Adsorption kinetics of (KL)$_4$K to a DMPG monolayer

The range of the used initial surface pressures are below the *LE/LC* phase transition for a DMPG monolayer, which starts at 40 mN m^{-1}, thus the monolayer is exclusively in the *LE* phase [256]. Experiments performed at higher initial surface pressures were omitted, because the lipid monolayer itself becomes unstable at these values and large errors determining the change in surface pressure occur.

After peptide injection, the surface pressure shows a fast and strong increase due to the insertion of the peptide into the monolayer, independent of the tested initial surface pressure (see Figure 4.4.1a). A second slower process follows and lowers the surface pressure of the monolayer. This can be explained by assuming an ordering of the lipid acyl chains. As the insertion process is much faster than the lipid condensation, an overshoot of the surface pressure is observed shortly after injection of the peptide. Higher initial surface pressures π_{ini},

leading to a more condensed *LE* monolayer, reduce the effect of peptide insertion and the coupled net increase of the surface pressure.
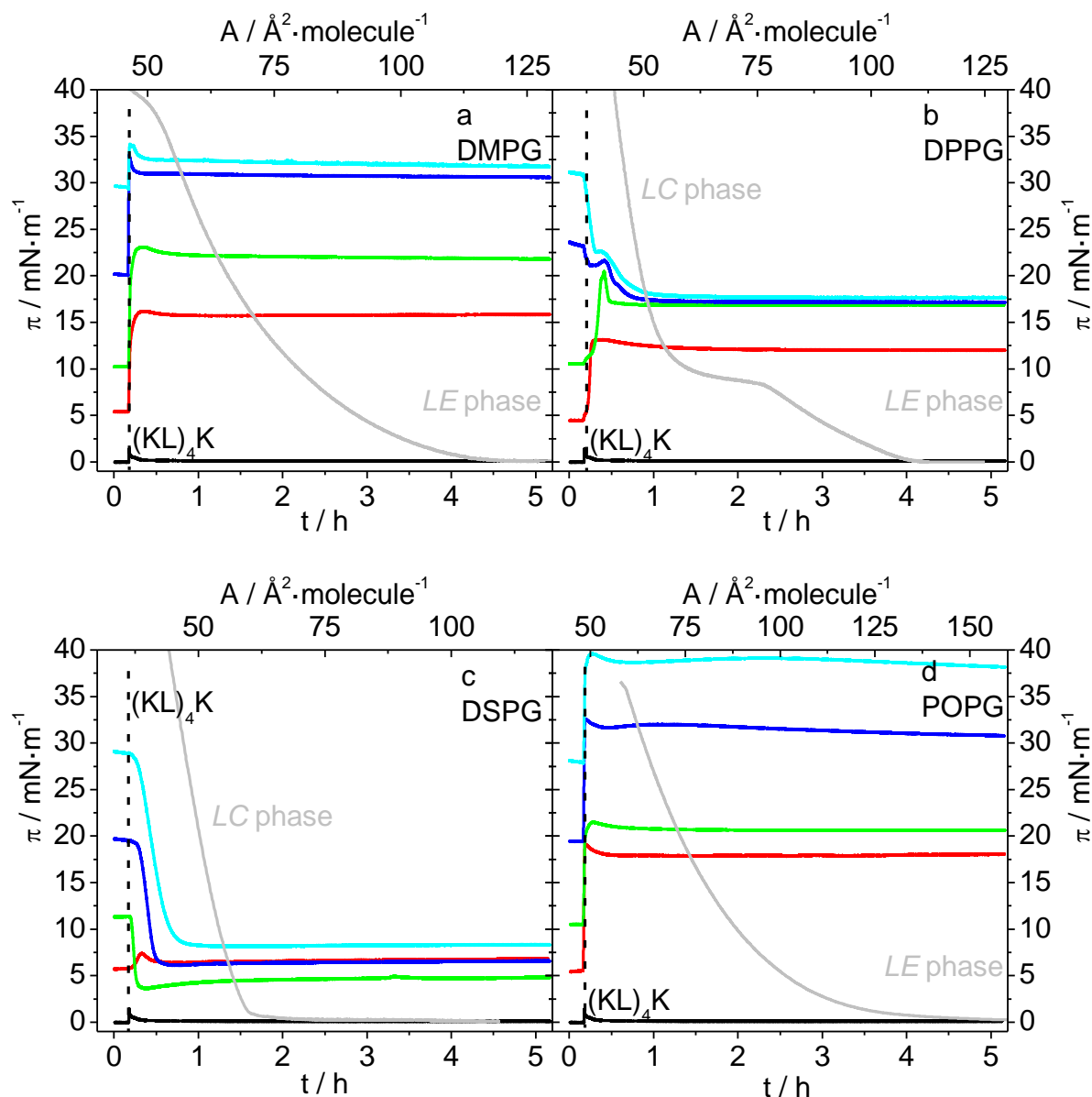

Figure 4.4.1 Change in surface pressure of different phosphatidylglycerol monolayer as a function of time after injection of (KL)₄K into the subphase ($T = 20\ °C$, 100 mM NaCl) at various initial surface pressure: a) DMPG, b) DPPG, c) DSPG, d) POPG monolayer. The lipid monolayer remains at a constant surface pressure prior to peptide injection at $t = 600$ s (marked with the dashed line). The final concentration of (KL)₄K in the subphase was 3.0 µM. Adsorption equilibrium was reached within 5 h. In all panels the surface pressure-area isotherm of pure lipid monolayer with their corresponding *LE* or *LC* phases are also shown in grey.

Adsorption kinetics of (KL)₄K to a DPPG monolayer

The binding of the peptide (KL)₄K to a DPPG monolayer was already presented before (see section 4.3.1). The adsorption kinetics of (KL)₄K to a DPPG monolayer in the *LE* phase are clearly dominated by the insertion of the hydrophobic peptide into the monolayer, as seen

before for DMPG. Independent of the initial surface pressure in the *LC* phase, a final surface pressure around 17 mN m^{-1} is reached.

Adsorption kinetics of (KL)$_4$K to a DSPG monolayer

Injection of (KL)$_4$K under the *LC* monolayer of DSPG decreases the surface pressure and the effect of lipid condensation scales linearly with the initial surface pressure (see Figure 4.4.1c). An exception to this behavior is visible for initial surface pressures around 5 mN m^{-1}. Here the lipid density at the air-water interface is low enough to enable peptide incorporation into the *LC* monolayer. A fast small increase in surface pressure is seen, followed by a slower decrease due to condensation. Both effects compensate each other so that the final change in surface pressure is zero. Compared to the behavior of DPPG in the *LC* phase, the peptide incorporation is less favored for DSPG, as no intermittent increase of the surface pressure is visible. The increased van der Waals interaction in the acyl chain region are too strong to be broken up by peptide incorporation assuming that the *LC*-domains of DSPG at the air-water interface remain nearly undisturbed. Thus, the peptide incorporates at the edge of the domains or only binds underneath the domains in the lipid headgroup region, leading to lipid condensation upon charge compensation.

According to the results found for DPPG and DSPG, the incorporation of (KL)$_4$K into a monolayer into the *LC* phase is hindered due to the dense monolayer and the strong interactions of the lipid acyl chains. Only close to the phase transition region, peptide incorporation is possible leading to a slight increase of the surface pressure. Lipid condensation dominates, reducing the surface pressure.

4.4.1.2 Influence of Lipid Acyl Chain Unsaturation

The presence of one unsaturated acyl chain in the case of POPG enhances the fluidity of the monolayer and the lipid requires more space at the air-water interface. With the double bond in the acyl chain, the formation of an *LC* phase upon compression is not observed at room temperature. Only the *LE* phase is present until the film collapses.

Adsorption kinetics of (KL)$_4$K to a POPG monolayer

Binding of (KL)$_4$K to a POPG monolayer shows a large increase of the surface pressure directly after peptide injection, followed by a slower process slightly decreasing the surface pressure (see Figure 4.4.1d). Comparing the results obtained with monolayer in the *LE* phase, POPG and DMPG, the incorporation leads to more pronounced effects using POPG

monolayer. A significant higher increase of surface pressure is visible, particularly at high initial surface pressure.

Comparing all results obtained from PGs, a strong dependence of the phase state of the lipid monolayer is observed. For an *LE* phase, a strong increase of the surface pressure is seen, because the incorporation of the peptide dominates.

4.4.1.3 Changes of Surface Pressure as a Function of π_{ini}

DMPG

For the adsorption of $(KL)_4K$ to DMPG monolayer, the influence of the peptide incorporation is enhanced over the lipid condensation (Figure 4.4.2). All observed $\Delta\pi$ values are positive. The range of the biphasic behavior is extended for a DMPG monolayer due to the wider stability range of the *LE* phase. The *LE* phase of the DMPG monolayer shows a similar behavior as the DPPG monolayer: the closer the π_{ini} to the *LC/LE* phase transition the more prominent is the effect of the lipid condensation. The exact calculation of π_{sp} is difficult due to missing data for *LC* phase monolayers. However, as the linear part starts already in the *LE* phase close to the phase transition region, the superposition pressure is approximated to $\pi_{sp} = 35 \pm 9$ mN m^{-1} (see Table 4.4.1). This value is above the tested initial surface pressure and in the main phase transition region of the DMPG monolayer.

DPPG

The behaviour of a DPPG monolayer upon injection of $(KL)_4K$ was discussed above (see section 4.3.1). The biphasic behavior for the adsorption shows an increase of $\Delta\pi$ up to a $\pi_{ini} = 10$ mN m^{-1} and in the range of π_{ini} from 10 mN m^{-1} up to 30 mN m^{-1} a linear decrease in $\Delta\pi$ is seen. The dependence of the interaction of the peptide on the phase state of the lipid monolayer is evident. In the *LE* phase, peptide incorporation into the loosely packed monolayer is favored over lipid condensation leading to a positive $\Delta\pi$, whereas in the *LC* phase the dense monolayer only lipid condensation can occur resulting in a negative $\Delta\pi$. The value of the superposition surface pressure π_{sp} of 17.5 ± 1.1 mN m^{-1} is a value, which lies in the stability region of the *LC* phase of the DPPG monolayers, it coincides with the final equilibrium surface pressure observed for all injection. The slope $m = -1.00$ of the linear fit is very steep, indicating strong electrostatic attraction.
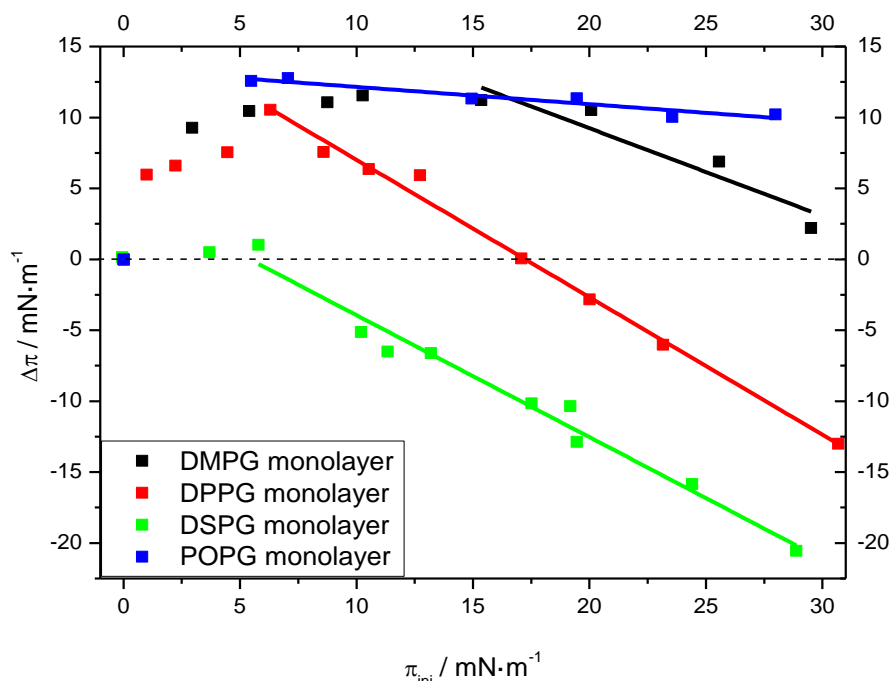
Figure 4.4.2: Difference of surface pressure $\Delta\pi$ after 5 h of adsorption of (KL)$_4$K solution to lipid monolayer with different initial surface pressure π_{ini}. The different monolayers consist of phosphatidylglycerols with different acyl chains: DMPG, DPPG, DSPG, or POPG. The line at $\Delta\pi = 0$ is drawn to guide the eye. The final concentration of the peptide in the subphase was 3.0 µM.

DSPG

Although for DSPG an *LC* phase is present over the whole range of the tested surface pressure, a linear relationship of $\Delta\pi$ vs. π_{ini} is only visible for π_{ini} larger than 5 mN m^{-1}. The obtained fit parameter from the linear regression *m*, *n,* and π_{sp} are presented in Table 4.4.1. The slope *m* = -0.86 is less negative than the one obtained for DPPG. The condensing effect of the peptide upon charge neutralization clearly dominates the behavior. Only at a surface pressure below 5 mN m^{-1}, the partial insertion of the peptide into the monolayer leads to a deviation from the linear behavior and $\Delta\pi$ is close to zero.

POPG

As the POPG monolayer is only in the *LE* phase the interaction with the peptide (KL)$_4$K leads always to positive values of $\Delta\pi$. The kinetically resolved curves in Figure 4.4.1d show that insertion as well as condensation effects are present. However, the insertion effect dominates so that even at high surface pressure an increase in π is observed. $\Delta\pi$ shows a maximal value of 13 mN m^{-1} and decreases only slightly up to a surface pressure of 30 mN m^{-1}.

Values for $\Delta\pi$ are slightly higher than those for DMPG. An increased influence of lipid condensation at higher π_{ini} leads to a slope *m* = -0.12. The slope is still shallower than the one of DMPG obtained also for the *LE* phase. Much more negative *m* values were obtained for *LC*

phases of DPPG and DSPG. Furthermore, the calculated superposition pressure of 113 mN m$^-$^{1} is out of the range of surface pressure values of an air-water interface and without any physical meaning. The maxima of the positive $\Delta\pi$ values decrease as follows: POPG > DMPG > DPPG > DSPG and seem to scale with the density of the lipid monolayer and the strength of the van der Waals interactions, underlining the suggestion that the peptide incorporation is favoured for lipids in the *LE* phase.

Table 4.4.1: Values of n, m, π_{sp} and R^2 obtained from the fitting of data for binding of (KL)$_4$K to a PG monolayer presented in Figure 4.4.2. A linear behavior of $\Delta\pi$ *vs.* π_{ini} was observed in the *LC* phases and in the *LE* phase in close proximity to the *LE/LC* phase transition region. Data from DMPG and POPG are exclusively from the *LE* phase having lower correlation coefficients. Errors of the parameters m, n, and π_{sp} from least square fit of the regression lines calculated with Origin 8.0.

lipid	intercept n / mN m^{-1}	slope m	superposition surface pressure, π_{sp} / mN m^{-1}	R^2
DMPG	21.6 ± 3.2	-0.62 ± 0.14	34.8 ± 9.4	0.86
DPPG	17.5 ± 0.9	-1.00 ± 0.04	17.5 ± 1.1	0.99
DSPG	4.7 ± 0.9	-0.86 ± 0.05	5.4 ± 1.1	0.97
POPG	13.4 ± 0.3	-0.12 ± 0.03	111.4 ± 18.8	0.90

4.4.2   Influence of the Lipid Headgroup Structure

Different structures of the lipid headgroup were tested to determine the influences of the headgroup structure and size on the interaction with the injected peptide (KL)$_4$K. To mask the influence of the acyl chain and focus on the headgroup of the lipid, monolayers of lipids with myristoyl chains and different headgroups were used. The size of the headgroup of the tested anionic lipids increases as follows: phosphatidic acid (DMPA) < cardiolipin (TMCL) = phosphatidylserine (DMPS) < phosphatidylglycerol (DMPG) (see Table 2.2.1). Although all lipids have the same acyl chain length, the different headgroup size as well the resulting different tilt angles of the chains influence the surface pressure of the *LE/LC* phase transition. For a DMPA, TMCL, DMPS, and DMPG monolayer, the surface pressure of the *LE/LC* phase transition increases in the same order as the headgroup size, occurring at 6 mN m^{-1}, 17 mN m^{-1}, 19 mN m^{-1} and 40 mN m^{-1}, respectively.

Adsorption kinetics of (KL)$_4$K to a DMPS monolayer

The initial surface pressure and the phase state of DMPS monolayer influences the adsorption kinetics of the peptide. For all tested π_{ini} up to 30 mN m^{-1}, the strong increase of surface pressure after injection is followed by a slower slight decrease of the surface pressure (see Figure 4.4.3b). The increase of surface pressure $\Delta\pi$ in the existence range of the *LE* phase does not depend on the surface pressure and is constant with 12 mN m^{-1}. In the range of the *LC* phase $\Delta\pi$ decreases with higher initial surface pressure up to $\pi_{ini} = 30$ mN m^{-1}, where no change in surface pressure is observed any more.

Adsorption kinetics of (KL)$_4$K to a DMPA monolayer

The two competing processes of peptide incorporation and lipid condensation are also visible upon injection of (KL)$_4$K under a DMPA monolayer. The overlay of the fast increase of the surface pressure and the following slower decrease result in a similar overshoot as discussed for DPPG (see Figure 4.4.3c). At higher initial surface pressure in the *LC* phase, the lipid condensation dominates and a net decrease of the surface pressure is recorded.

Adsorption kinetics of (KL)$_4$K to a TMCL monolayer

The adsorption kinetics of (KL)$_4$K to a TMCL monolayer are similar to those observed for DPPG and DMPA (see Figure 4.4.3d). At low π_{ini} an increase of the surface pressure occurs and at high π_{ini} lipid condensation reduces the surface pressure.
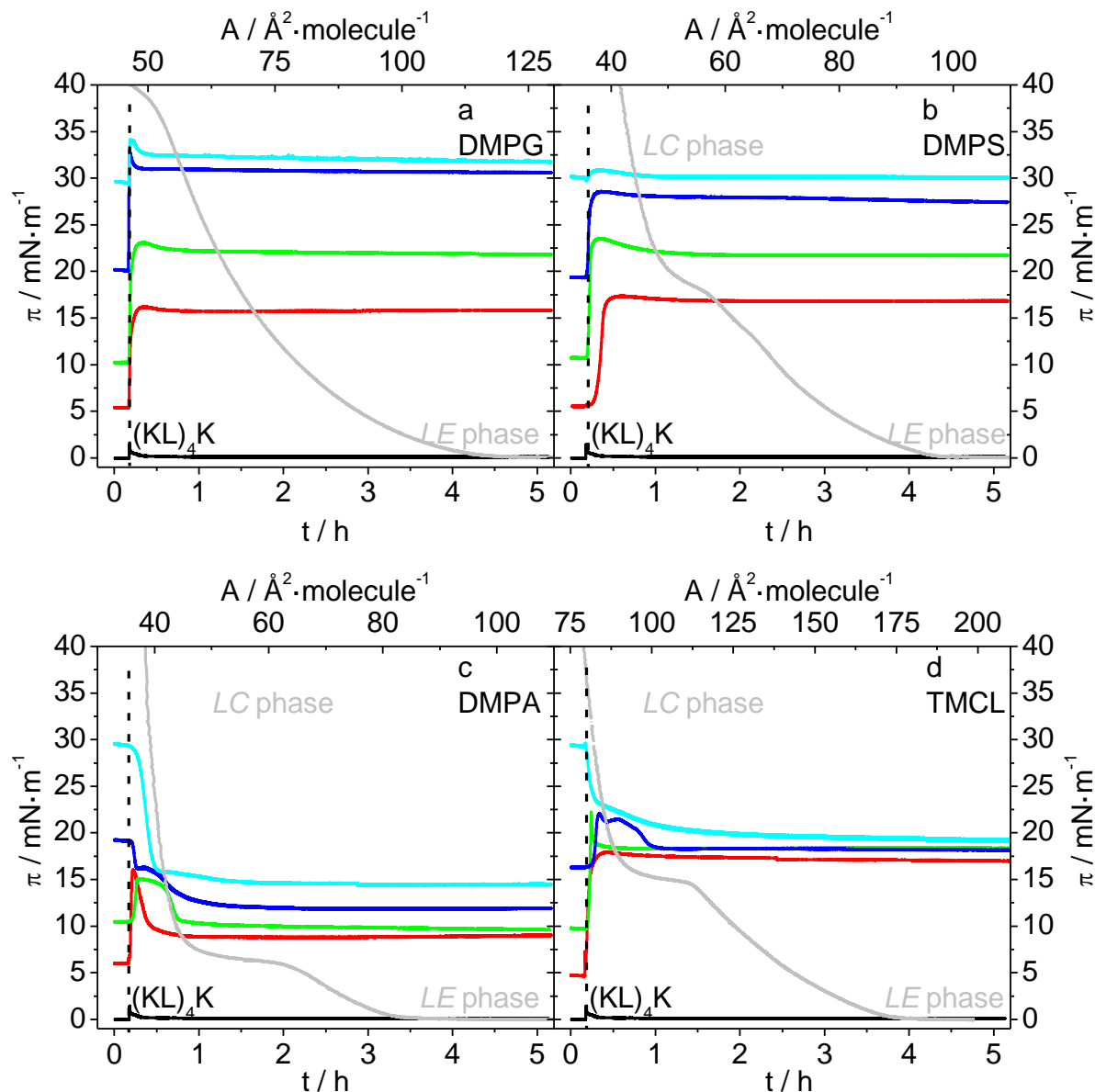
Figure 4.4.3: Change in surface pressure of different lipid monolayer composed of lipids with myristoyl chains as function of time after injection of (KL)$_4$K into the subphase (T = 20 °C, 100 mM NaCl) at various initial surface pressure: a) DMPG, b) DMPS, c) DMPA, d) TMCL monolayer. The lipid monolayer remains at a constant surface pressure prior to peptide injection at t = 600 s (marked with the dashed line). The final concentration of of (KL)$_4$K in the subphase was 3.0 μM. Adsorption equilibrium was reached within 5 h. In all panels the surface pressure-area isotherm of pure lipid monolayer with their corresponding *LE* or *LC* phases are also shown in grey.

4.4.2.1 Changes of Surface Pressure as a Function of π_{ini}

DMPS

Injection of (KL)$_4$K into the subphase of DMPS results in a biphasic behavior (see Figure 4.4.4) as seen before for DPPG and $\Delta\pi$ depends on the phase state of the lipid monolayer. For the whole stability range of the *LE* phase, a positive $\Delta\pi$ of 12 mN m^{-1} is observed. The effect of lipid condensation becomes more prominent at higher π_{ini} showing a linear relationship of

$\Delta\pi$ vs. π_{ini} in the *LC* phase and a calculated π_{sp} of 30 mN m^{-1}. The slope $m = -0.70$ determined for *LC* phase behavior is smaller compared to *m*-values found for DPPG and DSPG.
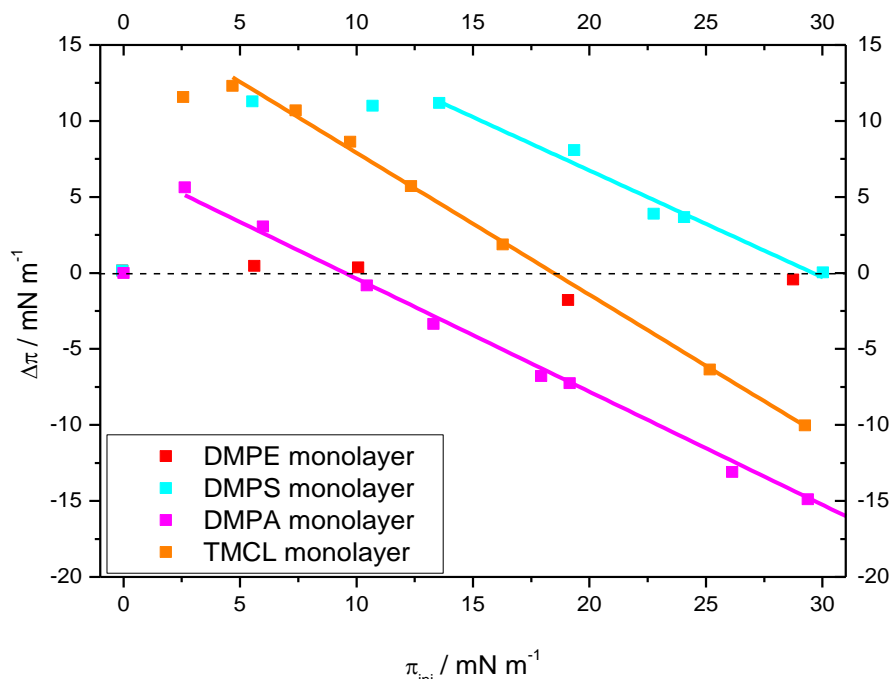

Figure 4.4.4: Difference of surface pressure $\Delta\pi$ after 5 h of adsorption of (KL)$_4$K solution to lipid monolayer with different initial surface pressure π_{ini}. The different monolayers consist of lipids, having myristoyl chains, but different headgroups: DMPE, DMPS, DMPA or TMCL (right panel). The line at $\Delta\pi = 0$ is drawn to guide the eye. The final concentration of the peptide in the subphase was 3.0 μM.

DMPA

DMPA has a low *LE/LC* phase transition pressure at $\pi = 6$ mN m^{-1}. The reduced range of the *LE* phase prevents the penetration of the peptide into the lipid monolayer. Lipid condensation is favored over peptide incorporation in the *LC* phase. The linear relationship of $\Delta\pi$ vs. π_{ini} with a π_{sp} of 10 mN m^{-1} and a slope of -0.74 is the result (see Figure 4.4.4).

TMCL

Although the phase transition pressures of DMPS and TMCL (19 and 17 mN m^{-1}) are similar, their interaction with (KL)$_4$K is different. The biphasic behavior is more pronounced for DMPS and lipid condensation effects are more prominent for TMCL monolayers, creating a steeper slope *m*.

Comparing all negatively charged lipids, the upshift of π_{sp} above the *LE/LC* phase transition scales with the size of the lipid headgroup. The larger headgroup moieties of DMPS and DPPG shift the superposition surface pressure by 10 mN m^{-1} or 8 mN m^{-1} above the *LE/LC* phase transition pressure. The smaller headgroups in DMPA and TMCL lead to an upshift of only 4 mN m^{-1} or 2 mN m^{-1}. Weaker van der Waals interaction of the acyl chains for lipids

with larger headgroups allow better the peptide incorporation close to the onset of *LC* phase formation.

The slopes of the regression lines for lipids with at least two glycerol moieties in the headgroup (DSPG, DPPG and TMCL) are steeper than those found for DMPS and DMPA. This might be an indication for a specific interaction of the peptide with the glycerol moiety enhancing the effect of lipid condensation and weakening the effect of peptide incorporation.

Table 4.4.2:Values of *n*, *m*, π_{sp} and R^2 obtained from the fitting of data for binding of (KL)$_4$K to a lipid monolayer presented in Figure 4.4.4. A linear behavior of $\Delta\pi$ *vs.* π_{ini} was observed in the *LC* phases and in the *LE* phase in close proximity to the *LE/LC* phase transition region. Errors of the parameters *m*, *n*, and π_{sp} from least square fit of the regression lines calculated with Origin 8.0.

lipid	intercept n / mN m^{-1}	slope m	superposition surface pressure, π_{sp} / mN m^{-1}	R^2
DMPG	21.6 ± 3.2	-0.62 ± 0.14	34.8 ± 9.4	0.86
DMPE	0.3 ± 0.6	-0.05 ± 0.04	7.0 ± 13.6	0.11
DMPS	20.8 ± 1.4	-0.70 ± 0.06	29.7 ± 3.3	0.97
DMPA	7.1 ± 0.4	-0.74 ± 0.02	9.6 ± 0.6	0.99
TMCL	17.2 ± 0.3	-0.93 ± 0.02	18.5 ± 0.5	0.99
all *LC* data	5.8 ± 0.8	-0.90 ± 0.05	6.5 ± 0.9	0.92

4.4.2.2 Is there a General Behavior for all Lipid Monolayers?

All tested negatively charged phospholipids show different phase behavior due to their different headgroup moieties and differences in acyl chain length and saturation. The interaction of (KL)$_4$K with these lipids depends on the phase state of the monolayer. To overcome the problem with the different *LE/LC* phase transition pressures ($\pi_{LE/LC}$) and to test whether a the binding of the peptide (KL)$_4$K to the different monolayers follows some general rule, the data for $\Delta\pi$ shown in Figure 4.4.2 and Figure 4.4.4 were re-plotted, by now using the reduced pressure $\pi_{red} = \pi - \pi_{LE/LC}$ on the abscissae. The resulting plot $\Delta\pi$ vs. π_{red} is shown in Figure 4.4.5. The vertical line at $\pi_{red} = 0$ divides the plot into a region with negative values of π_{red}, where the *LE* phase exists, and the other region with positive π_{red}, where the *LC* phase is stable. The horizontal line at $\Delta\pi = 0$ divides the plot into 4 different quadrants. In these regions, a different behavior of the monolayer after binding of the peptide (KL)$_4$K is observed.

All $\Delta\pi$ data observed for the *LE* phase monolayer are grouped in the upper left quadrant. Here, an increase of the surface pressure after peptide binding to the *LE* phase monolayer is

observed, A maximal value of $\Delta\pi = 13$ mN m^{-1} after binding to *LE* phase monolayers was observed for several different monolayers. Apparently, this value reflects the surface activity of the peptide in the presence of a lipid monolayer. Amino acids less hydrophobic than leucine lead to lower values of $\Delta\pi$. A more hydrophobic amino acid than leucine would increase $\Delta\pi$ for the incorporation of the peptide into an *LE* phase of an anionic lipid monolayer. The biphasic behavior due to the superposition of at least two processes is also visible in this plot, i.e. $\Delta\pi$ is lowered close to the phase transition region because of increased lipid condensation.
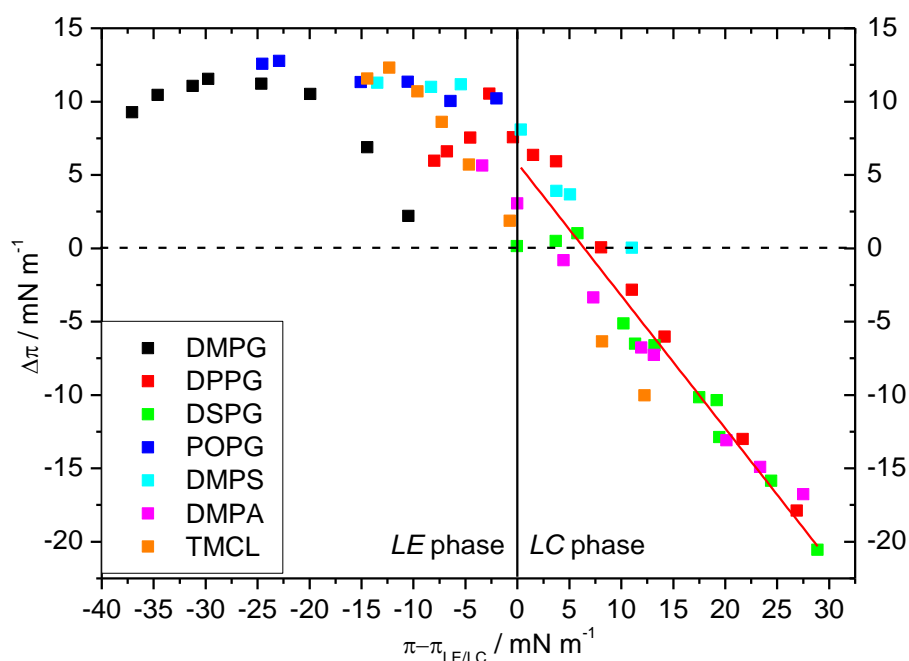

Figure 4.4.5: Difference of surface pressure $\Delta\pi$ after 5 h of adsorption of (KL)$_4$K solution to lipid monolayers with different surface pressure on a reduced scale $\pi_{red} = \pi - \pi_{LE/LC}$. Monolayers are composed of negatively charged lipids: DMPG (40 mN m^{-1}), DPPG (9 mN m^{-1}), DSPG (0 mN m^{-1}), POPG, DMPS (19 mN m^{-1}), DMPA (6 mN m^{-1}) or TMCL (17 mN m^{-1}). Values in brackets give the *LE/LC* phase transition pressure of the pure lipid. The lines at $\Delta\pi = 0$ is drawn to guide the eye and the line at π_{red} is drawn to discriminate between the *LE* and the *LC* phase. The final concentration of the peptide in the subphase was 3.0 µM.

For monolayers in the *LC* phase, a linear relationship of $\Delta\pi$ vs. π_{red} is seen (both quadrants of positive and negative $\Delta\pi$ values). Close above the phase transition, where the air-water interface is partly covered with condensed lipid domains, peptide incorporation is still possible. It is likely that the peptide inserts into still existing domain boundaries of the *LC* phase, as the phase transition is broad and residual *LE* type lipids are still present. A regression line for all data obtained from the *LC* phase leads to a slope of $m = -0.90$. The superposition of peptide incorporation and lipid condensation leading to $\Delta\pi = 0$ is reached at $\pi_{red} = 6.5 \pm 0.9$ mN m^{-1}.

4.5 Summary of Monolayer Experiments

4.5.1 Influence of Peptide Sequence

The injection of the peptides into a pure buffer solution shows no change of surface pressure. For these amphipathic peptides, no significant surface activity is observed. Due to their five positive charges, located at the side chains of the lysines or arginines, and despite their hydrophobic spacer amino acids, the peptides are well water soluble.

The results of binding experiments with the nine different peptides interacting with a DPPG monolayer show that there is a very subtle interplay between electrostatic and hydrophobic effects, which influences the binding properties of these cationic peptides. The time dependence of the surface pressure after peptide injection underneath the lipid monolayer showed two processes with different kinetics: a condensation of the lipid monolayer decreasing the surface pressure, and an incorporation increasing the surface pressure. The observed surface pressure changes $\Delta\pi$ as a function of initial surface pressure π_{ini} showed a complicated behavior, quite different from previously observed effects when peptides and proteins were incorporated into lipid monolayers [8, 148, 149, 241].

The impact of the hydrophobicity of the amino acid X in different nonapeptides of the structure $(KX)_4K$ on the binding behavior to negatively charged DPPG monolayers was investigated. The spacer amino acid X leads to a distance of the α-carbon atoms of the charged amino acids K of ~ 7.2 Å, a distance close to the headgroups separation of a DPPG monolayer in the *LE* phase, so that optimal electrostatic interactions can be expected.

For the nonapeptides $(KX)_4K$, the behavior of $\Delta\pi$ *vs.* π_{ini} depends on the hydrophobicity of the intervening amino acid X. At π_{ini} values below 10 mN m^{-1} the incorporation effect dominates for the more hydrophobic peptides $(KV)_4K$ and $(KL)_4K$, whereas condensation and incorporation effects more or less compensate for the other three peptides $(KG)_4K$, $(KA)_4K$ and $(KAbu)_4K$. Above an initial surface pressure of 10 mN m^{-1} the slopes of the $\Delta\pi$ *vs.* π_{ini} plots are negative and the $\Delta\pi$ values are all negative at high initial surface pressure of the monolayer, indicating the dominance of the electrostatic condensation effect (see Figure 4.5.1).

Introducing a second uncharged amino acid spacer X increases the charge distance, alters the periodicity of the peptide, and opens the possibilities for other conformations of the peptide. Adsorption kinetics of $(KGG)_4K$ are similar to those of $(KG)_4K$, although peptide incorporation is slower. The enhanced capability for lipid condensation is an effect of the higher peptide flexibility.
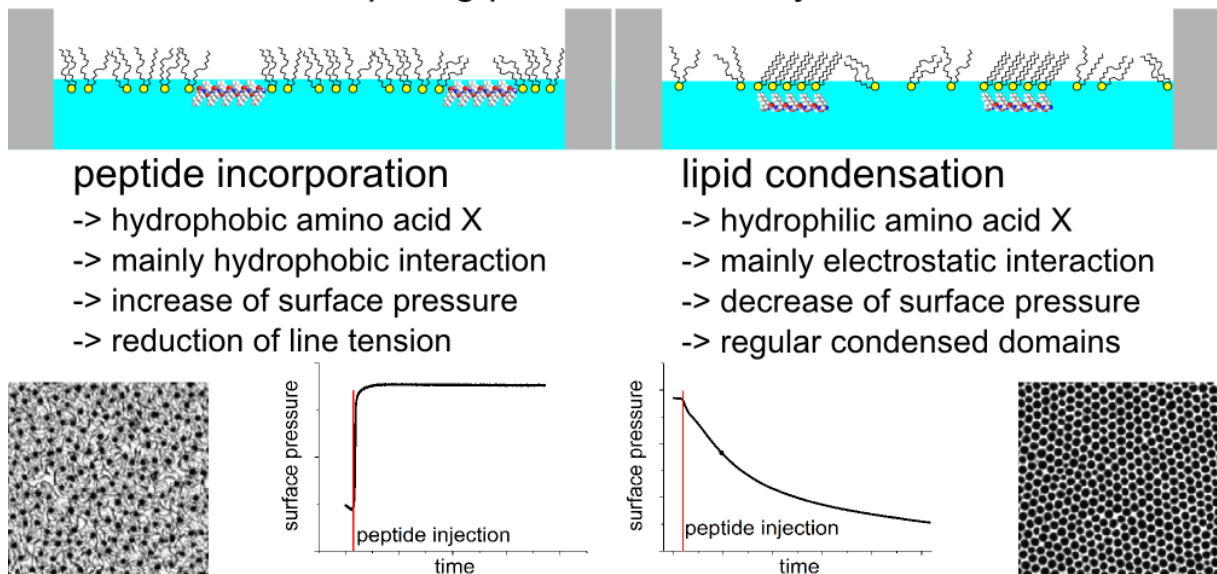
Figure 4.5.1: Two competing processes: peptide incorporation into the lipid monolayer due to hydrophobic interactions, and lipid condensation after peptide binding due to electrostatic interactions. The overlay of both processes determines the time dependent behavior of the surface pressure after peptide injection. For the peptides $(KX)_4K$, hydrophobicity of the uncharged amino acid X dictates the strength of both processes. The binding of $(KX)_4K$ to monolayer in the *LE* phase, induces the formation of *LC*-domains and changes their shapes upon compression.

When K is exchanged by R, minor effects are observed. The behavior of $(RG)_4R$ is again similar to $(KG)_4K$. The relative strength of the lipid condensation and peptide incorporation are larger, because the guanidinium residue is capable of bridging two lipid headgroups and contributes also more to the hydrophobic interaction with the lipid. For $(RA)_4R$, both effects nearly compensate each other resulting in a weak net effect on $\Delta\pi$.

The results of the fluorescence microscopy experiments support the results obtained by the sole adsorption experiments. An induction of *LC*-domains after peptide adsorption to a monolayer in the *LE* phase was observed for all peptides $(KX)_4K$. Upon compression of DPPG monolayers with pre-adsorbed peptides, the size of the domains remained almost constant and a regular quasi-hexagonal pattern of *LC*-domains at higher surface pressure is formed, indicating stabilization of the domain lattice by electrostatic repulsion. In the case of binding of the most hydrophobic peptide $(KL)_4K$, a significantly different domain shape was seen. Due to a stronger decrease in line tension, the domains formed longer filament-like extensions. The bound peptide alters the surface pressure-area isotherms, but seems to be squeezed out of the monolayer at higher surface pressure so that only the condensing effect remained.

IRRAS experiments show an increase of the OH vibrational band over time, upon peptide binding to the DPPG monolayer. Thus, it is concluded that the monolayer becomes thicker due to peptide adsorption compared to a pure DPPG monolayer. The obtained results for the increase in monolayer thickness are similar for all peptides, except for (KL)$_4$K binding, where an much larger increase was observed. Concomitant with the increase in thickness, the order in the acyl chains is increased. The tilt angles of the acyl chains show a decrease after peptide binding compared to pure DPPG. In the amide region, only broad bands with low peak intensities were observed, due to the unordered conformation of the adsorbed peptide. For the most hydrophobic peptide (KL)$_4$K, a β-sheet formation was detected upon binding to a DPPG monolayer.

The results show that for the binding of these peptides to charged lipid monolayers electrostatic as well as hydrophobic interactions are important. The different contributions can be separated by time dependent adsorption measurements. The observation of equilibrium values of the surface pressure alone might lead to wrong conclusions. For instance, fluorescence microscopy clearly shows that the decrease in surface pressure of *LE* phase DPPG found after binding of some of the peptides is correlated with the formation of *LC*-domains, although the isotherms seem to indicate that the monolayers are still completely in the *LE* phase.

4.5.2 Influence of Lipid Structure

Influence of the lipid headgroup charge

Injection experiments of the peptide (KL)$_4$K into the subphase of a monolayer composed of zwitterionic lipids show no change of surface pressure independent of the phase, assuming that the hydrophobic contributions from the leucine residues are too weak to penetrate a zwitterionic monolayer. A negative charge at the lipid headgroup of the monolayer is necessary for peptide binding (see Figure 4.5.2).

Influence of different acyl chains attached to a phosphatidylglycerol headgroup

The onset of the *LE/LC* phase transition is shifted to lower surface pressure for PGs with longer acyl chains. Upon injection of peptide into the subphase of the PG monolayer, an overlay of two processes is again observed as already discussed above.

Both effects, lipid condensation and peptide incorporation, show a strong phase dependence for their kinetics as well as for their relative strength. In the *LE* phase of DPPG monolayer at

low π_{ini}, a strong and fast increase of surface pressure is followed by a slower and weaker decrease, resulting in a net increase of surface pressure, because peptide incorporation is dominant. The situation in the *LC* phase in a DPPG monolayer at high π_{ini}, is reversed. Lipid condensation is now faster and more dominant than peptide incorporation causing a decrease of surface pressure. In the *LE* phase, a biphasic behavior of $\Delta\pi$ *vs.* π_{ini} is observed, due to the overlay of both effects. In the *LC* phase, $\Delta\pi$ *vs.* π_{ini} shows a linear relationship and the superposition surface pressure π_{sp}, where both effects compensate each other, is located at 17 mN m^{-1}.

The relative strength of both effects seems to be coupled with the density of the monolayer and the strength of the van der Waals interactions between the lipid acyl chains. Thus, the range of the biphasic behavior with favored peptide incorporation is extended to higher π_{ini} for the DMPG monolayer. In contrast, the densely packed DSPG monolayer enables nearly no peptide incorporation showing a linear relationship dominated by lipid condensation.

Influence of the lipid headgroup structure

Adsorption kinetics of the peptides to other negatively charged lipid monolayers are similar to those presented for PGs. Extent and rate of lipid condensation and peptide incorporation show the same phase dependency. From the equilibrium data, it was concluded that the position of the *LE/LC* phase transition determines the range of the biphasic behaviour. As seen for PGs, the biphasic range becomes larger, the higher the surface pressure for the *LE/LC* phase transition. The relative strength of the peptide incorporation compared to the lipid condensation determines the observed upshift of the superposition surface pressure π_{sp} above the *LE/LC* phase transition pressure. For negatively charged lipids with large headgroups (PS and PG) a less dense lipid layer promotes more peptide incorporation, shifting π_{sp} to values higher above the $\pi_{LE/LC}$ pressure, compared to lipids with small headgroups (PA and CL) and a denser lipid layer. Although, there are differences in π_{sp}, depending on the lipid headgroup size, the slope of the regression lines in the linear range of $\Delta\pi$ vs. π_{ini} shows another dependency. Lipid headgroups containing glycerol (DSPG, DPPG and TMCL) have a steeper slope in the *LC* phase compared to DMPA and DMPS, suggesting a specific interaction of the peptide in the headgroup region.
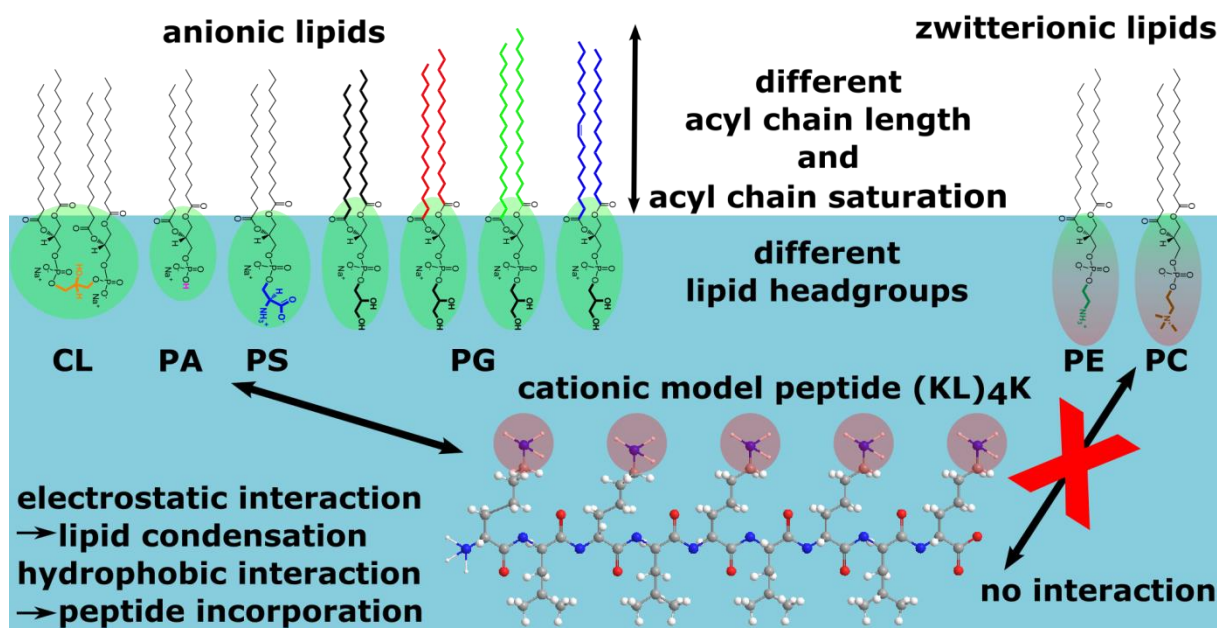
Figure 4.5.2: The interaction of cationic model peptide (KL)$_4$K with lipid monolayer is mainly determined by the headgroup charge. Negative charges (headgroups and phosphate groups) are colored in green and positive charges (lysine side chains and amino alcohol of zwitterionic lipid). No binding of (KL)$_4$K was observed to monolayers composed of zwitterionic lipids. The binding of the peptide to anionic lipids is determined by the structure of the headgroup, and the phase state of the lipid. An overlay of electrostatic and hydrophobic interactions is seen.

General behavior

Comparing the influence of different lipid acyl chains and headgroups a general behavior for negatively charged lipid monolayers is observed for the interaction with (KL)$_4$K at the air-water interface (see Figure 4.5.2). The extent of the two competing processes, lipid condensation and peptide incorporation, leading to opposing effects of the surface pressure, are determined by the phase state of the lipid and the density of the monolayer. In the *LE* phase, the increase of surface pressure occurs, because peptide incorporation driven by hydrophobic interaction dominates. The favored electrostatic interactions in the *LC* phase cause a decrease of surface pressure due to lipid condensation. The superposition of both effects leads to π_{sp} to values above the *LE/LC* phase transition pressure.

5   Comparison of Bilayer and Monolayer Results

5.1   Influence of Peptide Sequence

The classification of the peptides into three main categories based on the results of the bilayer experiments is also applicable for the monolayer results and corresponds to the presented matrix in Figure 2.3.1. The three parameters determining the groups are i) the hydrophobicity of the uncharged amino acid between the lysines or arginines, ii) the charge distance of the lysines, and iii) the different positively charged amino acids (K or R). The differences of the peptide behavior within the categories are smaller than between the peptides of different categories.

The main driving force for the interaction of the positively charged peptides with the negatively charged DPPG headgroups is electrostatic attraction. Peptide adsorption to the lipids reduces the repulsion of the identical charges at the headgroups and enables a better acyl chain packing leading to a stabilization of the more ordered phase. In the bilayer system, the gel phase is stabilized shifting the main phase transition to higher temperatures, whereas for the monolayer, the onset of the *LE/LC* phase transition is shifted to lower surface pressures.

In addition to the electrostatic effect, also the hydrophobicity of the spacer amino acid plays an important role. Based on the results for both model systems, a subtle interplay between electrostatic and hydrophobic interactions was detected. In contrast to the electrostatic screening in the headgroup region, the hydrophobic interaction of the peptide side chain takes place in the acyl chain region of the lipids. The latter should lead to a more unordered phase due to the perturbation of the lipid packing. The consequence upon peptide binding would be a decreased main phase transition temperature, a surface pressure increase, and an upshift of the *LE/LC* transition pressure.

For the peptides $(KX)_4K$, a domination of the electrostatic interaction is observed. The more hydrophobic the spacer amino acid X is, the stronger is the hydrophobic interaction. For the most hydrophobic peptide $(KL)_4K$, the main phase transition temperature is decreased compared to $(KAbu)_4K$, a more hydrophilic peptide. In the monolayer, the surface pressure increases in a certain range of the *LC*-phase upon adsorption of the peptides. With an increased peptide hydrophobicity, the slope of the regression line of the plot $\Delta\pi$ *vs* π_{ini} becomes more negative.

In addition to the hydrophobic and electrostatic effects discussed above, the geometry and the charge distances in the peptide strands and in the lipid monolayer are decisive as well. Therefore, the peptides interact more strongly with gel phase liposomes and can form β-sheet structures, "gluing" the bilayers together. A direct effect is the strong aggregation of the sample, which is also detectable by visible inspection. Upon mixing lipid vesicles with peptide solution, the samples became increasingly turbid and a separation into a clear bulk solution and flaky white lipid-peptide aggregates is observed.

Peptide binding to lipid bilayers in the liquid-crystalline phase affects their properties marginally. In contrast, the monolayer adsorption experiments show that there is an interaction of the peptides with *LE* monolayers, which is dominated by peptide incorporation and thereby overcompensates the electrostatic lipid condensation.

The peptides with the general sequence $(KX)_4K$ are able to adopt a β-sheet arrangement with a charged and a hydrophobic face. Except for $(KG)_4K$, all other $(KX)_4K$ peptides form antiparallel intermolecular β-sheets upon binding to DPPG vesicles. Comparing the results from the DPPG-bilayers and monolayers reveals that for bilayers both phases (the gel phase as well as the liquid-crystalline phase) act as template for β-sheet formation of $(KL)_4K$, whereas for monolayers only the *LC* phase triggers β-sheet formation. A reason might be the formation of stacked lipid bilayers separated by a peptide layer of aggregated β-sheets. In the monolayer system, the stabilization of the β-sheet by a second lipid layer is missing.

An increased charge distance in the peptide backbone lowers the ability to increase the main phase transition temperature in the bilayers and prevents the formation of a stable peptide structure.

Changing the charged amino acid from lysine to arginine decreases the influence of the peptide on the properties of the lipid. Additionally, the effects of the lipid condensation and the hydrophobic contribution of the guanidinium moiety compensate each other.

5.2   Influence of Lipid Structure

Influence of lipid headgroup charge

The results from the interaction of the peptide with zwitterionic lipids like phosphatidylcholine and phosphatidylethanolamine in bilayer and monolayer systems are consistent. Peptide binding is very weak and does not change the thermotropic behavior of the lipid bilayer and the lipid order at the air-water interface. Apparently, the peptides are not

hydrophobic enough to penetrate the headgroup region of the lipids in the absence of any net negative charges at the lipid layer.

Influence of different acyl chains attached to a phosphatidylglycerol headgroup

The thermotropic behavior of PGs with different acyl chain length and acyl chain saturation shows no differences on a reduced temperature scale. The lipid acyl chain melting as well as the secondary structure rearrangement of the adsorbed peptide occurs at the same temperature well above the main phase transition temperature of the pure lipid. These findings underline the fact that the lipid-peptide interaction mainly takes place at the lipid headgroup region. Similar results are obtained for the lipid monolayers at the air-water interface. Independent on the acyl chain, a maximal surface pressure change $\Delta\pi$ of 13 mN m^{-1} is observed upon peptide incorporation into an *LE* phase and the slope of the linear regressions of $\Delta\pi$ *vs* π_{ini} in the *LC* phase are similar.

Influence of the lipid headgroup structure

The headgroup sizes or the critical packing parameter (*cpp*) are decisive in bilayer systems. Smaller headgroups increase the gel phase stabilization for. Besides the peptide sequence, also the lipid headgroup determines the stability of the bound β-sheets. Larger lipid headgroups reduce the stability of the β-sheets. The *cpp* of the lipid in the monolayer determines the shift of the superposition pressure π_{sp} in relation to the *LE/LC* phase transition pressure. The slopes of the regression line of $\Delta\pi$ *vs.* π_{ini} and the secondary structure of peptides bound to lipid bilayers are comparable and only depend on the negative charge of the headgroup.

General behavior

A general behavior of negatively charged lipids interacting with cationic peptides is observed, if a reduced scale, i.e. temperature or surface pressure is applied. The acyl chain region, which mainly determines the phase state of the lipid, is less important compared to the headgroup region. Lipid vesicles interacting with peptides show an upshift of the main phase transition temperature by 15 to 31 K. The size of the headgroup determines the extent of the gel phase stabilization. Monolayer systems show a domination of peptide incorporation into the acyl chain region in the *LE* phase and a domination of lipid condensation in the *LC* phase. The compensation of both effects occurs at ca. 7 mN m^{-1} above the *LE/LC* phase transition. The shift is also dependent on the headgroup size.

6 Summary and Conclusions

Antimicrobial and cell penetrating peptides, originating from biological sources, show a complex behavior in interaction with bacterial membranes. The binding affinity is dependent on electrostatic and hydrophobic contributions and is further influenced by the different sequences and the secondary structure of these peptides.

The scope of this work is a systematic determination of the driving forces for the interaction of short cationic model peptides with lipid bilayers and monolayers. The cationic peptides are simplified models for the complex natural antimicrobial peptides. Lipid vesicles and monolayers at the air-water interface are models for biological membranes or bacterial membranes in special.

A systematic study of the binding properties was performed, where peptide sequence and lipid structures were altered to determine their influence on the interaction. Therefore, a small peptide library was used, consisting of peptides with the structures $(KX)_4K$, $(KXX)_4K$ and $(RX)_4R$, to investigate the impact of an increased hydrophobicity of the uncharged amino acid, of an elongated charge distance, and the exchange of the charged amino acid in the peptide sequence (see Figure 2.3.1). The uncharged amino acid X was varied from G, A, Abu, V, to L. To determine the influence of the lipid structure the acyl chain length and acyl chain saturation as well as the headgroup size and charge was altered. The lipids used were the negatively charged DMPG, DPPG, DSPG, POPG, DMPA, DMPS, and TMCL as well as the zwitterionic DMPE, and DPPC (see Figure 2.1.1). The combination of bilayer and monolayer experiments allows drawing a comprehensive picture of the lipid-peptide interaction.

Differential Scanning Calorimetry (DSC) was used to study the thermodynamic phase behavior of lipid bilayers complexed with peptide. With temperature dependent infrared spectroscopy the influence of the added peptide on the acyl chain order and interfacial hydration, as well as the secondary structure of the bound peptide were examined. Monolayer experiments provided information about the kinetics of the binding of the peptides, and the relative strength of the competing effects of lipid condensation and peptide incorporation. The combination of the monolayer technique with fluorescence microscopy enabled the determination of phase transitions and changes in domain formation upon peptide binding. Infrared Reflection Absorption Spectroscopy (IRRAS) provided information about the lipid acyl chain conformation and the chain tilt, the monolayer thickness, and the orientation of the peptide after binding.

The results of the studies show that the interaction of short cationic peptides with lipid monolayers and bilayers is a complex interplay of electrostatics, hydrophobicity, and geometry and depends on both, the peptide sequence and the lipids structure.

The lipid-peptide interaction is a subtle interplay of electrostatic interactions driven by opposite charges and hydrophobic interactions due to different contributions of the side chains of uncharged amino acids in the peptide. In addition, the geometry determined by the peptide sequence, its secondary structure, and the lipid headgroup distance plays a role. The peptide secondary structure is more important and the three different parameters of hydrophobicity, charge distance, and charge localization are the key elements determining the binding affinity.

An increased peptide hydrophobicity in the sequence $(KX)_4K$ increases for lipid-peptide mixtures the main phase transition temperature of the lipid, reduces the hydration in the lipid headgroup region and induces a β-sheet structure of the peptide (see Figure 3.5.1). In the monolayer adsorption experiments, the strength of the peptide incorporation and lipid condensation defines the slope of the regression lines of $\Delta\pi$ vs. π_{ini} (see Figure 4.5.1). For more hydrophobic peptides, the slope of the regression line becomes more negative, implying stronger interactions.

An increased charge distance of the positively charged amino acids in the peptides $(KXX)_4K$ alters the secondary structure of the peptide. The unordered structure in the bulk solution is preserved upon binding to lipid bilayer and the gel phase is only slightly stabilized. The lipid monolayer condensation suggests that only electrostatics are contributing to the binding.

By exchanging the lysine residues by arginines, the electrostatic interaction is counteracted by an increased hydrophobicity of the guanidinium moiety, leading to a weaker total effect (see Table 3.5.1).

The lipid component also influences the interaction with the model peptides. The lipid headgroup charge is the most important parameter for interaction. Only negatively charged headgroups enable the binding of these peptides. No significant binding to zwitterionic lipids was observed, regardless of the hydrophobicity of the amino acid X (see Figure 4.5.2). For a negatively charged lipid, the headgroup and the length and saturation of the acyl chain can be changed. Using a reduced scale for bilayers and monolayers systems, the nature of the acyl chain is nearly irrelevant for the binding affinity, suggesting that most of the lipid-peptide interaction takes place in the headgroup region of the lipid layer. The critical packing parameter determines the upshift of the main phase transition temperature for lipid bilayer systems with bound peptide, and the headgroup size correlates also the temperature dependent

stability of the adsorbed β-sheet. For monolayer systems, the lipid phase state determines the interaction with the peptide. Peptide incorporation dominates for the interaction with *LE* phase monolayers, whereas lipid condensation is favored for monolayers in the *LC* state. Condensation and incorporation effects compensate at the so-called superposition surface pressure π_{sp}, at ca. 7 mN m^{-1} above the *LE/LC* phase transition pressure. For initial surface pressures above this value a decrease in surface pressure throughout the interaction experiment is observed.

In summary, to investigate the complex interaction of cationic peptides with anionic lipids, the use of calorimetric and spectroscopic techniques is necessary. DSC reveals shifts of phase transition temperatures and IR data show that the conformational transition of the lipids and the peptides is a concerted process. The formed β-sheet structures are stabilized by lipid bilayers in a sandwich-like manner. However, DSC and IR experiments reveal only equilibrium data. The kinetics of the peptide binding can be recorded by monolayer adsorption experiments. Coupling of monolayer experiments with fluorescence microscopy and IRRA spectroscopy emphasizes the importance of hydrophobic contributions to the interaction between lipids and peptides. Nevertheless, the adsorption of the peptide via electrostatic interaction is not sufficient to form β-sheets underneath a lipid monolayer, when a second lipid layer is missing.

The general interaction of antimicrobial peptides with bacteria is very complex and hard to understand. To gain a deeper knowledge of this interaction, simplified models consisting of short cationic peptides and bilayer membranes with distinct lipid composition were studied. With the help of this work, a better understanding of the relationship between function and structure of the peptides and a more comprehensive insight about the overlay of electrostatic and hydrophobic interaction allows the design and production of cheaper and more efficient antimicrobial peptides.

7 Zusammenfassung

Antimikrobielle oder zellpenetrierende Peptide findet man in allen Reichen des Lebens. In Wechselwirkung mit Bakterienmembranen oder Zellen zeigen diese Peptide ein komplexes Verhalten. Die unterschiedlichen Sequenzen und Sekundärstrukturen beeinflussen die Interaktion des Peptides mit der Zellmembran. Elektrostatische und hydrophobe Beiträge tragen zur Bindungsaffinität bei.

Das Ziel dieser Arbeit bestand darin, die Triebkräfte der Wechselwirkung von kurzen kationischen Modellpeptiden mit Lipiddoppelschichten und Lipidmonoschichten aufzuklären. Die Kombinationen von verschiedenen Modellsystemen und Methoden ermöglichten, einen umfassenden Einblick zu erlangen.

Als Modellsysteme für natürlich vorkommende antimikrobielle Peptide dienten kationische Peptide mit einer definierten Sequenz. Lipidmonoschichten an der Luft-Wasser-Grenzfläche sowie Lipidvesikel stellen geeignete Modellsysteme für biologische, im Besonderen bakterielle Membranen dar.

Eine systematische Untersuchung der Lipid-Peptid-Wechselwirkungen in Abhängigkeit der chemischen Struktur der beiden Interaktionspartner ist bisher noch nicht erfolgt. Daher wurde die Struktur der eingesetzten Peptide und Lipide gezielt variiert. Um den Einfluss der Peptidsequenz auf die Wechselwirkung zu bestimmen, wurde eine Peptidbibliothek erstellt, welche die Peptide $(KX)_4K$, $(KXX)_4K$ and $(RX)_4R$ beinhaltet. Zunächst wurden die Auswirkungen einer erhöhten Hydrophobizität der ungeladenen Aminosäure X in den Peptiden mit der Sequenz $(KX)_4K$ untersucht und die folgenden ungeladenen Aminosäuren verwendet: X = G, A, Abu, V und L. Danach dienten $(KXX)_4K$ Peptide dazu, die Auswirkungen eines verlängerten Abstandes der geladenen Lysine auf die Wechselwirkungen zu bestimmen. Darüber hinaus wurde der Effekt des Austausches der geladenen Aminosäure Lysin durch Arginin in der Peptidsequenz ermittelt. Der Einfluss der Lipidstruktur wurde untersucht, indem die Länge der Alkylkette und deren Sättigungsgrad sowie die Landung und Größe der Kopfgruppe verändert wurde. Dafür wurden die Lipide DMPG, DPPG, DSPG, POPG, DMPA, DMPS, TMCL, DMPE und DPPC verwendet.

Das temperaturabhängige Phasenverhalten von Lipiddoppelschichten mit gebundenen Peptiden wurde mittels Differential Scanning Calorimetry (DSC) untersucht. Zusammen mit der ebenfalls temperaturabhängigen Infrarot-Spektroskopie konnte der Einfluss des zugesetzten Peptids auf die Alkylkettenordnung und die Hydratation der Kopfgruppenregion

der Lipide sowie die Sekundärstruktur des gebundenen Peptids aufgeklärt werden. Die durchgeführten Experimente an der Lipidmonoschicht erlauben Rückschlüsse auf die Bindungskinetiken sowie auf die relativen Stärken der beiden konkurrierenden Prozesse, des Peptideinbaus und der Lipidkondensation. In Verbindung mit der Fluoreszenzmikroskopie kann die Bildung von Lipiddomänen aufgrund der Peptidbindung visualisiert werden.

Die Ergebnisse der Untersuchungen von Lipiden in Wechselwirkung mit Peptiden zeigen ein komplexes Zusammenspiel durch die Überlagerung mehrerer Einzelbeiträge. Die elektrostatische Wechselwirkung wird durch die entgegengesetzten Ladungen der Peptidseitenketten und der Lipidkopfgruppen bedingt. Die hydrophoben Wechselwirkungen treten zwischen den Alkylketten des Lipids und den verschiedenen Peptidseitenketten auf. Des Weiteren spielen die geometrischen Verhältnisse zwischen den Peptiden, bestimmt durch die Sekundärstruktur, und den Lipiden, bestimmt durch den Phasenzustand, eine Rolle. Bei der Peptidstruktur sind folgende drei Parameter besonders entscheidend: die Hydrophobizität der ungeladenen Aminosäure, der Ladungsabstand der Lysine und der Austausch der geladenen Aminosäure von Lysin zu Arginin. Diese drei Parameter beeinflussen die Wechselwirkungen der Peptide mit der Lipidmonoschicht an der Luft-Wasser-Grenzfläche und das thermotrope Verhalten der Lipid-Peptide-Mischungen in der Volumenphase.

Eine erhöhte Hydrophobizität der ungeladenen Aminosäure X in Peptiden mit der allgemeinen Sequenz $(KX)_4K$, erhöht die Hauptphasenumwandlungstemperatur des Lipides, erniedrigt die Hydratation des Kopfgruppenbereiches und induziert eine β-Faltblattanordnung des Peptides. Bei der Adsorption des Peptides an die Lipidmonoschicht skaliert die Stärke des Peptideinbaus als auch der Anstieg der Regressionsgeraden der Auftragung $\Delta\pi$ vs. π_{ini} mit der Hydrophobizität des Peptides.

Ein verlängerter Abstand der positiv geladenen Aminosäure Lysin in den Peptiden $(KXX)_4K$ verändert die Sekundärstruktur des Peptides. Die ungeordnete Konformation des Peptides in der Volumenphase bleibt auch nach der Bindung an Lipiddoppelschichten erhalten. Demzufolge fällt auch die Stabilisierung der Gelphase des Lipides geringer aus. Jedoch bleibt der Effekt der Lipidkondensation erhalten, woraus sich schließen lässt, dass hierfür die Elektrostatik die treibende Kraft ist.

Bei dem Austausch der Lysinseitenkette gegen eine Argininseitenkette werden die hydrophoben Wechselwirkungen durch eine gesteigerte Hydrophobizität des Guanidiniumrestes erhöht. Durch die ebenfalls auftretenden elektrostatischen

Wechselwirkungen mit den negativ geladenen Lipidkopfgruppen kommt es zur Kompensation beider Effekte.

Die Lipidkomponente beeinflusst ebenfalls die Wechselwirkungen mit den hier untersuchten Modellpeptiden. Der wichtigste Parameter bei der Lipid-Peptid-Wechselwirkung ist die Ladung der Lipidkopfgruppe. Eine negativ geladene Kopfgruppe ermöglicht die Interaktion mit den Peptiden. Eine zwitterionische Kopfgruppe zeigt kaum Wechselwirkungen. Das negativ geladene Lipid kann durch Veränderung der Kopfgruppengröße sowie der Länge und dem Sättigungsgrad der Alkylkette modifiziert werden. Bei der Verwendung einer reduzierten Temperatur- bzw. Druckskala in Doppelschicht- bzw. Monoschichtsystemen hat die Alkylkette fast keinen Einfluss auf die Wechselwirkung mit den Peptiden. Dies bedeutet, dass die Wechselwirkung des Peptids mit dem Lipid hauptsächlich in der Kopfgruppenregion der Lipide stattfindet. Der kritische Packungsparameter des Lipides beeinflusst die Erhöhung der Hauptphasenumwandlungstemperatur von gemischten Lipid-Peptid-Systemen. Die Größe der Lipidkopfgruppe legt außerdem die Stabilität des adsorbierten β-Faltblattes fest. In Monoschichten bestimmt die vorliegende Phase die Wechselwirkung mit den Peptiden. Bei einer vorgelegten flüssig-expandierten (*LE*) Phase dominiert der Einbau der Peptide in die Lipidmonoschicht, während bei einer flüssig-kondensierten (*LC*) Phase die Lipidkondensation überwiegt. Die Überlagerung dieser beiden entgegengesetzten Effekte führt zu einer Kompensation bei ca. 7 mN m^{-1} über dem *LE/LC* Phasenübergang.

Das generelle Verhalten von antimikrobiellen Peptiden mit Bakterien ist sehr komplex und schwer zu verstehen. Um den Wirkmechanismus zu aufzuklären, wurden vereinfachte Modellsysteme bestehend aus kurzen kationischen Peptiden und Lipidmembranen mit definierter Zusammensetzung untersucht. Das bessere Verständnis von Funktion und Struktur der Peptide sowie eine umfassende Einsicht in die Überlagerung von elektrostatischen und hydrophoben Wechselwirkungen erlaubten es, effizientere antimikrobielle Peptide zu designen und auch günstiger herzustellen.

8 Appendix

8.1 Material

The lipids 1-palmitoyl-2-oleoyl-*sn*-glycero-3-phosphoglycerol (POPG), 1,2-distearyl-*sn*-glycero-3-phosphoglycerol (DSPG), 1,2-dimyristoyl-*sn*-glycero-3-phosphoethanolamine (DMPE), and 1,2-dimyristoyl-*sn*-glycero-3-phosphatidic acid (DMPA) were purchased from Genzyme Pharmaceuticals LLC (Liestal, Switzerland); 1,2-dimyristoyl-*sn*-glycero-3-phosphoglycerol (DMPG), 1,2-dipalmitoyl-*sn*-glycero-3-phosphoglycerol (DPPG) and 1,2-dimyristoyl-*sn*-glycero-3-phosphocholine (DMPC) from Lipoid GmbH (Ludwigshafen, Germany); 1,2-dimyristoyl-*sn*-glycero-3-phospho-L-serine (DMPS) and 1,1',2,2'-tetra myristoyl cardiolipin (TMCL) from Avanti Polar Lipids Inc. (Alabaster, USA).

The peptides were custom-made via Fmoc solid phase chemistry with purity above 98 % and purchased from GeneCust Europe (Dudelange, Luxemburg). For FT-IR measurements the TFA counter ion was exchanged by adding 0.5 mol l^{-1} DCl and lyophilizing the solution three times [269].

Chloroform, Methanol (both high performance liquid chromatography grade) and NaCl were purchased from Carl Roth GmbH&CO KG (Karlsruhe, Germany). All chemicals were used as received without further purification. Aqueous solutions were prepared with ultrapure water from a Milli-Q Advantage A10 system (Millipore S.A.S., Molsheim Cédex, France). Conductivity was lower than 0.055 μS cm^{-1} (25 °C) and TOC below 5 ppb.

8.2 Experimental

8.2.1 Differential Scanning Calorimetry

The pure lipid was suspended in 100 mM NaCl solution, followed by cyclic heating over the phase transition temperature and repeated vortexing. An Avanti Mini-Extruder (Avanti Polar Lipids Inc., Alabaster, USA) was used to prepare liposomes with a monodisperse size distribution by extruding repeatedly the sample solution through a polycarbonate filter with a pore size of 100 nm for 15 times. Differential Scanning Calorimetry was performed with a MicroCal VP-DSC (MicroCal Inc., Northhampton, USA). In all experiments the heating rate was 1 K min^{-1} and the time resolution of 4 s per data point was used. Aqueous lipid and peptide samples were prepared separately, mixed and degassed directly before measurement. The lipid concentration in the calorimetric cell was always 2 mM and the peptide concentration varied from 0.04 mM up to 0.4 mM according to the charge ratio R_c = PG:K 10:1, 5:1, 2:1, 1:1. The reference was always pure 100 mM NaCl solution. At least three up- and down-scans were performed for each sample to prove the reproducibility. All presented curves originate from the second heating scan, unless otherwise stated.

8.2.2 Attenuated Total Reflection Fourier-Transform Infrared Spectroscopy

Attenuated Total Reflection Fourier-transformed Infrared (ATR-FT IR) spectra with a spectral resolution of 4 cm^{-1} were recorded using a Tensor 27 spectrophotometer equipped with an N_2-cooled MCT detector and a BioATR II unit (Bruker Optics, Ettlingen, Germany). A total of 256 scans were averaged. As a reference, spectra of NaCl solution (100 mM) at each corresponding temperature were used. The final absorbance spectra were calculated by -log ($I_{sample}/I_{reference}$). The desired temperature was set by a computer-controlled circulating water bath (Haake C25P Phoenix II, Karlsruhe, Germany). To compare the results from DSC measurements with the IR experiments a similar preparation procedure was chosen. Aqueous lipid and peptide samples (10 mM) were prepared separately using a 100 mM NaCl solution in D_2O as solvent. The pure lipid was suspended and for 5minutes at 50 °C in a water bath. Samples were directly prepared on the crystal surface by mixing aliquots of lipid suspension (15 μl), peptide solutions (3 μl) and 100 mM NaCl solution in D_2O (12 μl) to obtain a charge ratio (R_c) of 1:1 and a lipid concentration of 5 mM. Before recording spectra, one heating and cooling scan was performed to ensure equilibration. Spectra were recorded in 2 °C intervals between 20 °C and 80 °C after temperature equilibration in a temperature interval (ΔT) of ± 0.1 °C for 15 min. The temperature was measured inside the cover plate of the sample holder by a Pt100 resistor (Omega Newport, Deckenpfronn, Germany). All absorbance spectra were

shifted to a zero baseline in a spectral region where no vibrational peak occurred. To determine the position of the vibrational bands in a certain wavenumber interval second derivative spectra were calculated and the 'peak picking' function included in the Bruker OPUS software was applied.

8.2.3 Adsorption Experiments

Adsorption experiments were performed with a home-built circular trough with a diameter of 6 cm and a height of 0.3 cm covered by a plastic hood to keep the temperature and humidity constant. The surface pressure was recorded using a microbalance (Riegler and Kirstein GmbH, Berlin, Germany) equipped with a Wilhelmy plate. Prior to each experiment the trough was thoroughly rinsed and filled with 100 mM NaCl solution. The pressure sensor was calibrated using the surface pressure of pure water (72 mN m^{-1}) and that of air (0 mN m^{-1}) as reference points. The subphase temperature was maintained at 20.0 ± 0.1 °C by a circulating water bath (Thermostat F3, Haake, Karlsruhe, Germany). The subphase was stirred during the experiment using a small stirring magnet to accelerate diffusion of the added solutes. First, a freshly prepared defined volume of a lipid solution in chloroform (1 mM) was spread onto the subphase forming a phospholipid monolayer to give and initial surface pressure π_{ini}. After waiting for 15 min for complete solvent evaporation the measurement was started and the surface pressure of the pure lipid monolayer was recorded for at least 10 min. Then an aqueous peptide solution was injected below the phospholipid monolayer through a channel just above the bottom of the trough. The injection volume was adjusted to give a peptide concentration of 3 μM in the subphase. Analysis and fitting of the kinetic adsorption curves were performed with routines of the software Origin 8.0 (Origin Lab Corp.).

8.2.4 Fluorescence Microscopy

Fluorescence microscopy imaging of monolayers at the air-water interface was performed using an Axio Scope A1 Vario epifluorescence microscope (Carl Zeiss MicroImaging, Jena, Germany). Underneath the microscope a home-build Langmuir Teflon trough with a maximal area of 20.8 cm^2 and a moveable computer-controlled Teflon barrier (Riegler & Kirstein, Berlin, Germany) was positioned on an x-y stage (Märzhäuser, Wetzlar, Germany) to be able to move the film surface with respect to the objective lens to any desired position. The x-y-z motion control was managed by a MAC5000 system (Ludl Electronic Products, Hawthorne, NY, USA). The trough was enclosed by a homebuilt Plexiglas hood to ensure a dust-free environment and to minimize evaporation of water. The temperature of 20 ± 0.1 °C was maintained with a circulating water bath and the whole setup was placed on a vibration-

damped optical table (Newport, Darmstadt, Germany). The air-water surface was illuminated using a 100 W mercury arc lamp, a long-distance objective (LD EC Epiplan-NEOFLUAR 50x) was used and the respective wavelengths were selected with a filter/beam splitter combination, which is appropriate for the excitation and detection of Rh-DHPE (Zeiss filter set 81HE: excitation band-pass BP 553/18 nm (HE), beam splitter QFT (400 + 503 + 570 + 650) nm (HE), emission band-pass QBP (432 + 519 + 590 + 680) nm (HE)). Images were recorded using an EMCCD camera (ImageEM C9100-13, Hamamatsu, Herrsching, Germany). Image analysis and data acquisition were done using the AxioVision software (Carl Zeiss MicroImaging, Jena, Germany). All presented images show areas of individually contrast-adjusted raw data. Monolayer films of DPPG were prepared by spreading from a stock solution with a total concentration of 1 mM in chloroform (HPLC-grade, Carl Roth, Karlsruhe, Germany) containing 0.01 mol% fluorescently labelled Rh-DHPE. The fluorescently labelled lipid Rh-DHPE prefers the liquid-expanded phase of a lipid monolayer so that liquid-condensed domains appear dark [158]. After waiting for 15 min for complete solvent evaporation, the measurement was started and the surface pressure of pure lipid monolayer was recorded for 1 h. Then an aqueous peptide solution was injected below the phospholipid monolayer through a channel just above the bottom of the trough. The injected amount yielded a peptide concentration of 3.0 µM in the subphase. The peptide adsorption was monitored for 4 h. After reaching the adsorption equilibrium, the monolayer was compressed using a compression speed of 2 $\mathring{A}^2$ molecule^{-1} min^{-1}. Microscopy images were taken during adsorption of the peptide and compression of the monolayer.

8.2.5 Infrared Reflection Absorption Spectroscopy

Infrared reflection absorption spectroscopy (IRRAS) was performed on a BRUKER Vector 70 FT-IR spectrometer equipped with a nitrogen cooled MCT detector and an A511 reflection unit (Bruker Optics, Germany), placed over the Langmuir trough setup (Riegler & Kirstein, Germany). A trough with two compartments in a hermetically sealed box was used. The circular sample trough with a diameter of 6 cm and a height of 0.3 cm was equipped with a Wilhelmy balance. The reference trough (30 cm x 6 cm) placed next to the sample trough can be brought into the focus of the IR beam by means of a shuttle. The temperature of 20 ± 0.1 °C was maintained with a circulating water bath. The filling levels of both troughs were kept equal and constant by means of an automated, laser reflection controlled, pumping system connected to reservoirs of purified, deionized water. The IR beam can be focused to the water surface in different angles of incidence with respect to the surface normal and was polarized

with a KRS-5 wire-grid polarizer. The reflectance absorbance spectra (RA) were calculated from the single-beam reflectance spectra recorded on the reference (I_0) and sample trough (I) according to RA = -log(I/I_0). The resolution and scanner speed in all experiments were 4 cm^{-1} and 80 kHz, 1000 scans or 500 scans were accumulated for measurements in p- or s-polarization, respectively. IRRAS experiments were performed in two different protocols:

1) Time dependent IRRA spectra

Prior to the recording of the IRRA spectra a fresh lipid monolayer was prepared. A defined volume of a lipid solution in chloroform (1 mM) was spread onto the subphase (100 mM NaCl) forming a phospholipid monolayer with an initial surface pressure π_{ini}. After waiting for 1 h for complete solvent evaporation and water vapour equilibration the IRRAS measurement was started. The surface pressure of the pure lipid monolayer was recorded for at least 1.5 h and simultaneously IRRA spectra of the pure lipid monolayer were accumulated. The spectra were recorded in p-polarization and at a fixed angle of incidence of 40°. A reference reflectivity spectrum was recorded right before each sample spectrum. The subphase level was adjusted before each data acquisition. Then an aqueous peptide solution was injected below the phospholipid monolayer through the film. The injection volume was adjusted to give a peptide concentration of 3.0 μM in the subphase. IRRAS measurement were continued to follow the adsorption of the injected peptide.

All IRRA spectra were shifted to a zero baseline in a spectral region where no vibrational peak occurred (1800 cm^{-1} - 1850 cm^{-1}). To determine the position of the vibrational bands in a certain wavenumber interval by calculating the second derivative of the spectra, the 'peak picking' function included in the Bruker OPUS software was used. For the time dependent plot of the band integrals and band positions five individual spectra were averaged to reduce the scattering of the data points.

2) Angle dependent IRRA spectroscopy

Subsequent to the time dependent measurements, the angle dependent measurements were performed on DPPG monolayer with the adsorbed peptide in the equilibrium state. The spectra were recorded in p- and s-polarization and at various angles of incidence, ranging from 26° to 70° in increments of 2°. A reference reflectivity spectrum was recorded right before each sample spectrum. The subphase level was adjusted before each data acquisition. At least two measurements were performed and averaged at each angle of incidence and polarization.

IRRA spectra simulation and fitting IRRA spectra were simulated using a 3 layer model (subphase/film/air) as described in Schwieger et al. [11].

To determine the layer thickness simulated spectra were fitted to experimental ones in a global fit, were spectra recorded in different angles of incidence (φ) and polarization (p or s) were fitted in one non-linear least square minimization using the Levenberg-Marquardt algorithm. The optical constants of the subphase water were taken from Berti et al. [270] and shifted -15 cm^{-1} for the determination of the layer thickness and the acyl chain tilt angle. The polarizer quality Γ was set to 0.005 (0.5%) in all simulation and fits. The layer thickness d, the absorption coefficient k, and the full width at half height $fwhh$ were free fitting parameters, while fitting angle and polarization dependent spectra recorded of the mixed monolayer. For all fits, the refractive index of the layer n was set to a constant value of 1.41, assuming a lipid layer. Spectra recorded at a φ close to the Brewster angle (52° - 56°) were not included into the fit due to their low signal to- noise ratio.

Spectra were fitted in the range of 3000 - 3600 cm^{-1}, which corresponds to the OH stretching vibrational band v(OH) to obtain the layer thickness. For the determination of the tilt angle of the acyl chains, spectra were fitted with two bands in the range of 2910 - 2930 cm^{-1}, and 2860 - 2840 cm^{-1}, corresponding to the asymmetric and symmetric v(CH$_2$) stretching bands. Peptide orientation was obtained by fitting the in the range of 1625 - 1610 cm^{-1} for the amide-I band, and 1525 - 1545 cm^{-1} for the amide-II band. A constant ratio of kI · $fwhh$I / kII · $fwhh$II = const. = 3 for the amide bands was used, as determined from transition IR measurements [268].

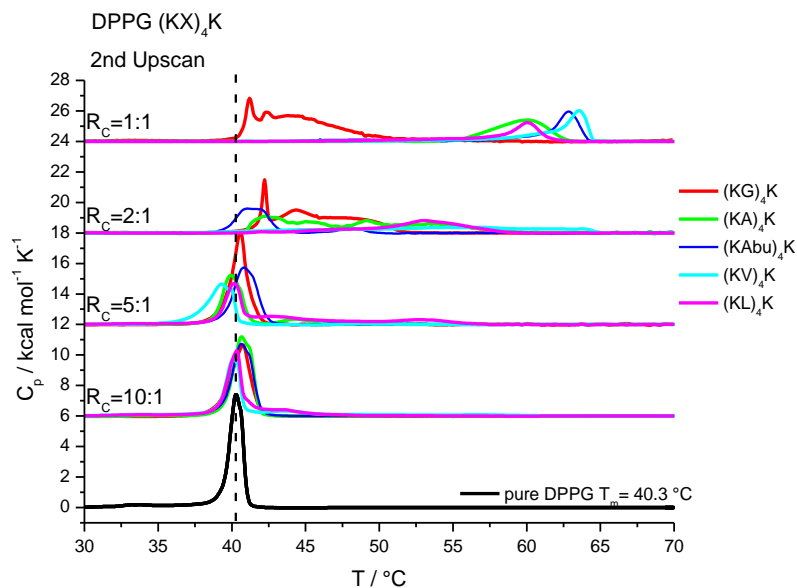# 8.3 Data Overview

8.3.1 DSC Data

Figure 8.3.1: Thermogram of pure DPPG vesicle (black) and different DPPG-$(KX)_4K$ mixtures with increasing charge ratio. The 2nd heating scan is shown, because equilibrium was only reached after passing the phase transition. Measurements were performed in 100 mM NaCl and a fixed lipid concentration of 2 mM.
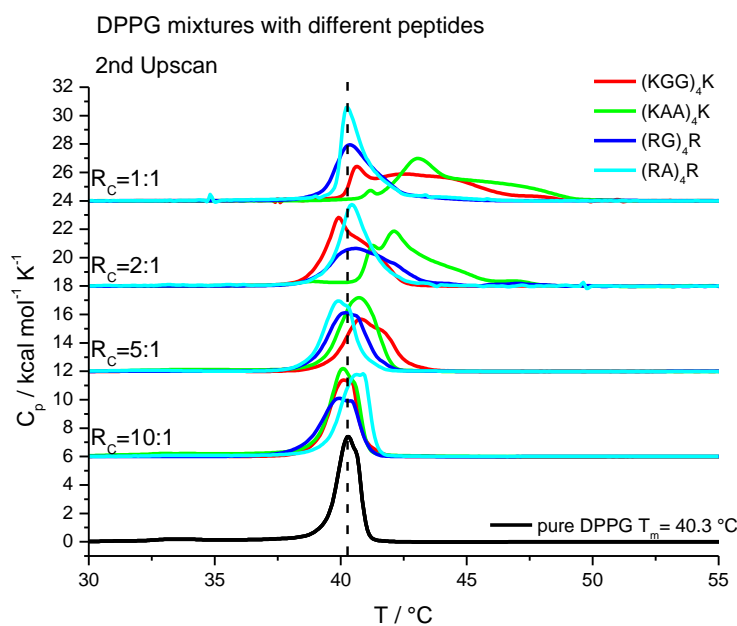

Figure 8.3.2: Thermogram of pure DPPG vesicle (black) and different DPPG-$(KXX)_4K$ or $(RX)_4R$ mixtures with increasing charge ratio. The 2nd heating scan is shown, because equilibrium was only reached after passing the phase transition. Measurements were performed in 100 mM NaCl and a fixed lipid concentration of 2 mM.
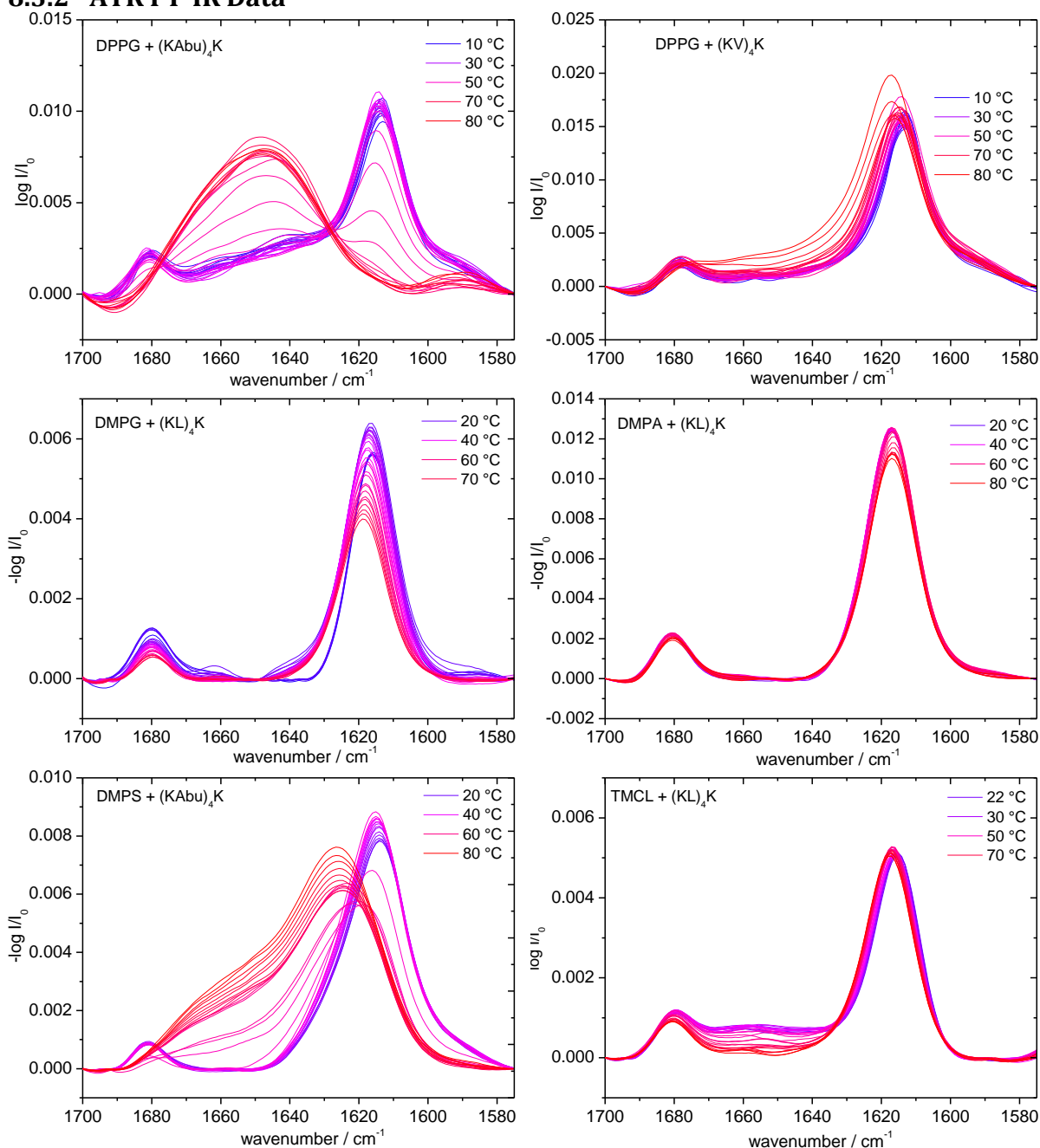
8.3.2 ATR FT-IR Data

Figure 8.3.3: Temperature dependent behavior of the amide-I band for anionic lipids mixed with $(KAbu)_4K$ or with the more hydrophobic peptide $(KL)_4K$. DPPG-$(KAbu)_4K$ mixtures (top left) and DMPS-$(KAbu)_4K$ mixtures (bottom right) show a β-sheet secondary structure at low temperatures with amide peaks at 1680 cm^{-1} and 1615 cm^{-1}, which converts into an unordered structure at higher temperature (amide-I peak at 1646 cm^{-1}). DPPG-$(KV)_4K$ mixtures (top left), DMPG-$(KL)_4K$ mixtures (middle left) DMPA-$(KL)_4K$ mixtures (middle right) and TMCL-$(KL)_4K$ mixtures (bottom right) show a β-sheet secondary structure for the whole tested temperature range. All samples had a charge ratio R_c = 1:1 and were prepared in D_2O containing 100 mM NaCl at pD = 7.2.

8.3.3   Peptide Adsorption to Lipid Monolayers

8.3.3.1 Fluorescence Microscopy coupled with Peptide Injection into the Subphase of a DPPG Monolayer in the *LE* Phase
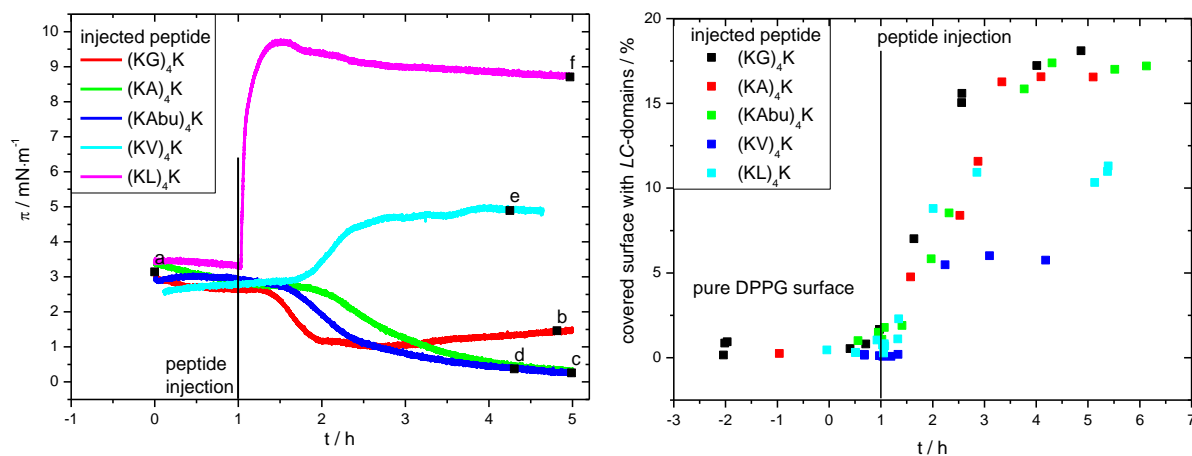

Figure 8.3.4: Left: Change in surface pressure as funktion of time of a DPPG monolayer at an initial surface pressure of about 3 mN m^{-1} after injection of different peptides into the subphase (T = 20 °C, 100 mM NaCl). The lipid monolayer remains at a constant surface pressure prior to peptide injection at t = 1 h (marked with the line). The final concentration of the peptides (panel a-e) in the subphase was 3.0 μM. Characters show the time points of the fluorescence pictures shown in Figure 4.3.6. Right: Coverage of the lipid monolayer with liquid-condensed domians as funktion of time before and after injection of the different peptides into the subphase.

8.3.3.2 Peptide Injection into the Subphase of a Zwitterionic Lipid Monolayer

Adsorption kinetics of (KL)$_4$K to a DMPE monolayer

The pure zwitterionic DMPE monolayer shows an *LE/LC* phase transition at 5 mN m^{-1}. After injection of the peptide solution into the subphase underneath a DMPE monolayer the surface pressure remains constant for all tested initial surface pressure (see Figure 8.3.5 top left panel). A compensation of the previous observed effects of peptide incorporation and lipid condensation is unlikely. The zwitterionic DMPE lacks a negative charge and binding of the peptide does not take place. Furthermore, if only one process would be present or clearly dominating, its relative strength would alter with π_{ini}, as seen for the peptide incorporation into DMPG monolayer. Similar results were also obtained for peptide injection into the subphase underneath a monolayer of DPPC, also a zwitterionic lipid (see Figure 8.3.5, top right panel). A negatively charged headgroup (see section 4.4) is therefore necessary for peptide binding. Data from differential scanning calorimetry also show no changes of the lipid phase transition, underlying the assumption that the peptide stays in the bulk phase without binding to zwitterionic lipids (see section 0).Furthermore, it can be concluded that the peptide is not hydrophobic enough to penetrate into a zwitterionic lipid monolayer or to accumulate at the bare air-water interface.

These results are in contrast to those reported by Castano et al. [71], where the adsorption of the modified peptide Dns-(KL)$_4$K to a DMPC monolayer increased the surface pressure upon incorporation of the peptide in a β-sheet conformation. A possible explanation of this behavior might be that the increase of the surface pressure is a result of increased hydrophobic interaction between the lipid acyl chain region and the attached dansyl (Dns) label of the peptide. The attachment of the dansyl fluorescence label to such a small peptide changes the behavior of the whole peptide as the label represents 18 % of the whole peptide mass.
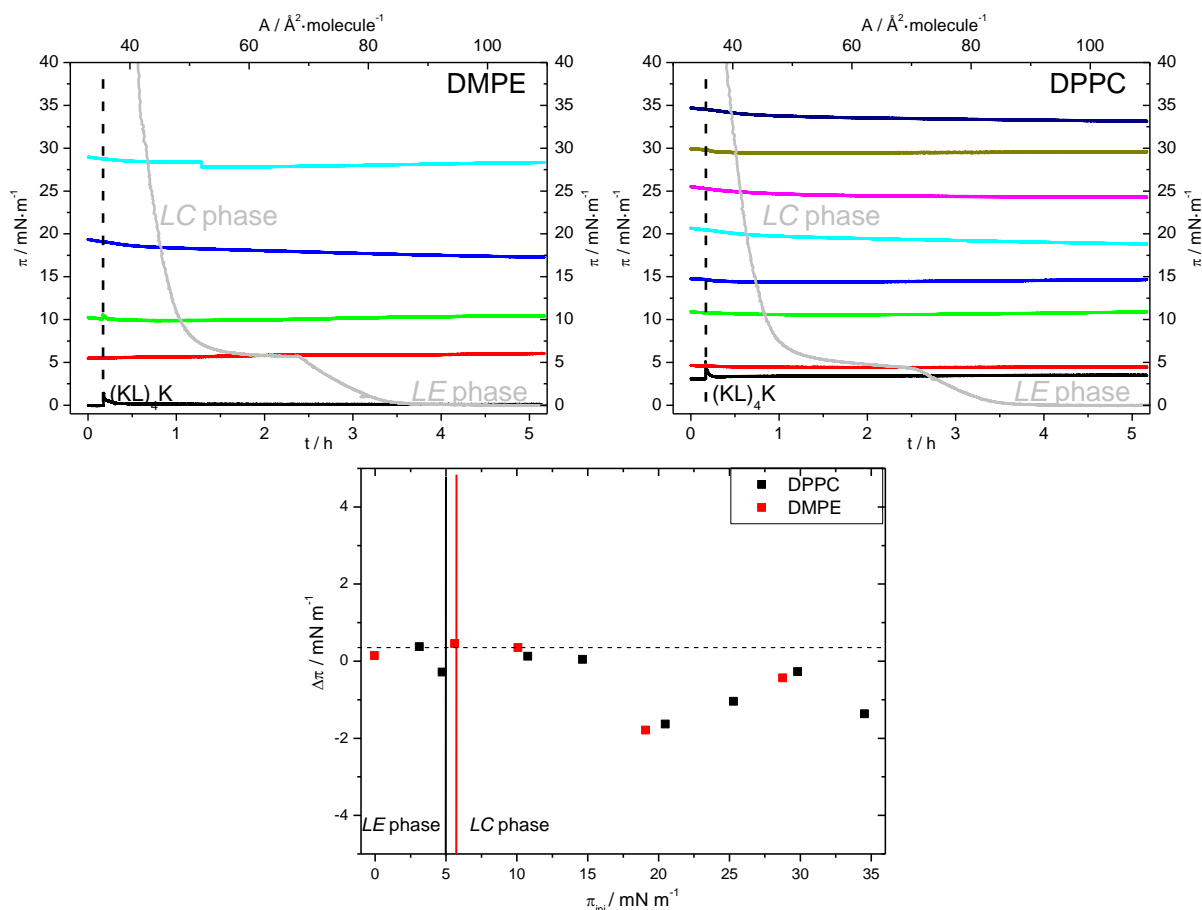
Figure 8.3.5: Change in surface pressure of DMPE (upper left panel) or DPPC (upper right panel) monolayer after injection of $(KL)_4K$ into the subphase ($T = 20\ °C$, 100 mM NaCl) at various initial surface pressure. The lipid monolayer remains at a constant surface pressure prior to peptide injection at $t = 600$ s (marked with the dashed line). The final concentration of of $(KL)_4K$ in the subphase was 3.0 μM. Adsorption equilibrium was reached within 5 h. The surface pressure-area isotherm of pure lipid monolayer with their corresponding *LE* or *LC* phases are also shown in grey. right panel: Difference of surface pressure $\Delta\pi$ after 5 h of adsorption of $(KL)_4K$ solution to a DMPE or DPPC monolayer with different initial surface pressure π_{ini}. The lines at $\Delta\pi = 0$ and $\pi_{ini} = 5$ mN m^{-1} are drawn to guide the eye and to distinguish between the different phases of the DPPC or DMPE monolayer.

8.3.3.3 Peptide Binding to a DPPG Monolayer Studied with IRRA Spectroscopy
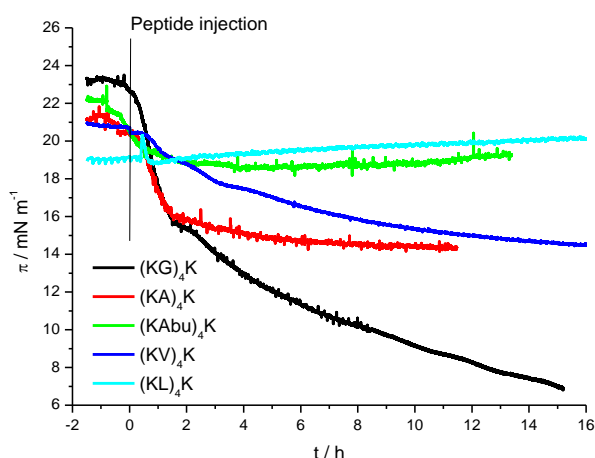
Adsorption kinetics of (KX)₄K to a DPPG monolayer

Figure 8.3.6: Change in surface pressure of a DPPG monolayer as a funktion of time after injection of different peptides into the subphase (T = 20 °C, 100 mM NaCl) at an initial surface pressure of about 20 mN m^{-1}. Experiments were performed within the IRRAS setup. The lipid monolayer remains at a constant surface pressure prior to peptide injection (marked with a line). The final concentration of the peptides in the subphase was 3.0 μM.

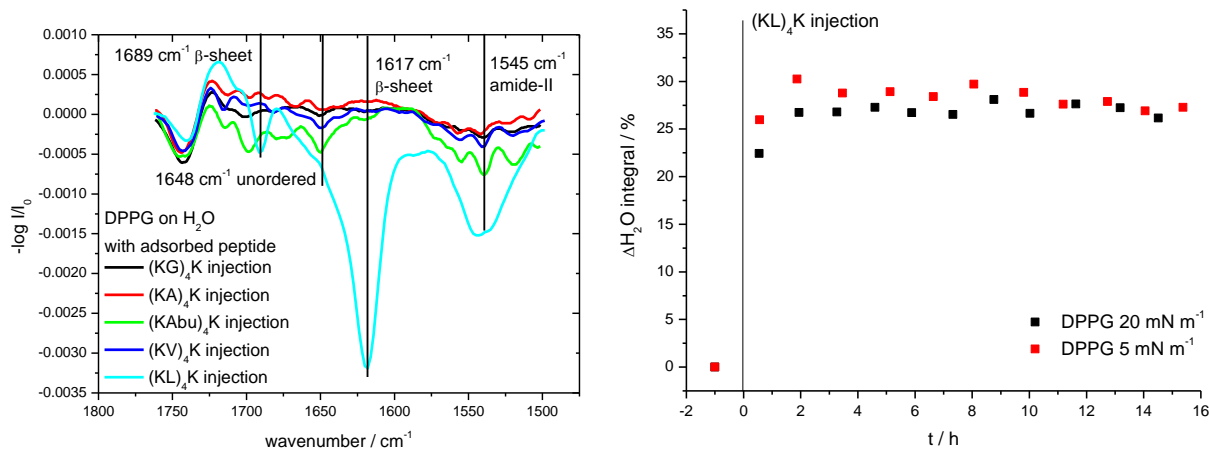*(KX)₄K structure after binding to a DPPG monolayer*

Figure 8.3.7: Left: Spectral region for the lipid carbonyl vibration and the peptide secondary structure of the difference spectra shown for the different tested peptides (difference spectra calculated from the spectra obtained from the lipid monolayer with the adsorbed peptide minus the spectra of pure DPPG prior to peptide adsorption). Right: time dependent difference of the integral of the water band (3000 cm^{-1} to 3800 cm^{-1}) upon peptide adsorption (avered values of 5 individual spectra). For all graphs the data point (-1;0) refers to the initial state of a pure DPPG monolayer prior to peptide injection.

Simulated IRRA spectra for a β-sheet structure bound to a DPPG monolayer

Figure 8.3.8: Experimental spectra of the mixed DPPG/(KL)$_4$K monolayer in the amid region, and simulated spectra of a mixed lipid/(KL)$_4$K monolayer in the amid region with different orientations of the β-sheet by variing the tilt angle *θ* and the twist angle *ψ*. Left: (p-polarization), Right: (s-polarization)

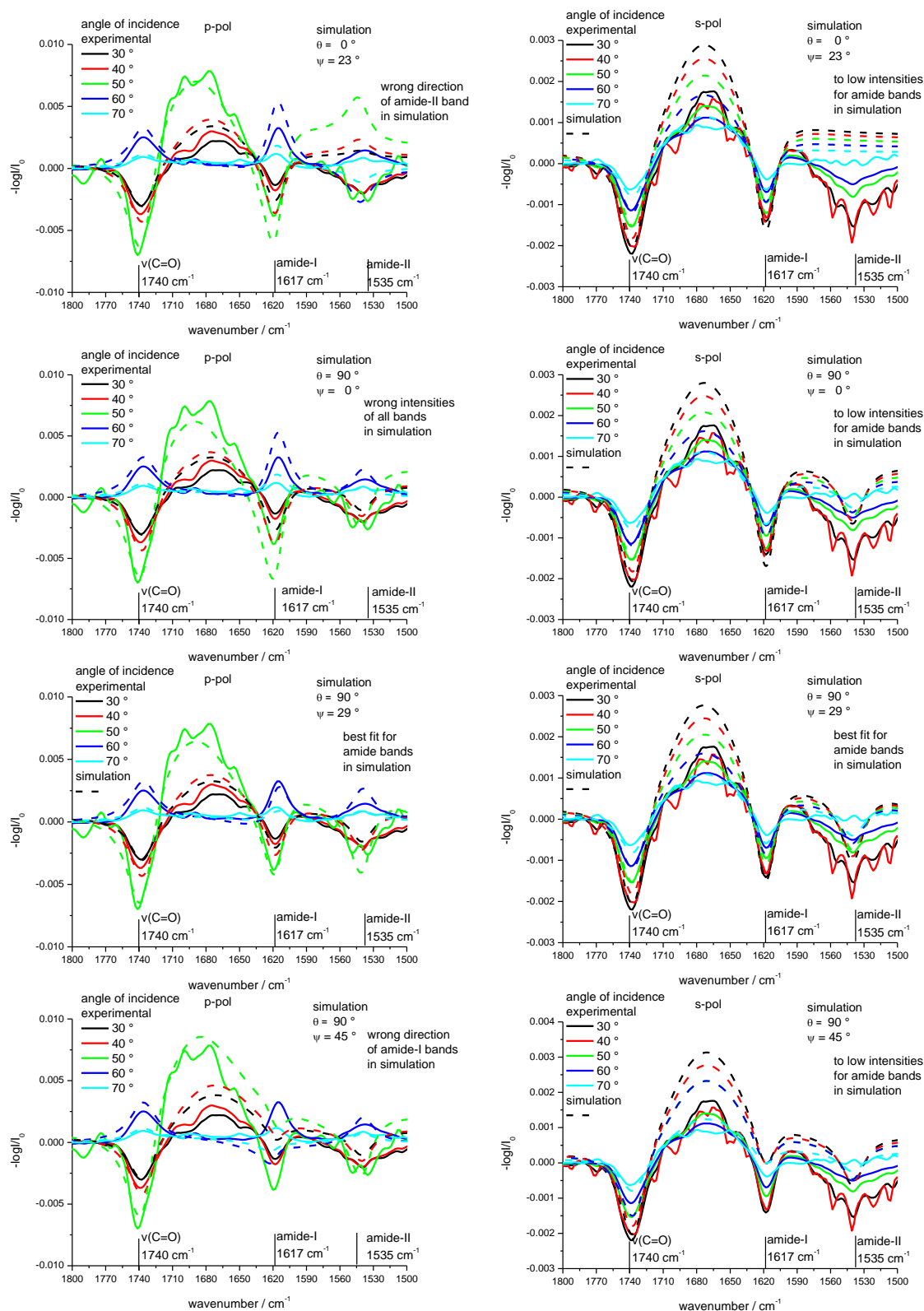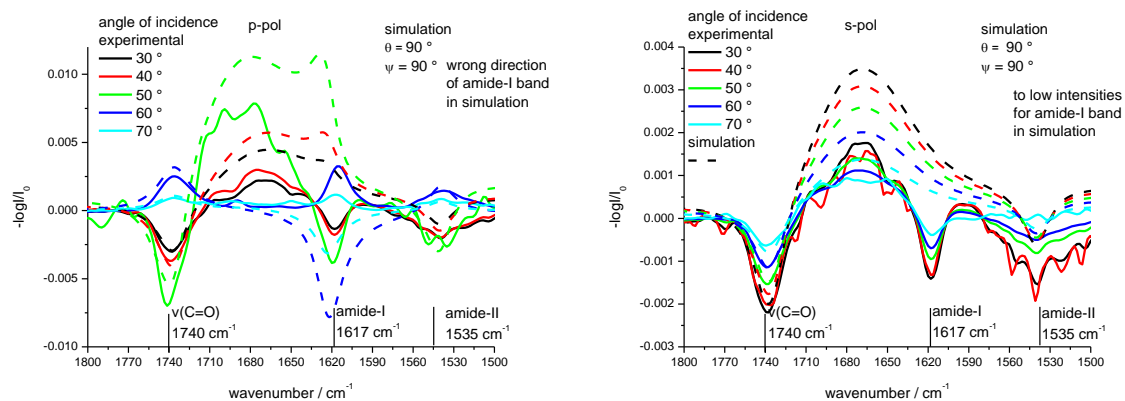Figure 8.3.7, continued: Experimental spectra of the mixed DPPG/(KL)$_4$K monolayer in the amid region, and simulated spectra of a mixed lipid/(KL)$_4$K monolayer in the amid region with different orientations of the β-sheet by variing the tilt angle θ and the twist angle ψ. Left: (p-polarization), Right: (s-polarization)

9 References

[1] S.J. Singer, G.L. Nicolson, The Fluid Mosaic Model of the Structure of Cell Membranes, Science, 175 (1975) 720-731.

[2] A. Blume, P. Garidel, Lipid Model Membranes and Biomembranes, in: R.B. Kemp (Ed.) Handbook of Thermal Analysis and Calorimetry, Elsevier Press, Amsterdam, 1999, pp. 109-173.

[3] J. Seelig, Titration calorimetry of lipid–peptide interactions, Biochimica et Biophysica Acta (BBA) - Reviews on Biomembranes, 1331 (1997) 103-116.

[4] L.K. Tamm, S.A. Tatulian, Infrared spectroscopy of proteins and peptides in lipid bilayers, Quarterly Reviews of Biophysics, 30 (1997) 365-429.

[5] R. Winter, F. Noll, Methoden der Biophysikalischen Chemie, Teubner-Verlag, Stuttgart, 1998.

[6] G. Brezesinski, H. Möhwald, Langmuir monolayers to study interactions at model membrane surfaces, Advances in Colloid and Interface Science, 100–102 (2003) 563-584.

[7] H. Brockman, Lipid monolayers: why use half a membrane to characterize protein-membrane interactions?, Current Opinion in Structural Biology, 9 (1999) 438-443.

[8] R. Maget-Dana, The monolayer technique: a potent tool for studying the interfacial properties of antimicrobial and membrane-lytic peptides and their interactions with lipid membranes, Biochimica et Biophysica Acta (BBA) - Biomembranes, 1492 (1999) 109-140.

[9] A. Arouri, A. Kerth, M. Dathe, A. Blume, The Binding of an Amphipathic Peptide to Lipid Monolayers at the Air/Water Interface Is Modulated by the Lipid Headgroup Structure, Langmuir, 27 (2011) 2811-2818.

[10] A. Hädicke, A. Blume, Interactions of Pluronic block copolymers with lipid monolayers studied by epi-fluorescence microscopy and by adsorption experiments, Journal of Colloid and Interface Science, 407 (2013) 327-338.

[11] C. Schwieger, B. Chen, C. Tschierske, J. Kressler, A. Blume, Organization of T-shaped facial amphiphiles at the air/water interface studied by infrared reflection absorption spectroscopy, The journal of physical chemistry. B, 116 (2012) 12245-12256.

[12] N.A. Alhakamy, A. Kaviratna, C.J. Berkland, P. Dhar, Dynamic Measurements of Membrane Insertion Potential of Synthetic Cell Penetrating Peptides, Langmuir, 29 (2013) 15336-15349.

[13] Y. Ishitsuka, D.S. Pham, A.J. Waring, R.I. Lehrer, K.Y.C. Lee, Insertion selectivity of antimicrobial peptide protegrin-1 into lipid monolayers: Effect of head group electrostatics and tail group packing, Biochimica et Biophysica Acta (BBA) - Biomembranes, 1758 (2006) 1450-1460.

[14] A. Blume, A. Kerth, Peptide and protein binding to lipid monolayers studied by FT-IRRA spectroscopy, Biochimica et Biophysica Acta (BBA) - Biomembranes, 1828 (2013) 2294-2305.

[15] K.A. Sepkowitz, One Hundred Years of Salvarsan, New England Journal of Medicine, 365 (2011) 291-293.

[16] K. Lohner, Development of Novel Antimicrobial Agents: Emerging Strategies, Horizon Scientific Press, Norfolk, 2001.

[17] Antibiotics Research: Problem and Perspectives, Academie of Science and Humanities in Hamburg / German National Academy of Sciences Leopoldina, 2013, pp. 1-66.

[18] R.P. Rubin, A Brief History of Great Discoveries in Pharmacology: In Celebration of the Centennial Anniversary of the Founding of the American Society of Pharmacology and Experimental Therapeutics, Pharmacological Reviews, 59 (2007) 289-359.

[19] J.F. Fisher, S.O. Meroueh, S. Mobashery, Bacterial Resistance to β-Lactam Antibiotics: Compelling Opportunism, Compelling Opportunity, Chemical Reviews, 105 (2005) 395-424.

[20] J.H. Powers, Antimicrobial drug development – the past, the present, and the future, Clinical Microbiology and Infection, 10 (2004) 23-31.

[21] D.A. Phoenix, F. Harris, S.R. Dennison, Novel Antimicrobial Agents and Strategies, Wiley, Somerset, NJ, USA, 2014.

[22] G. Wang, Database-Guided Discovery of Potent Peptides to Combat HIV-1 or Superbugs, Pharmaceuticals, 6 (2013) 728-758.

[23] W.C. Wimley, Describing the Mechanism of Antimicrobial Peptide Action with the Interfacial Activity Model, ACS Chemical Biology, 5 (2010) 905-917.

[24] Y.J. Gordon, E.G. Romanowski, A.M. McDermott, A Review of Antimicrobial Peptides and Their Therapeutic Potential as Anti-Infective Drugs, Current Eye Research, 30 (2005) 505-515.

[25] J.M. Sanderson, Peptide-lipid interactions: insights and perspectives, Organic & Biomolecular Chemistry, 3 (2005) 201-212.

[26] Y.H. Nan, K.H. Park, Y. Park, Y.J. Jeon, Y. Kim, I.-S. Park, K.-S. Hahm, S.Y. Shin, Investigating the effects of positive charge and hydrophobicity on the cell selectivity, mechanism of action and anti-inflammatory activity of a Trp-rich antimicrobial peptide indolicidin, 2009.

[27] S.H. White, W.C. Wimley, M.E. Selsted, Structure, function, and membrane integration of defensins, Current Opinion in Structural Biology, 5 (1995) 521-527.

[28] C. Yin, J.H. Wong, T.B. Ng, Recent Studies on the Antimicrobial Peptides Lactoferricin and Lactoferrampin, Journal of Applied Statistics, 14 (2014) 1139-1154.

[29] B. Bechinger, Structure and Functions of Channel-Forming Peptides: Magainins, Cecropins, Melittin and Alamethicin, J. Membrane Biol., 156 (1997) 197-211.

[30] U.H.N. Dürr, U.S. Sudheendra, A. Ramamoorthy, LL-37, the only human member of the cathelicidin family of antimicrobial peptides, Biochimica et Biophysica Acta (BBA) - Biomembranes, 1758 (2006) 1408-1425.

[31] R.E.W. Hancock, H.-G. Sahl, Antimicrobial and host-defense peptides as new anti-infective therapeutic strategies, Nature Biotechnology, 24 (2006) 1551-1557.

[32] M. Zasloff, Antimicrobial peptides of multicellular organisms, Nature, 415 (2002) 389-395.

[33] G. Wang, X. Li, Z. Wang, APD2: the updated antimicrobial peptide database and its application in peptide design, Nucleic Acids Research, 37 (2009) D933-D937.

[34] K. Matsuzaki, Control of cell selectivity of antimicrobial peptides, Biochimica et Biophysica Acta (BBA) - Biomembranes, 1788 (2009) 1687-1692.

[35] M.R. Yeaman, N.Y. Yount, Mechanisms of Antimicrobial Peptide Action and Resistance, Pharmacological Reviews, 55 (2003) 27-55.

[36] R.F.A. Zwaal, A.J. Schroit, Pathophysiologic Implications of Membrane Phospholipid Asymmetry in Blood Cells, 1997.

[37] C. Tanford, The Hydropobic Effect: Formation of Micells and Biological Membranes, Wiley, New York, 1980.

[38] R. Koynova, B. Tenchov, Transitions between lamellar and non-lamellar phases in membrane lipids and their physiological roles., OA Biochemistry, 1 (2013) 9.

[39] J.N. Israelachvili, D.J. Mitchell, B.W. Ninham, Theory of self-assembly of hydrocarbon amphiphiles into micelles and bilayers, Journal of the Chemical Society, Faraday Transactions 2: Molecular and Chemical Physics, 72 (1976) 1525-1568.

[40] J.M. Seddon, Structure of the inverted hexagonal (H_{II}) phase, and non-lamellar phase transitions of lipids, Biochimica et Biophysica Acta (BBA) - Reviews on Biomembranes, 1031 (1990) 1-69.

[41] R. Koynova, M. Caffrey, Phases and phase transitions of the hydrated phosphatidylethanolamines, Chemistry and Physics of Lipids, 69 (1994) 1-34.

[42] W.-K. Fong, T.L. Hanley, B. Thierry, A. Tilley, N. Kirby, L.J. Waddington, B.J. Boyd, Understanding the photothermal heating effect in non-lamellar liquid crystalline systems, and the design of new mixed lipid systems for photothermal on-demand drug delivery, Physical Chemistry Chemical Physics, 16 (2014) 24936-24953.

[43] V.V. Kumar, Complementary molecular shapes and additivity of the packing parameter of lipids, Proceedings of the National Academy of Sciences, 88 (1991) 444-448.

[44] R.N.A.H. Lewis, R.N. McElhaney, Surface Charge Markedly Attenuates the Nonlamellar Phase-Forming Propensities of Lipid Bilayer Membranes: Calorimetric and ^{31}P-Nuclear Magnetic Resonance Studies of Mixtures of Cationic, Anionic, and Zwitterionic Lipids, Biophysical Journal, 79 (2000) 1455-1464.

[45] Y.C. Lee, T.F. Taraschi, N. Janes, Support for the shape concept of lipid structure based on a headgroup volume approach, Biophysical Journal, 65 (1993) 1429-1432.

[46] A. Watts, K. Harlos, D. Marsh, Charge-induced tilt in ordered-phase phosphatidylglycerol bilayers Evidence from x-ray diffraction, Biochimica et Biophysica Acta (BBA) - Biomembranes, 645 (1981) 91-96.

[47] J. Pan, F.A. Heberle, S. Tristram-Nagle, M. Szymanski, M. Koepfinger, J. Katsaras, N. Kučerka, Molecular structures of fluid phase phosphatidylglycerol bilayers as determined by small angle neutron and X-ray scattering, Biochimica et Biophysica Acta (BBA) - Biomembranes, 1818 (2012) 2135-2148.

[48] J.F. Nagle, S. Tristram-Nagle, Structure of lipid bilayers, Biochimica et Biophysica Acta (BBA) - Reviews on Biomembranes, 1469 (2000) 159-195.

[49] G. Pabst, S. Danner, S. Karmakar, G. Deutsch, V.A. Raghunathan, On the Propensity of Phosphatidylglycerols to Form Interdigitated Phases, Biophysical Journal, 93 (2007) 513-525.

[50] I. Pascher, M. Lundmark, P.-G. Nyholm, S. Sundell, Crystal structures of membrane lipids, Biochimica et Biophysica Acta (BBA) - Reviews on Biomembranes, 1113 (1992) 339-373.

[51] I. Pascher, S. Sundell, K. Harlos, H. Eibl, Conformation and packing properties of membrane lipids: The crystal structure of sodium dimyristoylphosphatidylglycerol, Biochimica et Biophysica Acta (BBA) - Biomembranes, 896 (1987) 77-88.

[52] R.S. Armen, O.D. Uitto, S.E. Feller, Phospholipid Component Volumes: Determination and Application to Bilayer Structure Calculations, Biophysical Journal, 75 (1998) 734-744.

[53] U.R. Pedersen, C. Leidy, P. Westh, G.H. Peters, The effect of calcium on the properties of charged phospholipid bilayers, Biochimica et Biophysica Acta (BBA) - Biomembranes, 1758 (2006) 573-582.

[54] H.I. Petrache, S. Tristram-Nagle, K. Gawrisch, D. Harries, V.A. Parsegian, J.F. Nagle, Structure and Fluctuations of Charged Phosphatidylserine Bilayers in the Absence of Salt, Biophysical Journal, 86 (2004) 1574-1586.

[55] R.N.A.H. Lewis, D. Zweytick, G. Pabst, K. Lohner, R.N. McElhaney, Calorimetric, X-Ray Diffraction, and Spectroscopic Studies of the Thermotropic Phase Behavior and

Organization of Tetramyristoyl Cardiolipin Membranes, Biophysical Journal, 92 (2007) 3166-3177.

[56] F. Etienne, Y. Roche, P. Peretti, S. Bernard, Cardiolipin packing ability studied by grazing incidence X-ray diffraction, Chemistry and Physics of Lipids, 152 (2008) 13-23.

[57] J.F. Nagle, R. Zhang, S. Tristram-Nagle, W. Sun, H.I. Petrache, R.M. Suter, X-ray structure determination of fully hydrated L alpha phase dipalmitoylphosphatidylcholine bilayers, Biophysical Journal, 70 (1995) 1419-1431.

[58] S. Tristram-Nagle, R. Zhang, R.M. Suter, C.R. Worthington, W.J. Sun, J.F. Nagle, Measurement of chain tilt angle in fully hydrated bilayers of gel phase lecithins, Biophysical Journal, 64 (1993) 1097-1109.

[59] M.J. Janiak, D.M. Small, G.G. Shipley, Temperature and compositional dependence of the structure of hydrated dimyristoyl lecithin, Journal of Biological Chemistry, 254 (1979) 6068-6078.

[60] T.J. McIntosh, S.A. Simon, Area per molecule and distribution of water in fully hydrated dilauroylphosphatidylethanolamine bilayers, Biochemistry, 25 (1986) 4948-4952.

[61] T.P. Trouard, D.A. Mannock, G. Lindblom, L. Rilfors, M. Akiyama, R.N. McElhaney, Thermotropic phase properties of 1,2-di-O-tetradecyl-3-O-(3-O-methyl- beta-D-glucopyranosyl)-sn-glycerol, Biophysical Journal, 67 (1994) 1090-1100.

[62] D.A. Mannock, R.N. Lewis, R.N. McElhaney, M. Akiyama, H. Yamada, D.C. Turner, S.M. Gruner, Effect of the chirality of the glycerol backbone on the bilayer and nonbilayer phase transitions in the diastereomers of di-dodecyl-beta-D-glucopyranosyl glycerol, Biophysical Journal, 63 (1992) 1355-1368.

[63] R.N.A.H. Lewis, D.A. Mannock, R.N. McElhaney, D.C. Turner, S.M. Gruner, Effect of fatty acyl chain length and structure on the lamellar gel to liquid-crystalline and lamellar to reversed hexagonal phase transitions of aqueous phosphatidylethanolamine dispersions, Biochemistry, 28 (1989) 541-548.

[64] H. Eibl, A. Blume, The influence of charge on phosphatidic acid bilayer membranes, Biochimica et Biophysica Acta (BBA) - Biomembranes, 553 (1979) 476-488.

[65] T.H. Haines, N.A. Dencher, Cardiolipin: a proton trap for oxidative phosphorylation, FEBS Letters, 528 (2002) 35-39.

[66] M. Kates, J.-Y. Syz, D. Gosser, T.H. Haines, pH-dissociation characteristics of cardiolipin and its 2′-deoxy analogue, Lipids, 28 (1993) 877-882.

[67] W.F. DeGrado, J.D. Lear, Induction of peptide conformation at apolar water interfaces. 1. A study with model peptides of defined hydrophobic periodicity, Journal of the American Chemical Society, 107 (1985) 7684-7689.

[68] D. Dieudonné, A. Gericke, C.R. Flach, X. Jiang, R.S. Farid, R. Mendelsohn, Propensity for Helix Formation in the Hydrophobic Peptides $K_2(LA)_x$ (x = 6, 8, 10, 12) in Monolayer, Bulk, and Lipid-Containing Phases. Infrared and Circular Dichroism Studies, Journal of the American Chemical Society, 120 (1998) 792-799.

[69] L. Béven, S. Castano, J. Dufourcq, Å. Wieslander, H. Wróblewski, The antibiotic activity of cationic linear amphipathic peptides: lessons from the action of leucine/lysine copolymers on bacteria of the class Mollicutes, European Journal of Biochemistry, 270 (2003) 2207-2217.

[70] S. Castano, B. Desbat, M. Laguerre, J. Dufourcq, Structure, orientation and affinity for interfaces and lipids of ideally amphipathic lytic L_iK_j (i=2j) peptides, Biochimica et Biophysica Acta (BBA) - Biomembranes, 1416 (1999) 176-194.

[71] S. Castano, B. Desbat, J. Dufourcq, Ideally amphipathic β-sheeted peptides at interfaces: structure, orientation, affinities for lipids and hemolytic activity of $(KL)_mK$ peptides, Biochimica et Biophysica Acta (BBA) - Biomembranes, 1463 (2000) 65-80.

[72] J.E. Baio, A. Zane, V. Jaeger, A.M. Roehrich, H. Lutz, J. Pfaendtner, G.P. Drobny, T. Weidner, Diatom Mimics: Directing the Formation of Biosilica Nanoparticles by Controlled Folding of Lysine-Leucine Peptides, Journal of the American Chemical Society, 136 (2014) 15134-15137.

[73] T. Weidner, N.T. Samuel, K. McCrea, L.J. Gamble, R.S. Ward, D.G. Castner, Assembly and structure of α-helical peptide films on hydrophobic fluorocarbon surfaces, Biointerphases, 5 (2010) 9-16.

[74] J.R. Long, N. Oyler, G.P. Drobny, P.S. Stayton, Assembly of α-helical Peptide Coatings on Hydrophobic Surfaces, Journal of the American Chemical Society, 124 (2002) 6297-6303.

[75] L. Fu, J. Liu, E.C.Y. Yan, Chiral Sum Frequency Generation Spectroscopy for Characterizing Protein Secondary Structures at Interfaces, Journal of the American Chemical Society, 133 (2011) 8094-8097.

[76] R.L. York, G.J. Holinga, D.R. Guyer, K.R. McCrea, R.S. Ward, G.A. Somorjai, A New Optical Parametric Amplifier Based on Lithium Thioindate Used for Sum Frequency Generation Vibrational Spectroscopic Studies of the Amide I Mode of an Interfacial Model Peptide, Applied Spectroscopy, 62 (2008) 937-940.

[77] M. Narita, Y. Tomotake, S. Isokawa, T. Matsuzawa, T. Miyauchi, Syntheses and properties of resin-bound oligopeptides. 2. Infrared spectroscopic conformational analysis of cross-linked polystyrene resin bound oligoleucines in the swollen state, Macromolecules, 17 (1984) 1903-1906.

[78] M. Gustafsson, G. Vandenbussche, T. Curstedt, J.-M. Ruysschaert, J. Johansson, The 21-residue surfactant peptide (LysLeu$_4$)$_4$Lys (KL4) is a transmembrane α-helix with a mixed nonpolar/polar surface, FEBS Letters, 384 (1996) 185-188.

[79] A. Sáenz, O. Cañadas, L.A. Bagatolli, M.E. Johnson, C. Casals, Physical properties and surface activity of surfactant-like membranes containing the cationic and hydrophobic peptide KL4, FEBS Journal, 273 (2006) 2515-2527.

[80] J.A. Whitsett, T.E. Weaver, Hydrophobic Surfactant Proteins in Lung Function and Disease, New England Journal of Medicine, 347 (2002) 2141-2148.

[81] P. Cai, C.R. Flach, R. Mendelsohn, An Infrared Reflection−Absorption Spectroscopy Study of the Secondary Structure in (KL$_4$)$_4$K, a Therapeutic Agent for Respiratory Distress Syndrome, in Aqueous Monolayers with Phospholipids, Biochemistry, 42 (2003) 9446-9452.

[82] J. Ma, S. Koppenol, H. Yu, G. Zografi, Effects of a Cationic and Hydrophobic Peptide, KL$_4$, on Model Lung Surfactant Lipid Monolayers, Biophysical Journal, 74 (1998) 1899-1907.

[83] L. Martínez-Gil, J. Pérez-Gil, I. Mingarro, The Surfactant Peptide KL$_4$ Sequence Is Inserted with a Transmembrane Orientation into the Endoplasmic Reticulum Membrane, Biophysical Journal, 95 (2008) L36-L38.

[84] C. Cochrane, S. Revak, Pulmonary surfactant protein B (SP-B): structure-function relationships, Science, 254 (1991) 566-568.

[85] J.B. Rothbard, T.C. Jessop, R.S. Lewis, B.A. Murray, P.A. Wender, Role of Membrane Potential and Hydrogen Bonding in the Mechanism of Translocation of Guanidinium-Rich Peptides into Cells, Journal of the American Chemical Society, 126 (2004) 9506-9507.

[86] N. Sakai, S. Matile, Anion-Mediated Transfer of Polyarginine across Liquid and Bilayer Membranes, Journal of the American Chemical Society, 125 (2003) 14348-14356.

[87] L. Li, I. Vorobyov, T.W. Allen, The Different Interactions of Lysine and Arginine Side Chains with Lipid Membranes, The Journal of Physical Chemistry B, 117 (2013) 11906-11920.

[88] M. Mosior, S. McLaughlin, Binding of basic peptides to acidic lipids in membranes: effects of inserting alanine(s) between the basic residues, Biochemistry, 31 (1992) 1767-1773.

[89] K.J. Hallock, D.-K. Lee, J. Omnaas, H.I. Mosberg, A. Ramamoorthy, Membrane Composition Determines Pardaxin's Mechanism of Lipid Bilayer Disruption, Biophysical Journal, 83 (2002) 1004-1013.

[90] L. Zhang, A. Rozek, R.E.W. Hancock, Interaction of Cationic Antimicrobial Peptides with Model Membranes, Journal of Biological Chemistry, 276 (2001) 35714-35722.

[91] B. Bechinger, Rationalizing the membrane interactions of cationic amphipathic antimicrobial peptides by their molecular shape, Current Opinion in Colloid & Interface Science, 14 (2009) 349-355.

[92] L.T. Nguyen, E.F. Haney, H.J. Vogel, The expanding scope of antimicrobial peptide structures and their modes of action, Trends in Biotechnology, 29 (2011) 464-472.

[93] Y. Shai, Mechanism of the binding, insertion and destabilization of phospholipid bilayer membranes by K-helical antimicrobial and cell non-selective membrane-lytic peptides, Biochimica et Biophysica Acta (BBA) - Biomembranes, 1462 (1999) 55-70.

[94] B. Bechinger, K. Lohner, Detergent-like actions of linear amphipathic cationic antimicrobial peptides, Biochimica et Biophysica Acta (BBA) - Biomembranes, 1758 (2006) 1529-1539.

[95] K.A. Brogden, Antimicrobial peptides: pore formers or metabolic inhibitors in bacteria?, Nature Reviews, 3 (2005) 238-250.

[96] A. Blume, Apparent Molar Heat Capacities of Phospholipids in Aqueous Dispersion. Effects of Chain Length and Head Group Structure, Biochemistry, 22 (1983) 5436-5442.

[97] M. Reuter, C. Schwieger, A. Meister, G. Karlsson, A. Blume, Poly-L-lysines and poly-L-arginines induce leakage of negatively charged phospholipid vesicles and translocate through the lipid bilayer upon electrostatic binding to the membrane, Biophysical Chemistry, 144 (2009) 27-37.

[98] M.R.R. de Planque, J.A. Killian, Protein–lipid interactions studied with designed transmembrane peptides: role of hydrophobic matching and interfacial anchoring (Review), Molecular Membrane Biology, 20 (2003) 271-284.

[99] W. Schmidt, M. Buschle, W. Zauner, H. Kirlappos, K. Mechtler, B. Trska, M.L. Birnstiel, Cell-free tumor antigen peptide-based cancer vaccines, Proceedings of the National Academy of Sciences, 94 (1997) 3262-3267.

[100] P.A. Wender, D.J. Mitchell, K. Pattabiraman, E.T. Pelkey, L. Steinman, J.B. Rothbard, The design, synthesis, and evaluation of molecules that enable or enhance cellular uptake: Peptoid molecular transporters, Proceedings of the National Academy of Sciences, 97 (2000) 13003-13008.

[101] D.J. Mitchell, L. Steinman, D.T. Kim, C.G. Fathman, J.B. Rothbard, Polyarginine enters cells more efficiently than other polycationic homopolymers, The Journal of Peptide Research, 56 (2000) 318-325.

[102] B. de Kruijff, A. Rietveld, N. Telders, B. Vaandrager, Molecular aspects of the bilayer stabilization induced by poly(l-lysines) of varying size in cardiolipin liposomes, Biochimica et Biophysica Acta (BBA) - Biomembranes, 820 (1985) 295-304.

[103] J. Kim, M. Mosior, L.A. Chung, H. Wu, S. McLaughlin, Binding of peptides with basic residues to membranes containing acidic phospholipids, Biophysical Journal, 60 (1991) 135-148.

[104] C. Schwieger, A. Blume, Interaction of poly(L-lysines) with negatively charged membranes: an FT-IR and DSC study, European Biophysics Journal, 36 (2007) 437-450.

[105] C. Schwieger, A. Blume, Interaction of Poly(L-arginine) with Negatively Charged DPPG Membranes: Calorimetric and Monolayer Studies, Biomacromolecules, 10 (2009) 2152-2161.

[106] S.E. Blondelle, K. Lohner, M.-I. Aguilar, Lipid-induced conformation and lipid-binding properties of cytolytic and antimicrobial peptides: determination and biological specificity, Biochimica et Biophysica Acta (BBA) - Biomembranes, 1462 (1999) 89-108.

[107] D. Carrier, J. Dufourcq, J.-F. Faucon, M. Pézolet, A fluorescence investigation of the effects of polylysine on dipalmitoylphosphatidylglycerol bilayers, Biochimica et Biophysica Acta (BBA) - Biomembranes, 820 (1985) 131-139.

[108] D. Carrier, M. Pezolet, Investigation of polylysine-dipalmitoylphosphatidylglycerol interactions in model membranes, Biochemistry, 25 (1986) 4167-4174.

[109] G. Förster, C. Schwieger, F. Faber, T. Weber, A. Blume, Influence of poly(L-lysine) on the structure of dipalmitoylphosphatidylglycerol/water dispersions studied by X-ray scattering, European Biophysics Journal, 36 (2007) 425-435.

[110] W. Hartmann, H.-J. Galla, Binding of polylysine to charged bilayer membranes. Molecular organization of a lipid · peptide complex, Biochimica et Biophysica Acta (BBA) - Biomembranes, 509 (1978) 474-490.

[111] H. Takahashi, S. Matuoka, S. Kato, K. Ohki, I. Hatta, Effects of poly(l-lysine) on the structural and thermotropic properties of dipalmitoylphosphatidylglycerol bilayers, Biochimica et Biophysica Acta (BBA) - Biomembranes, 1110 (1992) 29-36.

[112] M. Jackson, P.I. Haris, D. Chapman, Conformational transitions in poly(l-lysine): studies using Fourier transform infrared spectroscopy, Biochimica et Biophysica Acta (BBA) - Protein Structure and Molecular Enzymology, 998 (1989) 75-79.

[113] K. Fukushima, Y. Muraoka, T. Inoue, R. Shimozawa, Conformational study of poly(l-lysine) interacting with acidic phospholipid vesicles, Biophysical Chemistry, 34 (1989) 83-90.

[114] D. Carrier, M. Pézolet, Raman spectroscopic study of the interaction of poly-L-lysine with dipalmitoylphosphatidylglycerol bilayers, Biophysical Journal, 46 (1984) 497-506.

[115] M. Mosior, S. McLaughlin, Electrostatics and reduction of dimensionality produce apparent cooperativity when basic peptides bind to acidic lipids in membranes, Biochimica et Biophysica Acta (BBA) - Biomembranes, 1105 (1992) 185-187.

[116] M. Roux, J.M. Neumann, M. Bloom, P.F. Devaux, ^{2}H and ^{31}P NMR study of pentalysine interaction with headgroup deuterated phosphatidylcholine and phosphatidylserine, European Biophysics Journal, 16 (1988) 267-273.

[117] N. Ben-Tal, B. Honig, R.M. Peitzsch, G. Denisov, S. McLaughlin, Binding of small basic peptides to membranes containing acidic lipids: theoretical models and experimental results, Biophysical Journal, 71 (1996) 561-575.

[118] N. Ben-Tal, B. Honig, C.K. Bagdassarian, A. Ben-Shaul, Association Entropy in Adsorption Processes, Biophysical Journal, 79 (2000) 1180-1187.

[119] D. Murray, A. Arbuzova, G. Hangyás-Mihályné, A. Gambhir, N. Ben-Tal, B. Honig, S. McLaughlin, Electrostatic Properties of Membranes Containing Acidic Lipids and Adsorbed Basic Peptides: Theory and Experiment, Biophysical Journal, 77 (1999) 3176-3188.

[120] G. Denisov, S. Wanaski, P. Luan, M. Glaser, S. McLaughlin, Binding of Basic Peptides to Membranes Produces Lateral Domains Enriched in the Acidic Lipids Phosphatidylserine and Phosphatidylinositol 4,5-Bisphosphate: An Electrostatic Model and Experimental Results, Biophysical Journal, 74 (1998) 731-744.

[121] B. Bonev, A. Watts, M. Bokvist, G. Grobner, Electrostatic peptide-lipid interactions of amyloid-β peptide and pentalysine with membrane surfaces monitored by ^{31}P MAS NMR, Physical Chemistry Chemical Physics, 3 (2001) 2904-2910.

[122] C.A. Buser, J. Kim, S. McLaughlin, R.M. Peitzsch, Does the binding of clusters of basic residues to acidic lipids induce domain formation in membranes?, Molecular Membrane Biology, 12 (1995) 69-75.

[123] M. Hoernke, C. Schwieger, A. Kerth, A. Blume, Binding of cationic pentapeptides with modified side chain lengths to negatively charged lipid membranes: Complex interplay of electrostatic and hydrophobic interactions, Biochimica et Biophysica Acta (BBA) - Biomembranes, 1818 (2012) 1663-1672.

[124] G.W.H. Höhne, W. Hemminger, H.-J. Flammersheim, Differential Scanning Calorimetry, Springer Verlag, Berlin, 1996.

[125] A. Blume, Applications of Calorimetry to Lipid Model Membranes, in: C. Hidalgo (Ed.) Physical Properties of Biological Membranes and Their Functional Implications, Plenum Press, New York, 1988, pp. 71-121.

[126] R.N. McElhaney, The use of differential scanning calorimetry and differential thermal analysis in studies of model and biological membranes, Chemistry and Physics of Lipids, 30 (1982) 229-259.

[127] A. Blume, Biological calorimetry: membranes, Thermochimica Acta, 193 (1991) 299-347.

[128] D. Chapman, R.M. Williams, B.D. Ladbrooke, Physical studies of phospholipids. VI. Thermotropic and lyotropic mesomorphism of some 1,2-diacyl-phosphatidylcholines (lecithins), Chemistry and Physics of Lipids, 1 (1967) 445-475.

[129] D.F. Evans, H. Wennerström, The Colloidal Domain, 2nd ed., Wiley-VCH, New York, 1999.

[130] K. Lohner, E.J. Prenner, Differential scanning calorimetry and X-ray diffraction studies of the specificity of the interaction of antimicrobial peptides with membrane-mimetic systems., Biochimica et Biophysica Acta (BBA) - Biomembranes, 1462 (1999) 141-156.

[131] R.N. McElhaney, Differential scanning calorimetric studies of lipid-protein interactions in model membrane systems, Biochimica et Biophysica Acta (BBA) - Reviews on Biomembranes, 864 (1986) 361-421.

[132] P.L. Privalov, V.V. Plotnikov, V.V. Filimonov, Precision scanning microcalorimeter for the study of liquids, Journal of Chemical Thermodynamics, 7 (1975) 41-47.

[133] H.H. Mantsch, R.N. McElhaney, Phospholipid phase transitions in model and biological membranes as studied by infrared spectroscopy, Chemistry and Physics of Lipids, 57 (1991) 213-226.

[134] M. Jackson, H.H. Mantsch, The Use and Misuse of FTIR Spectroscopy in the Determination of Protein Structure, Critical Reviews in Biochemistry and Molecular Biology, 30 (1995) 95-120.

[135] P.H. Axelsen, M.J. Citra, Orientational order determination by internal reflection infrared spectroscopy, Progress in Biophysics and Molecular Biology, 66 (1996) 227-253.

[136] R.A. Dluhy, S.M. Stephens, S. Widayati, A.D. Williams, Vibrational spectroscopy of biophysical monolayers. Applications of IR and Raman spectroscopy to biomembrane model systems at interfaces, Spectrochimica Acta Part A: Molecular and Biomolecular Spectroscopy, 51 (1995) 1413-1447.

[137] E. Goormaghtigh, V. Raussens, J.-M. Ruysschaert, Attenuated total reflection infrared spectroscopy of proteins and lipids in biological membranes, Biochimica et Biophysica Acta (BBA) - Reviews on Biomembranes, 1422 (1999) 105-185.

[138] U.P. Fringeli, H.H. Günthard, Infrared Membrane Spectroscopy, in: E. Grell (Ed.) Membrane Spectroscopy, Springer Berlin Heidelberg, Berlin, Heidelberg, 1981, pp. 270-332.

[139] R.A. Dluhy, Infrared Spectroscopy of Biophysical Monomolecular Films at Interfaces: Theory and Applications, Applied Spectroscopy Reviews, 35 (2000) 315-351.

[140] A.W. Adamson, Physical Chemistry of Surfaces, John Wiley & Sons, Inc., New York, Chichester, Brisbane, Toronto, Singapore, 1990.

[141] G.L. Gaines, Insoluble Monolayers at Liquid-Gas Interfaces, Inetrscience Publisher, New York, 1966.

[142] H. Möhwald, Phospholipid Monolayers, in: R. Lipowsky, E. Sackmann (Eds.) Structure and Dynamics of Membranes. From Cells to Vesicles., North Holland, Amsterdam, 1995, pp. 161-211.

[143] H. Möhwald, Phospholipid and Phospolipid-Protein Monolayers at the Air/Water Interface, Annual Review of Physical Chemistry, 41 (1990) 441-476.

[144] H. Brockman, Lipid monolayers: why use half a membrane to characterize protein-membrane interactions?, Curr. Opin. Struct. Biol., 9 (1999) 438-443.

[145] M. Ahlers, W. Müller, A. Reichert, H. Ringsdorf, J. Venzmer, Spezifische Wechselwirkungen von Prteinen mit funktionellen Lipidmonoschichten - Wege zur Simulation von Biomembranprozessen, Angewandte Chemie, 102 (1990) 1310-1327.

[146] A. Hädicke, A. Blume, Binding of Short Cationic Peptides $(KX)_4K$ to Negatively Charged DPPG Monolayers: Competition between Electrostatic and Hydrophobic Interactions, Langmuir, 31 (2015) 12203-12214.

[147] É. Boisselier, P. Calvez, É. Demers, L. Cantin, C. Salesse, Influence of the Physical State of Phospholipid Monolayers on Protein Binding, Langmuir, 28 (2012) 9680-9688.

[148] P. Calvez, S. Bussières, E. Demers, C. Salesse, Parameters modulating the maximum insertion pressure of proteins and peptides in lipid monolayers, Biochimie, 91 (2009) 718-733.

[149] P. Calvez, E. Demers, E. Boisselier, C. Salesse, Analysis of the Contribution of Saturated and Polyunsaturated Phospholipid Monolayers to the Binding of Proteins, Langmuir, 27 (2011) 1373-1379.

[150] M. Lhor, S.C. Bernier, H. Horchani, S. Bussières, L. Cantin, B. Desbat, C. Salesse, Comparison between the behavior of different hydrophobic peptides allowing membrane anchoring of proteins, Advances in Colloid and Interface Science, 207 (2014) 223-239.

[151] T. Brehmer, A. Kerth, W. Graubner, M. Malesevic, B. Hou, T. Bruser, A. Blume, Negatively Charged Phospholipids Trigger the Interaction of a Bacterial Tat Substrate Precursor Protein with Lipid Monolayers, Langmuir, 28 (2012) 3534-3541.

[152] A. Baszkin, W. Norde, Physical chemistry of Biological Interfaces, in: F. MacRitchie (Ed.) Proteins at Liquid Interfaces, Marcel Dekker, New York, 2000.

[153] 2016.

[154] C.M. Knobler, Seeing Phenomena in Flatland: Studies of Monolayer by Fluorescence Microscopy, Science, 249 (1990) 870-874.

[155] M. Lösche, E. Sackmann, H. Möhwald, A Fluorescnece Microscopic Study Concerning the Phase Diagram of Phospholipids, Berichte der Bunsengeschaft für Physikalische Chemie, 87 (1983) 848-852.

[156] H. McConnell, Structures and transitions in lipid monolayers at the air-water interface., Annual Review of Physical Chemistry, 42 (1991) 171-195.

[157] R.M. Weis, Fluorescence microscopy of phospholipid monolayer phase transitions, Chemistry and Physics of Lipids, 57 (1991) 227-239.

[158] M. Dyck, M. Lösche, Interaction of the Neurotransmitter, Neuropeptide Y, with Phospholipid Membranes: Film Balance and Fluorescence Microscopy Studies, The Journal of Physical Chemistry B, 110 (2006) 22143-22151.

[159] R.A. Dluhy, D.G. Cornell, In situ measurement of the infrared spectra of insoluble monolayers at the air-water interface, The Journal of Physical Chemistry, 89 (1985) 3195-3197.

[160] R.A. Dluhy, R. Mendelsohn, Emerging techniques in biophysical FT-IR, Analytical Chemistry, 60 (1988) 269A-278A.

[161] E. Bellet-Amalric, D. Blaudez, B. Desbat, F. Graner, F. Gauthier, A. Renault, Interaction of the third helix of Antennapedia homeodomain and a phospholipid monolayer, studied by ellipsometry and PM-IRRAS at the air–water interface, Biochimica et Biophysica Acta (BBA) - Biomembranes, 1467 (2000) 131-143.

[162] S. Castano, B. Desbat, I. Cornut, P. Méléard, J. Dufourcq, α-Helix to β-sheet transition within the Leu $_i$ Lys $_j$ (i=2j) series of lytic amphipathic peptides by decreasing their size, Lett Pept Sci, 4 (1997) 195-200.

[163] C. Fuchs, H. Hussain, C. Schwieger, M. Schulz, W.H. Binder, J. Kressler, Molecular arrangement of symmetric and non-symmetric triblock copolymers of poly(ethylene oxide) and poly(isobutylene) at the air/water interface, Journal of Colloid and Interface Science, 437 (2015) 80-89.

[164] H. Hussain, A. Kerth, A. Blume, J. Kressler, Amphiphilic Block Copolymers of Poly(ethylene oxide) and Poly(perfluorohexylethyl methacrylate) at the Water Surface and Their Penetration into the Lipid Monolayer, The Journal of Physical Chemistry B, 108 (2004) 9962-9969.

[165] A. Kerth, P. Garidel, J. Howe, C. Alexander, J.-P. Mach, T. Waelli, A. Blume, E.T.h. Rietschel, K. Brandenburg, An Infrared Reflection-Absorption Spectroscopic (IRRAS) Study of the Interaction of Lipid A and Lipopolysaccharide Re with Endotoxin-Binding Proteins, Medicinal Chemistry, 5 (2009) 535-542.

[166] K. Knauf, A. Meister, A. Kerth, A. Blume, Interaction of alkyltrimethylammonium bromides with DMPC-d$_{54}$ and DMPG-d$_{54}$ monolayers studied by infrared reflection absorption spectroscopy (IRRAS), Journal of Colloid and Interface Science, 342 (2010) 243-252.

[167] A. Meister, C. Nicolini, H. Waldmann, J. Kuhlmann, A. Kerth, R. Winter, A. Blume, Insertion of Lipidated Ras Proteins into Lipid Monolayers Studied by Infrared Reflection Absorption Spectroscopy (IRRAS), Biophysical Journal, 91 (2006) 1388-1401.

[168] H. Nakahara, A. Dudek, Y. Nakamura, S. Lee, C.-H. Chang, O. Shibata, Hysteresis behavior of amphiphilic model peptide in lung lipid monolayers at the air–water interface by an IRRAS measurement, Colloids and Surfaces B: Biointerfaces, 68 (2009) 61-67.

[169] H. Nakahara, S. Lee, O. Shibata, Specific interaction restrains structural transitions of an amphiphilic peptide in pulmonary surfactant model systems: An in situ PM-IRRAS investigation, Biochimica et Biophysica Acta (BBA) - Biomembranes, 1798 (2010) 1263-1271.

[170] R. Mendelsohn, J.W. Brauner, A. Gericke, External Infrared Reflection Absorption Spectrometry of Monolayer Films at the Air-Water Interface, Annual Review of Physical Chemistry, 46 (1995) 305-334.

[171] R. Mendelsohn, G. Mao, C.R. Flach, Infrared reflection–absorption spectroscopy: Principles and applications to lipid–protein interaction in Langmuir films, Biochimica et Biophysica Acta (BBA) - Biomembranes, 1798 (2010) 788-800.

[172] D. Blaudez, T. Buffeteau, J.C. Cornut, B. Desbat, N. Escafre, M. Pezolet, J.M. Turlet, Polarization-Modulated FT-IR Spectroscopy of a Spread Monolayer at the Air/Water Interface, Applied Spectroscopy, 47 (1993) 869-874.

[173] D. Blaudez, T. Buffeteau, J.C. Cornut, B. Desbat, N. Escafre, M. Pezolet, J.M. Turlet, Polarization modulation FTIR spectroscopy at the air-water interface, Thin Solid Films, 242 (1994) 146-150.

[174] D. Blaudez, T. Buffeteau, B. Desbat, J. Marie Turlet, Infrared and Raman spectroscopies of monolayers at the air–water interface, Current Opinion in Colloid & Interface Science, 4 (1999) 265-272.

[175] J. Ebenhan, Orientierung amphiphiler Terphenylderivate an der Wasser-Luft-Grenzfläche, Naturwissenschaftliche Fakultät II - Chemie, Physik und Mathematik, Martin-Luther-Universität, Halle, 2012.

[176] A. Kerth, Infrarot-Reflexions-Absorptions-Spektroskopie an Lipid-, Peptid- und Flüssigkristall-Filmen an der Luft/Wasser-Grenzfläche, Mathematisch-Naturwissenschaftliche-Technische Fakultät, Martin-Luther-Universität, Halle, 2003.

[177] T. Heimburg, A Model for the Lipid Pretransition: Coupling of Ripple Formation with the Chain-Melting Transition, Biophysical Journal, 78 (2000) 1154-1165.

[178] M.F. Schneider, D. Marsh, W. Jahn, B. Kloesgen, T. Heimburg, Network formation of lipid membranes: Triggering structural transitions by chain melting, Proceedings of the National Academy of Sciences, 96 (1999) 14312-14317.

[179] G. Cevc, Polymorphism of the bilayer membranes in the ordered phase and the molecular origin of the lipid pretransition and rippled lamellae, Biochimica et Biophysica Acta (BBA) - Biomembranes, 1062 (1991) 59-69.

[180] V.V. Andrushchenko, H.J. Vogel, E.J. Prenner, Interactions of tryptophan-rich cathelicidin antimicrobial peptides with model membranes studied by differential scanning calorimetry, Biochimica et Biophysica Acta (BBA) - Biomembranes, 1768 (2007) 2447-2458.

[181] A. Hildebrand, K. Beyer, R. Neubert, P. Garidel, A. Blume, Solubilization of negatively charged DPPC/DPPG liposomes by bile salts, Journal of Colloid and Interface Science, 279 (2004) 559-571.

[182] A. Hildebrand, R. Neubert, P. Garidel, A. Blume, Bile Salt Induced Solubilization of Synthetic Phosphatidylcholine Vesicles Studied by Isothermal Titration Calorimetry, Langmuir, 18 (2002) 2836-2847.

[183] R.V. Durvasula, C.-h. Huang, Thermotropic phase behavior of mixed-chain phosphatidylglycerols: implications for acyl chain packing in fully hydrated bilayers, Biochimica et Biophysica Acta (BBA) - Biomembranes, 1417 (1999) 111-121.

[184] Y.-P. Zhang, R.N.A.H. Lewis, R.N. McElhaney, Calorimetric and Spectroscopic Studies of the Thermotropic Phase Behavior of the n-Saturated 1,2-Diacylphosphatidylglycerols, Biophysical Journal, 72 (1997) 779-793.

[185] R.G. Snyder, H.L. Strauss, C.A. Elliger, Carbon-hydrogen stretching modes and the structure of n-alkyl chains. 1. Long, disordered chains, The Journal of Physical Chemistry, 86 (1982) 5145-5150.

[186] A. Blume, W. Huebner, G. Messner, Fourier transform infrared spectroscopy of $^{13}C=O$ labeled phospholipids hydrogen bonding to carbonyl groups, Biochemistry, 27 (1988) 8239-8249.

[187] D.D. Lasic, Liposomes, from Physics to Applications, Elsevier, Amsterdam, 1993.

[188] D.D. Lasic, Y. Barenholz, Handbook of Nonmedical Applications of Liposomes, CRC Press, Boca Raton, 1996.

[189] K.K. Eklund, I.S. Salonen, P.K.J. Kinnunen, Monovalent cation dependent phase behaviour of dipalmitoylphosphatidylglycerol, Chemistry and Physics of Lipids, 50 (1989) 71-78.

[190] V. Baumruk, D. Huo, R.K. Dukor, T.A. Keiderling, D. Lelievre, A. Brack, Conformational study of sequential Lys and Leu based polymers and oligomers using vibrational and electronic CD spectra, Biopolymers, 34 (1994) 1115-1121.

[191] B. Hernández, F.Z. Boukhalfa-Heniche, O. Seksek, Y.-M. Coïc, M. Ghomi, Secondary conformation of short lysine- and leucine-rich peptides assessed by optical spectroscopies: Effect of chain length, concentration, solvent, and time, Biopolymers, 81 (2006) 8-19.

[192] G. Guiffo-Soh, B. Hernández, Y.-M. Coïc, F.-Z. Boukhalfa-Heniche, G. Fadda, M. Ghomi, Vibrational Analysis of Amino Acids and Short Peptides in Hydrated Media. 3. Successive KL Repeats Induce Highly Stable β-Strands Capable of Forming Non-H-Bonded Aggregates, The Journal of Physical Chemistry B, 112 (2008) 1282-1289.

[193] S. Finger, A. Kerth, M. Dathe, A. Blume, The efficacy of trivalent cyclic hexapeptides to induce lipid clustering in PG/PE membranes correlates with their antimicrobial activity, Biochimica et Biophysica Acta (BBA) - Biomembranes, 1848 (2015) 2998-3006.

[194] S. Finger, C. Schwieger, A. Arouri, A. Kerth, A. Blume, Interaction of linear polyamines with negatively charged phospholipids: the effect of polyamine charge distance, Biological Chemistry, 395 (2014) 769-778.

[195] I.D. Alves, N. Goasdoué, I. Correia, S. Aubry, C. Galanth, S. Sagan, S. Lavielle, G. Chassaing, Membrane interaction and perturbation mechanisms induced by two cationic cell penetrating peptides with distinct charge distribution, Biochimica et Biophysica Acta (BBA) - General Subjects, 1780 (2008) 948-959.

[196] A. Shibata, S. Murata, S. Ueno, S. Liu, S. Futaki, Y. Baba, Synthetic copoly(Lys/Phe) and poly(Lys) translocate through lipid bilayer membranes, Biochimica et Biophysica Acta (BBA) - Biomembranes, 1616 (2003) 147-155.

[197] B.Z. Chowdhry, A.W. Dalziel, Phase transition properties of 1,2- and 1,3-diacylphosphatidylethanolamines with modified head groups, Biochemistry, 24 (1985) 4109-4117.

[198] D. Papahadjopoulos, M. Moscarello, E.H. Eylar, T. Isac, Effects of proteins on the thermotropic phase transitions of phospholipid membranes, Biochimica et Biophysica Acta (BBA) - Biomembranes, 401 (1975) 317-335.

[199] J.H. Kleinschmidt, D. Marsh, Spin-label electron spin resonance studies on the interactions of lysine peptides with phospholipid membranes, Biophysical Journal, 73 (1997) 2546-2555.

[200] G. Schwarz, S. Stankowski, Linear cooperative binding of large ligands involving mutual exclusion of different binding modes, Biophysical Chemistry, 10 (1979) 173-181.

[201] S. Stankowski, Large-ligand adsorption to membranes: I. Linear ligands as a limiting case, Biochimica et Biophysica Acta (BBA) - Biomembranes, 735 (1983) 341-351.

[202] S. Stankowski, Large-ligand adsorption to membranes III. Cooperativity and general ligand shapes, Biochimica et Biophysica Acta (BBA) - Biomembranes, 777 (1984) 167-182.

[203] B. Bonev, A. Watts, M. Bokvist, G. Grobner, Electrostatic peptide-lipid interactions of amyloid-[small beta] peptide and pentalysine with membrane surfaces monitored by 31P MAS NMR, Physical Chemistry Chemical Physics, 3 (2001) 2904-2910.

[204] M. Hörnke, Wechselwirkung von Oligopeptiden mit Lipidmembranmodellen, Naturwissenschaftliche Fakultät II Institut für Chemie, Martin-Luther-Universität Halle-Wittenberg, Halle, 2008.

[205] C. Schwieger, Electrostatic and Non-Electrostatic Interactions of Positively Charged Polypeptides with Negatively Charged Lipid Membranes, Institut für Chemie, Martin-Luther-Universität Halle-Wittenberg, Halle, 2008.

[206] R.M. Epand, B. Gabel, R.F. Epand, A. Sen, S.W. Hui, A. Muga, W.K. Surewicz, Formation of a new stable phase of phosphatidylglycerols, Biophysical Journal, 63 (1992) 327-332.

[207] F.M. Menger, V.A. Seredyuk, M.V. Kitaeva, A.A. Yaroslavov, N.S. Melik-Nubarov, Migration of Poly-l-lysine through a Lipid Bilayer, Journal of the American Chemical Society, 125 (2003) 2846-2847.

[208] V.R. Kodati, R. El-Jastimi, M. Lafleur, Contribution of the Intermolecular Coupling and Librotorsional Mobility in the Methylene Stretching Modes in the Infrared Spectra of Acyl Chains, The Journal of Physical Chemistry, 98 (1994) 12191-12197.

[209] D.M.H. Small, Donald J., The physical chemistry of lipids : from alkanes to phospholipids, Plenum Press, New York, NY, 1986.

[210] U. Shmueli, W. Traub, An X-ray diffraction study of poly-L-lysine hydrochloride, Journal of Molecular Biology, 12 (1965) 205-IN220.

[211] E.R. Blout, H. Lenormant, Reversible Configurational Changes in Poly-L-Lysine Hydrochloride Induced by Water, Nature, 179 (1957) 960-963.

[212] C. Nick Pace, J. Martin Scholtz, A Helix Propensity Scale Based on Experimental Studies of Peptides and Proteins, Biophysical Journal, 75 422-427.

[213] E.G. Hutchinson, J.M. Thornton, A revised set of potentials for β-turn formation in proteins, Protein Science, 3 (1994) 2207-2216.

[214] W.J. Sun, S. Tristram-Nagle, R.M. Suter, J.F. Nagle, Structure of gel phase saturated lecithin bilayers: temperature and chain length dependence, Biophysical Journal, 71 (1996) 885-891.

[215] J. Wang, A. Gambhir, S. McLaughlin, D. Murray, A Computational Model for the Electrostatic Sequestration of PI(4,5)P$_2$ by Membrane-Adsorbed Basic Peptides, Biophysical Journal, 86 (2004) 1969-1986.

[216] G. Ye, A. Gupta, R. DeLuca, K. Parang, G.D. Bothun, Bilayer disruption and liposome restructuring by a homologous series of small Arg-rich synthetic peptides, Colloids and Surfaces B: Biointerfaces, 76 (2010) 76-81.

[217] S. Futaki, T. Suzuki, W. Ohashi, T. Yagami, S. Tanaka, K. Ueda, Y. Sugiura, Arginine-rich Peptides, Journal of Biological Chemistry, 276 (2001) 5836-5840.

[218] J.B. Rothbard, E. Kreider, C.L. VanDeusen, L. Wright, B.L. Wylie, P.A. Wender, Arginine-Rich Molecular Transporters for Drug Delivery: Role of Backbone Spacing in Cellular Uptake, Journal of Medicinal Chemistry, 45 (2002) 3612-3618.

[219] A. Barth, C. Zscherp, What vibrations tell about proteins, Quarterly Reviews of Biophysics, 35 (2002) 369-430.

[220] A. Walrant, I. Correia, C.-Y. Jiao, O. Lequin, E.H. Bent, N. Goasdoué, C. Lacombe, G. Chassaing, S. Sagan, I.D. Alves, Different membrane behaviour and cellular uptake of three basic arginine-rich peptides, Biochimica et Biophysica Acta (BBA) - Biomembranes, 1808 (2011) 382-393.

[221] W.C. Wimley, S.H. White, Experimentally determined hydrophobicity scale for proteins at membrane interfaces, Nature Structural Biology, 3 (1996) 842-848.

[222] M. Vazdar, F. Uhlig, P. Jungwirth, Like-Charge Ion Pairing in Water: An Ab Initio Molecular Dynamics Study of Aqueous Guanidinium Cations, The Journal of Physical Chemistry Letters, 3 (2012) 2021-2024.

[223] M. Vazdar, J. Vymětal, J. Heyda, J. Vondrášek, P. Jungwirth, Like-Charge Guanidinium Pairing from Molecular Dynamics and Ab Initio Calculations, The Journal of Physical Chemistry A, 115 (2011) 11193-11201.

[224] B.D. Fleming, K.M.W. Keough, Thermotropic mesomorphism in aqueous dispersions of 1-palmitoyl-2-oleoyl- and 1,2-dilauroyl-phosphatidylglycerols in the presence of excess Na^+ or Ca^{2+}, Canadian Journal of Biochemistry and Cell Biology, 61 (1983) 882-891.

[225] G. Cevc, A. Watts, D. Marsh, Non-electrostatic contribution to the titration of the ordered-fluid phase transition of phosphatidylglycerol bilayers, FEBS Letters, 120 (1980) 267-270.

[226] R.F. Epand, R.I. Lehrer, A. Waring, W. Wang, R. Maget-Dana, D. Lelièvre, R.M. Epand, Direct comparison of membrane interactions of model peptides composed of only Leu and Lys residues, Peptide Science, 71 (2003) 2-16.

[227] M. Sathappa, N.N. Alder, The ionization properties of cardiolipin and its variants in model bilayers, Biochimica et Biophysica Acta (BBA) - Biomembranes.

[228] M.B. Sankaram, B. de Kruijff, D. Marsh, Selectivity of interaction of spin-labelled lipids with peripheral proteins bound to dimyristoylphosphatidylglycerol bilayers, as determined by ESR spectroscopy, Biochimica et Biophysica Acta (BBA) - Biomembranes, 986 (1989) 315-320.

[229] P.W.M. van Dijck, B. de Kruijff, A.J. Verkleij, L.L.M. van Deenen, J. de Gier, Comparative studies on the effects of pH and Ca^{2+} on bilayers of various negatively charged phospholipids and their mixtures with phosphatidylcholine, Biochimica et Biophysica Acta (BBA) - Biomembranes, 512 (1978) 84-96.

[230] A. Watts, K. Harlos, W. Maschke, D. Marsh, Control of the structure and fluidity of phosphatidylglycerol bilayers by pH titration, Biochimica et Biophysica Acta (BBA) - Biomembranes, 510 (1978) 63-74.

[231] M. Vazdar, E. Wernersson, M. Khabiri, L. Cwiklik, P. Jurkiewicz, M. Hof, E. Mann, S. Kolusheva, R. Jelinek, P. Jungwirth, Aggregation of Oligoarginines at Phospholipid Membranes: Molecular Dynamics Simulations, Time-Dependent Fluorescence Shift, and Biomimetic Colorimetric Assays, The Journal of Physical Chemistry B, 117 (2013) 11530-11540.

[232] K. Matsuzaki, K.-i. Sugishita, N. Ishibe, M. Ueha, S. Nakata, K. Miyajima, R.M. Epand, Relationship of Membrane Curvature to the Formation of Pores by Magainin 2, Biochemistry, 37 (1998) 11856-11863.

[233] W. Jing, E.J. Prenner, H.J. Vogel, A.J. Waring, R.I. Lehrer, K. Lohner, Headgroup structure and fatty acid chain length of the acidic phospholipids modulate the interaction of membrane mimetic vesicles with the antimicrobial peptide protegrin-1, Journal of Peptide Science, 11 (2005) 735-743.

[234] G. Laroche, D. Carrier, M. Pezolet, Study of the effect of poly(L-lysine) on phosphatidic acid and phosphatidylcholine/phosphatidic acid bilayers by Raman spectroscopy, Biochemistry, 27 (1988) 6220-6228.

[235] F. Jaehnig, K. Harlos, H. Vogel, H. Eibl, Electrostatic interactions at charged lipid membranes. Electrostatically induced tilt, Biochemistry, 18 (1979) 1459-1468.

[236] H. Takahashi, S. Matuoka, S. Kato, K. Ohki, I. Hatta, Electrostatic interaction of poly(l-lysine) with dipalmitoylphosphatidic acid studied by X-ray diffraction, Biochimica et Biophysica Acta (BBA) - Biomembranes, 1069 (1991) 229-234.

[237] G.G. Hammes, S.E. Schullery, Structure of macromolecular aggregates. II. Construction of model membranes from phospholipids and polypeptides, Biochemistry, 9 (1970) 2555-2563.

[238] Y.A. Ovchinnikov, V.T. Ivanov, Conformational states and biological activity of cyclic peptides, Tetrahedron, 31 (1975) 2177-2209.

[239] D.C. Hodgkin, B.M. Oughton, Possible molecular models for gramicidin S and their relationship to present ideas of protein structure, Biochemical Journal, 65 (1957) 752-756.

[240] E.J. Prenner, R.N.A.H. Lewis, L.H. Kondejewski, R.S. Hodges, R.N. McElhaney, Differential scanning calorimetric study of the effect of the antimicrobial peptide gramicidin S on the thermotropic phase behavior of phosphatidylcholine, phosphatidylethanolamine and phosphatidylglycerol lipid bilayer membranes, Biochimica et Biophysica Acta (BBA) - Biomembranes, 1417 (1999) 211-223.

[241] A. Giehl, T. Lemm, O. Bartelsen, K. Sandhoff, A. Blume, Interaction of the GM2-activator protein with phospholipid–ganglioside bilayer membranes and with monolayers at the air–water interface, European Journal of Biochemistry, 261 (1999) 650-658.

[242] N.R. Pallas, B.A. Pethica, Liquid-expanded to liquid-condensed transition in lipid monolayers at the air/water interface, Langmuir, 1 (1985) 509-513.

[243] M. Eeman, M. Deleu, From biological membranes to biomimetic model membranes, Biotechnologie, Agronomie, Société et Environnement, 4 (2010) 719.

[244] O.G. Travkova, G. Brezesinski, Adsorption of the antimicrobial peptide arenicin and its linear derivative to model membranes – A maximum insertion pressure study, Chemistry and Physics of Lipids, 167–168 (2013) 43-50.

[245] J. Marra, Direct measurement of the interaction between phosphatidylglycerol bilayers in aqueous electrolyte solutions, Biophysical Journal, 50 (1986) 815-825.

[246] J. Dufourcq, J.F. Faucon, R. Maget-Dana, M.P. Pileni, C. Hélène, Peptide-membrane interactions A fluorescence study of the binding of oligopeptides containing aromatic and basic residues to phospholipid vesicles, Biochimica et Biophysica Acta (BBA) - Biomembranes, 649 (1981) 67-75.

[247] D. Murray, A. Arbuzova, B. Honig, S. McLaughlint, The role of electrostatic and nonpolar interactions in the association of peripheral proteins with membranes, in: T.J.M. Sidney A. Simon (Ed.) Current Topics in Membranes, Academic Press2002, pp. 277-307.

[248] P. Garidel, A. Blume, 1,2-Dimyristoyl-sn-glycero-3-phosphoglycerol (DMPG) monolayers: influence of temperature, pH, ionic strength and binding of alkaline earth cations, Chemistry and Physics of Lipids, 138 (2005) 50-59.

[249] P.J. Casey, P.A. Solski, C.J. Der, J.E. Buss, p21ras is modified by a farnesyl isoprenoid, Proceedings of the National Academy of Sciences, 86 (1989) 8323-8327.

[250] F.L. Zhang, P.J. Casey, Protein Prenylation: Molecular Mechanisms and Functional Consequences, Annual Review of Biochemistry, 65 (1996) 241-269.

[251] A. Erbe, A. Kerth, M. Dathe, A. Blume, Interactions of KLA Amphipathic Model Peptides with Lipid Monolayers, ChemBioChem, 10 (2009) 2884-2892.

[252] C. Mangavel, R. Maget-Dana, P. Tauc, J.-C. Brochon, D. Sy, J.A. Reynaud, Structural investigations of basic amphipathic model peptides in the presence of lipid vesicles studied by circular dichroism, fluorescence, monolayer and modeling, Biochimica et Biophysica Acta (BBA) - Biomembranes, 1371 (1998) 265-283.

[253] T. Hitz, R. Iten, J. Gardiner, K. Namoto, P. Walde, D. Seebach, Interaction of α-and β-Oligoarginine-Acids and Amides with Anionic Lipid Vesicles: A Mechanistic and Thermodynamic Study, Biochemistry, 45 (2006) 5817-5829.

[254] D. Trommeshauser, H.-J. Galla, Interaction of a basic amphipathic peptide from the carboxyterminal part of the HIV envelope protein gp41 with negatively charged lipid surfaces, Chemistry and Physics of Lipids, 94 (1998) 81-96.

[255] M.M. Sacré, J.F. Tocanne, Importance of glycerol and fatty acid residues on the ionic properties of phosphatidylglycerols at the air—water interface, Chemistry and Physics of Lipids, 18 (1977) 334-354.

[256] J.F. Tocanne, P.H.J.T. Ververgaert, A.J. Verkleij, L.L.M. van Deenen, A monolayer and freeze-etching study of charged phospholipids I. Effects of ions and pH on the ionic properties of phosphatidylglycerol and lysylphosphatidylglycerol, Chemistry and Physics of Lipids, 12 (1974) 201-219.

[257] D. Andelman, F. Broçhard, J.F. Joanny, Phase transitions in Langmuir monolayers of polar molecules, The Journal of Chemical Physics, 86 (1987) 3673-3681.

[258] H.M. McConnell, Theory of hexagonal and stripe phases in monolayers, Proceedings of the National Academy of Sciences, 86 (1989) 3452-3455.

[259] R.M. Weis, H.M. McConnell, Cholesterol stabilizes the crystal-liquid interface in phospholipid monolayers, The Journal of Physical Chemistry, 89 (1985) 4453-4459.

[260] S. Nakamura, H. Nakahara, M.P. Krafft, O. Shibata, Two-Component Langmuir Monolayers of Single-Chain Partially Fluorinated Amphiphiles with Dipalmitoylphosphatidylcholine (DPPC), Langmuir, 23 (2007) 12634-12644.

[261] P. Krüger, M. Lösche, Molecular chirality and domain shapes in lipid monolayers on aqueous surfaces, Physical Review E, 62 (2000) 7031-7043.

[262] P. Scholtysek, Z. Li, J. Kressler, A. Blume, Interactions of DPPC with Semitelechelic Poly(glycerol methacrylate)s with Perfluoroalkyl End Groups, Langmuir, 28 (2012) 15651-15662.

[263] E. Maltseva, A. Kerth, A. Blume, H. Möhwald, G. Brezesinski, Adsorption of Amyloid β (1–40) Peptide at Phospholipid Monolayers, ChemBioChem, 6 (2005) 1817-1824.

[264] M. Dyck, A. Kerth, A. Blume, M. Lösche, Interaction of the Neurotransmitter, Neuropeptide Y, with Phospholipid Membranes: Infrared Spectroscopic Characterization at the Air/Water Interface, The Journal of Physical Chemistry B, 110 (2006) 22152-22159.

[265] A. Dicko, H. Bourque, M. Pézolet, Study by infrared spectroscopy of the conformation of dipalmitoylphosphatidylglycerol monolayers at the air–water interface and transferred on solid substrates, Chemistry and Physics of Lipids, 96 (1998) 125-139.

[266] F. Neville, Y. Ishitsuka, C.S. Hodges, O. Konovalov, A.J. Waring, R. Lehrer, K.Y.C. Lee, D. Gidalevitz, Protegrin interaction with lipid monolayers: grazing incidence X-ray diffraction and X-ray reflectivity study, Soft Matter, 4 (2008) 1665-1674.

[267] O.G. Travkova, J. Andrä, H. Möhwald, G. Brezesinski, Influence of Arenicin on Phase Transitions and Ordering of Lipids in 2D Model Membranes, Langmuir, 29 (2013) 12203-12211.

[268] T. Buffeteau, E. Le Calvez, S. Castano, B. Desbat, D. Blaudez, J. Dufourcq, Anisotropic Optical Constants of α-Helix and β-Sheet Secondary Structures in the Infrared, The Journal of Physical Chemistry B, 104 (2000) 4537-4544.

[269] V.V. Andrushchenko, H.J. Vogel, E.J. Prenner, Optimization of the hydrochloric acid concentration used for trifluoroacetate removal from synthetic peptides, Journal of Peptide Science, 13 (2007) 37-43.

[270] J.E. Bertie, Z. Lan, Infrared Intensities of Liquids XX: The Intensity of the OH Stretching Band of Liquid Water Revisited, and the Best Current Values of the Optical Constants of $H_2O(l)$ at 25°C between 15,000 and 1 cm^{-1}, Applied Spectroscopy, 50 (1996) 1047-1057.

10 Acknowledgements

This work could not have been accomplished without the help and support of many people. Therefore, I would like to address thanks to:

First of all, I want to thank Prof. Dr. Alfred Blume for including me in his group, which is actually several years ago, and the chance to work on this interesting topic with all the granted freedom. I am grateful to him for supervising this work and for the stimulating scientific discussions.

I am extremely grateful to all members of the DFG Graduiertenkolleg 1026 "Conformational Transitions in Macromolecular Interactions", for the stimulating atmosphere and for the continuous help and financial support.

My co-workers for the introduction in the new techniques, experimental help, the convenient atmosphere in the group, many discussions, and help to solve big and small problems of the daily scientific life. Thanks are directed to: Dr. Andreas Kerth, Dr. Christian Schwieger, Dr. Annette Meister, Dr. Peggy Scholtysek, Dr. Bob-Dan Lechner, Sebastian Finger, Andreas Lonitz, Waqar Shah and all other in the group AK Blume and the group AK Hinderberger.

I would like to acknowledge Prof. Dr. Margitta Dathe (Forschungsinstitut für Molekulare Pharmakologie, Berlin) for giving me the opportunity to carry out measurements determining the MIC of the peptides and to perform CD spectroscopy measurements in her lab and for her guidance, as well as to her group for all sorts of help, especially Kathy Scheinpflug and Heike Nikolenko.

Furthermore, I would like to express my love and gratitude to the two most important people in my life, my parents, whose unflinching love and support have helped me reach this far.

Finally, a very special debt of gratitude goes to my brother, my friends, and all members of the "Osternienburger Hockey Club" and all other persons who are not listed above. Without their support this work could never be done.

11 Publications

1) Hädicke, A. and A. Blume, *Binding of the cationic peptide (KL)$_4$K to lipid monolayers at the air-water interface - effect of the lipid headgroup charge, acyl chain length, and acyl chain saturation*. The Journal of Physical Chemistry B, 2016, **120**, 3880-3887

2) Hädicke, A. and A. Blume, *Binding of cationic peptides (KX)$_4$K to DPPG bilayers. Increasing the hydrophobicity of the uncharged amino acid X drives formation of membrane bound β-sheets: A DSC and FT-IR study.* Biochimica et Biophysica Acta-Biomembranes, 2016. **1858**, 1196-1206.

3) Hädicke, A. and A. Blume, *Binding of Short Cationic Peptides (KX)$_4$K to Negatively Charged DPPG Monolayers: Competition between Electrostatic and Hydrophobic Interactions.* Langmuir, 2015. **31,** 12203-12214.

4) Hädicke, A. and A. Blume, *Interactions of Pluronic block copolymers with lipid vesicles depend on lipid phase and Pluronic aggregation state.* Colloid and Polymer Science, 2015. **293,** 267-276.

5) Hädicke, A. and A. Blume, *Interactions of Pluronic block copolymers with lipid monolayers studied by epi-fluorescence microscopy and by adsorption experiments.* Journal of Colloid and Interface Science, 2013. **407**, 327-338.

Oral Contributions:

24.06.12 - 29.06.12   "Interaction of positively charged model peptides with bilayer membranes", 2nd EBSA BIOPHYSICS COURSE: "Membrane Biophysics and Lipid-Protein Interaction", Bordeaux/Lacanau

09.05.13 - 11.05.13   "Interaction of short cationic peptides with bilayer membranes and monolayers", 112. Bunsentagung: "Theory meets Spectroscopy", Karlsruhe

31.05.14 - 02.06.14   "Role of lipid monolayer at interaction with cationic model peptides at the air/water interface", 113. Bunsentagung: "Physical Chemistry on the Nanometer Scale", Hamburg

Poster Contributions:

12.03.12 - 14.03.12   International Workshop: "Membranes in Health and Disease", Gomadingen

17.05.12 - 19.05.12   111. Bunsentagung: „Ionic Liquids", Leipzig

13.07.13 - 17.07.13   9th European Biophysics Congress, Lisbon

04.11.13 - 06.11.13   Third International Meeting: "Conformational transitions in macromolecular interactions"

03.03.14 - 05.03.14   International Workshop "Molecular Membrane Biophysics", Hünfeld

14.09.14 - 17.09.14   Annual Meeting of the German Biophysical Society: "Molecular Biophysics · Membranes, Cells, Networks · Medical Biophysics", Lübeck

18.07.15 - 22.07.15   10th European Biophysics Congress, Dresden

28.09.15 - 29.09.15   21st Ostwald Kolloquium: "Biomolecules, Macromolecules and Particles at Fluid Interfaces", Potsdam

12.10.15 - 13.10.15   Soft interfacial materials: from fundamentals to formulation, London

12 Curriculum Vitae

Personal Data:

Family Name:	*Hädicke*
First Name:	*André*
Date of Birth:	*July 14, 1985*
Place of Birth:	*Köthen, Germany*
Nationality:	*German*

Education and Working Experience:

10/2011 – 07/2016	PhD student on the topic "Interactions of Cationic Peptides with Anionic Lipid Bilayers and Monolayers - Influence of Peptide and Lipid Modifications on Binding" in the group of Prof. Dr. A. Blume, Institute of Physical Chemistry, Martin-Luther-University Halle-Wittenberg
09/2011	Master of Science
04/2011 - 09/2011	Master Thesis on "Interactions of Pluronic block copolymers with lipid monolayers and lipid vesicles" in the group of Prof. Dr. A. Blume, Institute of Physical Chemistry, Martin-Luther-University Halle-Wittenberg
10/2009 - 09/2011	Study of Chemistry at Martin-Luther-University Halle-Wittenberg (Master of Science)
08/2009	Bachelor of Science
04/2009 - 07/2009	Bachelor Thesis on "Untersuchungen zur Wechselwirkung von Pluronic-Blockcopolymeren mit Lipidvesikeln" in the group of Prof. Dr. A. Blume, institute of physical chemistry, Martin-Luther-University Halle-Wittenberg
10/2006 - 09/2009	Study of Chemistry at Martin-Luther-University Halle-Wittenberg (Bachelor of Science)
07/2005 - 03/2006	Military service 1./Nachschubbataillon 462 in Diez
07/2005	Abitur
1996-2005	Grammar school "Burggymnasium" Aken
1992-1996	Primary school "Alfred Wirth" Osternienburg